The **relationship** between **geometric** and **mechanical properties** of **shell structures**

Andrew Borgart

Picture title page:
Morpharchitecture workshop in Lyon 2011

The relationship between geometric and mechanical properties of shell structures

Dissertation

for the purpose of obtaining a degree of doctor
at Delft University of Technology
by the authority of the Rector Magnificus prof.dr.ir. T.H.J.J. van der Hagen
chair of the Board of Doctorates
to be defended publicly on
Tuesday the 9th of July 2024 at 10:00 o'clock

by

Andrew BORGART

Master of Science in Architecture, Delft University of Technology
born in De Bilt, The Netherlands

This dissertation has been approved by the promotors.

Composition of the doctoral committee:

Rector Magnificus,	chairman
Prof.dr. M. Overend	Delft University of Technology, promotor
Dr.ir. P.J.C. Hoogenboom	Delft University of Technology, copromotor
Independent members:	
Dr.ir. A.D.C. Pronk	Eindhoven University of Technology
Dr. C. Andriotis	Delft University of Technology
Prof. A. McRobie	University of Cambridge, United Kingdom
Prof.dr. S. Adriaenssens	Princeton University, United States
Prof.dr.ir. A. van Keulen	Delft University of Technology
Prof.dr.ir. L.J. Sluys	Delft University of Technology, reserve member

Contents

Preface and acknowledgements

In 1994 as a student at the Delft University of Technology with an individual study programme containing mostly courses on structural mechanics I approached professor of Structural Mechanics at the faculty of Architecture, W.J. Beranek, to do my graduation project with him. My initial proposal was to do research on shell structures, my longtime topic of great fascination. Instead my thesis was part of the research project lead by Beranek together with my highly regarded former colleague Gerrie Hobbelman on a new constitutive model for brittle material such as concrete and masonry, the so-called "structuur mechanica".
After my graduation I stayed on at the chair of Structural Mechanics as a teacher and researcher. But my fascination with shell structures was still alive, so I pursued my interest to unravel its secrets by conducting this PhD thesis.

From prof. Beranek I learned classical mechanics, he was one of the last giants of classical mechanics. His greatest contribution was the introduction, in addition to the moment-hill, of the "shower analogy" for slab theory and which forms an important basis for this thesis. The other professor of Structural Mechanics from which I learned classis mechanics was prof. Blaauwendraad. As a student I followed all his courses with intense interest at the faculty in Civil Engineering.

In all modesty I hope this thesis adds to the great tradition of concrete shell research at the Delft University of Technology, following in the large unfillable footsteps of prof. Bouma, prof. Haas, prof. Loof and prof. Ernst. Their insights leaves me in their debt, without these great professors I would not have achieved this result.

My gratitude also goes to the younger guard, as former students or present colleagues of mine, who share my passion for shell structures and helped me to conduct this research. They discussed with me, argued with me, made valuable tools and came-up with innovations. For this I thank them all warmly.

My dear paranymphs Peter Eigenraam and Pim Buskermolen, who with their inquisitive nature have contributed greatly to my research. They always challenge my follies, but sometimes I get away with it, resulting in a discovery. To the talented former students whom I had the privilege to work with: Wout Baecke, Niels van Dijk, Matthijs van den Dool, Marcel Haasnoot, Henno Hanselaar, Alex Kouwenhoven, Marc de Leuw, Daoxuan Liang, Yannick Liem,

Michiel Oosterhuis, Kris Riemens, Jeroen Ros, Rik Rozendaal and Lonneke Tiggeler. They all endures my relentless search for insight and endless requests for raising the bar. But they all stood firm and we achieved great results, and had some fun along the way.
My dear former PhD students Qingpeng Li and Yu-Chou Chiang. They have endured the brunt of my quest for knowledge. Sometimes driving them to desperation, we had many inspiring conversations and their help was unsurpassed, I thank them.

I want to gratefully thank my colleague Pierre Hoogenboom for always being available for many long years as a valuable sparring partner. Jan Rots has contributed by ensuring the thesis got its introduction and conclusions, and provided as always the right words as commentary.
Mauro Overend and Fred Veer, my colleagues at Architecture, were among my greatest supporters in getting the thesis approved and provided valuable comments, for which I thank them. Michiel Kreutzer, as department head, was instrumental in getting the thesis actually finished, my gratitude for that.

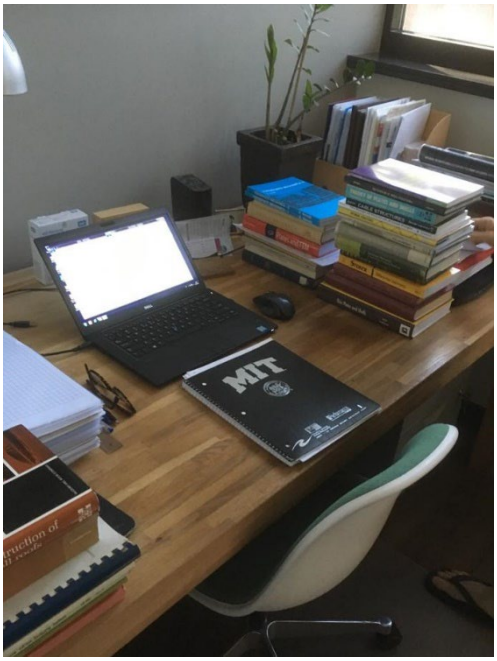

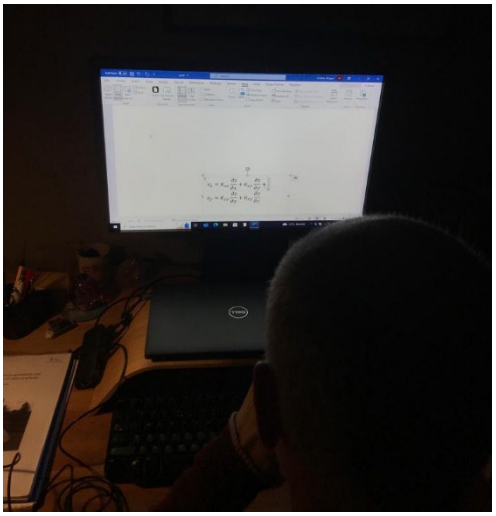

I have no words to express my debt to my dear late parents Robert and Hilda Borgart, and father in-law Bob de Wit, who lovingly supported me. I would not have wished anything more than for them to have seen this finished thesis. My mother in-law Marijke de Wit – Knottenbelt cheeringly supported me. And my brother Bart, my sister Vanessa and aunt Ada where always rooting for me.

My greatest gratitude goes to my husband, Jan-Willem. Nobody has endured more the many years of anguish of me struggling, often in the depth of night, to complete this thesis.

May 9th 2024

Addendum version, July 7th 2024

Summary

Shell structures can be either calculated with complex mathematics and differential geometry, or with the help of finite element method (FEM) software. Neither method gives the designer sufficient insight about the behaviour of the shell in the early design stage. The first method is for most designers too complex, it requires proficiency in at higher order mathematics and it can be only used for shells the geometry of which can be described by analytical equations. The second method is more accessible for most designers, and in combination with 3D modelling software is an attractive alternative to the cumbersome mathematics. However, the disadvantage of using FEM software is that the analytical relations between the different parameters important for obtaining insight into the structural behaviour of the shell is lost.

The ideal tool for designers would take the best of both methods: the analytical insight of the mathematics and the relatively easy access of FEM and 3D modelling software. The aim of the research done presented in this thesis is to do precisely that. By extending the well-known beam-analogy and its relations for an arch to shell structures a construct of relations is available for providing the designer with insight and means to influence the geometry of the shell and the resulting stress state.

The proposed hypotheses are based on classic analytical geometry and mechanics, especially analogies and methods developed in the past to elucidate the complex mathematics and mechanics for the purpose of insight [1]. The theory of graphic statics, reciprocal diagrams, complementary and potential energy was used to develop the method of solving the thrust network. Analogies such as the moment-hill for out-of-plane loaded slabs and the static-geometric analogy for thin shells as well as the load path theorem and stress functions were used to develop the slab – shell analogy.

Two approximate hypotheses are proposed in this thesis, the first is used to solve 3D indeterminate thrust networks by using complementary energy. The second hypothesis extends the beam – arch analogy in two directions to the slab – shell analogy; this method produces results in range of solutions found in classical shell theory.

The result of the different examples has been checked with the help of well-known solutions of classical shell mechanics, FEM calculations or graphic statics. Examples with relatively basic analytical formulas have been used to

elucidate the proposed method and for other examples simple purpose made tools based on the method have been used. Some simplifications have been made to avoid unnecessary complications in the derivation of the proposed method, such as only applying a uniformly distributed load. But most of the simplifications are not technically necessary; the conclusion and recommendations section include some suggestions have been added for extending the method.

The inception of numeric methods for analysing structures in the 1960^{s} was the end of the development of analytical mechanics for shell structures. This thesis aims to continue this development by tying the used theories and analogies together and bridge the gap with the numeric methods and to increase the understanding of the structural performance of shell structures.

Samenvatting

Het berekenen van schaalconstructies kan op twee manieren, met behulp van complexe wiskundige toegepaste mechanica en met de eindige elementen methode (EEM). Beide methoden zijn niet bevredigend om in een vroeg stadium de ontwerper bij te staan met het maken van onderbouwde beslissingen. De eerste wijze is voor de meeste ontwerpers en ingenieurs te complex en tijd rovend. De tweede wijze is, in combinatie met 3D modelleer programma's, veel toegankelijker voor de meeste ontwerpers en ingenieurs, het nadeel is wel dat bij numerieke methoden de analytische samenhang tussen de verschillende parameters die inzicht geven in het constructieve gedrag van de schaal verdwijnt.

De meeste ideale werkwijze zou een compromis zijn met de beste ingrediënten van beide methoden, het analytische inzicht van de complexe wiskunde en schaalmechanica en het gebruikersgemak van EEM en 3D modelleersoftware. De doelstelling van dit onderzoek is een methode te ontwikkelen die precies dat doet. De bekende balk – kabel / booganalogie zal uitgebreid worden naar schalen. Dit geeft de ontwerper en ingenieur voldoende inzicht om in de eerste ontwerpfase afgewogen beslissingen te maken over het ontwerp.

De voorgestelde hypothesen voor benaderingen zijn gebaseerd op klassieke geometrie en mechanica. Er wordt gebruik gemaakt van eerder ontwikkelde analogieën die als doel hadden om naast de complexe wiskunde en mechanica inzicht te bieden, en deze zijn gebruikt voor het ontwikkelen van de theorieën en methodes van dit onderzoek. De grafo-statica, de leer van wederkerige diagrammen en complementaire en potentiële energie zijn gebruikt om druk netwerken op te lossen. Analogieën als de momentenheuvel van platen, de statisch-geometrische analogie voor dunne schalen alsmede spanningsfuncties en de "load path" theorie zijn gebruikt voor de ontwikkeling van de plaat – schaal analogie.

Twee hypothesen worden gepresenteerd in dit onderzoek, de eerste lost statisch onbepaalde 3D stangenveelhoeken (druk netwerken) op met behulp van complementaire energie. The tweede methode breidt de balk – boog analogie uit in twee richtingen, de plaat – schaal analogie, deze methode levert resultaten vergelijkbaar met oplossingen uit de klassieke schaaltheorie.

De verschillende resultaten in dit onderzoek zijn geverifieerd met behulp van bekende oplossingen in de schaalmechanica, EEM berekeningen en grafo-

statica. Voorbeelden zijn uitgewerkt met relatief eenvoudige analytische formules, anderen met voor dit onderzoek speciaal ontwikkelde tools. Om in staat te zijn de voorgesteld methoden helder te presenteren zijn vereenvoudigingen aangenomen, zoals uitsluitend gelijkmatig verdeelde belastingen. De meeste vereenvoudigingen zijn technisch gezien niet noodzakelijk; in de aanbevelingen worden suggesties gedaan voor het uitbreiden van de methode.

De geboorte van numerieke methoden voor het analyseren van constructies in de jaren 60 van de vorige eeuw betekende nagenoeg het einde van de ontwikkeling van analytische mechanica voor schalen. Deze thesis beoogd de ontwikkeling weer op te pakken en een brug te slaan naar de numerieke methoden, met als doel om het inzicht in schalen te verhogen.

Notations

w	displacement
q	uniformly distributed line load, force density
EI	bending stiffness
M	bending moment
z	shape function
H	horizontal thrust, mean curvature
f, f^*	rise
V	support reaction, shear force, vertical load distribution, volume
m_{xx}, m_{yy}	bending moment slab
ν	Poisson's ratio
ϕ	redundancy, stress function
$\bar{M}$	Moment-hill
ζ	thurst surface
p	uniformly distributed surface load
v_x, v_y, v_n, v_t	shear force slab, vertical load distribution
Q	total force density
N	axial / normal force
F	point load
l	span, length
s	scaling factor, slope
α	angle, (shape) coefficient, ratio of strip length
σ	stress
EA	extensional stiffness
ε	strain
u	displacement
E	energy
A	area
C, c	constant
r	position vector
Π	functional
κ_{xx}, κ_{yy}, κ_{xy}	curvature (deformation)
k_x, k_y, k_{xy}	curvature (geometry)
a	length, distance
n_{xx} n_{yy}, n_{xy}	membrane force
$\bar{n}_{xx}$ $\bar{n}_{yy}$, $\bar{n}_{xy}$	projected membrane force
r_x, r_y, r_{xy}	radii
b	width, distance
t	height cross section

e	eccentricity
h	height, distributed horizontal thrust
β	angle, ratio of loads
φ	rotation
θ	slope of fold, rotation
P	total uniformly distributed surface load
r	radius
K	bending stiffness strip
D	bending stiffness slab
g	change of Gaussian curvature

1 Introduction

1.1 Background and motivation

This research is partly based on more than 25 years of experience teaching structural mechanics and spatial structures to students of Architecture and Civil Engineering of Delft University of Technology and internationally. Therefore, this part of the introduction strays somewhat from the conventional introduction of a PhD thesis. It is impossible not to take into account the very different background to which this thesis has been developed. For the readers to get a level of understanding of the motives behind this research some words should be dedicated to the authors position as teacher and researcher, they were instrumental to writing this thesis.

The text of the thesis should be read as one continuous “train of thought”, whereby the written words, the images and formulas form one coherent proposition resulting in the hypotheses. The propositions will be underpinned by analytical and pictorial validations.

The purpose of this thesis is to analyse the structural behaviour of shell structures by studying the way the applied loads flow naturally through the shells surface (cross section) to its supports and how the flow off forces relates to the shell’s geometry. This will give a fundamental understanding of the behaviour of shell structures and will thus provide the means to design these with form efficiently and elegance, as has been done by engineers such as Heinz Isler, Felix Candela and Eduardo Torroja.

Shells have geometrical and mechanical properties which have a close relationship for transferring loads and determine its structural performance. For many years shell structures have excited interest, especially their seemingly enigmatic states of equilibrium in relation to their form. Thin shells spanning long distances are a sight of beauty. However, just as professor Ekkehard Ramm [2] once called shells are the prima donnas of structures, the designing of these gracious structures has many pitfalls. An ill-shaped curved geometry, which is not always a real shell in the sense that the predominant part of the load is carried by membrane forces but are just curved surfaces loaded in bending, or incorrect shaped edge can totally ruin the shell’s structural behaviour and the shell consequently performs poorly resulting in a failed design.

Many scientists, from Timoshenko to Flügge, over the years have formulated very useful shell theories for analytically calculating the internal forces and stresses in shells. These theories are usually very mathematically complex but give some insight into the relation between the stresses and the shell's geometry and are nearly always only applicable to shells with simple mathematically describable geometries. Some engineers, like Heinz Isler, have performed physical experiments on shell structures to try to uncover more of the form-force relationship [3].

Nowadays, 3D modelling software and computational structural analysis are utilized by architects and engineers in the design of irregular curved surfaces. Most of the classical shell theories fail to provide analytical solutions for these complex shapes and thus the structures are calculated numerically with the help of the finite element method (FEM). In doing so, the relations, which are enclosed in analytical solutions are lost, making the relationship between the internal forces and the geometry even less insightful. This lack of insight makes designing these types of shells even more difficult for the designer and engineer.

The designer gets insight of the relation between the internal forces, loads and their geometry by graphical solutions, force polygons and form diagrams, for linear 2D structures such as cables and arches and thrust networks for discretized shells [4]. What even graphical solutions do not always reveal is why a (ratio of) curve(s) or the number and location of supports results in a certain load path. This is especially the case for 3D thrust networks.

The principal load path of an applied load to a shell is not easy to determine, because most shells are highly indeterminate. The principal stresses and their trajectories, often calculated with the aid of finite element methods, are not exactly the load path, the trajectories of the vertical component of the internal forces which carries the load. This means that to determine a thrust network for analysing a shell's state of stress, with or without making an additional finite element calculation, an infinite amount of possible load paths have to be considered as they are all possible. The best fit solutions are several possible states of equilibriums within the thickness of the shell's surface or predefined design envelope. However, the "correct" solution is not provided by this method which makes it impossible without the finite element method to find the correct internal forces for a given geometry, loading and boundary conditions.

As can be seen with experiments of hanging models of deformable cloth or latex sheets, they are naturally shaped by gravity loading. Their load path and unique thrust surface are inseparably linked with the gravity shaped surface and its curvature. This means that there is a unique solution for each shell's thrust surface under a specific loading and boundary condition. In this case the thrust surface is the shell's shape function. But these do not always have to be the same surface. As an example, the shape function of a spherical dome is not equal to its thrust surface.

The ratio of curvatures of the surface in conjunction with the boundary conditions determine the shell's state of indeterminacy. By solving the relationship between curvature and load path the unique thrust surface can be derived and thus the problem has been solved: a qualitative and quantitative relation between form and force.

The author's curiosity and search for knowledge and insight into shells started with the Blob revolution at the start of the 21st century [5]. Students of Architecture discovered the extensive possibilities ushered by the newly available 3D modelling software and in particular the ease with which complex curved surfaces could be drawn and explored in CAD. These types of forms were quickly called Blobs. It is unclear where the word BLOB came from, some sources refer to Binary Large OBject another to shapeless object as can be seen in the 50's movie "The Blob", which was very popular with students at the time of the Blob revolution.

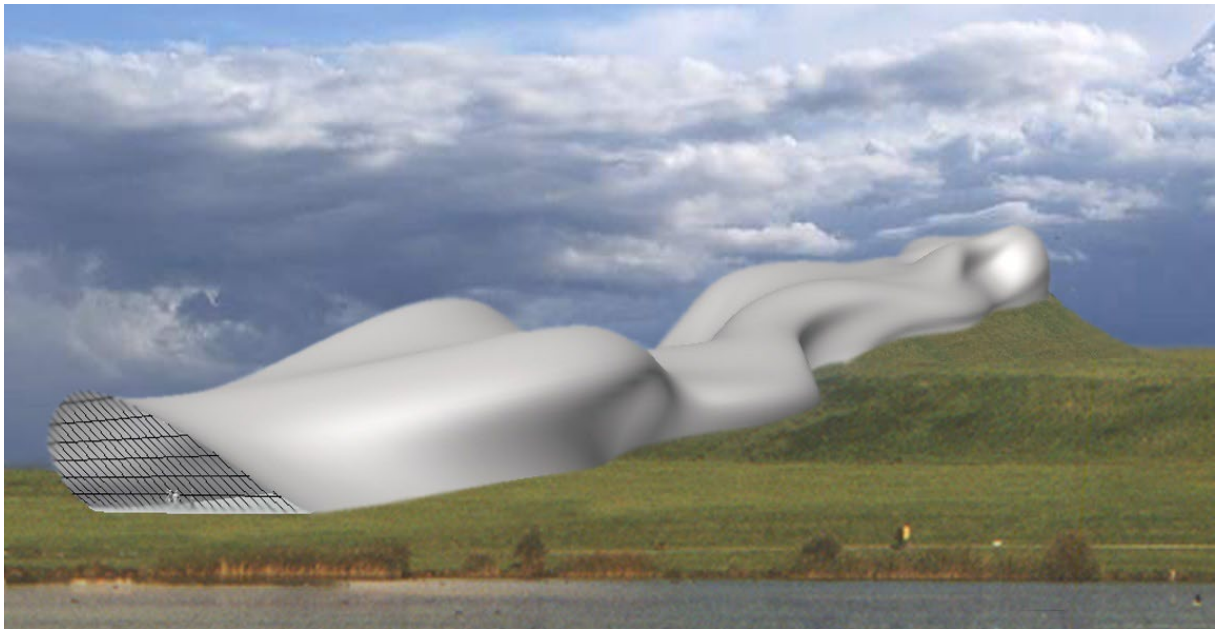

Figure 1 Ski Hall [image 6], design by Henno Hanselaar (2003)

One of the early blob-like shell structures the author encountered was the ski-hall designed by a graduate student of his at the time of the Blob revolution, Henno Hanselaar, fig. 1 [6]. Together with colleague Karel Vollers the author ran in the first decade of this century the Blob graduation studio of the master track Building Technology at TU Delft.

As a curvature analysis of the ski-hall shows the “shell-like” blob or “blob-like” shell is highly irregular curved, with areas where clastic and anti-clastic curvatures alternate. As can be observed of a Gaussian curvature analysis of the designs surface. The irregular curvature, illustrated in the Gaussian curvature analysis (fig. 2), makes it impossible to calculate the stresses with analytical equations.

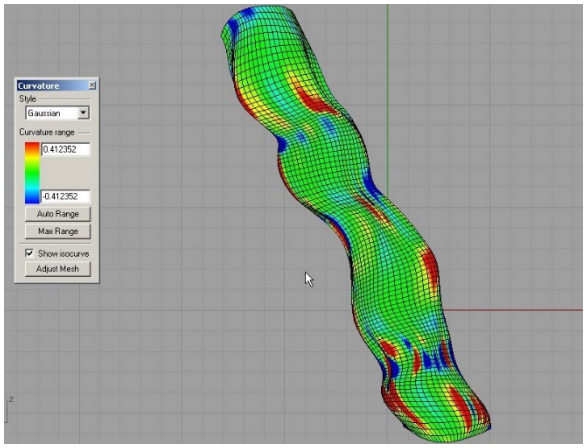

Figure 2 Gaussian curvature analysis Ski Hall [image 6]

Therefore, a FEM calculation was performed in order to determine the internal forces, stresses and deformations. For the FEM analysis shell elements where used. The outcome was unsurprising in that the location of the best and worst preforming areas on the surface were unpredictable. On the one hand this highlights the power of FEM calculation, but on the other hand the complexity of the geometry makes it difficult to intuitively predict the performance. It is therefore cumbersome to steer the design in a certain desired direction.

Due to the extreme curvature change in the lower part of the ski-hall the displacements in the valley are considerable. By altering the curvature problems would arise in another part of the surface. It is not easy to mentally predict which local curvatures would have a positive or negative effect. The only way to find this out was by trial and error and by altering the geometry and run another FEM calculation. Hanselaar “solved” the weak valley by adding a spider like truss on the of the surface, this proved to be effective, fig. 3.

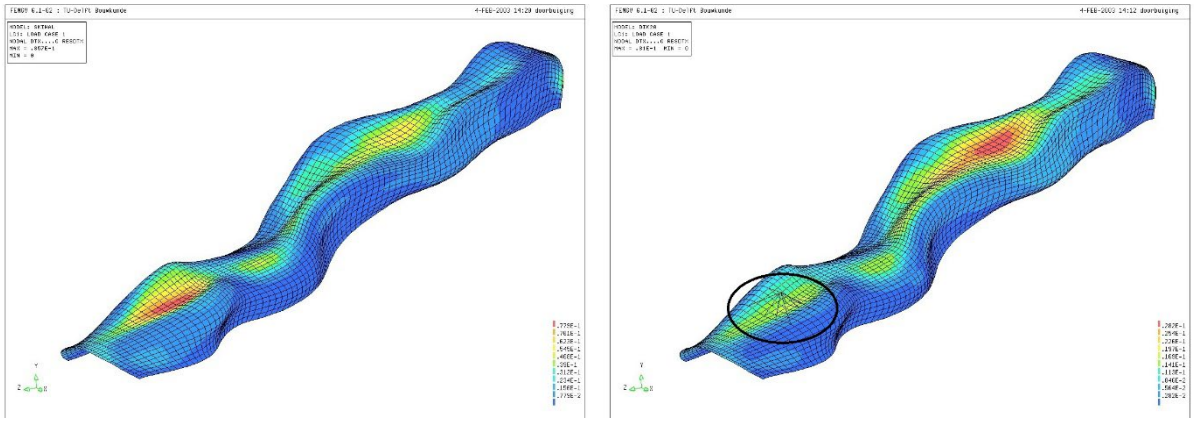

Figure 3 deflections by FEM calculation Ski Hall before and after added spider truss [image 6]

In particular the Ski-hall design of 2003 became a recurring theme in subsequent years and are present to this day. The problematic nature of the structural behaviour versus the fascinating shape proved to be a challenge for the author and the student research group. Methods would be developed to get a grip on the this “shell”, not always successfully but the understanding of “complex geometry surfaces”, the new name for blobs, slowly grew [7].

Nowadays there are optimization routines, like Bi-Directional Evolutionary Structural Optimization (BESO) [8], available to come to the best possible irregular curved surfaces with the minimum of stresses and deformations [9]. But these numerical routines are in fact automatized “black box” methods, they provide little analytical or qualitative insight. The goal of the Blob graduation studio was to develop methods and tools to expand the insight whilst designing shell structures.

One of the methods developed was the “Rain Flow” analysis [10] [11]. The hypothesis of this method was: “*Like a rain flow, loads will flow along curves with the steepest ascent on the shell to its supports*”. This is not correct, as will be shown later in this thesis, but gave the input for this research, fig. 4. The aim of this method is to use particles to simulate the flow of the loads that role over the surface, close to the gradient representing the vertical component of the axial forces of a thrust line of an arch or cable. This is similar, to the gradients of the moment hill, which represent the shear forces of a slab, loaded out-of-plane.

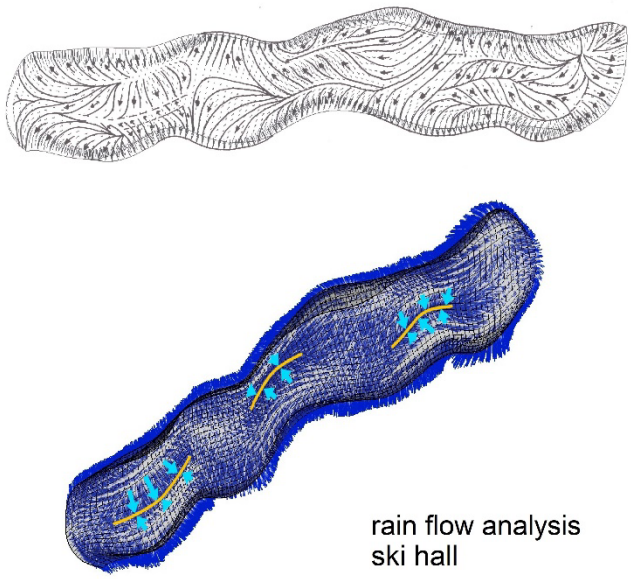

Figure 4 "Rain flow" analysis Ski hall [images 10, 52]

Although the "rain flow" analysis is not correct it does give some insight into how the edges of shells need to be shaped for an optimal performance. If the particles flow over an edge, usually curved downwards, then it can be expected that a large part of the load needs to be carried by shear forces and bending moments, fig. 5. The load cannot be sufficiently resolved in-plane to make equilibrium with internal membrane forces.

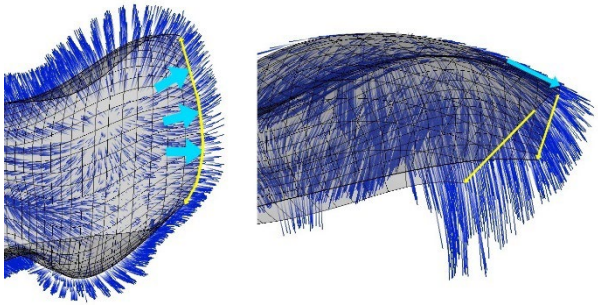

Figure 5 downward edge Ski Hall [image 52]

Edges which are turned upward divert the loads away from the edge, these edges are unloaded and will perform well, fig. 6. The shells of Felix Candela often have these types of edges.

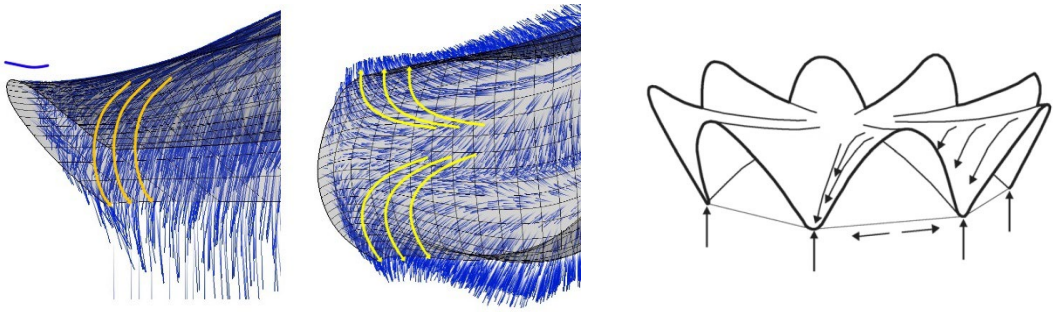

Figure 6 upward edge Skil Hall [52], Los Manantiales by Felix Candela [images 6]

Another student project is the shell designed and constructed by students from Delft and Montpellier during the Morpharchitecture workshop in Lyon. This shell also adheres to the “rain flow” principle. The result is a very light weight shell with all the right curves to ensure the most optimal load transfer, fig.7.

Figure 7 shell Morpharchitecture workshop Lyon

The research for this thesis starts from the fascination to uncover the fundamental principles that govern the structural behaviour of shell structures. The curiosity was fed by work done with students by making models, physical, analytic and numeric. The work presented in this thesis was done in silence, contemplating over what was discovered, after the fun part with the students was completed. And page after page trying to turn this insight into analytical formulas, so that the relations expressed in elegant mathematics can be the basis of new graphic models. To be used for the exploration and design of elegant shell structures.

In the past research was mostly concerned with finding analytical formulas to be able to calculate a design of shell structures. Many classic handbooks have been written in the first part of the last century, such by Timoshenko [12], Flügge [13], Novozhilov [14], Love [15], Haas [16], Csonka, Girkman [17], Billington [18], Ramaswamy, Heyman, Calladine [19], Born, Dischinger [20] and many other. Their content is predominately mathematical, and for most designers and modern-day engineers difficult to read. Other engineers, such as Candela [21], Torroja [22], Nervi [23] and Isler (fig. 8) [24] took a more practical approach. Between approximately 1930 and 1990 they built many elegantly shaped thin concrete shells [25]. By the 1960^{s} the main wave of shell building was all but over, different reasons have been suggested to explain this. Such as rising labour costs of building shells, to shells being out of fashion etc [26].

The other important development in the 1960[s] was the inception of computational methods such as the finite element method (FEM) which made it possible to calculate complex structures without the cumbersome mathematics [27]. Especially for irregular shapes, which are nearly impossible to describe with mathematical formulas, the FEM was a good alternative and made their analysis possible. This development all but stopped the further progress of analytical methods which slowly faded and was eventually mostly confined to libraries.

At the beginning of the 21st century due to newly developed parametric software graphic statics was rediscovered by researchers, architects and engineers. This made it possible to create interactive animation between the different form diagrams and their respective force polygons. O'Dwyer [28], Ochsendorf and Block [29] expanded graphic statics from arches and cable to 3D thrust networks. William Baker, Allan McRobie, Chris Williams any many others took the development on graphic statics further with the help of rediscovered work from James Clerk Maxwell on reciprocal diagrams. These principles were used to develop the polyhedral Airy stress function. Researchers such as Chris Calladine and Sergio Pellegrino worked on mechanics and rigidity theory. Wolfgang Beranek was the first to introduce the "shower analogy" as an addition to the moment hill for slabs, which analogies will be used and expanded for use to shells in this dissertation [30]. Their research is part of the basis of this thesis.

Figure 8 scanning of the Bellinzona shell model of Heinz Iser, Burgdorf, Switzerland by team from TU Delft, July 2011

1.2 Research objectives

The aim of this thesis is it to close the gap between the mathematical theory of shell structures and the recent developments in the field of graphic statics and reciprocal diagrams and to apply these to the understanding of shells structures. Because of the inability of computational methods such as FEM, to give analytical insight into the behaviour of shell structures this thesis will concentrate on trying to continue with the development of analytical methods, but without the complex mathematics. The aim is to develop semi-analytical methods which can form the basis of computational tools, like the example of parametric software being used for graphic statics, such as RhinoVAULT. In this thesis some results will be presented of the use of parametric tools used for creating M-hills, stress functions and thrust surfaces.

From the start of the research for this thesis it was always presumed by the author that the load path or distribution was the key for understanding the behaviour of shells. Aided by the curvatures of the shell the load path determines the internal membrane forces and whether out-of-plane ones are needed to ensure equilibrium, this in case due to incorrect curvatures the membrane forces would not be able to do this by themselves. The relational diagram below shows the initial hypothesis from which the research started. It will be shown that the load path is determined by the moment hill of the load on an equivalent flat slab. The curvatures are represented by the shape function of the shell. In addition, it will be explained that the force network is a simplified discretized version of the thrust surface. The initial relational diagram has slightly changed into the one which forms the basis of the research hypothesis as result of knowledge gained over the years, fig. 9 [31].

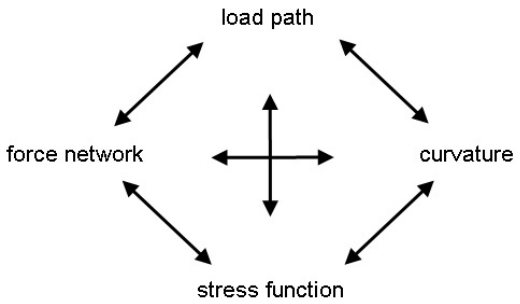

Figure 9 initial relational diagram

The differential equations which govern beams, slabs and shell structures consists of two parts. The first relates to equilibrium, the second part to cross sectional and material properties, these are the constitutive and kinematic relations, respectively.

$$beam\ equation:$$
$$\frac{d^4w}{dx^4} = \frac{q}{EI} \begin{cases} \frac{d^2M}{dx^2} = -q \\ \frac{d^2w}{dx^2} = -\frac{M}{EI} \end{cases}$$

The solutions for statically determined structures only concerns the first part of the differential equations. Like the cable / arch equation, which can be represented by graphic statics via a form diagram of the structure and its reciprocal force polygon. Once the load distribution has been determined what remains is a scaling issue, this occurs when moving the pole in the direction of the closing string. The rise of the arch *f* is reciprocal to the thrust *H*, and their product is constant. If the pole moves perpendicular to the closing string the load distribution alters, the vertical support reactions change as does the curvature of the arch, fig. 10.

$$cable\ equation:$$
$$q = -H\frac{d^2z}{dx^2} \qquad with: Hf = constant$$

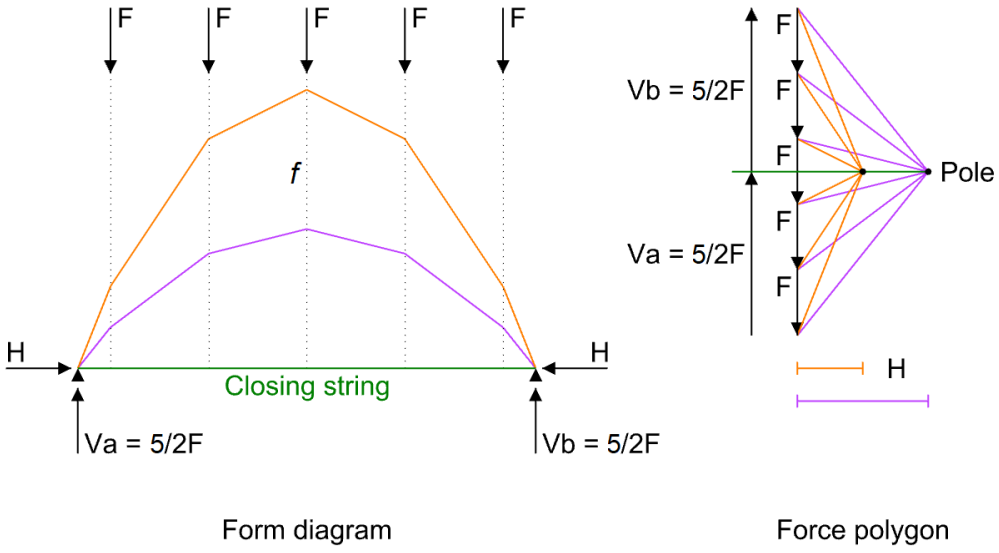

$$2D, when\ moving\ the\ pole\ along\ the\ closing\ string:$$
$$\rightarrow V_a = V_b = constant$$
$$the\ load\ path\ /\ distribution\ remains\ unchanged$$

Figure 10 reciprocity between form diagram and force polygon

For shell structures statically determined solutions are less straight forward, due to their 3D geometry. For a funicular cable or arch structure, the tension or thrust line is equal to their shape function. For arches it is important not to have bending, although for arches a discrepancy between the thrust line and shape is possible resulting in bending. Shells have an extra dimension in space compared to arches which can provide for membrane forces that cancel out-of-plane bending, like hoop forces in domes.

For shells the load distribution is coupled to the curvatures of its geometry and the type of the boundary condition. If the curvatures (*k*) are fixed but the overall height of the shell is changed it is a scaling problem, i.e. the load distribution remains unchanged. But when the ratio of the curvature is changed the load distribution changes accordingly, fig. 11.

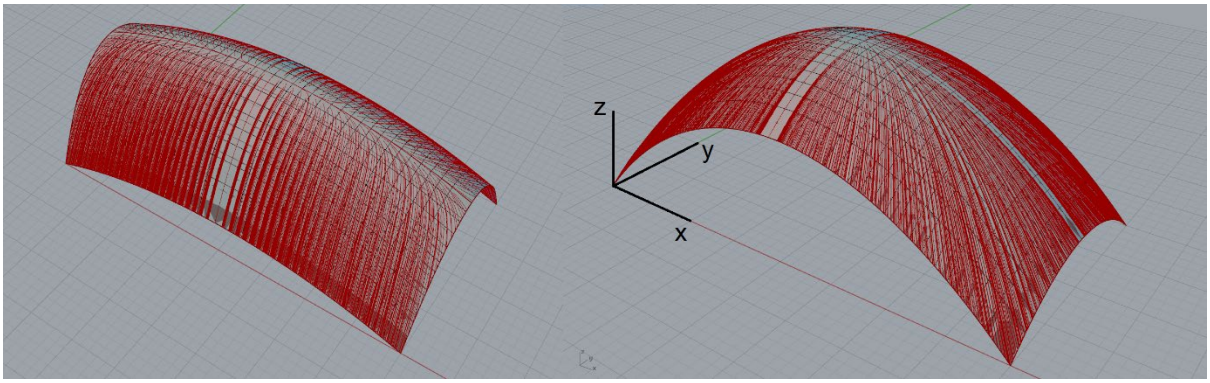

$$k_{xx} = \frac{\partial^2 z}{\partial x^2}$$
$$k_{yy} = \frac{\partial^2 z}{\partial y^2}$$
$$k_{xy} = \frac{\partial^2 z}{\partial x \partial y}$$

$3D, when\ changing\ the\ shells\ ratio\ of\ the\ curvatures$:
$the\ load\ path\ /\ distribution\ changes$

Figure 11 load path of shell in relation to its curvature [image 61]

Thrust networks are statically indeterminate; they are in fact three dimensional trusses, whose configuration is made-up of lines of actions along which its forces act and which as a whole is in equilibrium with the loads (imposed and/or self-weight). It is proposed that the indeterminacy is solved with the help of complementary energy, in which the constitutive relations are used. This is elaborated in the first part of the thesis, in the second part the load path theorem (moment-hill) of slabs loaded out-of-plane is extended to shells structures. The moment-hill is the 3-dimensional representation of weighted sum of the bending moment of the slab in two directions ($\bar{M}$).

$$\bar{M} = \frac{m_{xx} + m_{yy}}{1 + \nu}$$

The moment hill ($\bar{M}$) is the alternative solution, next to that of the deflections *w*, of the slab equation, which in most cases is a statically indeterminant problem. The slab equation can be split via the M-hill in two parts, one that allows the M-hill to be solved via the membrane analogy due to the similar structure of the differential equation, see section 8.3. The other part is a direct relation of the M-hill with the load *p*, this provides the route to the load path: the "shower analogy", fig. 12 [30].

$$slab\ equation:$$

$$p = D\left(\frac{\partial^4 w}{\partial x^4} + 2\frac{\partial^4 w}{\partial x^2 \partial y^2} + \frac{\partial^4 w}{\partial y^4}\right) \Rightarrow \begin{cases} \bar{M} = -D\left(\dfrac{\partial^2 w}{\partial x^2} + \dfrac{\partial^2 w}{\partial y^2}\right) \\ p = -\left(\dfrac{\partial^2 \bar{M}}{\partial x^2} + \dfrac{\partial^2 \bar{M}}{\partial y^2}\right) \end{cases}$$

Like a rain flow the loads will discharge along the curves with the steepest ascent (*n*-direction) on the surface of the moment-hill. This determines the load distribution and thus the load path.

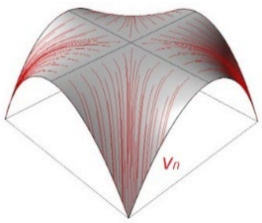

$$load\ path, load\ distribution:$$

$$v_n = \frac{\partial \bar{M}}{\partial n} = max$$

$$v_t = \frac{\partial \bar{M}}{\partial t} = 0$$

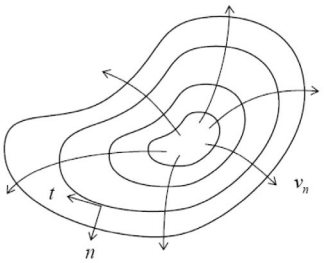

Figure 12 the moment-hill and the "shower analogy" [image right 30]

When considering the equilibrium of halve of a uniformly distributed load *q* a function can be derived, this is the line of equilibrium. It depends on a geometry of the loaded structure what this line represents, for a straight beam it is the moment diagram, for a structure without internal bending moments it is equivalent to their shape function. These curved structures are either arches or cables, depending if they are curved upwards or downwards. For both cases the slope of *M* represents the vertical load distribution *V*.

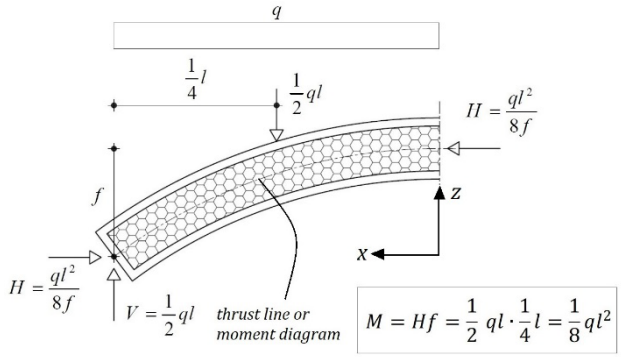

$$M = \frac{ql}{2}\cdot\frac{l}{4} - qx\cdot\frac{x}{2} = \frac{1}{8}q(l^2 - 4x^2)$$

$$\begin{cases} M = Hz \Rightarrow H = constant \\ M \equiv z \end{cases}$$

$$V = \frac{dM}{dx} = -qx$$

1.3 Research hypothesis

For cables and arches the relationship between the shape function, the thrust line, the moment diagram and the stress function is unambiguous. The relation is direct because the cable or arch has a horizontal component *H*, which is constant in any cross section. The thrust line is in fact equal to the shape function and equivalent to the moment diagram, the stress function plays a subordinate role because of the two-dimensional nature of the cable and arch and the fact that the horizontal thrust is constant, fig.13. For arches the difference between the thrust line and its shape function is equal to the resulting bending moment imposed onto the arch.

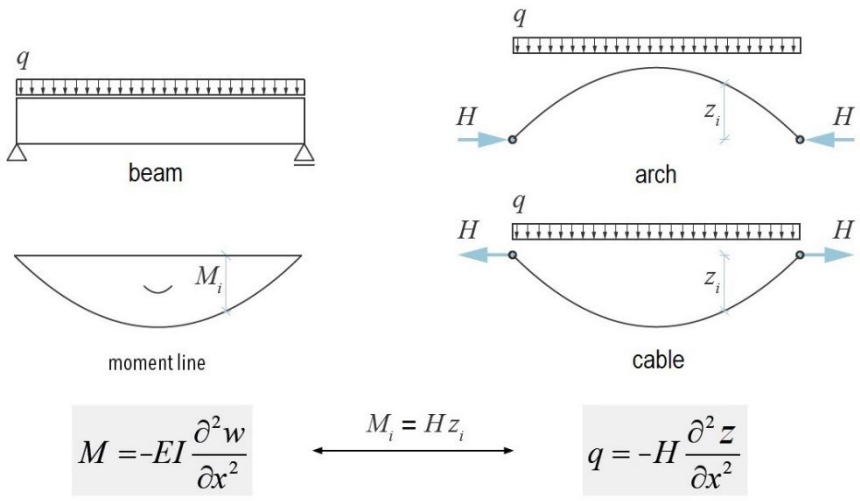

Figure 13 the beam - arch analogy [image 101]

For shell structures the relationship between the shape function (*z*), the stress function (ϕ), the thrust surface (*ζ*) and the moment hill ($\bar{M}$) is more complicated, fig. 14. This is because of the 3-dimensional nature of shell structures which, compared with 2-dimensional arches, leads to a larger number of possible solutions for a given situation. It can be stated that the relation between the four functions for arches is a reduction of a higher order hierarchy.

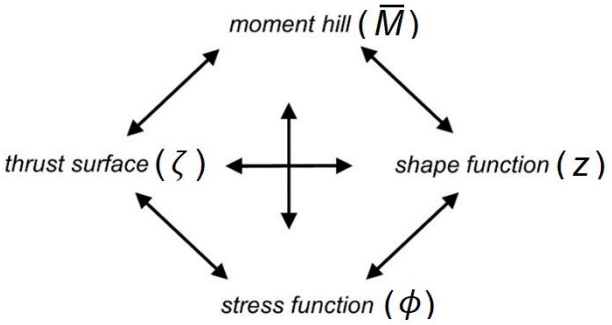

Figure 14 relational diagram hypothesis

The driver of the relation between geometry and mechanical behaviour of shell structures is the flow of forces. For arches this is unambiguous, but for shell structures there are for a given load case many lower bound solutions possible that ensure equilibrium. In contrast to arches, if the thrust surface deviates from the shape function this does not automatically result in out-of-plane bending. Also, the thrust surface is not necessarily equal to the moment hill. In fact, now there is a trade-off possible between the four functions, yet they are all linked to the flow of forces / load path.

arch:

$$\underbrace{\frac{dM}{dx}}_{\substack{moment\\ hill}} = V = \underbrace{H\ \frac{dz}{dx}}_{\substack{shape\ function\ /\\ stress\ function}}$$

$$q = -\frac{dV}{dx}$$

$$\begin{cases} arch\colon q = -H\dfrac{d^2z}{dx^2} \\ beam\colon q = -\dfrac{d^2M}{dx^2} \end{cases}$$

The beam – arch analogy

shell structure:

$$\underbrace{\frac{d\bar{M}}{dx}}_{\substack{moment\\ hill}} = v_x = \underbrace{\frac{\partial^2\phi}{\partial y^2}\frac{\partial z}{\partial x} - \frac{\partial^2\phi}{\partial x\partial y}\frac{\partial z}{\partial y}}_{\substack{stress\ function\ /\\ shape\ function}}$$

$$\underbrace{\frac{d\bar{M}}{dy}}_{\substack{moment\\ hill}} = v_y = \underbrace{\frac{\partial^2\phi}{\partial x^2}\frac{\partial z}{\partial y} - \frac{\partial^2\phi}{\partial x\partial y}\frac{\partial z}{\partial x}}_{\substack{stress\ function\ /\\ shape\ function}}$$

$$p = -\left(\frac{\partial v_x}{\partial x} + \frac{\partial v_y}{\partial y}\right)$$

$$\begin{cases} shell\colon p = -\left(\dfrac{\partial^2\phi}{\partial y^2}\dfrac{\partial^2 z}{\partial x^2} - 2\dfrac{\partial^2\phi}{\partial x\partial y}\dfrac{\partial^2 z}{\partial x\partial y} + \dfrac{\partial^2\phi}{\partial x^2}\dfrac{\partial^2 z}{\partial y^2}\right) \\ slab\colon p = -\left(\dfrac{\partial^2\bar{M}}{\partial x^2} + \dfrac{\partial^2\bar{M}}{\partial y^2}\right), with\ \bar{M} = m_{xx} + m_{yy} \end{cases}$$

The slab – shell analogy

In this thesis the relation between the four functions will be explored, and how they shape the flow of forces of the shell in conjunction with its geometry.

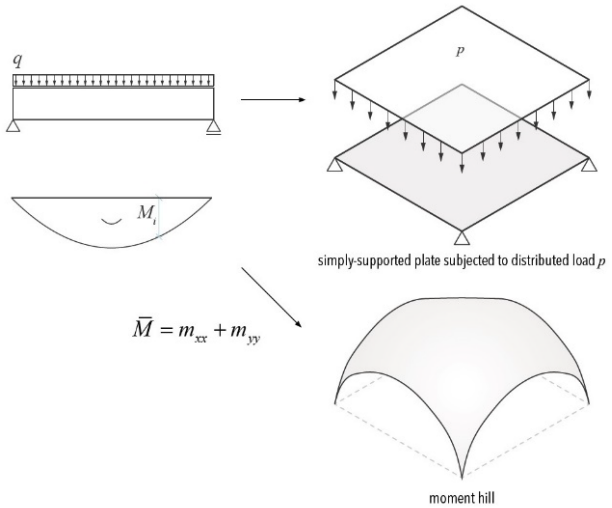

Figure 15 the beam - arch & slab - shell analogy [image 101]

The hypothesis states that the established relation between the moment diagram of a beam, the stress function and the thrust line / shape function of the equivalent arch, having a corresponding load and boundary conditions, also holds for the moment-hill of out-of-plane loaded slabs and their equivalent shell structure.

The hypothesis is valid for thin shells. In fact, the beam – arch analogy is the simplified version for one direction of the slab – shell analogy, fig. 15. The thrust surface is a reciprocal diagram, see chapter 8, of the stress function and it therefore not part of the slab – shell analogy equations.

The flow of forces or load transfer is central for both the slab- and the shell structure. For the slab the load transfer goes via the moment hill. For the membrane shells, thus without bending moments needing to assist in transferring the load, the load transfer goes via an interaction between the curvatures of the shape function and the stress function of the shell (fig. 16), see chapter 7 and 8.

$$\underbrace{p = -\left(\frac{\partial v_x}{\partial x} + \frac{\partial v_y}{\partial y}\right)}_{load\ transfer}$$

slab structure:

$$v_x = \frac{d\bar{M}}{dx}$$
$$v_y = \frac{d\bar{M}}{dy}$$

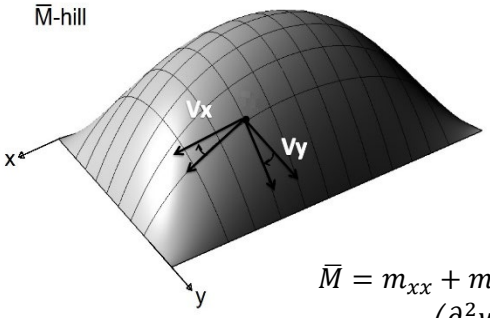

$$\bar{M} = m_{xx} + m_{yy}$$
$$\bar{M} = -D\left(\frac{\partial^2 w}{\partial x^2} + \frac{\partial^2 w}{\partial y^2}\right)$$

$$\Rightarrow p = -\left(\frac{\partial^2 \bar{M}}{\partial x^2} + \frac{\partial^2 \bar{M}}{\partial y^2}\right)$$

shell structure:

$$v_x = h_x \frac{\partial z}{\partial x} + h_{xy} \frac{\partial z}{\partial y} = \bar{n}_{xx} \frac{\partial z}{\partial x} + \bar{n}_{xy} \frac{\partial z}{\partial y}$$
$$v_y = h_y \frac{\partial z}{\partial y} + h_{yx} \frac{\partial z}{\partial x} = \bar{n}_{yy} \frac{\partial z}{\partial y} + \bar{n}_{xy} \frac{\partial z}{\partial x}$$

$$h_x = \bar{n}_{xx} = \frac{\partial^2 \phi}{\partial y^2}$$
$$h_y = \bar{n}_{yy} = \frac{\partial^2 \phi}{\partial x^2}$$
$$h_{xy} = \bar{n}_{xy} = -\frac{\partial^2 \phi}{\partial x \partial y}$$
$$with: h_{xy} = h_{yx}$$

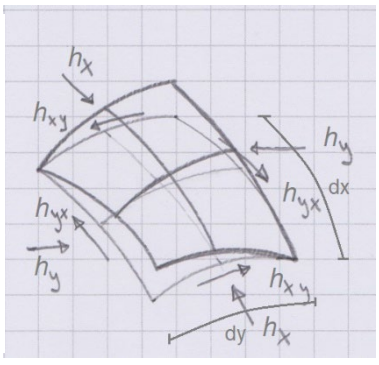

$$p = -\left(h_x \frac{\partial^2 z}{\partial x^2} + 2h_{xy} \frac{\partial^2 z}{\partial x \partial y} + h_y \frac{\partial^2 z}{\partial y^2}\right)$$
$$p = -\left(\bar{n}_{xx} \frac{\partial^2 z}{\partial x^2} + 2\bar{n}_{xy} \frac{\partial^2 z}{\partial x \partial y} + \bar{n}_{yy} \frac{\partial^2 z}{\partial y^2}\right)$$
$$\Rightarrow p = -\left(\frac{\partial^2 \phi}{\partial y^2} \frac{\partial^2 z}{\partial x^2} - 2\frac{\partial^2 \phi}{\partial x \partial y} \frac{\partial^2 z}{\partial x \partial y} + \frac{\partial^2 \phi}{\partial x^2} \frac{\partial^2 z}{\partial y^2}\right)$$

Figure 16 the beam - arch & slab - shell relations [image left 100]

The bending stiffness of the slab *D* is equivalent to the ratio of the curvatures and the stress function of the shell and their interdependency, and determines the load transfer.

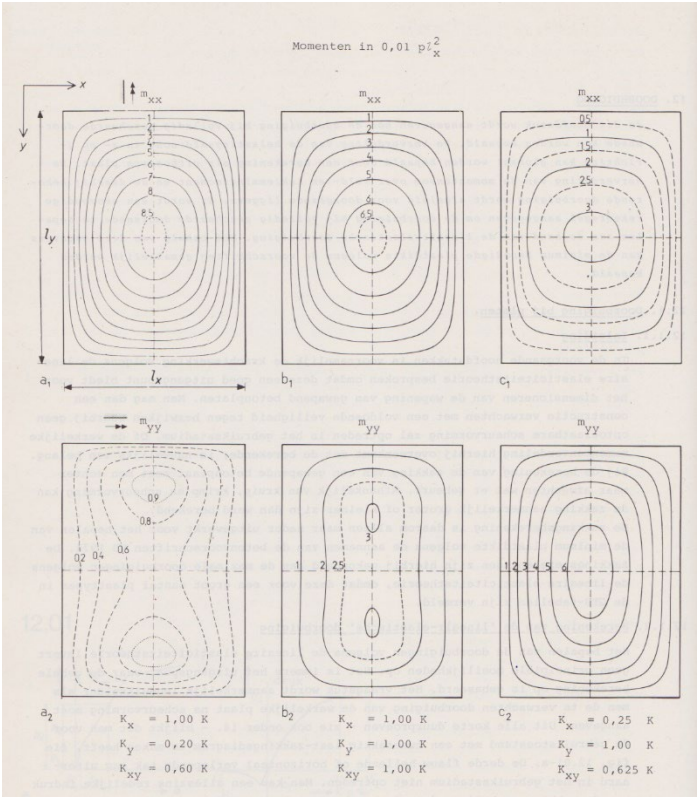

slab, simply supported along all edges:
uniformly distributed load p
$l_y = 1.4\ l_x$

slab b is isotropic: $D = K_x = K_y = K_{xy}$
slab a & c are orthotropic: $K_x \neq K_y \neq K_{xy}$

The moment hill, and thus the load distribution depends on the ratio between the bending stiffnesses K_x *and* K_y *and the torsional stiffness* $K_{xy} = \frac{K_x + K_y}{2}$.

For shell structures the load distribution depends on the ratio between the curvatures: k_{xx}, k_{yy} *and* k_{xy}.

image [30]

As an example of the slab – shell analogy are the skylights, fig. 18. These where form found by inflating a membrane [32], which is equivalent to the moment-hill of an out-of-plane loaded slab. The flow of forces (load path) of the skylight (shell) is represented by the trajectories of the maximum shear forces v_n of the slab, which are the curves of steepest ascent of the M-hill, fig. 17. For further elaboration see section 8.3.

Figure 18 "rain flow" of skylight, image provided with courtesy by John Chilton

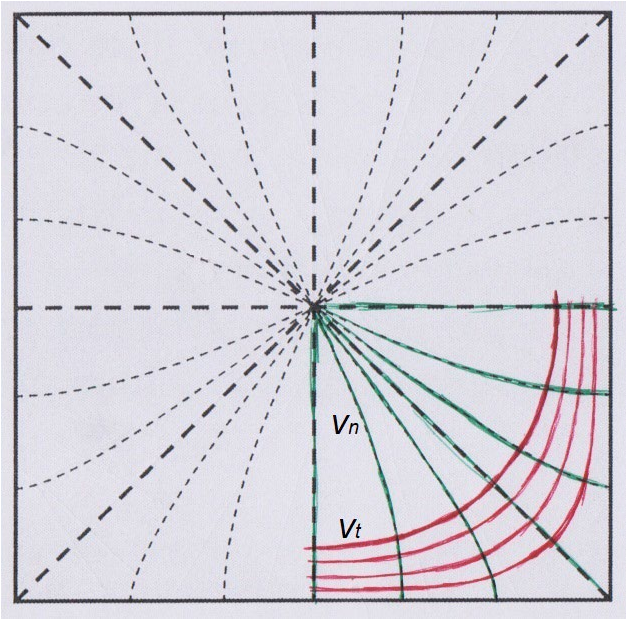

Figure 17 trajectories of the moment hill with a square base, hinge supported along all edges

1.4 Thesis structure

The thesis is structured in three parts, the first part (chapters 2 to 4) concerns trusses and cables and the second part (chapters 5 and 6) arches and the third part (chapters 7 and 8) focusses on shell structures.

The thesis starts with a round up and an additional perspective to the classic approach on the fundamentals of form diagrams and force polygons. Reciprocal characteristics of trusses and cables are discussed, to which the theory of rigidity will be applied. Indeterminacy in graphic statics will be introduced and applied to 3D graphic statics with the help of complementary and potential energy.

The second part starts with statically indeterminate arches and to solve these with complementary energy and concludes with a discussion of the stress function in relation to the other fundamental function of arches, the shape function and the thrust line.

The third part concentrates around the relationship of the four fundamental function for shell structures; the shape function, the thrust surface, the moment hill and the stress function. Different shapes of shells will be used to exemplify this relationship and different methods will be presented to solve these equations. The second part concludes with a method to also take into account out-of-plane bending if the geometry of the shell is such that it is not possible to carry all the loads via membrane forces.

Results throughout the thesis will be shown of analytical examples, or from computational tools based on theories and methods that have been developed in the context of this thesis. These tools have been developed with help of master graduate students from the faculties of Architecture and the Built Environment and Civil Engineering and Geosciences of the Delft University of Technology, whereby the theoretical input was provided by the author.

2 General properties of force polygons and form diagrams

2.1 Introduction

The practical use of graphic statics for visually representing the state of equilibrium of funicular structures, such as cables and arches, has been well established for centuries [33]. Funicular in the sense means structures whose centroidal axis coincides with the line of action of all its forces, known for arches as a “thrust line”. Another way of describing a funicular is the infinite collection of points forming a line in which in each point all its forces are in equilibrium.
The force polygon is the graphical representation of the equilibrium of the forces in the structure which topology is the form diagram, such as the shape of an arch or a cable. It is a well-established fact that the force polygon (FP) and form diagram (FD) are reciprocal diagrams, fig. 19 [34].

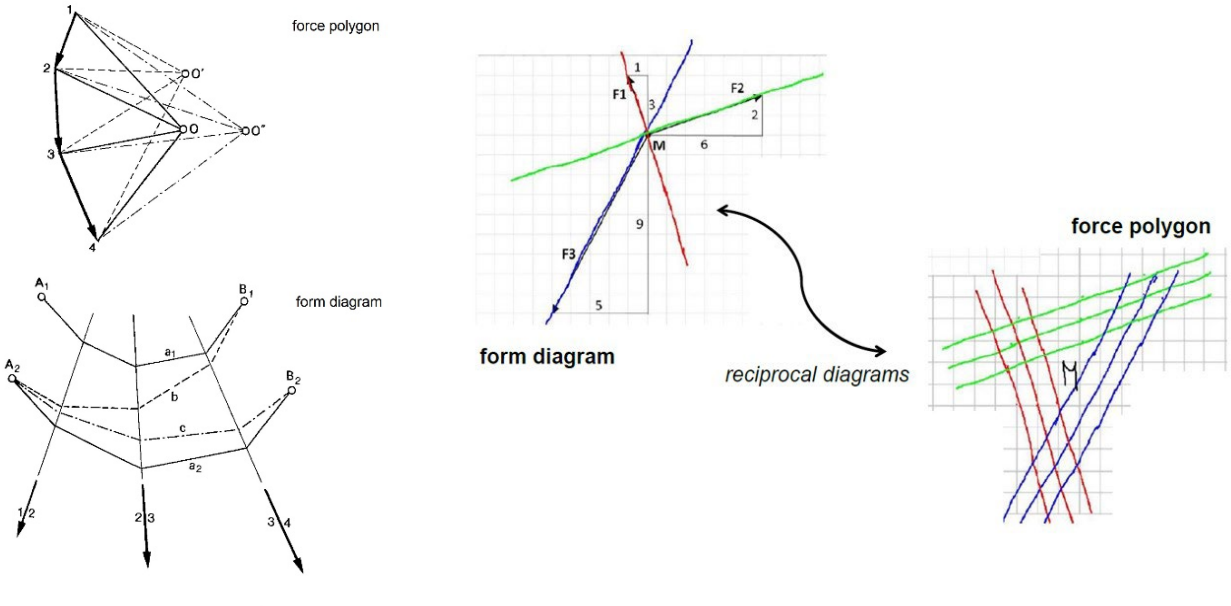

Figure 19 reciprocal relation between form diagram and force polygon

Some of the properties that describe this reciprocity, meaning mutually corresponding and dependent, will be further elaborated in this chapter with the help of formulas.

2.2 Sign convention

In this thesis we will not be using the classic Bow’s notation for graphic statics [35]. Bow’s notation uses the reciprocal properties between the form diagram and force polygon. It numbers the surfaces in the form diagram which refer

their reciprocal point in the force polygon. In this thesis the surfaces of the force polygons will be numbered which will refer to their reciprocal points in the form diagram, fig. 20 [36]. This makes it easier to directly observe the forces which act on a point in the structure. This is also a direct link between the pairs of lines of both diagrams, which represent the forces and their respective lines of action.

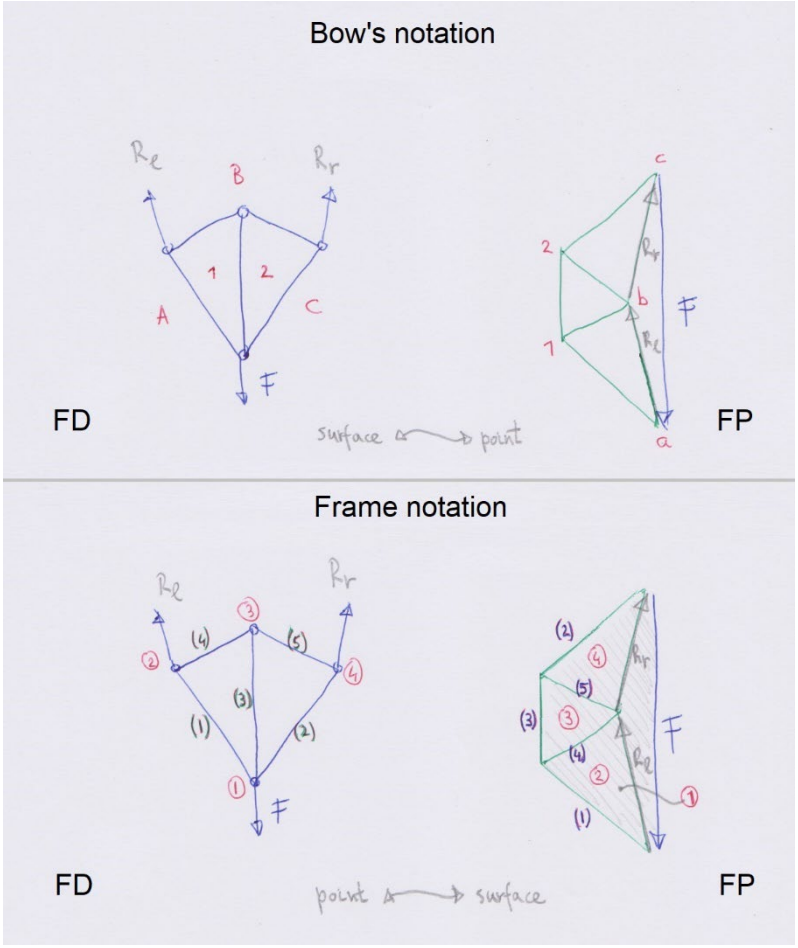

Bow's notation:
of a force in the force polygon between two points, begin and end point, its corresponding line of action in the form diagram lies between the two reciprocal surfaces of the two points

Frame notation:
there is a direct correspondence between the force in the force polygon and its line action in the form diagram

Figure 20 notation of form diagram and force polygon

2.3 General reciprocity of a basic form diagram and its force polygon

In this chapter general rules will be established concerning 2D force polygons and form diagrams, such as cables and arches. In chapters 3 and 4 these will be expanded to 3D for the purpose of constructing thrust surfaces for shell structures.

To exemplify the reciprocity a basic form diagram will be explored representing a cable with one point load ($\sum F$) and with level supports. Their form diagram and a force polygon have a reciprocal relation as can be observed through uniform triangles (eq. 1), fig. 21. Because the structure is statically determined any change in the rise f will not change the vertical support reactions V_i .

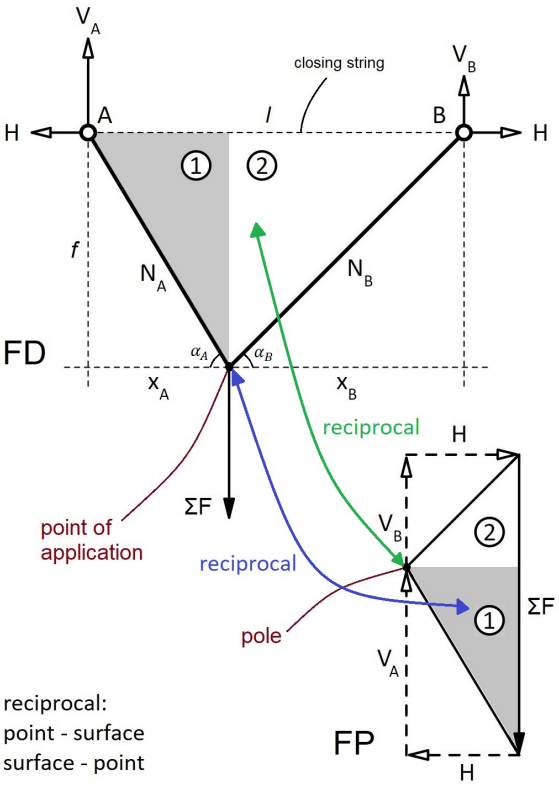

$$f, H \text{ are variables; } x_i, V_i \text{ are constants}$$

$$\tan\alpha_A = \frac{f}{x_A} = \frac{V_A}{H} \rightarrow Hf = V_A\, x_A = constant$$

$$\tan\alpha_B = \frac{f}{x_B} = \frac{V_B}{H} \rightarrow Hf = V_B\, x_B = constant$$

$$\rightarrow \quad \frac{x_A}{x_B} = \frac{V_B}{V_A} \qquad (1)$$

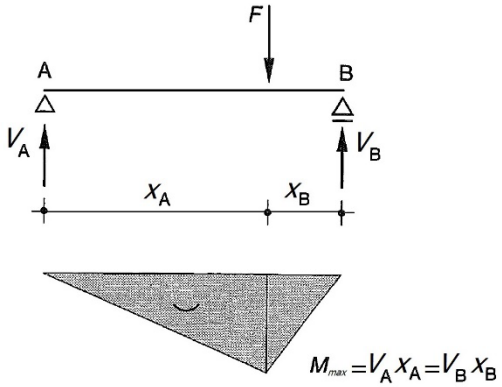

Figure 21 basic form diagram

Compared to an equivalent beam with the same span and load the shape of the form diagram corresponds with the shape of its bending moment diagram. The product of the horizontal force *H* and the rise *f* of the cable is constant and remains such for any change of *f* and is equal to the maximum moment M_{max} of the equivalent beam (eq. 2).

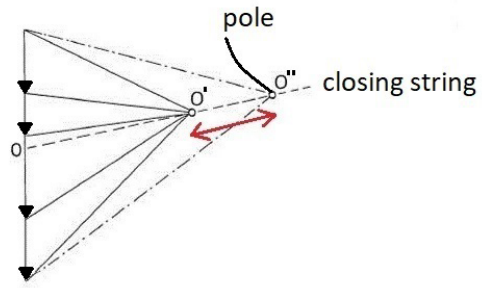

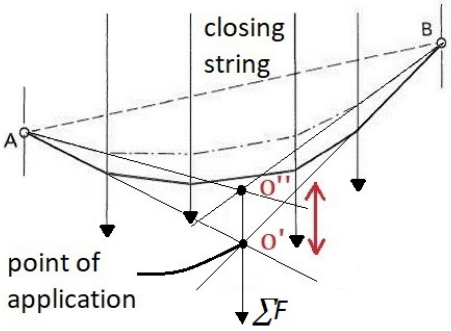

$$M_{max} = V_A\, x_A = V_B\, x_B$$

$$V_A + V_B = \Sigma F \rightarrow \frac{Hf}{x_A} + \frac{Hf}{x_A} = \Sigma F$$

$$with: x_A + x_B = l$$

$$\rightarrow Hf = \Sigma F \frac{(x_A x_B)}{l} = M_{max} \qquad (2a)$$

$$x_A + x_B = l \rightarrow \frac{Hf}{V_A} + \frac{Hf}{V_B} = l$$

$$\rightarrow Hf = l \frac{(V_A V_B)}{\Sigma F} = M_{max} \qquad (2b)$$

Any change in position of the pole of the force polygon has a reciprocal effect on the point of application of the total force $\sum F$ in the form diagram and vice versa. So if either the rise *f* or the horizontal force *H* changes and because their product is constant these two points, the pole and point of application, move in opposite directions.

The force density of a bar is the ratio of its axial force over the length of the bar (eq. 3). The total force density *Q*, the summation of all the individual force densities of each bar, of this system can also be expressed in either a function of the horizontal force *H* or the total load $\sum F$ (eq. 5). The geometric factor s_f (eq. 6) for the change of *f* in the form diagram represents the reciprocal effect on the force polygon. The total force density will also change accordingly to the same factor (eq. 7).

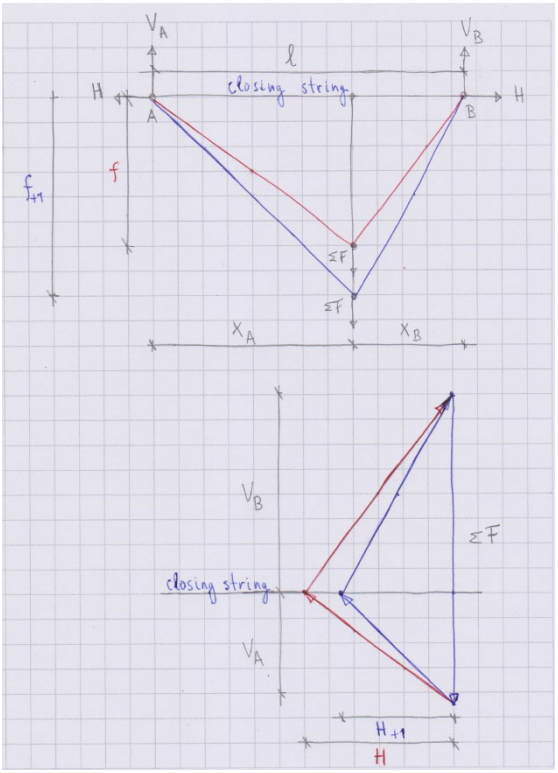

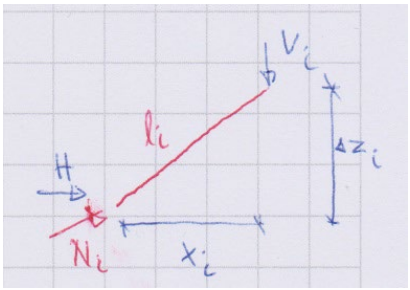

$$Q = \frac{N_A}{l_A} + \frac{N_B}{l_B} \qquad (3)$$

$$with: \frac{N_i}{H} = \frac{l_i}{x_i} \; ; \frac{N_i}{V_i} = \frac{l_i}{f} \qquad (4)$$

$$\rightarrow Q = \frac{H}{x_A} + \frac{H}{x_B} = \frac{\Sigma F}{f} \qquad (5)$$

$$s_f = \frac{f_{+1}}{f} \; ; \frac{1}{s_f} = \frac{H_{+1}}{H} \qquad (6)$$

$$Q_{+1} = \frac{1}{s_f} Q \qquad (7)$$

The principles of these relations hold for all cable and arch structures with different loads, apart from the last part of (eq. 5), which for truncated form diagrams will be altered, this will be discussed further in section 2.7.

There are a few basic ways to reconfigure a form diagram and its reciprocal force polygon. When one of them is reconfigured the other will automatically follow and the basic relations will remain applicable to both. The properties of reconfiguration through scaling the FP / FD or changing the load distribution, by horizontally moving the point of application, will be briefly discussed.

a. *scaling FP / FD*

It is possible to scale either the form diagram or the force polygon by a scaling factor. The properties below will alter according to this scaling factors, s_{FP} and s_{FD}.

$$scaling\ force\ polygon:$$
$$s_{FP} = \frac{H_{+1}}{H} = \frac{\Sigma F_{+1}}{\Sigma F}$$
$$Q_{i+1} = s_{FD}\ Q_i$$

$$scaling\ form\ diagram:$$
$$s_{FD} = \frac{f_{+1}}{f} = \frac{l_{+1}}{l}$$
$$Q_{+1} = \frac{1}{s_{FD}}\ Q$$

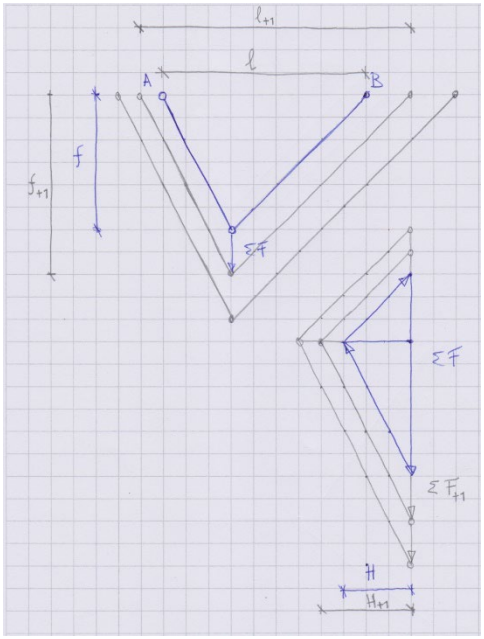

By scaling the force polygon but leaving the form diagram intact the total force density increases. And by scaling the form diagram and leaving the force polygon intact the total force density decreases.

b. *moving horizontally the point of application of the total load ∑F*

The horizontal force *H* stays constant but the position of the total load shifts horizontally and thus the total force density changes accordingly as does the load distribution. The vertical support reactions in A and B change in the same ratio s_{mo} as the horizontal distance of *∑F*.

Note that if the pole of the force polygon moves whilst having a constant *H* and constant total load the rise *f* of the form diagram changes. This is due to the uniformity of their respective triangles.

$$s_{mo} = \frac{x_{A,i}x_{B,i}}{x_{A,i+1}x_{B,i+1}} = \frac{V_{A,i}V_{B,i}}{V_{A,i+1}V_{B,i+1}}$$
$$Q_{+1} = s_{mo}\ Q_i$$

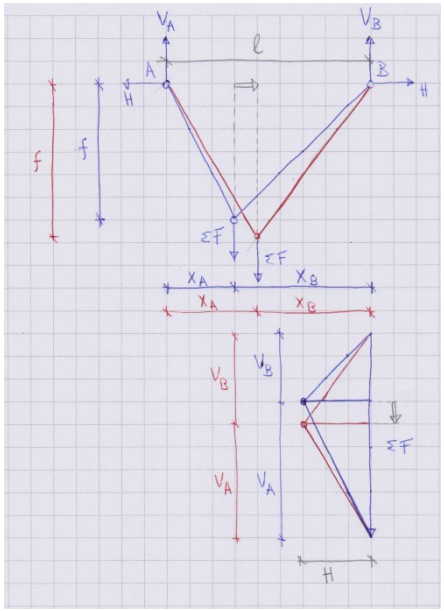

2.4 General reciprocity of a basic configuration with non-level supports

In a more general case consider a cable with non-level supports loaded by a point load. Like the case with level supports the uniform triangles, which can be observed in the form diagram and the force polygon, have a reciprocal relation (eq. 8). Also with non-level supports, by moving the point of application of the total load in the form diagram, the pole of the force polygon moves in a reciprocal manner along the closing string.
The force polygon can be split along a line parallel to the closing string, both parts belong to one of the supports. Hereby the vertical support reactions S_A and S_B are determined as well as the support reaction along the closing string S_0. This line in the force polygon cuts the vector of the total force $\sum F$ in point *0*.

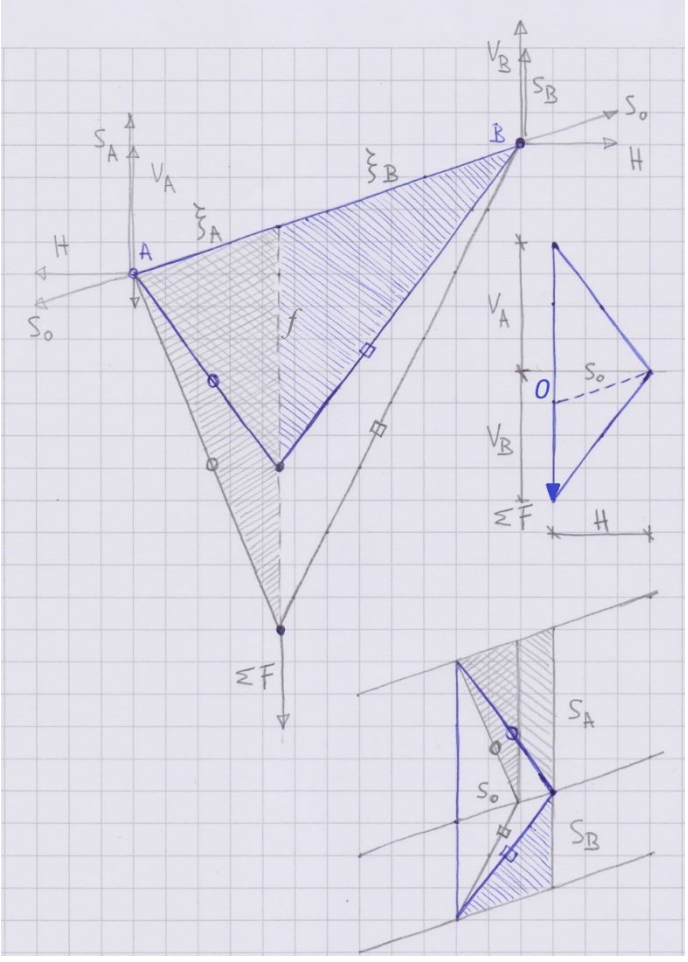

$$f, S_0 \text{ are variables; } \xi_i, S_i \text{ are constants}$$

$$\frac{f}{\xi_A} = \frac{S_A}{S_0} \Rightarrow S_0 f = S_A \xi_A \text{ are constant}$$

$$\frac{f}{\xi_B} = \frac{S_B}{S_0} \Rightarrow S_0 f = S_B \xi_B \text{ are constant}$$

$$\Rightarrow \frac{\xi_A}{\xi_B} = \frac{S_B}{S_A} \quad (8)$$

$$Hf = M_{max} = constant \quad (9)$$

For an equivalent beam with the same span and load the shape of the form diagram corresponds with its bending moment diagram, and has the same maximum moment (eq. 9).

The ratio of the position of the line of action l_F of the total force $\sum F$ is equal to the ratio of the vertical support reactions, the line of action l_F and point *0* are reciprocal.
When the pole of the force polygon is moved the shape of the form diagram changes. By moving point *0* in the force polygon the line of action l_F and thus the point of application moves in the form diagram, as seen in section 2.3.

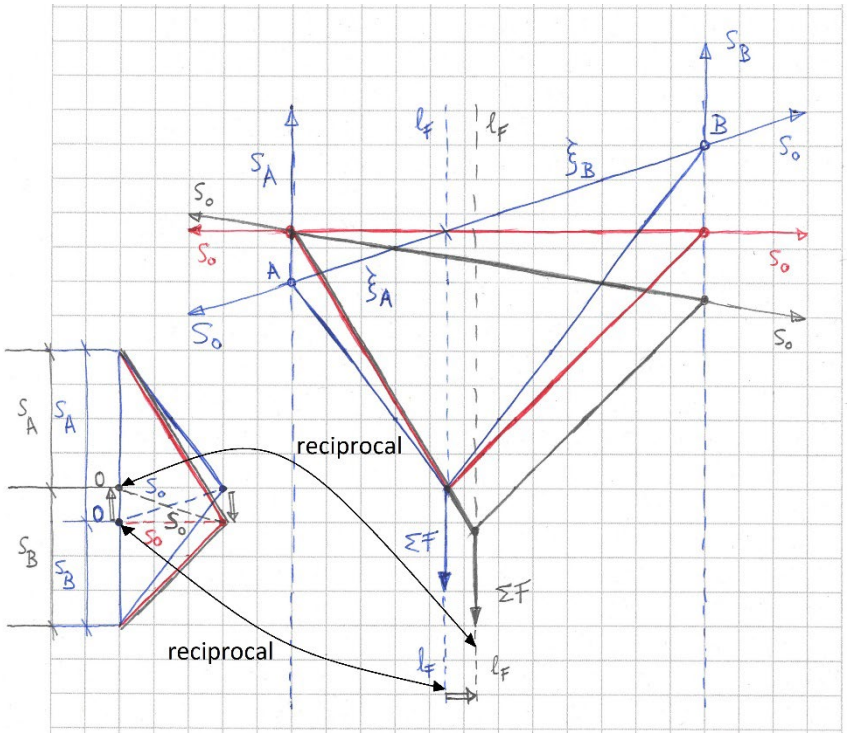

$$ratio: \frac{\xi_A}{\xi_B} = \frac{S_B}{S_A}$$

2.5 Truncated form diagrams, subdivision of the total load

Cables and arches usually have multiple loads, for this a truncated basic configuration can be used. The truncation of the form diagram is the result of splitting the total load in several point loads. The total load $\sum F$ and its corresponding point of application is the vertex of the envelope of the form diagram where the lines of action of the total load and of the reactions forces R_i , which are also the tangents of the form diagram at the supports, meet. This point is in the case of a uniformly distributed load comparable to a control point of a quadratic Bezier curve.

The force polygon retains its overall shape when the total load is split, yet the point of application stays the same, but will be subdivided into more triangles representing the different point loads. The rays of the force polygons are the tangents of the parabola in the case of a uniformly distributed load and in the case of discreet point loads it coincides with the straight members which form the form diagram.
When the form diagram is scaled, by increasing or decreasing *f* and thus moving the control point, the other location coordinate for each node z_i which define the form diagram in respect to the closing string will be scaled according to the same factor (eq. 10).

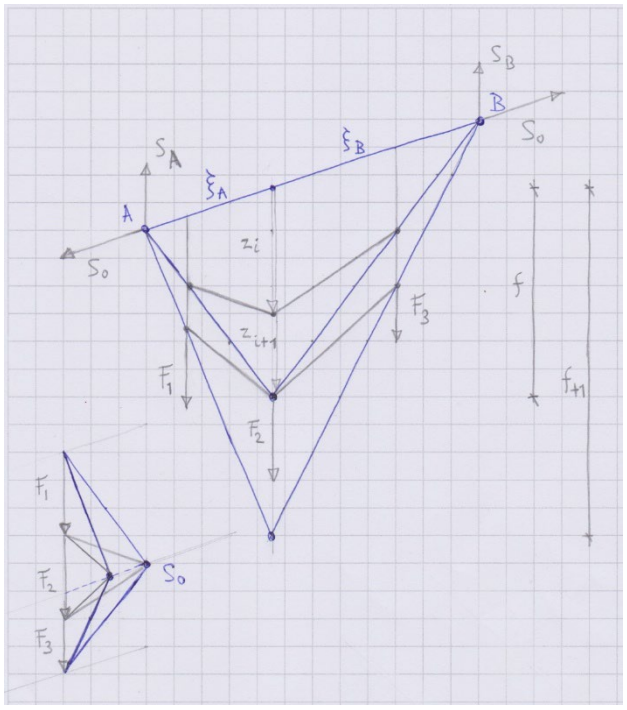

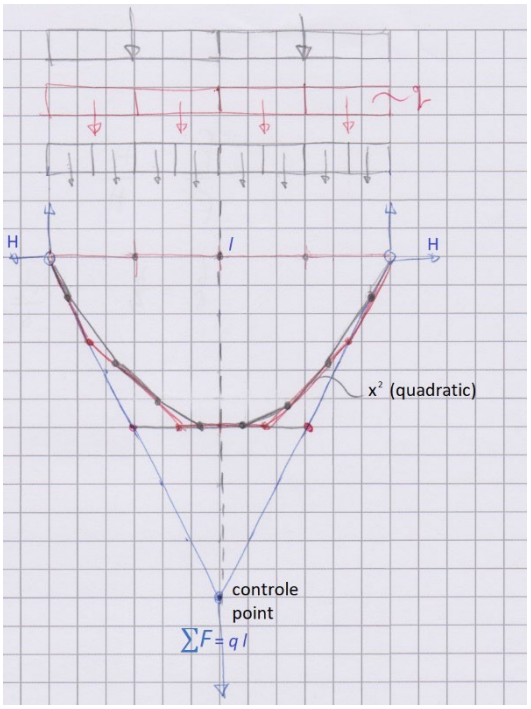

$$S_f = \frac{f_{+1}}{f} = \frac{z_{i+1}}{z_i} \rightarrow z_{i+1} = S_f \cdot z_i \qquad (10)$$

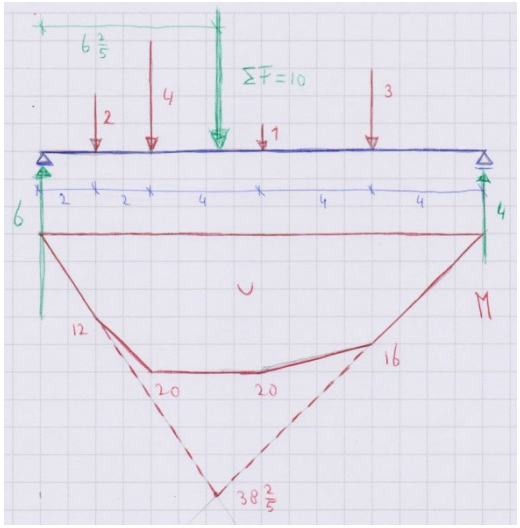

$$V_A + V_B = \Sigma F = 10$$

$$Hf = \Sigma F \frac{(x_A x_B)}{l} = 10 \frac{6\frac{2}{5} \cdot 9\frac{3}{5}}{16} = 38\frac{2}{5} = M_{max}$$

2.6 Relation form diagram and force polygon

The classic understanding of the geometric reciprocity between a (truncated) form diagram and it's force polygons is between points and triangles.

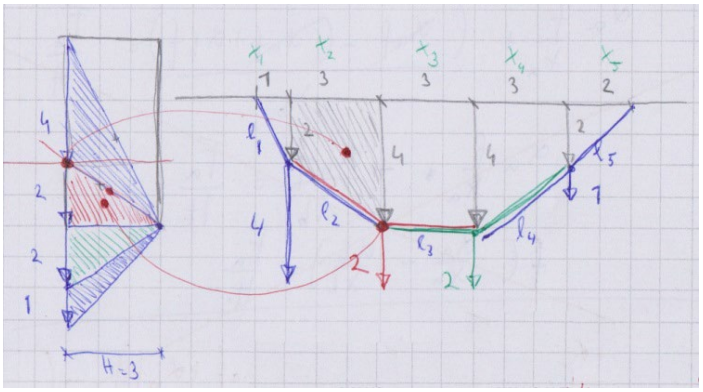

A reciprocal relation between the form diagram and the force polygon has already been introduced in sections 2.3 and 2.4 are the uniform triangles which are observed in both and are reciprocal to each other (eq. 11). These can also be found in a truncated form diagram. When the basic form diagrams from 2.3 and 2.4 are truncated, thus with more than one load, more triangles will appear in the form diagram. This has as a consequence that both of the two uniform triangles which constitute the basic form diagram will be scaled back to accommodate additional triangles as a result more loads (eq. 12). The slopes of reciprocal triangles in the form diagram and the force polygons are equal (eq. 13). The rise of each triangle in the form diagram Δz_i is equal to the incremental equivalent moment over the base of the triangle if it was part of a beam divided by the horizontal thrust *H*. This is essentially the same relationship as between the rise *f* of the envelope of the truncated form diagram and the equivalent maximum moment (eq. 2 & 14). And it also represents the discretization of expression for the load transfer of a cable with a uniformly distributed load (eq. 15).

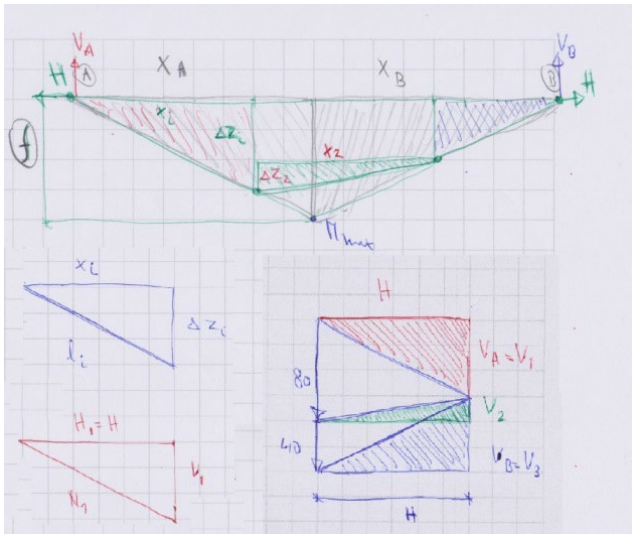

$$\frac{H}{V_a} = \frac{x_a}{f} \tag{11}$$

$$\frac{x_a}{f} = \frac{x_i}{\triangle z_i} \tag{12}$$

$$\frac{V_i}{H} = \frac{\triangle z_i}{x_i} \Rightarrow \triangle z_i = \frac{V_i}{H} x_i = \frac{\triangle M_i}{H} \tag{13}$$

$$f = \frac{M_{max}}{H} \tag{14}$$

$$V_i = H \frac{\triangle z_i}{x_i} \equiv V = H \frac{dz}{dx} \tag{15}$$

Each element of the form diagram has a triangle that corresponds to its reciprocal in the force polygon. If the triangles of the form diagram are assembled in a similar configuration of that of a force polygon this will most likely not result in the polygon being in equilibrium. To achieve this each triangle needs to be scaled individually. This scaling is the force density (eq. 16), which connects each triangle in the form diagram with its reciprocal in the force polygon. Thus the correct force polygon is obtained.

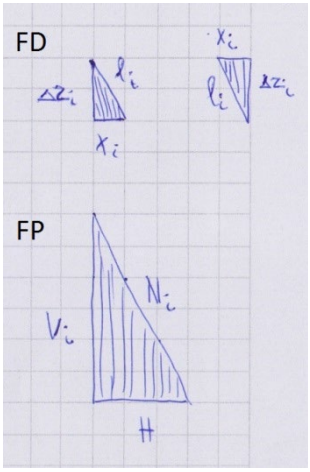

$$q_i = \frac{N_i}{l_i} = \frac{V_i}{\triangle z_i} = \frac{H}{x_i} \quad (16)$$

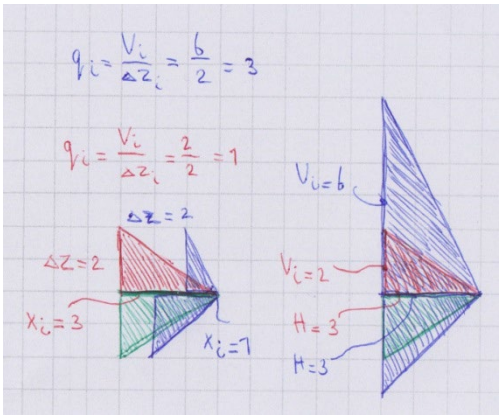

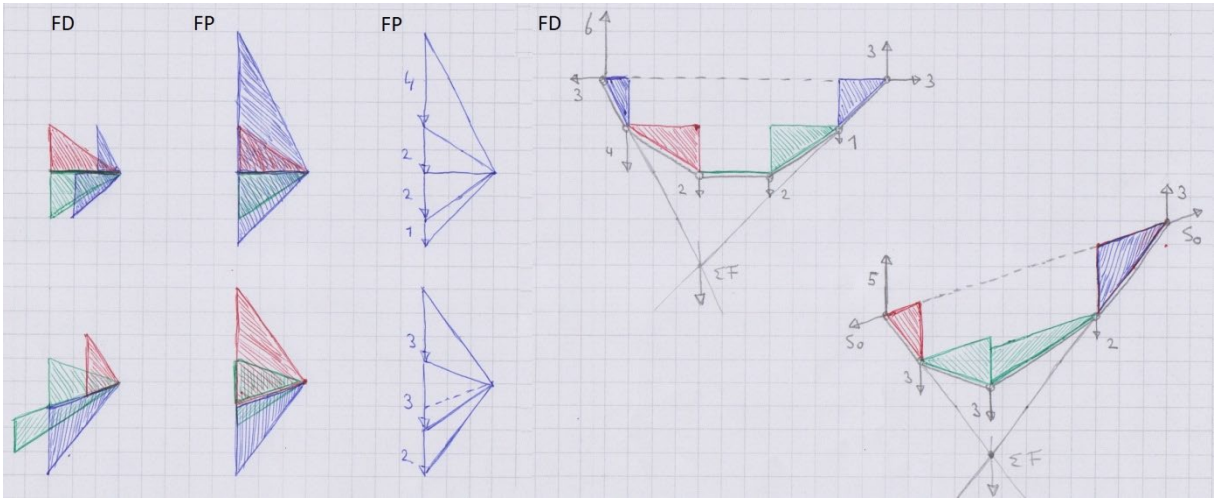

An example where all the individual force densities are equal is a cable with a discretized uniformly distributed load, which result in a form diagram with the shape of a parabola.

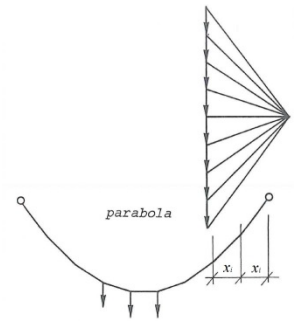

$$q_i = \frac{H}{x_i} : Q = \sum \frac{H}{x_i}$$

$x_i = constant, thus\ uniform\ distributed\ load\ is\ discretized: q_i = 1$

$x_i \Rightarrow \infty, thus\ uniform\ distributed\ load\ is\ continuous: Q \Rightarrow \infty$

If the discretisation of the parabolic cable goes to infinity the total force density *Q* also goes to infinity.

Although each assemblage of triangles can be scaled to produce a closed force polygon, in which all forces are in equilibrium, they do not automatically result in a closed form diagram, in which all the loads are in equilibrium. If total summation of the rises of triangles is not zero, then the closing string will be discontinuous and thus there will be no equilibrium (eq. 17).

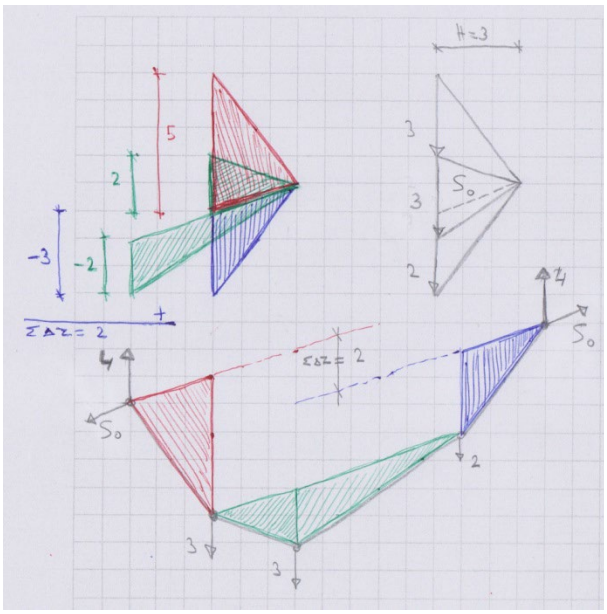

$$closed\ form\ diagram: \sum \triangle z_i = 0 \qquad (17)$$

2.7 Relation force density and equilibrium

If the difference of the two location coordinates at each end of a member Δz_i , the rise of a triangle, is taken as a ratio of *f* we get the shape coefficients of the form diagram α_i (eq. 18). These remain constant when the form diagram is scaled.

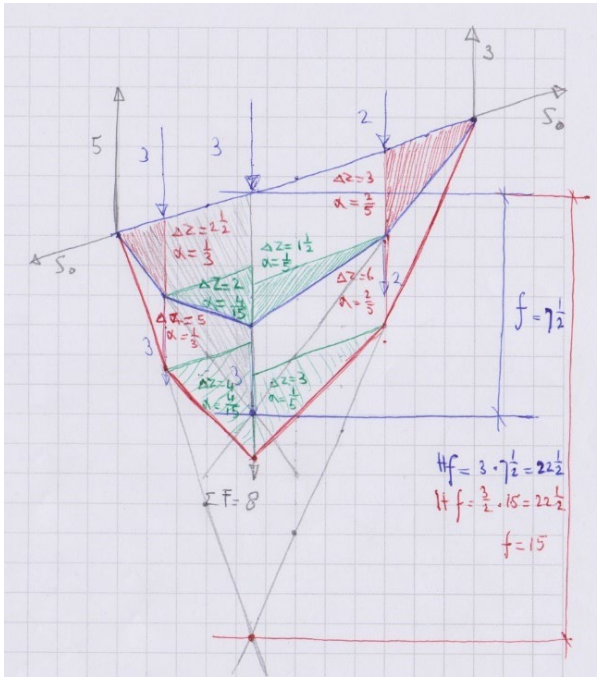

$$\alpha_i = \frac{\triangle z_i}{f} \qquad (18)$$

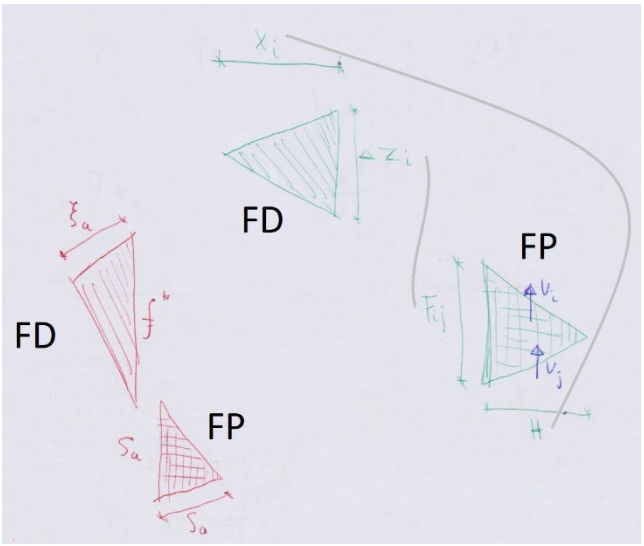

$$\frac{\triangle z_i}{x_i} = \frac{F_{ij}}{H} \Rightarrow H\frac{\triangle z_i}{x_i} = F_{ij} \quad (19)$$

$$with: q_i = z\frac{H}{x_i} = \frac{N_i}{l_i}$$

$$\Rightarrow \triangle z_i \frac{N_i}{l_i} = F_{ij} \quad (20)$$

$$\frac{f^*}{\xi_a} = \frac{S_a}{S_0} \quad (19)$$

By comparing a set of reciprocal triangles from the form diagram and the force polygon it can be observed that the ratio of two sides are equal (eq. 19). By reworking this ratio with the triangle scaling factor, the force density, the result is the kernel of the well-known expression of equilibrium used in the force-density method to find equilibrium solutions for cable nets (eq. 20).

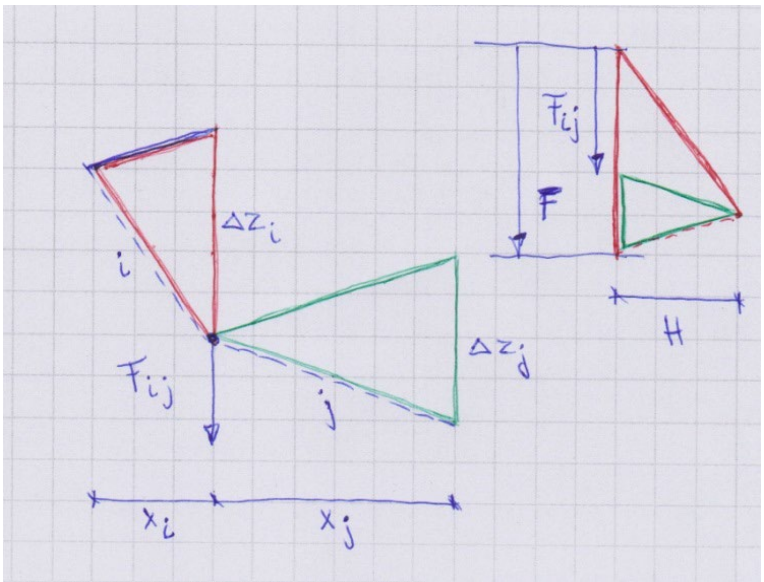

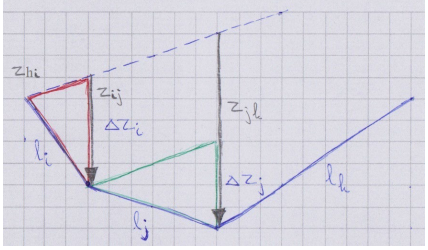

$$\frac{\triangle z_i}{x_i} = \frac{F}{H}$$

$$\frac{\triangle z_j}{x_j} = \frac{F - F_{ij}}{H}$$

$$\frac{\triangle z_i}{x_i} - \frac{\triangle z_j}{x_j} = \frac{F_{ij}}{H} \quad (21)$$

$$with: q_i = \frac{H}{x_i} = \frac{N_i}{l_i}, q_j = \frac{H}{x_j} = \frac{N_j}{l_j}$$

$$\triangle z_i \frac{N_i}{l_i} - \triangle z_j \frac{N_j}{l_j} = F_{ij} \Rightarrow \quad (22)$$

$$\triangle z_i = z_{ij} - z_{hi},\ \triangle z_j = z_{jk} - z_{ij}$$

$$(z_{ij} - z_{hi})\frac{N_i}{l_i} + (z_{ij} - z_{jk})\frac{N_j}{l_j} = F_{ij}$$

Expanding the procedure to a point of a cable with point loads (eq. 21), the derivation results in the classic force-density relations (eq. 22). Thus graphic statics has been used to established the relation between the form diagram, the force polygon and the force density (eq. 23), and is a function of horizontal

thrust *H* and the rise *f*. The negative sign in equation 22 becomes positive at the node where the slope of the form diagram changes from positive to negative. Which also acts like a drainage divide of the load transfer.

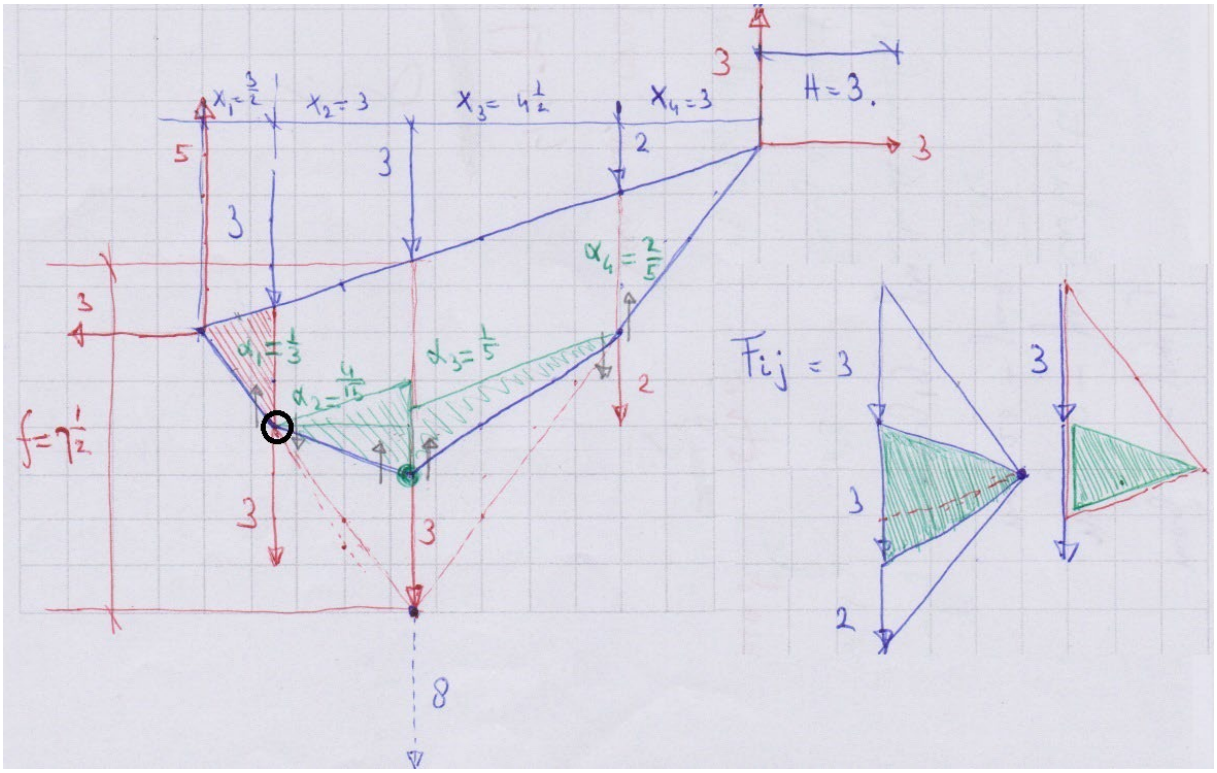

$$\frac{\triangle z_i}{x_i} - \frac{\triangle z_j}{x_j} = \frac{F_{ij}}{H}$$

$$with: \alpha_i = \frac{\triangle z_i}{f}, \alpha_j = \frac{\triangle z_j}{f}$$

$$\Rightarrow \underbrace{f\left(\frac{\alpha_i}{x_i} - \frac{\alpha_j}{x_j}\right)}_{form\ diagram} = \underbrace{\frac{F_{ij}}{H}}_{force\ polygon} \qquad (23)$$

For each node of the form diagram, which has a point load, an equilibrium equation (eq. 24) can be set-up using the derived expression (eq. 22). When all these equations are put together there can be observed from the result that all the relations relating to the nodes between the two outmost free nodes (*a* and *d*), which are directly connected to the supports (*l* and *r*), fall away (eq. 25). The ratio of the location coordinate z_a of node *a* and the length of member 1, which connects node *a* to support *l*, is equal to the ratio *f* and length of the envelop of the form diagram between the support *l* and the point of application of the total load, the uniform triangle (eq. 26).

The relation between the force density and the equilibrium of the system has been established (eq. 27). This expression is equal to that for the basic system with only one point load discussed in section 2.2, which actually forms the envelope of the form diagram with multiple point loads or a uniformly distributed load.

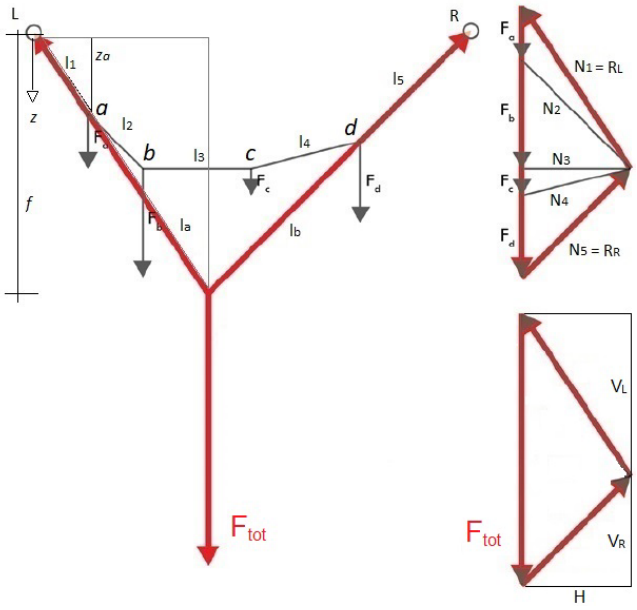

$$z_l = z_r = 0$$

$$(z_a - z_l)\frac{N_1}{l_1} + (z_a - z_b)\frac{N_2}{l_2} - F_a = 0 \qquad (24)$$

$$(z_b - z_a)\frac{N_2}{l_2} + (z_b - z_c)\frac{N_3}{l_3} - F_b = 0$$

$$(z_c - z_b)\frac{N_3}{l_3} + (z_c - z_d)\frac{N_4}{l_4} - F_c = 0$$

$$(z_d - z_c)\frac{N_4}{l_4} + (z_d - z_r)\frac{N_5}{l_5} - F_d = 0 \quad +$$

$$z_a\frac{N_1}{l_1} + z_d\frac{N_5}{l_5} = F_a + F_b + F_c + F_d = \Sigma F \Rightarrow \qquad (25)$$

$$\frac{z_a}{l_1} = \frac{f}{l_a}, \frac{z_d}{l_5} = \frac{f}{l_b} \qquad (26)$$

$$f\frac{N_1}{l_a} + f\frac{N_5}{l_b} = V_l + V_r = F_{tot} = \Sigma F \qquad (27)$$

The total force density of a form diagram can also be determined by using the shape coefficients and the vertical projection of the axial force (V_i). This is however only possible for inclined elements not for a horizontal one for which Δz_i and α_i are zero. A horizontal element is the watershed of the load transfer (V_i). Using this alternate formulation (eq. 28) allows the total force density to give insight into the load transfer of the system in relation to the rise, i.e. morphology of the system.

$$Q = \Sigma\frac{N_i}{l_i} = H\left(\Sigma\frac{1}{x_i}\right) = \frac{M_{max}}{f}\left(\Sigma\frac{1}{x_i}\right) \Rightarrow \frac{1}{f}\left(\Sigma\frac{V_i}{\alpha_i}\right) + \underbrace{\left(\frac{H}{l_i}\right)}_{only\ horizontal\ element} \qquad (28)$$

Expanding on this expression for the force density (eq. 28) for a system with multiple point loads it can be observed that the first part relates to the envelope (or a system with just one point load). The other parts are a result of the division of the total load into multiple point loads and thus the truncation of the form diagram of which the envelop forms its tangent and with the latter part referring to a horizontal element.

By using the expressions of (eq. 1) from section 2.3, the part that relates to an eventual horizontal element can be rewritten so that the entire relation of the total force density is a function of the rise of the point of application of the total load *f* (eq. 29). Because all the elements of the function remain constant when either *f* or its reciprocal *H* change it is established that the total force density of a funicular system (cable of arch) is a function of *f*.

$$\Sigma F = V_l + V_r$$

$$Q = \frac{\Sigma F}{f} + \frac{1}{f}\left(\frac{V_l(1-\alpha_l)}{\alpha_l} + \frac{V_r(1-\alpha_r)}{\alpha_r}\right) + \frac{1}{f}\left(\Sigma \frac{V_{in}}{\alpha_{in}}\right) + \underbrace{\left(\frac{H}{l_i}\right)}_{only\ horizontal\ element}$$

$$Q = \frac{\Sigma F}{f} + \frac{1}{f}\left(\frac{V_l(1-\alpha_l)}{\alpha_l} + \frac{V_r(1-\alpha_r)}{\alpha_r}\right) + \frac{1}{f}\left(\Sigma \frac{V_{in}}{\alpha_{in}}\right) + \underbrace{\frac{1}{f}\left(\frac{V_l x_l + V_r x_r}{2l_i}\right)}_{only\ horizontal\ element} \quad (29)$$

By comparing a cable to the equivalent beam the total force density can be determined in three ways:

- total force density expressing the load transfer (V_i)
- total force density related to the “moment” distribution
- total force density relating to the cable

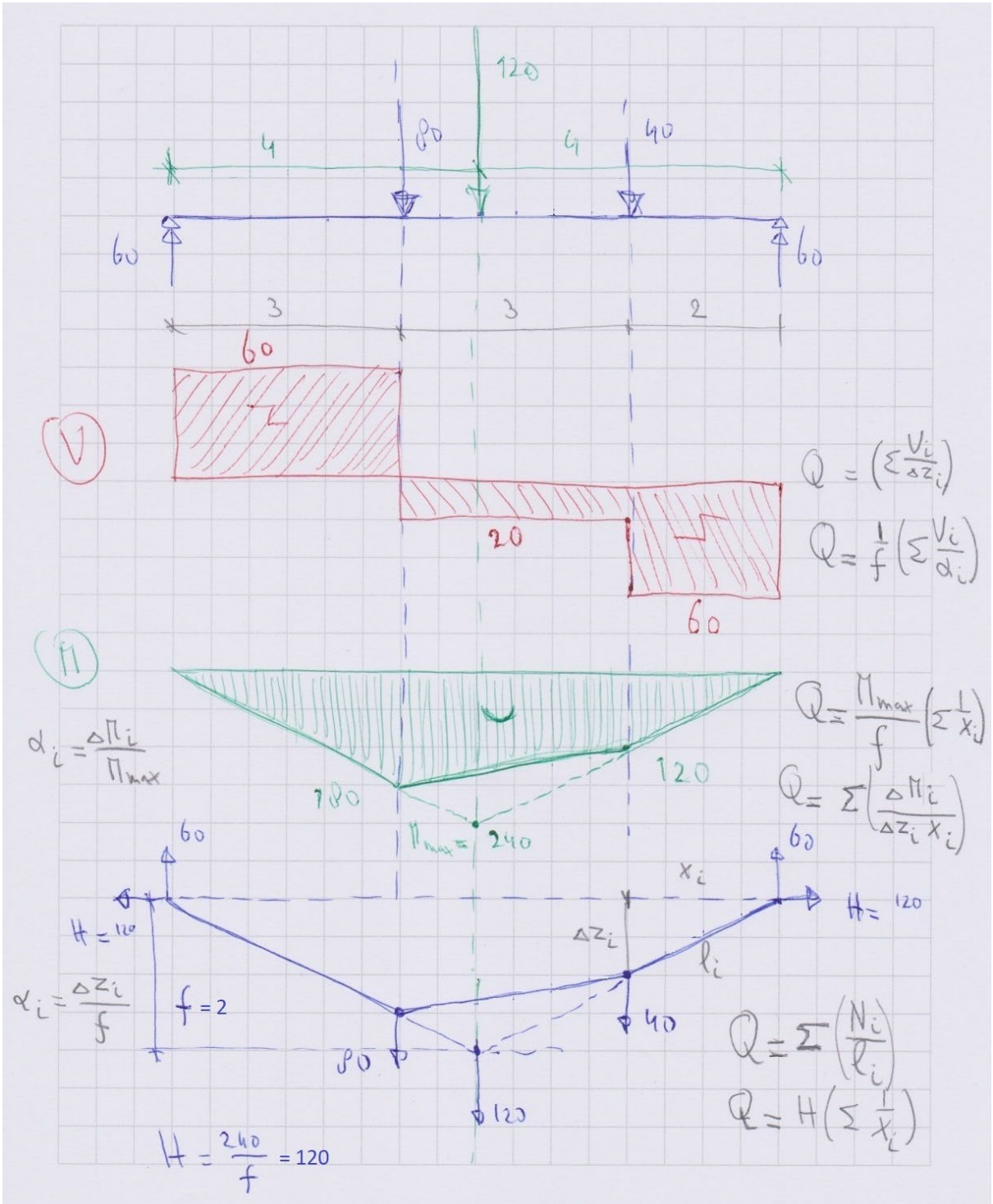
120
80
40
4
4
60
60
3
3
2
60
V
20
60
П
180
120
Π_{max} = 240
60
60
x_i
H = 120
H = 120
Δz_i
l_i
$\alpha_i = \frac{\Delta z_i}{f}$
f = 2
40
80
120
$\alpha_i = \frac{\Delta \Pi_i}{\Pi_{max}}$
$Q = \left(\Sigma \frac{V_i}{\Delta z_i}\right)$
$Q = \frac{1}{f}\left(\Sigma \frac{V_i}{\alpha_i}\right)$
$Q = \frac{\Pi_{max}}{f}\left(\Sigma \frac{1}{x_i}\right)$
$Q = \Sigma\left(\frac{\Delta \Pi_i}{\Delta z_i x_i}\right)$
$Q = \Sigma\left(\frac{N_i}{l_i}\right)$
$Q = H\left(\Sigma \frac{1}{x_i}\right)$
$H = \frac{240}{f} = 120$

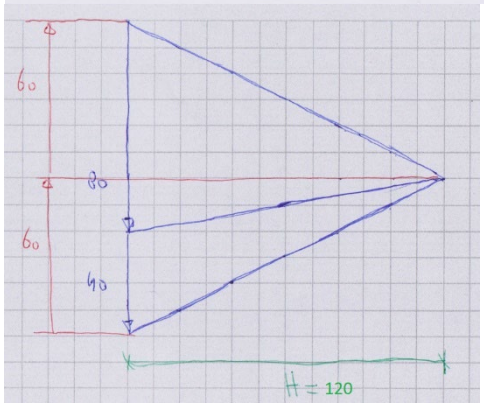
60
80
60
40
H = 120

2.8 Relation equilibrium, discretization and cable equation

In section 2.7 the classic force-density equilibrium relation was derived. This equilibrium equation is used by the force-density method (Sheck, Linkwitz) [37] to form find membrane structures but also forms the basis of the thrust network analysis (O'Dwyer, Block, Ochsendorf). This relation is in fact the discretized version of the cable relation using the finite difference method.

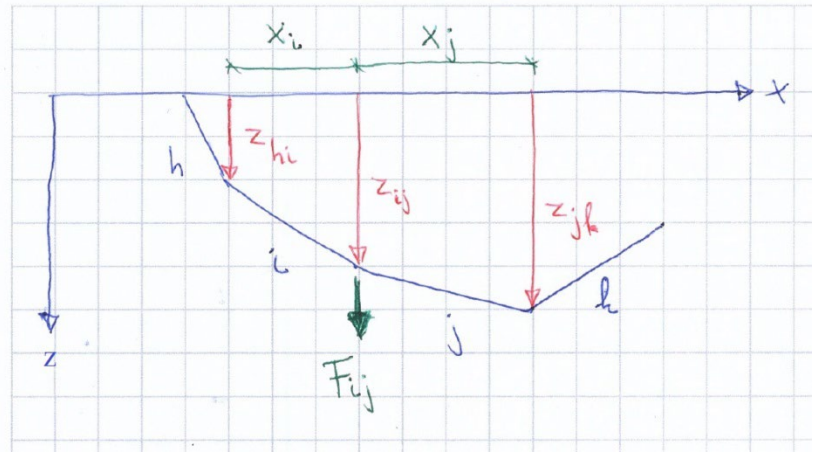

$$\frac{\triangle z_j}{x_j} - \frac{\triangle z_i}{x_i} = \frac{F_{ij}}{H}$$

$$with: \triangle z_i = z_{ij} - z_{hi},\ \triangle z_j = z_{jk} - z_{ij}$$
$$and: x_i = x_j = \triangle x,$$
$$F_{ij} = \triangle x\, q$$

$$\frac{z_{jk} - z_{ij} - z_{ij} + z_{hi}}{\triangle x} = -\frac{\triangle x\, q}{H} \Rightarrow H\frac{z_{jk} - 2z_{ij} + z_{hi}}{(\triangle x)^2} = -q \quad (30)$$

$$cable\ equation:$$
$$\Rightarrow H\frac{d^2z}{dx^2} = -q$$

Because the force polygon is the reciprocal diagram of the form diagram, in this case a cable, it also represents the discretized version of the differential equation. Because of the similar structure of the first part of the beam equation to the cable equation the bending moment diagram can be constructed using a force polygon.

$$first\ part\ of\ beam\ equation:$$
$$q = -\frac{d^2M}{dx^2}$$
$$V = \frac{dM}{dx}$$

$$cable\ equation:$$
$$q = -H\frac{d^2z}{dx^2}$$
$$V = H\frac{dz}{dx}$$

An example of a cantilever with loads and the construction of the bending moment diagram with the help of the force polygon and its reciprocal form diagram [38].

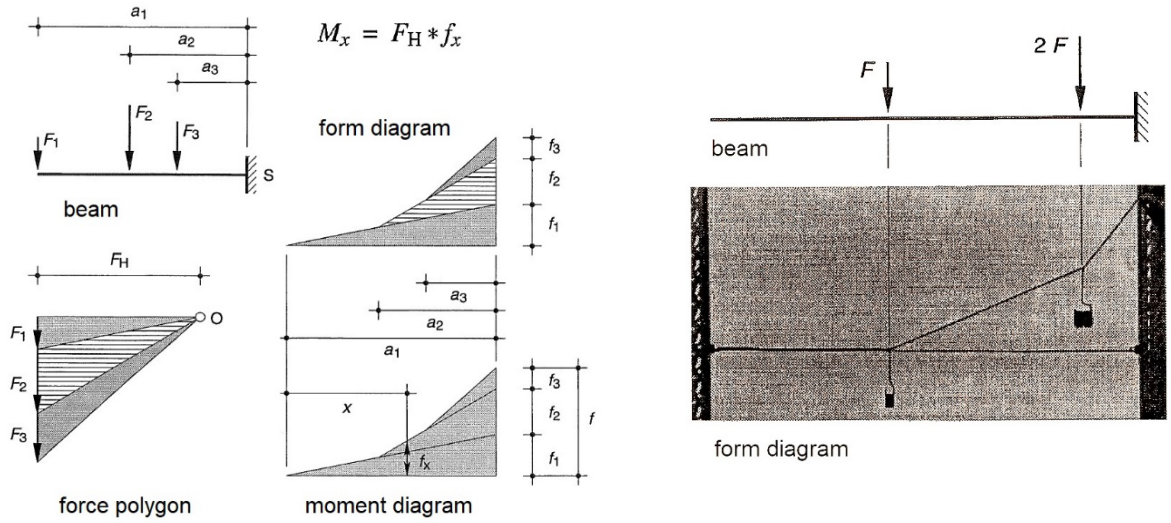

Figure 22 drawing the moment diagram by using the beam - cable analogy [images 38]

The form diagram and the force polygon of a cable or arch are in fact the graphical representation of their differential equation.

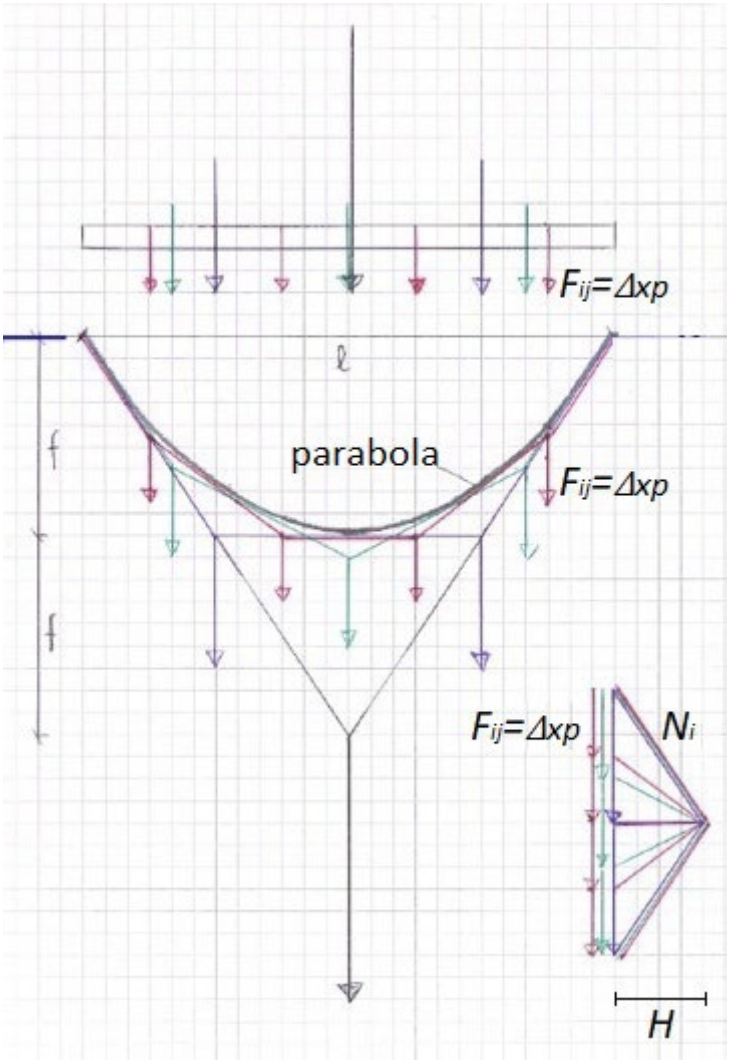

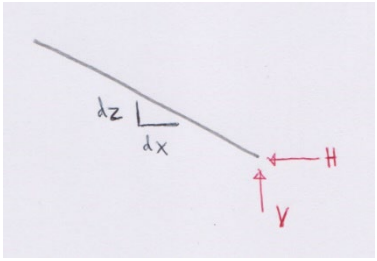

$$V_i = \frac{\triangle z_i}{x_i} H = \sum (\triangle x \cdot p)$$

$$N_i = \left(H^2 + {V_i}^2\right)^{1/2}$$

$$= \left(H^2 + \left(\frac{\triangle z_i}{x_i} H\right)^2\right)^{\frac{1}{2}}$$

$$= H\left(1 + \left(\frac{\triangle z_i}{x_i}\right)^2\right)^{\frac{1}{2}}$$

The version presented in section 2.7 is for cables and arches but can be expanded in 3D for membranes and thrust networks. Derived here, is the 3D version for an orthogonal grid as basis for the discretization. For both force-density and thrust networks other non-orthotropic grids as bases can also be used. This does not change the load transfer in x- and y-directions.

The discretization used for the force-density and thrust networks results in a version of the cable equation [39] with the part relating to the twist of the grid omitted, which means there are no in-plane shear forces to help carry the load. This is of course a result of discretizing the membrane and thrust surface into a grid. For an anti-clastic membrane as a minimal surface or a cable nets this is reasonable, but for thrust surfaces this does not result in the optimal load transfer and is therefore a sub-optimal shape.

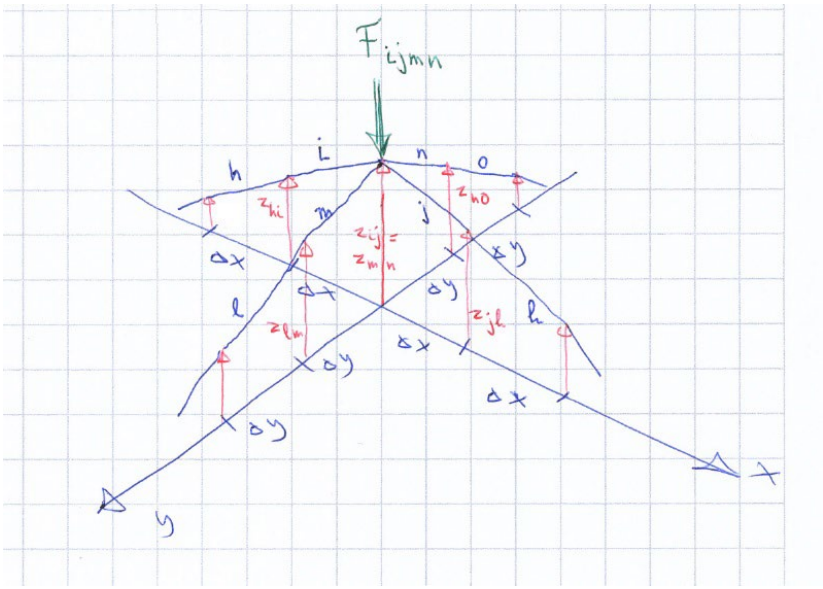

$$with: F_{ijmn} = \triangle x \triangle y \, p_z$$
$$z_{mn} = z_{ij}$$

$$\Rightarrow H_x \frac{z_{jk} - 2z_{ij} + z_{hi}}{(\triangle x)^2} + H_y \frac{z_{no} - 2z_{ij} + z_{lm}}{(\triangle y)^2} = -F_{ijmn}$$

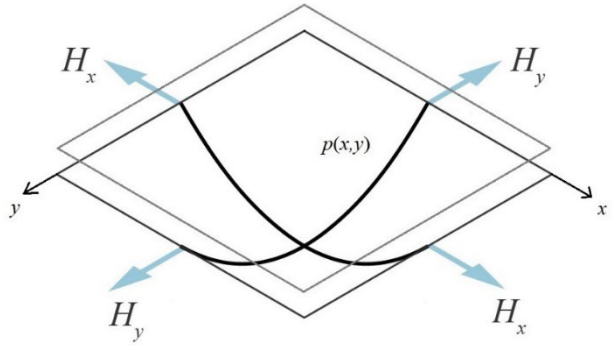

$$cable\ equation:$$
$$\Rightarrow H_x \frac{\partial^2 z}{\partial x^2} + H_y \frac{\partial^2 z}{\partial y^2} = -p_z$$

2.9 From the cable equation via force density to the thrust network

The discretized version of the cable equation from section 2.8 can be generalized. The result is the force-density equation in the version for the horizontal projected forces. The classic force-density equation contains the axial forces in the links of the mesh and their length. But their force-densities are equal to those in the horizontally projected plane.

$$H_i \frac{\triangle z_i}{l_{p,i}} + H_j \frac{\triangle z_j}{l_{p,j}} + H_n \frac{\triangle z_n}{l_{p,n}} + H_m \frac{\triangle z_m}{l_{p,m}} - F_{ijmn} = 0$$

$$with: l_{p,i} = \sqrt{\Delta x^2 + \Delta y^2}$$

$$\triangle z_i = z_{ij} - z_{hi},\ \triangle z_j = z_{ij} - z_{jk},$$
$$\triangle z_n = z_{ij} - z_{no},\ \triangle z_m = z_{ij} - z_{lm}\ , and\ z_{mn} = z_{ij}$$

$$\left(z_{ij} - z_{hi}\right)\frac{H_i}{l_{p,i}} + \left(z_{ij} - z_{jk}\right)\frac{H_j}{l_{p,j}} + \left(z_{ij} - z_{no}\right)\frac{H_n}{l_{p,n}} + \left(z_{ij} - z_{lm}\right)\frac{H_m}{l_{p,m}} - F_{ijmn} = 0$$

$$force\ density: q_i = \frac{N_i}{l_i} = \frac{H_i}{l_{p,i}}$$

The version presented here form the basis for the thrust network analysis [40]. As with the cable and arch for a thrust network the form diagram and the force polygon are reciprocal diagrams.
The height of the thrust network has yet to be determined, there are many solutions possible which ensure equilibrium. Multiple reciprocal force polygons are possible for the same horizontal projection (primal grid) of the thrust networks form diagram.

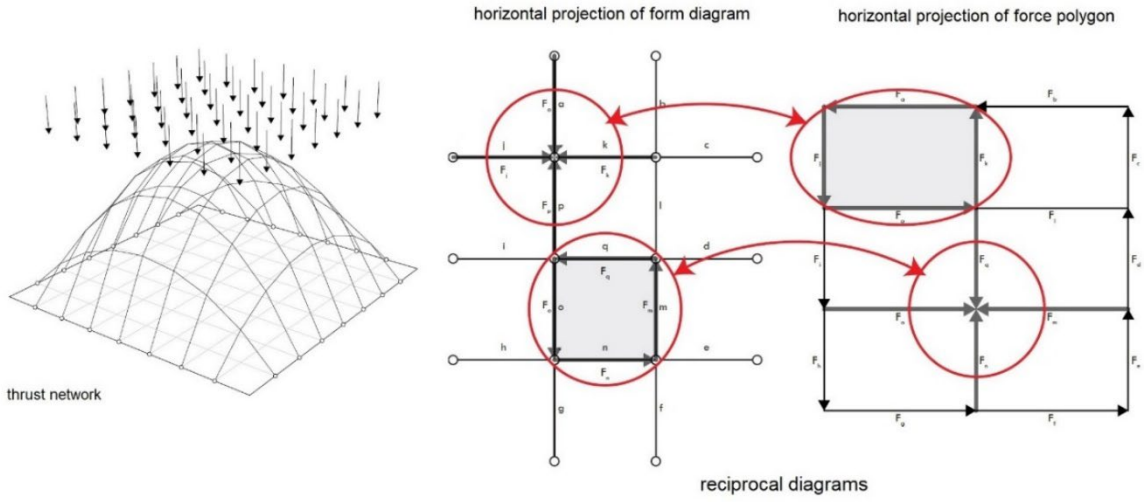

Figure 23 thrust network and its horizontal projections [images 89]

Each viable solution has a different set of z-coordinates and thus different ratio of “curvatures” of the network and accompanying load distribution. It should be noted that for the thrust network shear elements are omitted. The individual link can only take up axial forces.

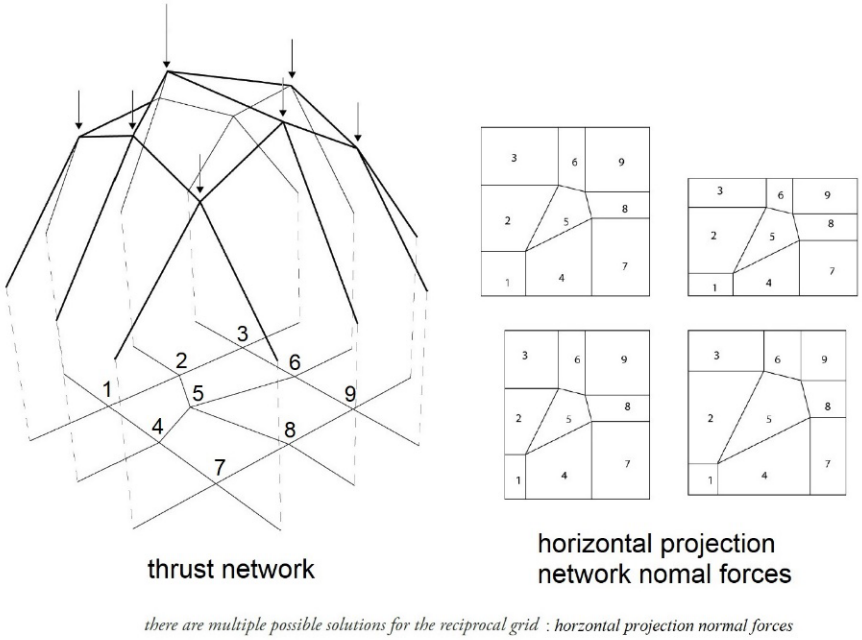

Figure 24 thrust network and possible solutions [images 103]

Once a solution has been chosen, a closed polygon of the horizontally projected force is set, the ratio between the z-coordinates for each node of the network is fixed. As with the force polygon and form diagram of the arch, the thrust network is scalable. Whereby the load distribution remains unaltered. The horizontal forces are reciprocal to the z-coordinates and just as for the arch their product is constant throughout the scaling.
In fact the thrust network is equivalent to the moment hill of a twistless case of a slab loaded out-of-plane, this will be explained in more detail in section 8.2.

$$scaling\ the\ thrust\ network:$$
$$H_i\ z_i = constant\ throughout\ the\ network$$

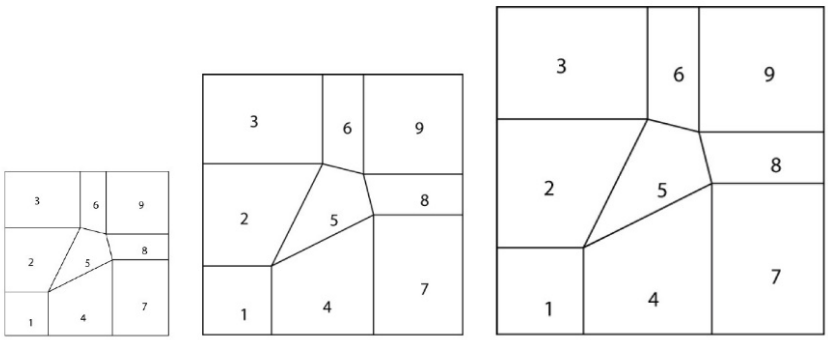

the scaling affects the size of the projected horizontal forces

3 Reciprocal characteristics of cables and trusses; and energy methods

3.1 Introduction

The relation between funicular cables and a specific type of truss structures is explored in this chapter. What will be established is the reciprocity of the force diagram of the funicular cable structure and the force polygon of the truss structure and thus the reciprocity of their respective force polygon and form diagram. This reciprocity concerns their state of rigidity [41], the funicular cable structure having mechanisms and the truss structure having independent states of self-stress (degree of static indeterminacy) of the same order [42].

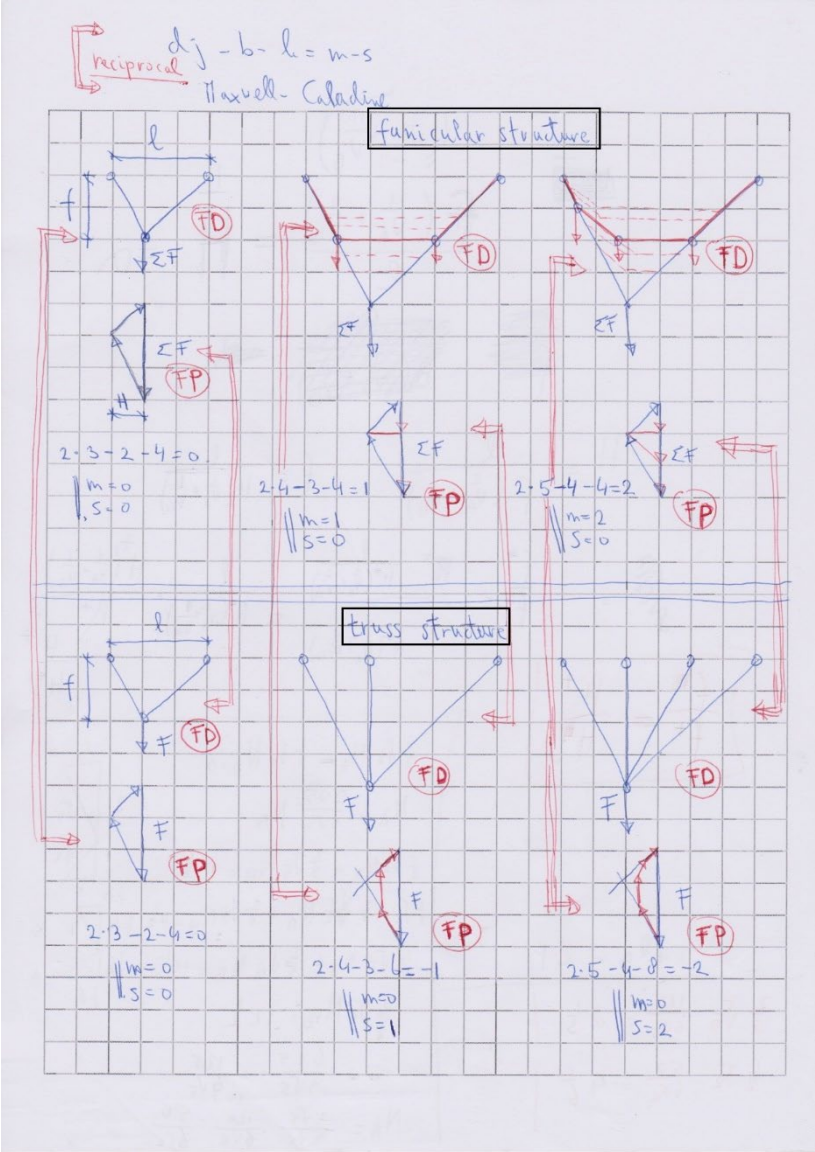

Maxwell / Calladine

$$dj - b - k = m - s$$

d = dimension
j = number of joints
b = number of bars
k = kinematic constraints
m = number of mechanisms
s = state of self-stress

Cables are used to illustrate this approach here, but the general properties also hold for the other type of funicular structure, the arch. But because these can

be statically indeterminate relations become more complicated, which will be further discussed in chapter 4.

It can be observed in the force polygons of the trusses which are statically indeterminate (s >1), that its state of equilibrium of the applied load and the state of self-stress are complementary. The difference in the force polygon between the statically determinate and statically indeterminate state is the force polygon of the state of self-stress.

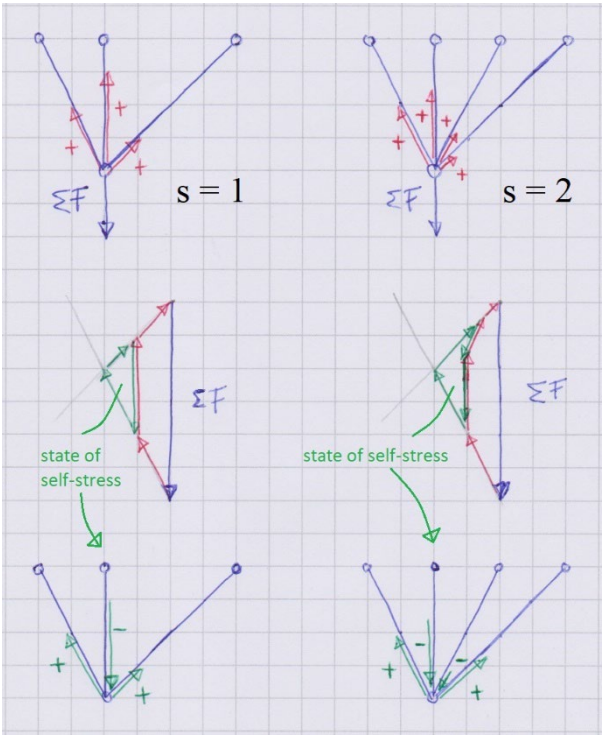

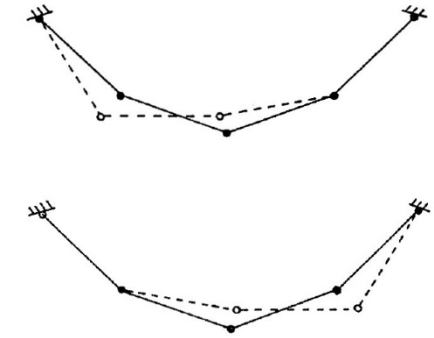

Two independent mechanisms of the hanging cable $m = 2$

$$dj - b - k = m - s$$
$$2 \cdot 5 - 4 - 2 \cdot 2 = 2$$
$$m = 2$$
$$s = 0$$

Figure 25 image right of mechanisms of cable is from "Mechanics of Kinematically Indeterminate Structures" by Sergio Pellegrino.

3.2 Some properties of the state of rigidity

In a closed system the internal horizontal force due to the vertical load and the topology of the structures is taken up by the structure itself. The internal forces form a "closed loop" with respect to its horizontal component. If the horizontal component has to be taken up by the structures support reaction it is called an open system.
For example a truss with a redundancy of *s* = 1 will keep its state of rigidity if one of its support reactions is altered but an extra strut is added to take up the horizontal component, in that case it changes from an open system to a closed system.

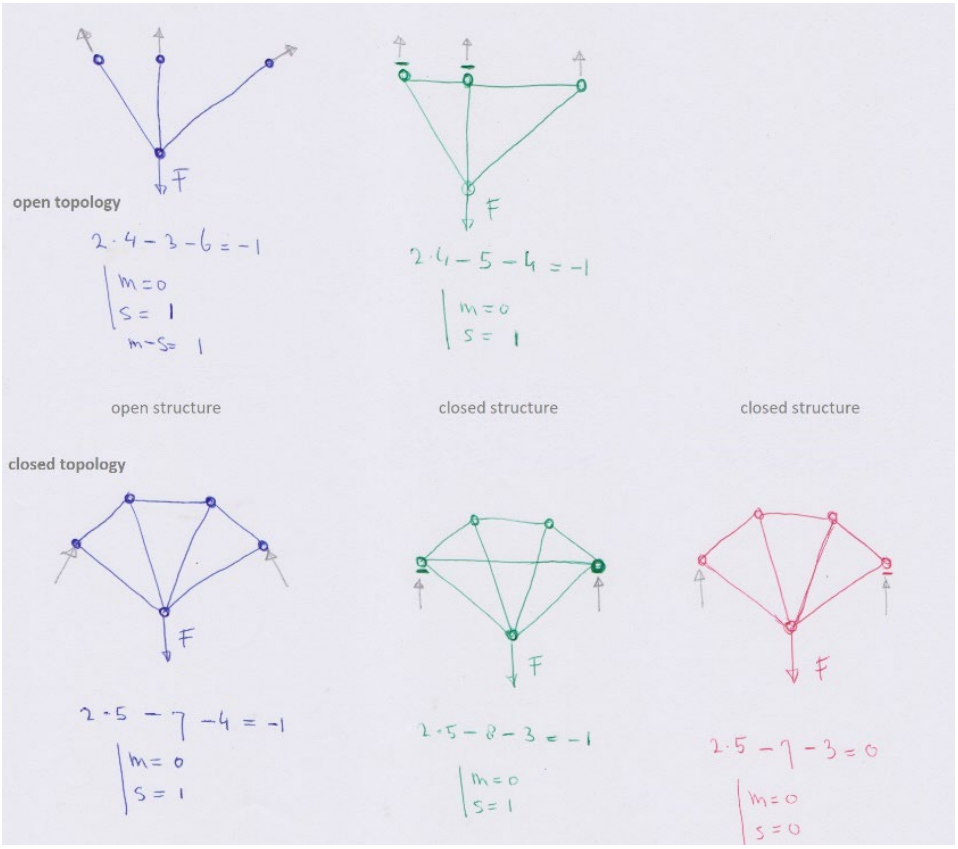

3.3 Statically (in)determinate trusses

A funicular cable and a truss structure with only one load and respectively two ties or bars are both statically determinate ($s = 0$). If the total load $\sum F$ is divided into more point loads along the cable, and thus the force polygon is subdivided, it still remains statically determinate. If its reciprocal diagram for the truss structure, the form diagram, is subdivided and thus extra bars are added it becomes statically indeterminate. This will further be discussed with the help of an example.

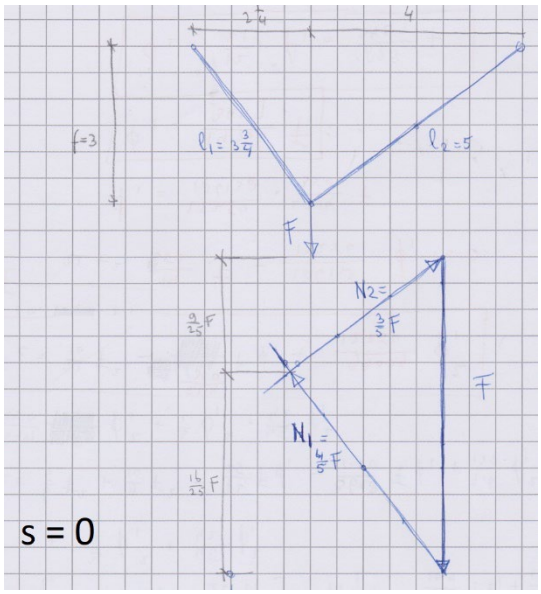

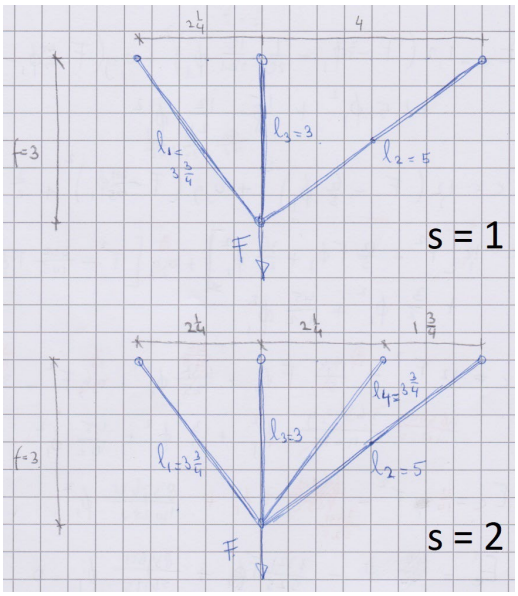

$l_1 = 15/4$
$l_2 = 3$
$l_3 = 3$

A two bar truss is suspended from two hinges and has one load and is statically determinate. The internal forces can be represented unambiguously by its reciprocal diagram, the force polygon .
When the truss structure becomes statically indeterminate by adding an extra bar there are theoretically an infinite amount of solutions possible which ensures equilibrium [43]. The initial force polygon belonging to the two bar truss can be endlessly truncated to suit these possibilities. There is only one exact solution, the one with the lowest complementary energy [44]. This solution can also be obtained by making for example a FEM calculation of the problem.

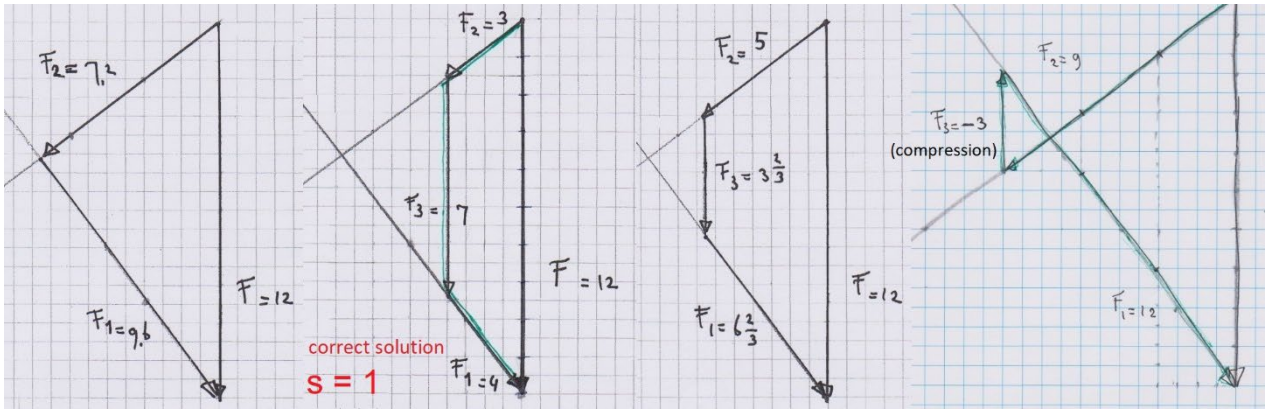

For the purpose of comparing the statically determinate truss (s = 0) with two cases of statically indeterminate trusses (s = 1 and 2), first some properties of the statically determinate truss are given. They are the total force density of the system and the equilibrium equation, their relation was discussed in 2.7.

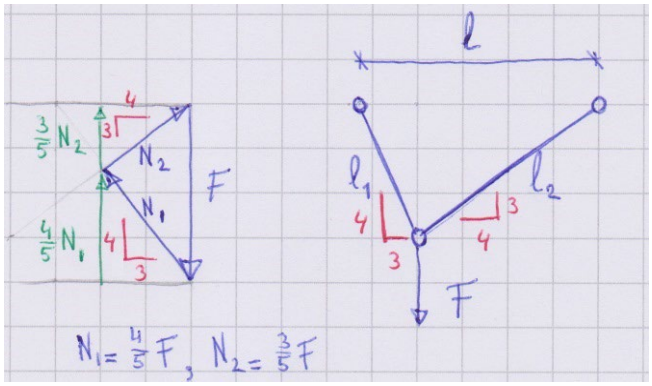

$$for\ s = 0$$

$$Q = \frac{N_1}{l_1} + \frac{N_2}{l_2} = \frac{N_1}{15/4} + \frac{N_2}{5} = \frac{4/5\,F}{15/4} + \frac{3/5\,F}{5} = \frac{1}{3}F = \frac{F}{f} \Rightarrow$$

$$Q \cdot f = \frac{4}{5}N_1 + \frac{3}{5}N_2 = F\text{: } equilibrium\ equation$$

The solution for the statically indeterminate trusses are determined next.

a. *solving the redundancy for s = 1*

The redundant ϕ , which is the force in the vertical bar, will be solved by determining the lowest complementary energy of the system.

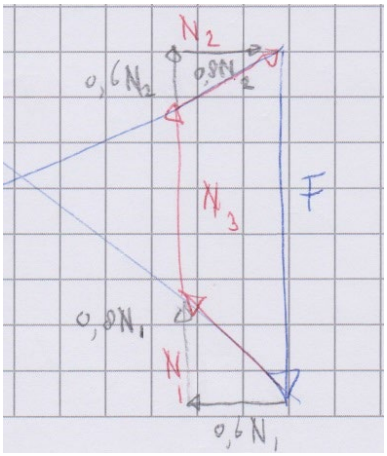

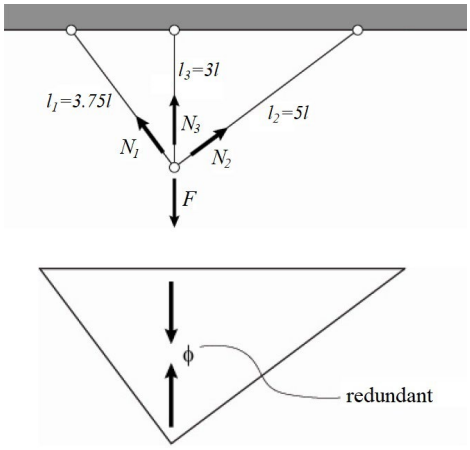

complementary energy is expressed in stresses:

$$E_{compl} = \frac{1}{2}\frac{\sigma^2}{E}$$

the complementary energy per unit of bar length:

$$E_{compl} = \int_0^V \frac{1}{2}\frac{\sigma^2}{E}\, dV = \frac{1}{2}\frac{N^2}{EA}$$

for the bar with length l:

$$E_{compl} = \frac{1}{2}\frac{N^2}{EA} l$$

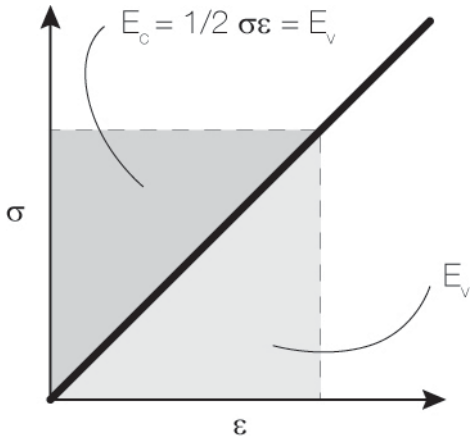

For determining the total complementary energy the equilibrium equations need to be set up (*EA* is presumed to be constant).The total complementary energy can be accordingly calculated and minimized, thus resulting in the exact solution. When the redundant ϕ has been solved the other internal forces can be calculated. This method is relatively simple.

$$\Sigma F_{vert} = 0 \Rightarrow \frac{4}{5}N_1 + \phi + \frac{3}{5}N_2 = F$$
$$\Sigma F_{hor} = 0 \Rightarrow \frac{3}{5}N_1 - \frac{4}{5}N_2 = 0 \Rightarrow N_1 = \frac{4}{3}N_2$$

$$N_1 = \frac{4}{5}(F-\phi)$$
$$N_2 = \frac{3}{5}(F-\phi)$$
$$N_3 = \phi$$

$$E_{compl,N} = N_1^2 l_1 + N_2^2 l_2 + N_3^2 l_3$$
$$E_{compl,N} = \frac{21}{10}F^2 - \frac{42}{10}F\phi + \frac{36}{10}\phi^2$$
$$\frac{dE_{compl,N}}{d\phi} = 0 \Rightarrow \phi = \frac{7}{12}F$$
$$N_1 = \frac{4}{12}F, N_2 = \frac{3}{12}F, N_3 = \frac{7}{12}F$$

member	N_i	l_i	E_c
1	$0{,}8(F-\phi)$	3,75l	$1{,}2\frac{l}{EA}(F-\phi)^2$
2	$0{,}6(F-\phi)$	5l	$0{,}9\frac{l}{EA}(F-\phi)^2$
3	ϕ	3l	$1{,}5\frac{l}{EA}\phi^2$

b. solving the redundancy for s = 2

As a follow-up to the previous example an additional bar is added to the truss, thus making the degree of indeterminacy equal to two. This means that there are two redundancies: ϕ_1 and ϕ_2, the consequence of this being one equation for the complementary energy with two unknowns. In addition to equilibrium equation to set up the total complementary energy we will use compatibility to express one redundancy in another and thus reducing to number of unknowns to one and directly solve the problem.

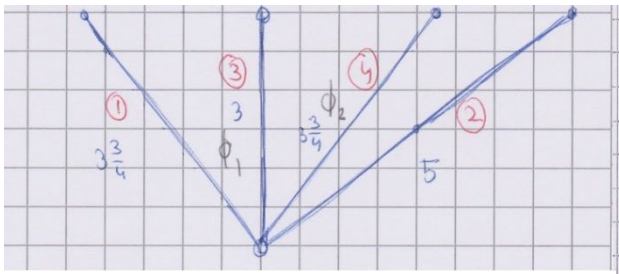

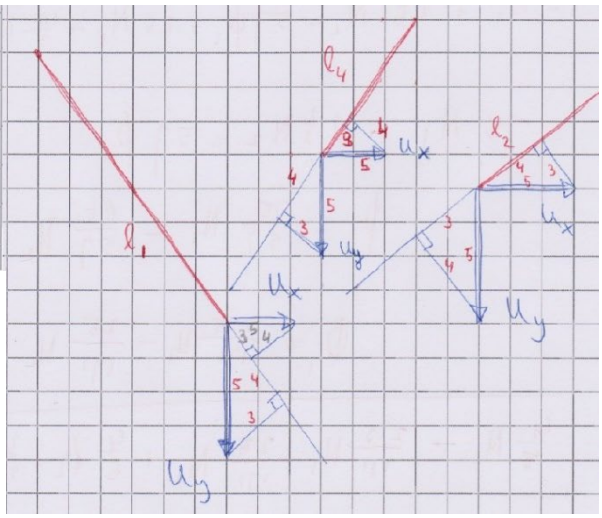

$$\varepsilon_1 = \frac{{}^4\!/_5\, u_y}{l_1} + \frac{{}^3\!/_5\, u_x}{l_1} : \varepsilon_2 = \frac{{}^3\!/_5\, u_y}{l_2} - \frac{{}^4\!/_5\, u_x}{l_2}$$

$$\varepsilon_3 = \frac{u_y}{l_3} : \varepsilon_4 = \frac{{}^4\!/_5\, u_y}{l_4} - \frac{{}^3\!/_5\, u_x}{l_4}$$

$$50\varepsilon_1 + 25\varepsilon_2 - 57\varepsilon_3 + 25\varepsilon_4 = 0$$
$$\Rightarrow 50N_1 + 25N_2 - 57N_3 + 25N_4 = 0$$

The equilibrium equation again is used to set up the equation for the complementary energy:

$$\Sigma F_{vert} = 0 \Rightarrow \frac{4}{5}N_1 + \phi_1 + \frac{4}{5}\phi_2 + \frac{3}{5}N_2 = F$$
$$\Sigma F_{hor} = 0 \Rightarrow \frac{3}{5}N_1 - \frac{3}{5}\phi_2 - \frac{4}{5}N_2 = 0$$

$$N_1 = \frac{4}{5}\left(F - \phi_1 - \frac{7}{20}\phi_2\right)$$
$$N_2 = \frac{3}{5}\left(F - \phi_1 - \frac{8}{5}\phi_2\right)$$
$$N_3 = \phi_1, N_4 = \phi_2$$

Including compatibility the equation for the complementary energy and its solution becomes:

$$E_{compl,N} = \frac{43125}{676}F^2 - \frac{367440}{1352}F\phi_1 + \frac{12364356}{42250}\phi_1^2$$
$$\frac{dE_{compl,N}}{d\phi_1} = 0 \Rightarrow \phi_1 = \frac{625}{1346}F$$
$$\phi_2 = \frac{55}{13}F - \frac{112}{13}\phi_1 = \frac{310}{1346}F$$
$$N_1 = \frac{490}{1346}F, \quad N_2 = \frac{135}{1346}F$$
$$N_3 = \phi_1 = \frac{625}{1346}F, \quad N_4 = \phi_2 = \frac{310}{1346}F$$

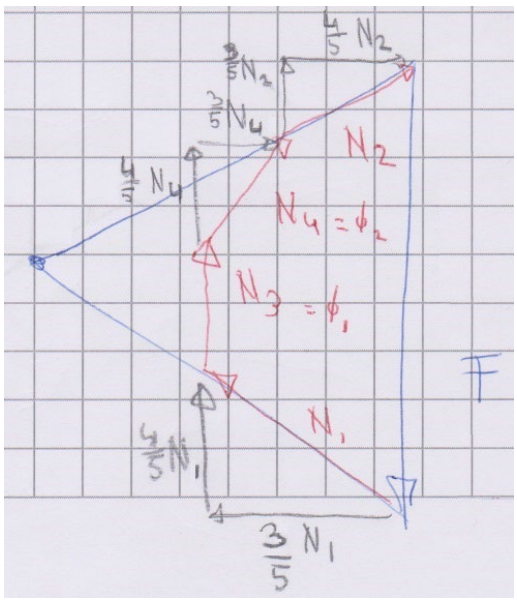

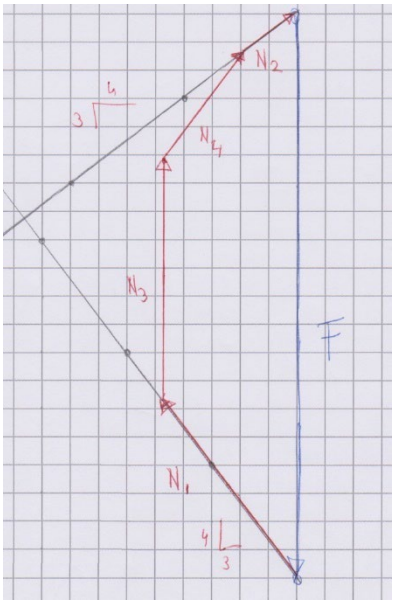

If we use the full variational method to set up the equation for the complementary energy we can dispense with the additional compatibility condition, this is satisfied by the minimisation of the complementary energy. We arrive at the same solution.

$$E_{compl,N} = \frac{3(350F^2 - 700F\phi_1 - 620F\phi_2 + 600\phi_1^2 + 620\phi_1\phi_2 + 721\phi_2^2)}{500}$$

$$\frac{dE_{compl,N}}{\partial\phi_1} = \frac{3(60\phi_1 + 31\phi_2 - 35F)}{25} = 0 \Rightarrow \phi_1 = \frac{625}{1346}F$$

$$\frac{dE_{compl,N}}{\partial\phi_2} = \frac{3(310\phi_1 + 721\phi_2 - 310F)}{250} = 0 \Rightarrow \phi_2 = \frac{310}{1346}F$$

$$N_1 = \frac{490}{1346}F, \quad N_2 = \frac{135}{1346}F$$

$$N_3 = \phi_1 = \frac{625}{1346}F, \quad N_4 = \phi_2 = \frac{310}{1346}F$$

In other words: if there are more states of equilibrium statically admissible, the situation with the minimum complementary energy will prevail.

The method discussed above can be generalised:

$$- \textit{variational method of the lowest complementary energy}:$$

$$E_{compl,N} = \sum_i N_i^2\, l_i \Rightarrow minumum$$

$$\sum_i \frac{\partial E_{compl,N}}{\partial N_i} = 0$$

For completeness the general method will be demonstrated by solving the first example in this section with *s = 1*.

$$E_{compl,N} = \sum_i N_i^2\, l_i \;\rightarrow minumum$$

$$E_{compl,N} = N_1^2\, 3\frac{3}{4} + N_2^2\, 5 + N_3^2\, 3 \;\rightarrow min$$

$$with\ equilibrium:$$

$$\Sigma F_{vert} = 0 \Rightarrow F - (V_1 + V_2 + V_3) = 0 \Rightarrow F - \left(\frac{4}{5}N_1 + \frac{3}{5}N_2 + N_3\right) = 0 \Rightarrow N_3 = \frac{5}{3}N_2 - F$$

$$\Sigma F_{hor} = 0 \Rightarrow H_1 - H_2 = 0 \Rightarrow \frac{3}{5}N_1 - \frac{4}{5}N_2 = 0 \Rightarrow N_1 = \frac{4}{3}N_2$$

$$\Rightarrow E_{compl,N} = 2N_2^2 - FN_2 + F^2 \rightarrow min$$

$$\sum_i \frac{\partial E_{compl,N}}{\partial N_i} = 4N_2 - F = 0 \Rightarrow N_2 = \frac{3}{12}F$$

$$\Rightarrow N_1 = \frac{4}{12}F, \qquad N_3 = \frac{7}{12}F$$

The following observations can be made:
1. When calculating the total force density *Q* of both examples the redundancies ϕ_i fall out of the addition. Which means that for each possible solution for equilibrium the total force density is constant, including the exact solution. The total force density is equal to a parameter α times the total load. In the next section it is shown that the coefficient α is the reciprocal value of the rise *f* of the form diagram.
The total force density is stays constant and is equal to the coefficient α, for both systems. So by adding a bar to the truss and thus increasing the degree of indeterminacy does not change the value of α.

$$statically\ determinate\ example, s = 0:$$

$$Q = \frac{N_1}{l_1} + \frac{N_2}{l_2} = \frac{N_1}{15/4} + \frac{N_2}{5} = \frac{4/5\,F}{15/4} + \frac{3/5\,F}{5} = \frac{1}{3}F$$

$$statically\ indeterminate\ example, s = 1:$$

$$Q = \frac{N_1}{l_1} + \frac{N_2}{l_2} + \frac{N_3}{l_3} = \frac{\frac{4}{5}(F-\phi)}{15/4} + \frac{\frac{3}{5}(F-\phi)}{5} + \frac{\phi}{3} = \frac{1}{3}F$$

$$statically\ indeterminate\ example, s = 2:$$

$$Q = \frac{N_1}{l_1} + \frac{N_2}{l_2} + \frac{N_3}{l_3} + \frac{N_4}{l_4} = \frac{\frac{4}{5}\left(F - \phi_1 - \frac{7}{20}\phi_2\right)}{15/4} + \frac{\frac{3}{5}\left(F - \phi_1 - \frac{8}{5}\phi_2\right)}{5} + \frac{\phi_1}{3} + \frac{\phi_2}{15/4} = \frac{1}{3}F$$

$$\Rightarrow Q = \Sigma\frac{N_i}{l_i} = \alpha F$$

2. As already has been shown is that if the individual force density for each bar is multiplied with the parameter α the equation of the total force density turns into the equilibrium equation, see also 2.7.

$$statically\ indeterminate\ example\ s = 1:$$
$$Q = \frac{N_1}{l_1} + \frac{N_2}{l_2} + \frac{N_3}{l_3} = \frac{N_1}{15/4} + \frac{N_2}{5} + \frac{N_3}{3} = \alpha F = \frac{1}{3}F \Rightarrow$$
$$\frac{4}{5}N_1 + \frac{3}{5}N_2 + N_3 = F: equilibrium\ equation$$
$$statically\ indeterminate\ example\ s = 2:$$
$$Q = \frac{N_1}{l_1} + \frac{N_2}{l_2} + \frac{N_3}{l_3} + \frac{N_4}{l_4} = \frac{N_1}{15/4} + \frac{N_2}{5} + \frac{N_3}{3} + \frac{N_4}{15/4} = \frac{1}{3}F \Rightarrow$$
$$\frac{4}{5}N_1 + \frac{3}{5}N_2 + N_3 + \frac{4}{5}N_4 = F: equilibrium\ equation$$

3. The total force density of the complementary state of self-stress, see section 3.1, is equal to zero for a certain type of geometry, see section 3.7.

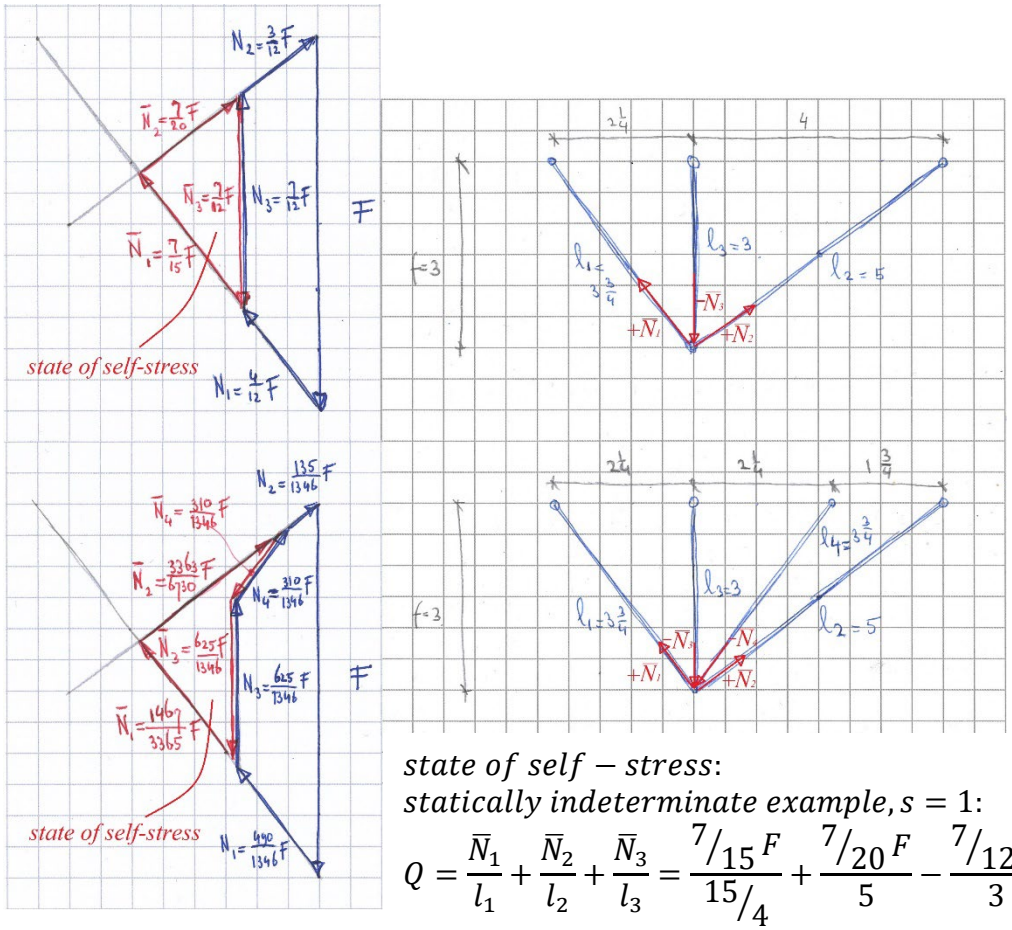

$$state\ of\ self-stress:$$
$$statically\ indeterminate\ example, s = 1:$$
$$Q = \frac{\bar{N}_1}{l_1} + \frac{\bar{N}_2}{l_2} + \frac{\bar{N}_3}{l_3} = \frac{7/15\,F}{15/4} + \frac{7/20\,F}{5} - \frac{7/12\,F}{3} = 0$$

$$statically\ indeterminate\ example, s = 2:$$
$$Q = \frac{\bar{N}_1}{l_1} + \frac{\bar{N}_2}{l_2} + \frac{\bar{N}_3}{l_3} + \frac{\bar{N}_4}{l_4} = \frac{1467/3365\,F}{15/4} + \frac{3363/6730\,F}{5} - \frac{625/1346\,F}{3} - \frac{310/1346\,F}{15/4} = 0$$

3.4 Example from statically determinate to statically indeterminate truss

This example starts with a statically indeterminate truss, with a central vertical axis of symmetry [45]. The internal axial forces and the support reaction will be determined by using the variational method of the lowest complementary energy. With this outcome the force polygon of the truss can be drawn. By altering the support conditions by adding two struts to the truss, thus the kinematic constraints, it becomes statically determinate.

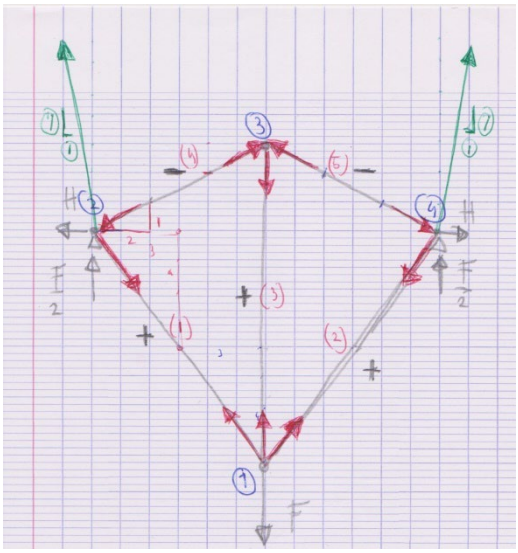

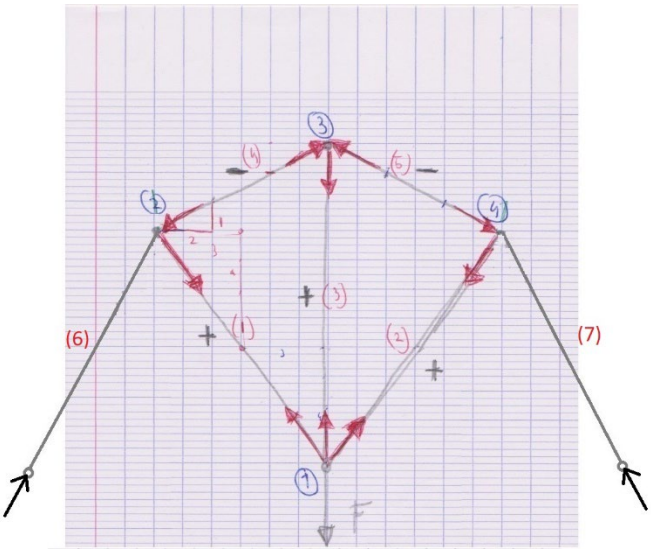

$2 \cdot 4 - 5 - 4 = -1$
$m = 0$
$s = 1$

$2 \cdot 6 - 7 - 4 = 1$
$m = 1$
$s = 0$

Not only does the truss become statically determinate, it also becomes a mechanism. If their respective force polygons are compared it can be observed that the slope of the supports reaction align with their accompanying struts for the statically determinate truss. This is not so for the statically indeterminate truss.

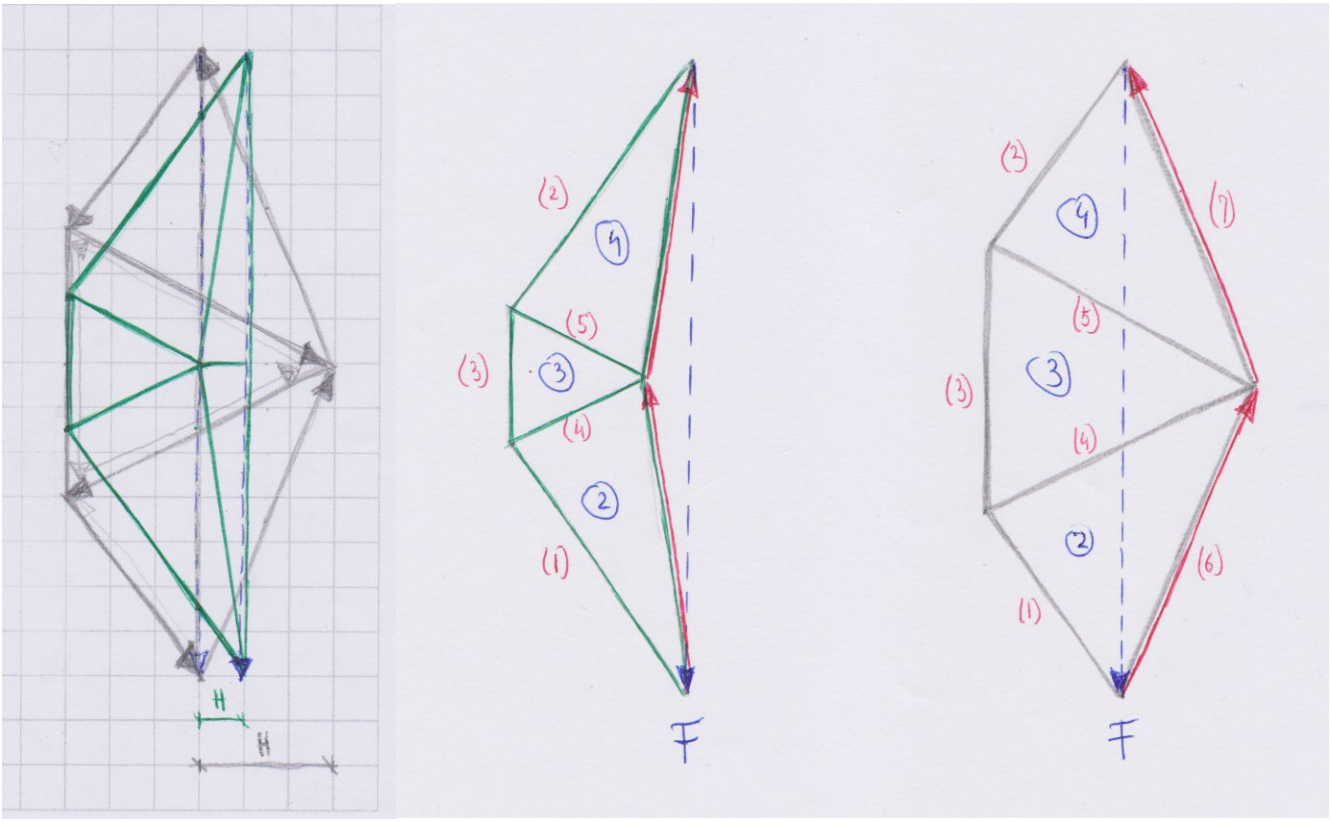

$$E_{compl,N} = \sum_i N_i^2 l_i \rightarrow minimum$$

$$E_{compl,N} = N_1^2 10 + N_2^2 10 + N_3^2 11 + N_4^2 3\sqrt{5} + N_5^2 3\sqrt{5} \rightarrow min$$

due to symmetry: $N_1 = N_2$ *and* $N_4 = N_5$

with vertical and horizontal equilibrium:

$$F - (V_1 + V_2 + V_4 + V_5) = 0 \Rightarrow F - \left(\frac{8}{5}N_1 + \frac{2}{5}\sqrt{5}N_4\right) = 0 \Rightarrow N_1 = \frac{5}{8}F - \frac{1}{4}\sqrt{5}N_4$$

$$V_4 + V_5 - N_3 = 0 \Rightarrow \frac{1}{5}\sqrt{5}N_4 + \frac{1}{5}\sqrt{5}N_4 - N_3 = 0 \Rightarrow N_1 = \frac{2}{5}\sqrt{5}N_4$$

$$H - (H_1 + H_4) = 0 \Rightarrow H - \frac{3}{5}N_1 + \frac{2}{5}\sqrt{5}N_4 = 0 \Rightarrow H = \frac{11}{5}N_1 - F$$

$$\Rightarrow E_{compl,N} = \left(6\sqrt{5} + \frac{1204}{80}\right)N_4^2 - \frac{500}{80}\sqrt{5}FN_4 + \frac{625}{80}F^2 \rightarrow min$$

$$\sum_i \frac{\partial E_{compl,N}}{\partial N_i} = \left(12\sqrt{5} + \frac{602}{80}\right)N_4 - \frac{125}{80}\sqrt{5}F = 0 \Rightarrow N_4 = \frac{125\left(301\sqrt{5} - 600\right)}{37202}F$$

$$N_1 = \frac{10\left(1875\sqrt{5} - 2378\right)}{37202}F, N_3 = \frac{50\left(-600\sqrt{5} + 1505\right)}{37202}F$$

$$H = \frac{22(1875\sqrt{5} - 4069)}{37202}F$$

3.5 General reciprocity of cables and trusses

The relation between the total force density *Q* and the equilibrium equation has been discussed in sections 2.7 and 3.3. The relation between the force density and the load *F* is constant and is determined by the coefficient *α*.

equilibrium equation	*force density*
$\Sigma \frac{N_i}{\alpha l_i} = F$	$Q = \Sigma \frac{N_i}{l_i} = \alpha F$

The coefficient *α* is the reciprocal value of the rise *f* of the FD. The total force density and the equilibrium equation can now be expressed as a function of *f*, see also 2.3 equation (5).

$$truss:$$

$$Q = \sum \frac{N_i}{l_i} = \alpha F \Rightarrow \sum \frac{N_i}{\alpha l_i} = F$$

$$equilibrium\ equation:$$

$$\sum N_i \sin\theta_i = F \Leftrightarrow \sum \frac{N_i}{\alpha l_i} = F$$

$$\left\{ \sin\theta_i = \frac{f}{l_i} \quad \Leftrightarrow \quad \sin\theta_i = \frac{1}{\alpha l_i} \right\} \Rightarrow \alpha = \frac{1}{f}$$

$$\Rightarrow \sum \frac{N_i f}{l_i} = F$$

$$Q = \sum \frac{N_i}{l_i} = \frac{F}{f}$$

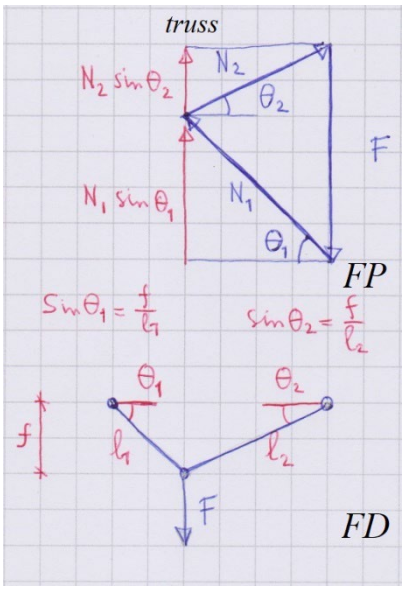

Using the reciprocity of the properties between the truss and funicular structures, it is possible to derive a similar set of relations for the funicular system. The equivalent coefficient *α** is the reciprocal value of the thrust *H* of the FP.

due to reciprocity

$funicular$:

$$\sum \frac{l_i}{N_i} = \alpha^* l \Rightarrow \sum \frac{l}{\alpha^* N_i} = l$$

$compatibility\ equation$:

$$\sum l_i \sin\theta_i = l \Leftrightarrow \sum \frac{l_i}{\alpha^* N_i} = l$$

$$\left\{\sin\theta_i = \frac{H}{N_i} \quad \Leftrightarrow \quad \sin\theta_i = \frac{1}{\alpha^* N_i}\right\} \Rightarrow \alpha^* = \frac{1}{H}$$

$$\Rightarrow \sum \frac{l_i H}{N_i} = l$$

$$\sum \frac{l_i}{N_i} = \frac{l}{H}$$

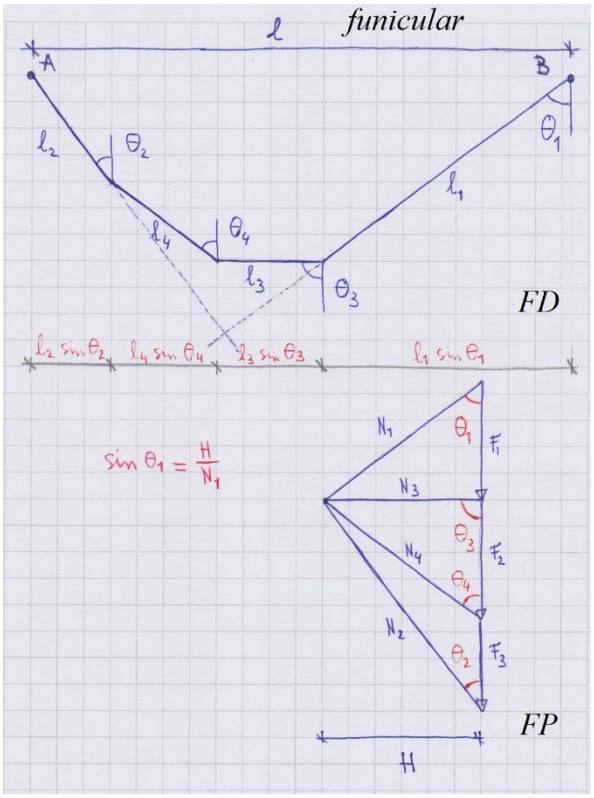

This chapter shows the relation between funicular systems and their reciprocal truss structures. It is interesting that there are multiple solutions that ensure equilibrium for the type of statically indeterminate trusses discussed in this chapter which means its force polygon changes and thus the form diagram of the funicular systems changes accordingly. But what does not change in this situation are the form diagram of the truss and the force polygon of the funicular system.

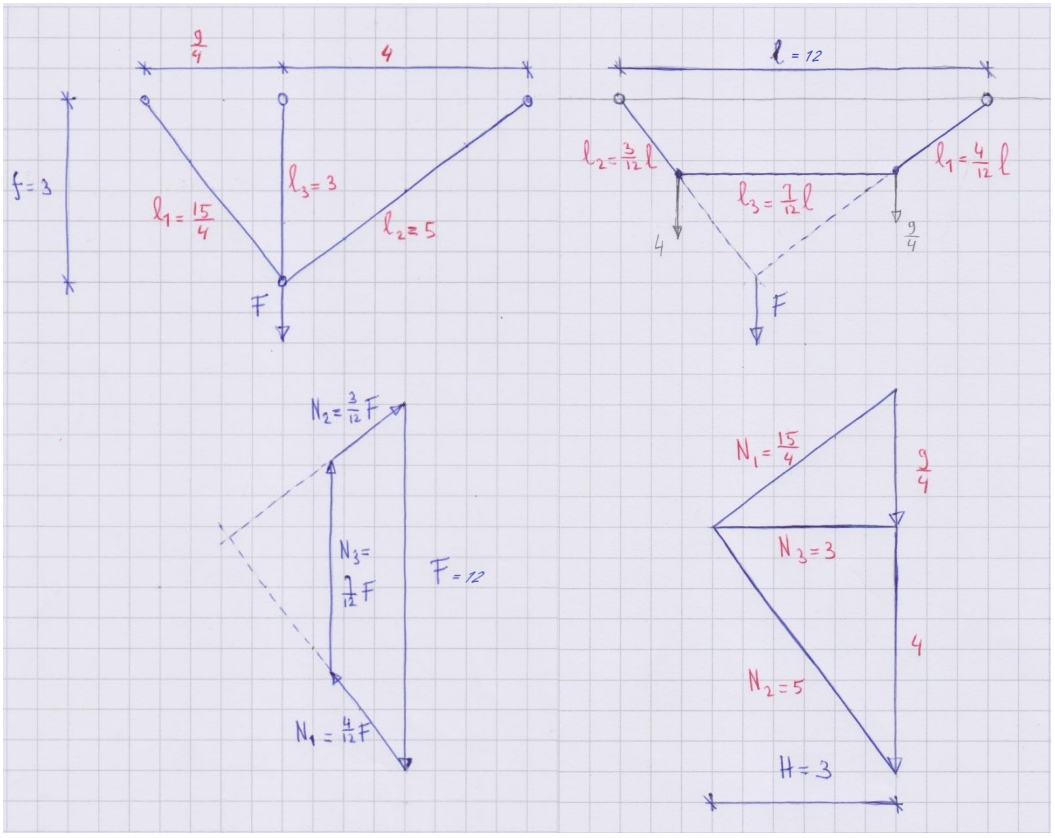

The next two diagrams show an overview of the reciprocal relation between funicular systems and truss structures.

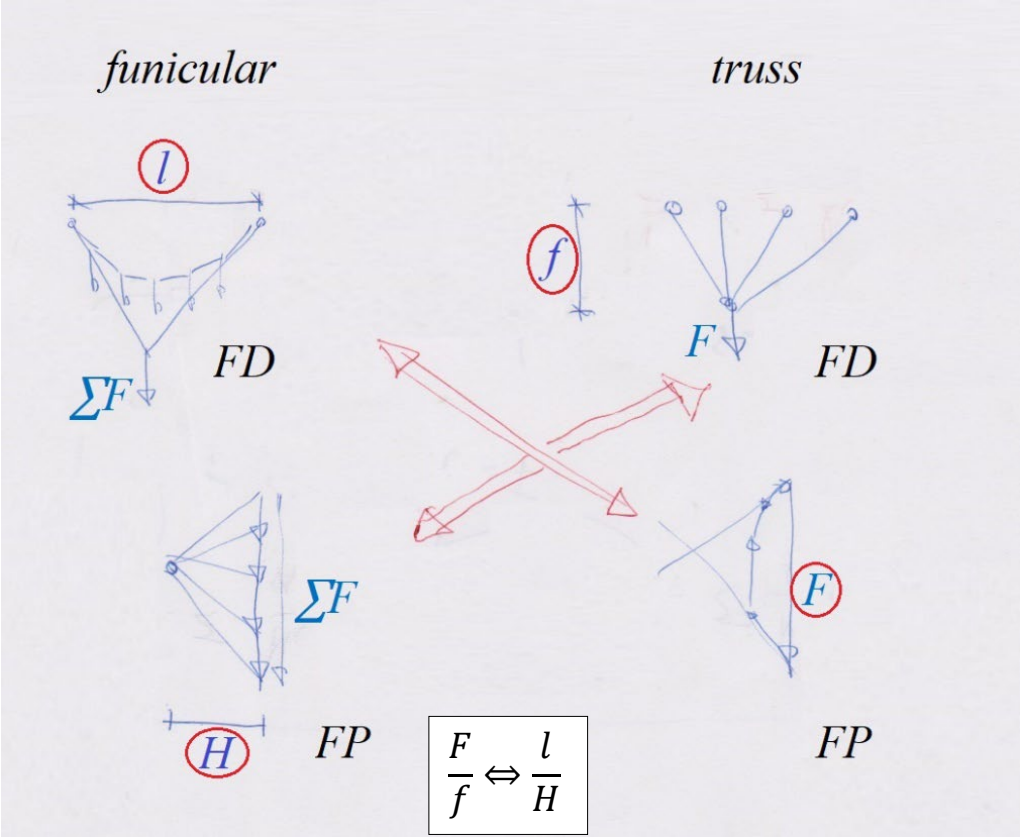

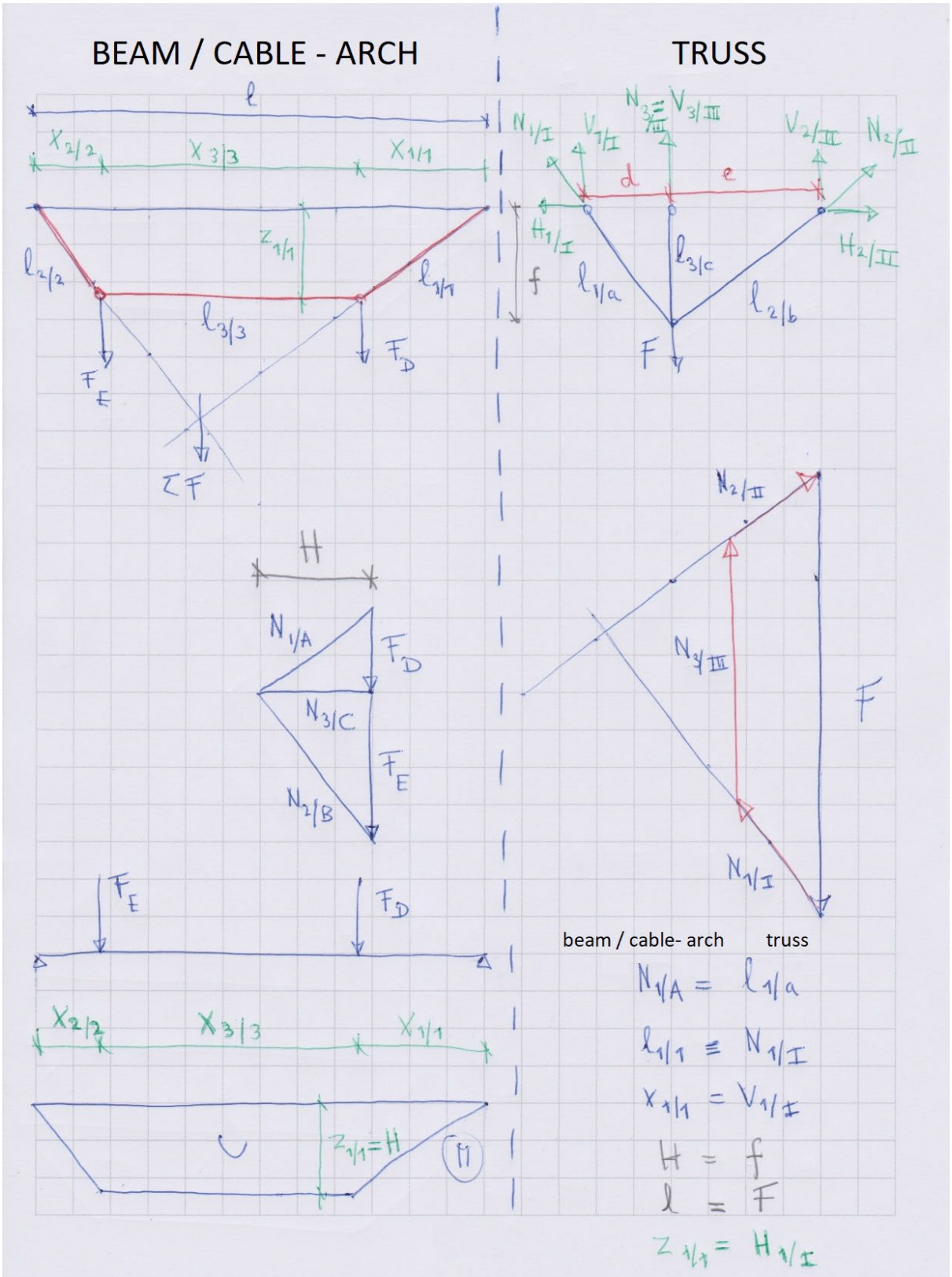
BEAM / CABLE - ARCH
TRUSS
beam / cable- arch
truss
N1/A = l1/a
l1/1 ≡ N1/I
X1/1 = V1/I
H = f
l = F
Z1/1 = H1/I

3.6 Maxwell's load path of cables and arches

Maxwell's load path theorem [46] is well known, especially in relation to trusses, and basically states that the difference in the sum of the tension load paths (product of the axial force N_i in a member and its length l_i) and the compression load paths is equal to the dot product of the external loads and reactions and their position vectors from an arbitrary point. The latter comes down to the dot product of the magnitude of the external force and its line of action, the distance of the external force travels over its line of action in relation to the supports of the structure. Maxwell's theorem means that the internal energy generated by the axial forces is equal to the work done by external loads. Maxwell's theorem is usually applied to truss structures, hence members which are in tension and compression.

$$Maxwell\ load\ path:$$
$$\underbrace{\sum_i N_{t_i} l_{t_i} - \sum_i N_{c_i} l_{c_i}}_{internal\ forces} = \underbrace{\sum_i \vec{F_i} \cdot \vec{r_i}}_{loads,\ reactions}$$

If the theorem is applied to cables and arches then the internal forces are only compression or tension respectively.
Maxwell theorem can be used to find a minimal load path by minimizing the total volume of the structure for a given allowable σ stress in all members.

$$optimal\ load\ path, minimum\ volume:$$
$$min \sum_i V_i = min \sum_i A_i l_i = min \frac{1}{\sigma} \sum_i |N_i| l_i$$

In the first example, a precursor for load path of a dome in section 7.1, the optimum ratio between the rise f^* and the span l of a parabolic arch with a uniformly distributed load will be found. The span will remain constant [47].

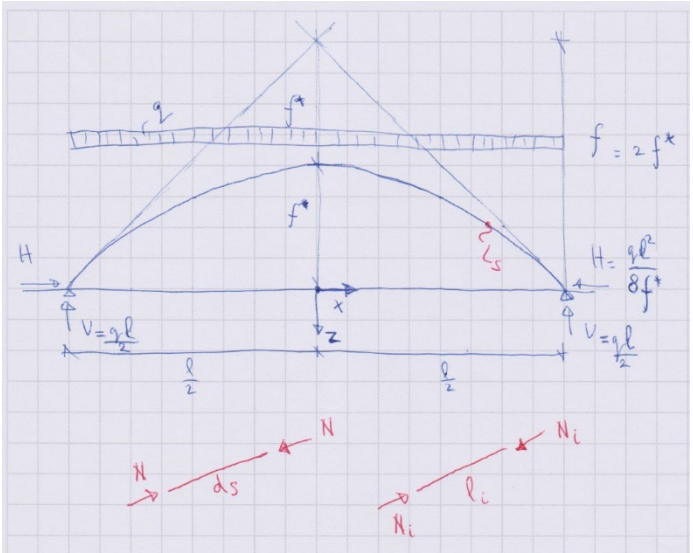

Because of the shape function the geometry of the parabolic arch is fixed. The shape function is a function of the rise f^* of the arch. Thus the only parameter determining the optimization is the rise f^*, the shape coefficients α_i remain constant for every value of f^*.

$$z = f^* \frac{(l^2 - 4x^2)}{l^2};\ L_s = \int_{-\frac{1}{2}l}^{\frac{1}{2}l} ds\,;\, ds = \left(1 + \left(\frac{dz}{dx}\right)^2\right)^{\frac{1}{2}} dx$$

$$ds = \left(1 + \frac{64 f^{*2} x^2}{l^4}\right)^{\frac{1}{2}} dx$$

$$N = [(H)^2 + (V)^2]^{\frac{1}{2}} = \left(\left(\frac{ql^2}{8f^*}\right)^2 + (qx)^2\right)^{\frac{1}{2}} = \frac{q(l^4 + 64 f^{*2} x^2)^{\frac{1}{2}}}{8f^*}$$

$$Nds = \left(\frac{q(l^4 + 64 f^{*2} x^2)^{\frac{1}{2}}}{8f^*}\right)\left(1 + \frac{64 f^{*2} x^2}{l^4}\right)^{\frac{1}{2}} dx = \frac{q(l^4 + 64 f^{*2} x^2)}{8 l^2 f^*} dx$$

the total load path:

$$V = \frac{1}{\sigma}\int_{-\frac{1}{2}l}^{\frac{1}{2}l} N\, ds = \frac{1}{\sigma}\int_{-\frac{1}{2}l}^{\frac{1}{2}l} \frac{q(l^4 + 64 f^{*2} x^2)}{8 l^2 f^*} dx\ = \frac{ql(3l^2 + 16 f^{*2})}{24 f^* \sigma} \rightarrow min$$

the lowest value of the load path gives the optimal ratio:

$$\Rightarrow \frac{d}{df^*} = \frac{ql(16 f^{*2} - 3l^2)}{24 f^{*2}} = 0 \Rightarrow f^* = \frac{\sqrt{3}}{4} l$$

$$\frac{f^*}{l} = \frac{\sqrt{3}}{4} \approx 0.433$$

In the next example, a precursor for section 3.7, the optimum ratio between the rise f^* and the span l of a discretized arch with point loads will be found. The shape coefficients of the form diagram α_i and rise of the point of application of the total load f will be used. Also in this example the geometry is fixed and the horizontal spacing x_i between the loads remains constant.

$$\sum_i N_i\, l_i = min$$

$$N_i l_i = V_i \triangle z_i + H x_i$$

$$with:\ \triangle z_i = \alpha_i f; Hf = C_{Hf} = \text{constant}$$

$$\Rightarrow N_i l_i = V_i \alpha_i f + \frac{C_{Hf}}{f} x_i$$

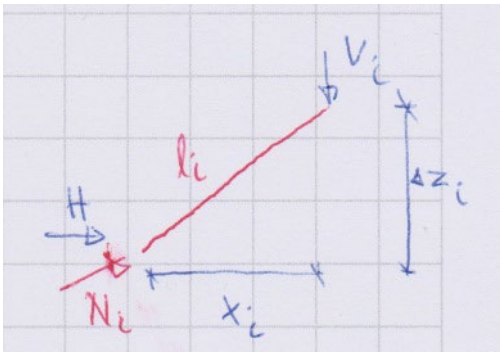

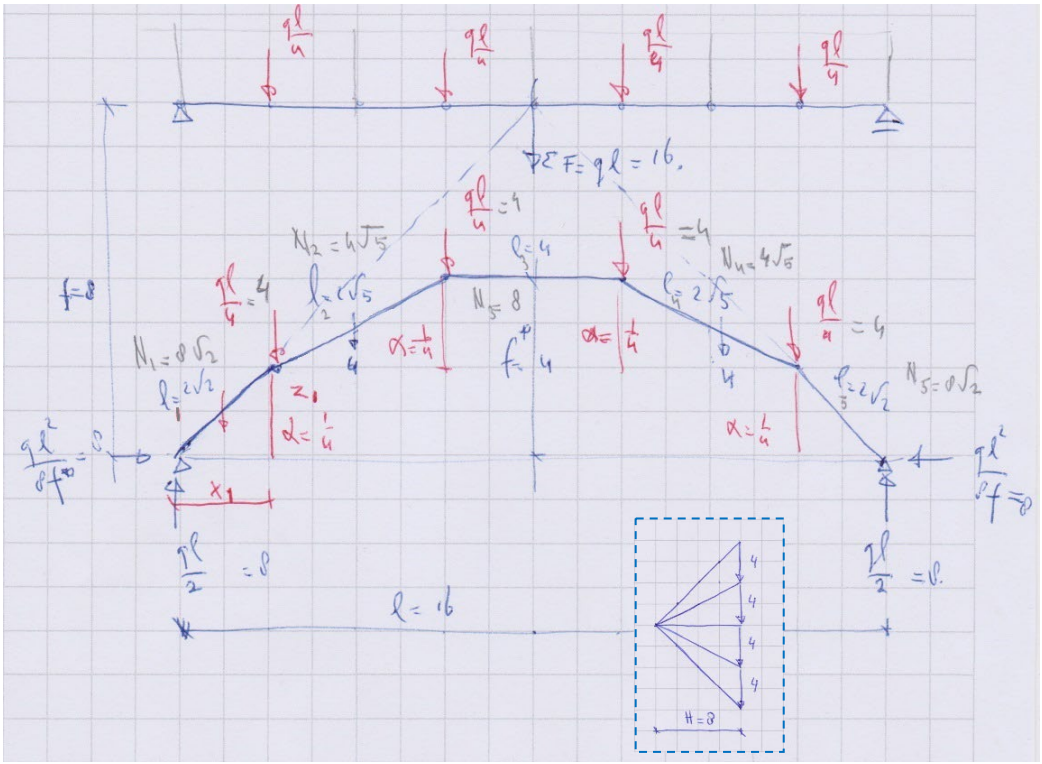

constant:
$Hf = 8 \cdot 8 = 64$

the total load path:
$N_1 l_1 + N_2 l_2 + N_3 l_3 + N_4 l_4 + N_5 l_5 \rightarrow \min$

$$\left(8\frac{1}{4}f + \frac{64}{f}2\right) + \left(4\frac{1}{4}f + \frac{64}{f}4\right) + \left(\frac{64}{f}4\right) + \left(4\frac{1}{4}f + \frac{64}{f}4\right) + \left(8\frac{1}{4}f + \frac{64}{f}2\right) \rightarrow min$$

$$\Rightarrow 6f + \frac{1024}{f} = \frac{6f^2 + 1024}{f} \rightarrow min$$

the lowest value of the load path gives the optinal ratio:

$$\Rightarrow \frac{d}{df} = \frac{6f^2 - 1024}{f^2} = 0 \Rightarrow f = \frac{16\sqrt{6}}{3} \approx 13.064$$

$$f^* = \frac{f}{2} = \frac{16\sqrt{6}}{6} \approx 6.532 \Rightarrow \frac{f^*}{l} = \frac{\sqrt{6}}{6} \approx 0.408$$

$$Hf = 64 \Rightarrow H = \frac{64}{\frac{16\sqrt{6}}{3}} = 2\sqrt{6} \approx 4.899$$

The result corresponds to that to that one of the parabolic arch. There is a small difference due to the discretization.

The only parameter as object for optimization when Maxwell's theorem is used in this example is *f*, in other words only the span – rise ratio can be altered. Because the product *Hf* is constant, the form diagram and the force polygon change in reciprocal ways.

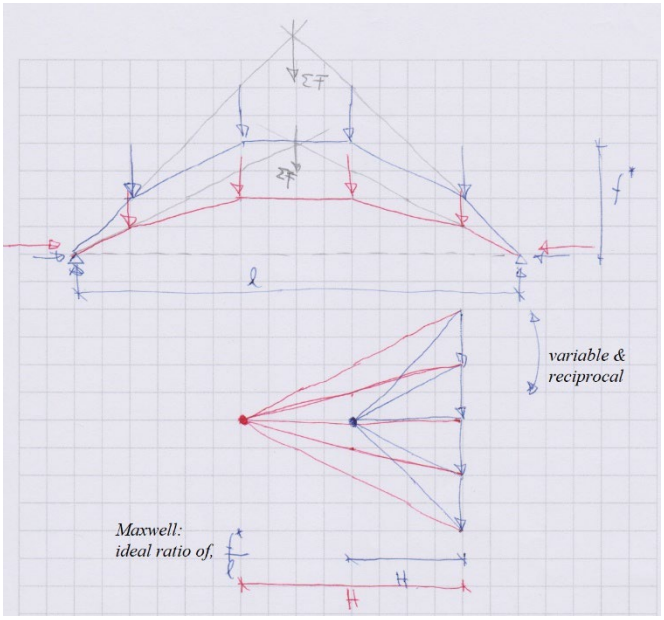

What cannot be examined by using Maxwell's theorem as described in the previous examples is the determination of the position of the loads along the axis of the arch, thus different values for the shape coefficients α_i and the horizontal spacing x_i between the different loads along the arch or cable that make up the total load $\sum F$. This total load can be subdivided in different loads in infinite ways provided the form diagram stays within the bounding envelop and the two reactions left and right of the arch follow the slope of the boundary envelop so the vertical support reactions remain unaltered.

When Maxwell's theorem is used while keeping the force polygon constant, notably the horizontal reaction *H*, it results in an optimal arch or cable with a rise f^* that goes to zero. The reason for this is that although the product of *H* and its line of action *l* remains constant, the line of action of the loads goes to zero and thus the external work done decreases and thus the lower the total load path the more optimal the structure according Maxwell's theorem. But a very shallow arch or cable is not practical.

The next section discusses how Maxwell's theorem is used to test solutions for an optimal position for the subdivided loads, with different values for the horizontal spacing x_i and the shape coefficients α_i. This principle is a result of the reciprocal properties of cables and trusses.

3.7 Variational principles of cables and trusses

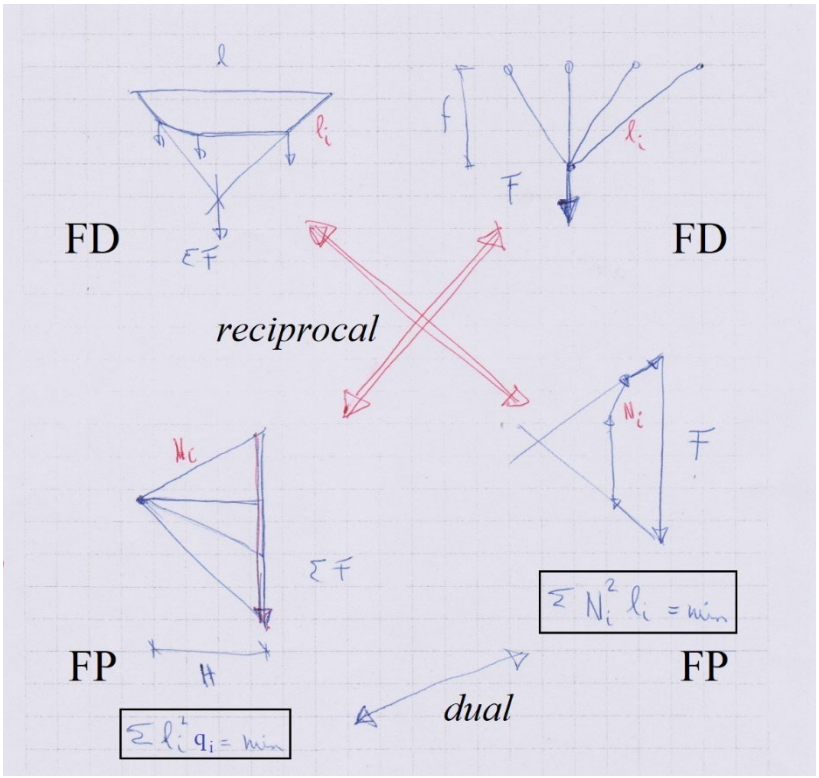

As is observed that for a statically indeterminate truss with any given number of branches there are an infinite amount of solutions possible which ensure equilibrium. In the case of the truss the topology of the form diagram remains constant for each alternative solution of the force diagram, although its solution remains within the bounding envelop. The redundancies can be solved by using the variational method of the lowest complementary energy and taking into account the relations of equilibrium.

$$E_{compl,N} = \sum_i N_i^2 \, l_i \rightarrow minimum$$

It is also observed that in general for a given load there are equal amounts of configurations possible for the cable which ensure equilibrium within its bounding envelope. The force polygon of the cable is the reciprocal diagram of the form diagram of the truss. In section 3.3 it was shown that the reciprocal parameters of the cables / arches and trusses are the axial force of a member and the length a member, and vice versa. The dual relation for an unloaded cable (network) is the functional of the force density method, which is equivalent to the result of a form finding process by means of solved force density equations.
The functional of the force density method $\overline{\Pi}$ is the variational principle of the force density method.

$$\overline{\Pi} = \sum_i l_i^2 \, q_i \rightarrow minimum$$

If the state of self-stress (*s* in the Maxwell-Calladine equation) is not zero for a truss it is statically indeterminant which redundants can be solved with the variational method of the lowest complementary energy. If the state of self-stress is not zero for a cable its (unloaded) equilibrium geometry has to be form found which can be done with the variational principle of the force density method.

This is explained with the next example, a small 3D anti-clastic cable configuration comprising of 4 ties. All nodes except node 1, which is to be form found, are pinned. The dimension of the design space is 2 by 2 by 2, and chosen force density of all ties is equal to 2.

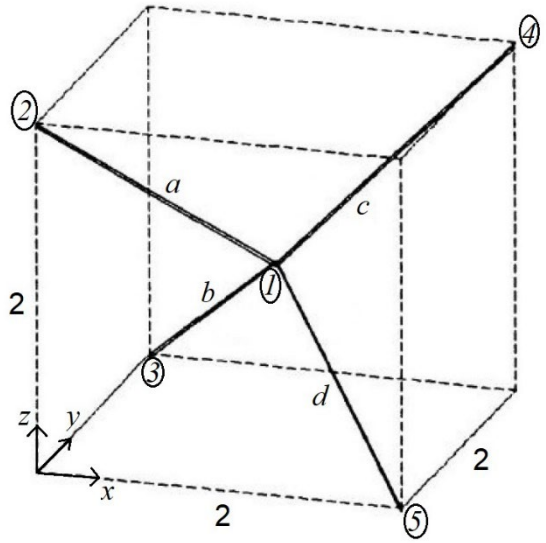

$$anti-clastic:$$
$$dj-b-k=m-s$$

$$3\cdot 5-4-4\cdot 3=-1$$
$$\rightarrow m-s=-1$$
$$m=0$$

In order to solve the coordinates of node 1 first the force density equation are solved.

$$\frac{N_a}{l_a}(x_1-x_2)+\frac{N_b}{l_b}(x_1-x_3)+\frac{N_c}{l_c}(x_1-x_4)+\frac{N_d}{l_d}(x_1-x_5)=0$$
$$\frac{N_a}{l_a}(y_1-y_2)+\frac{N_b}{l_b}(y_1-y_3)+\frac{N_c}{l_c}(y_1-y_4)+\frac{N_d}{l_d}(y_1-y_5)=0$$
$$\frac{N_a}{l_a}(z_1-z_2)+\frac{N_b}{l_b}(z_1-z_3)+\frac{N_c}{l_c}(z_1-z_4)+\frac{N_d}{l_d}(z_1-z_5)=0$$

$$with: q=\frac{N_a}{l_a}=\frac{N_b}{l_b}=\frac{N_c}{l_c}=\frac{N_d}{l_d}=2$$

$$and: x_2=x_3=y_2=y_5=z_3=z_5=0$$
$$x_4=x_5=y_3=y_4=z_2=z_4=2$$

$$\rightarrow solve: x_1=y_1=z_1=1$$

The variational principle of the force density method will now be applied to check the previously found coordinates. An established theorem of the force density method is: for each equilibrium state of an unloaded network the sum of the squared lengths weighted by the force densities is minimal [48, 49].

$$\overline{\Pi} = \sum_i l_i^2 \, q_i \rightarrow minimum$$
$$q(l_a^2 + l_b^2 + l_c^2 + l_d^2) \rightarrow minimum$$

$$with: q = 2$$

$$l_a^2 = (x_1 - 0)^2 + (y_1 - 0)^2 + (z_1 - 2)^2$$
$$l_b^2 = (x_1 - 0)^2 + (y_1 - 2)^2 + (z_1 - 0)^2$$
$$l_c^2 = (x_1 - 2)^2 + (y_1 - 2)^2 + (z_1 - 2)^2$$
$$l_d^2 = (x_1 - 2)^2 + (y_1 - 0)^2 + (z_1 - 0)^2$$

$$\rightarrow 2(4x_1^2 + 4y_1^2 + 4z_1^2 - 8x_1 - 8y_1 - 8z_1 + 24) \rightarrow minimum$$
$$\frac{\partial}{\partial x_1} = 16x_1 - 16 = 0 \rightarrow x_1 = 1$$
$$\frac{\partial}{\partial y_1} = 16y_1 - 16 = 0 \rightarrow y_1 = 1$$
$$\frac{\partial}{\partial z_1} = 16z_1 - 16 = 0 \rightarrow z_1 = 1$$

As expected, the results are equal. The length of the ties are now known and the axial forces can be determined which represent the pre-stress of the unloaded network.

This example demonstrates the dual relation of cables and trusses. For statically indeterminant trusses the sum of the squared bar axial forces weighted by their length has to be minimal. Similarly, the equilibrium geometry of cable structures can be determined from the sum of the squared tie lengths weighted by their force densities has to be minimal.

In section 3.4 it was observed that in case of a state of self-stress for a certain type of geometry the total force density *Q* is equal to zero, these geometries are synclastic. For anti-clastic geometries, such as tent structures, the total force density of a state of self-stress is positive and not zero. Anti-clastic geometries can be pre-stressed which results in an overall state of stress in tension, because pre-stress of an anti-clastic geometry is possible without an

external surface load *p*. Synclastic structures cannot be submitted to a pre-stress without an external load *p*.

To illustrate this principle, consider the anti-clastic form found geometry will be changed into a synclastic geometry by bringing the two top members down to the same plane as the other two members. For this synclastic geometry there is a state of self-stress, two members in compression and two in tension.

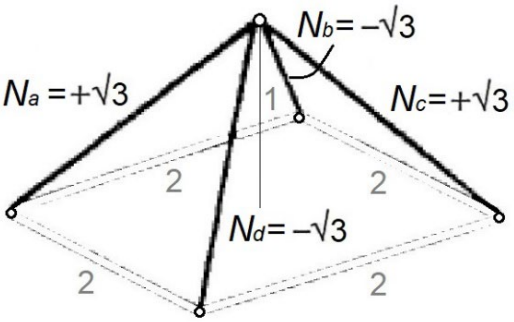

$$synclastic:$$
$$dj - b - k = m - s$$

$$3 \cdot 5 - 4 - 4 \cdot 3 = -1$$
$$\rightarrow m - s = -1$$
$$m = 0$$

$$state\ of\ self-stress:$$

$$statically\ indeterminate\ synclastic\ example:$$
$$Q = \frac{N_a}{l_a} + \frac{N_b}{l_b} + \frac{N_c}{l_c} + \frac{N_d}{l_d} = \frac{\sqrt{3}}{\sqrt{3}} - \frac{\sqrt{3}}{\sqrt{3}} + \frac{\sqrt{3}}{\sqrt{3}} - \frac{\sqrt{3}}{\sqrt{3}} = 0$$

$$statically\ indeterminate\ anti-clastic\ example:$$
$$Q = \frac{N_a}{l_a} + \frac{N_b}{l_b} + \frac{N_c}{l_c} + \frac{N_d}{l_d} = 2 + 2 + 2 + 2 = 8$$

If the geometry of an anti-clastic surface goes from a discretized network to a continuous field (function) it becomes a membrane or a tent.

When the network is increasingly refined its upper limit case of summing the individual force densities of the increasing number of members results in the total force density *Q* going to infinity.

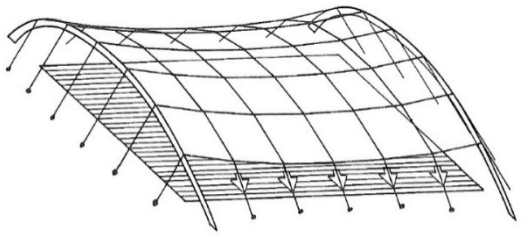

$$anti-clastic:$$
$$\Rightarrow \left[Q = \sum \frac{N_i}{l_i} \Rightarrow \infty\right] \Rightarrow$$

Figure 26 anti-clastic network / surface, image right of membrane by courtesy of Arno Pronk

The energy and functional relations are also applicable to 3D truss and cable structures. For soap films, such as a catenoid the potential surface energy is minimized, the constitutive relation does not influence the shape [50]. The catenoid is a minimal surface, thus it's mean curvature is equal to zero, as a consequence of the potential surface energy being proportional to the surface area [51, 52], and being minimal. A soap film has no out of plane loads.

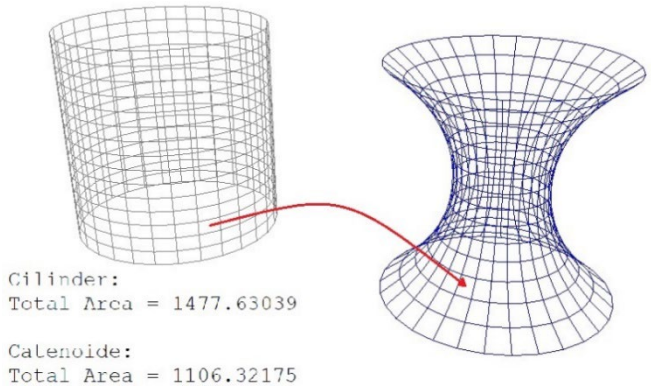

Figure 27 area optimization of cylinder [image 52]

$$catenoid: minimal\ surface$$
$$H = \frac{1}{2}(\kappa_1 + \kappa_2) = 0$$
$$H = mean\ curvature$$
$$E_{pot,surface} = D \sum_i l_i^2 \rightarrow minimum$$
$$D = constitutive\ constant$$
$$with: p_z = 0$$

The 3D statically indeterminate truss is the reciprocal of a (soap film) catenoid. The 2D version of the truss is the reciprocal of the catenary, the catenoid is the surface of revolution of the catenary. The loads of the catenary are a result of the hoop force of the catenoid, and are not out of plane loads.

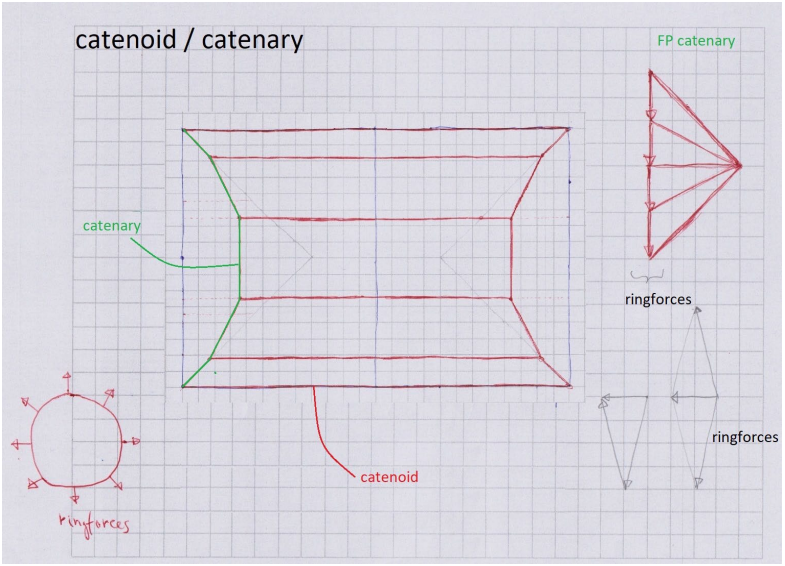

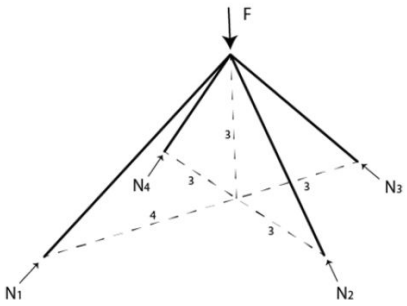

If the slopes of the lengths l_i are set, the force density can be replaced by the axial force N_i.

$$\overline{\Pi} = \sum_i l_i^2\ q_i \rightarrow minimum$$
$$with: q_i = \frac{N_i}{l_i} = \frac{H}{x_i}, if\ the\ network\ is\ loaded\ and\ the\ FP\ is\ set\ \rightarrow$$
$$E_{pot,tot} = \sum_i l_i^2\ N_i \rightarrow minimum$$

As an example the shape of a symmetric arch with two point loads will be found.

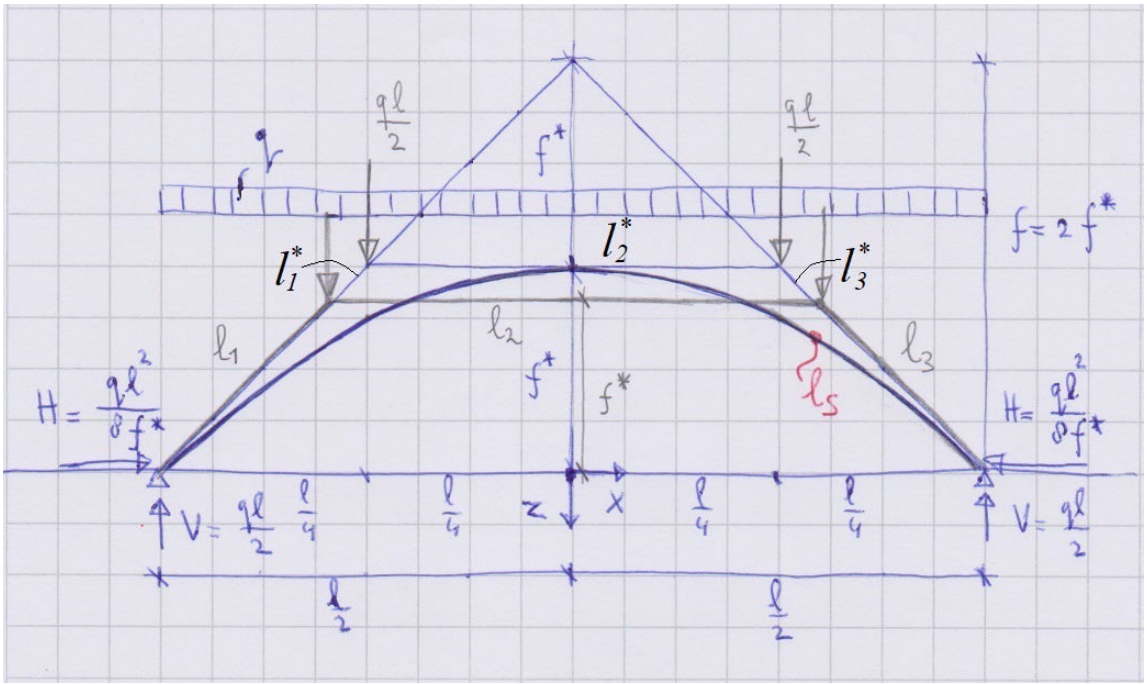

The example is derived from an arch with a uniformly distributed load, which is split into the two equivalent point loads. It is the first step from the development of drawing a bending moment diagram of a thrust line from one point load (the total load $\sum F$) to a uniformly distributed load which results in a parabola. This results in the position of the two loads at one quarter of the span at either side from the supports. The variational method is used in which the equilibrium equations are replaced by the minimisation of the potential energy. The horizontal thrust H is constant and the arc segments have the same slopes as their equivalent rays in the force polygon: x_i is set by l_i.

$$E_{pot,tot} = \sum_i l_i^2 N_i \rightarrow minimum$$

$$E_{pot,tot} = l_1^2 \frac{1}{2}\sqrt{2}ql + l_2^2 \frac{1}{2}ql + l_3^2 \frac{1}{2}\sqrt{2}ql \rightarrow min$$

$with\ compatibility$:

$$l - (x_1 + x_2 + x_3) = 0 \Rightarrow l - \left(\frac{1}{2}\sqrt{2}l_1 + l_2 + \frac{1}{2}\sqrt{2}l_3\right) = 0 \Rightarrow l_1 = \sqrt{2}l - \sqrt{2}l_2 - l_3$$

$$\sum \frac{\partial E_{pot,tot}}{\partial l_2} = 0 \Rightarrow l_3 = \sqrt{2}l - l_2\left(\sqrt{2} + \frac{1}{2}\right)$$

$$\sum \frac{\partial E_{pot,tot}}{\partial l_3} = 0 \Rightarrow l_2 = l - \sqrt{2}l_3$$

$$\Rightarrow l_1 = l_3 = \left(1 - \frac{1}{2}\sqrt{2}\right)l;\ l_2 = (2 - \sqrt{2})l$$

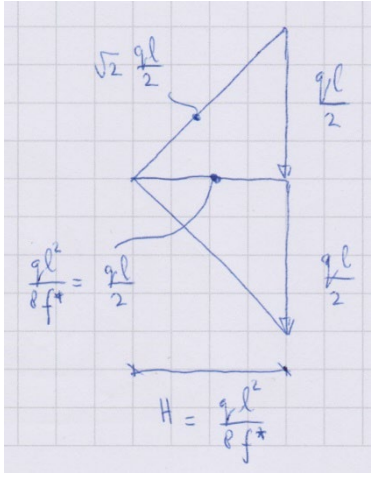

The result of this procedure is surprising, it is not the same as the first step of splitting the total load *∑F* resulting in a parabola. The length of the segments of the arch either side of the point load is equal. The total load path according to Maxwell is lower than the “parabolic” solution, although the total length l_s of the arch is approximately the same.

$$N_1 = \sqrt{2}\frac{ql}{2} : N_2 = \frac{ql}{2} : N_3 = \sqrt{2}\frac{ql}{2}$$

$$"parabola"$$
$$l_1^* = l_3^* = \frac{1}{4}\sqrt{2}\, l : l_2^* = \frac{1}{2} l$$
$$Maxwell: N_1 l_1^* + N_2 l_2^* + N_3 l_3^* = \frac{3}{4} q l^2 = 0.75\, q l^2$$
$$l_s = \frac{\sqrt{2}+1}{2} l \approx 1.20710\, l$$
$$f^* = \frac{1}{4} l = 0.25\, l$$

$$"catenary"$$
$$l_1 = l_3 = \left(1 - \frac{1}{2}\sqrt{2}\right)\, l : l_2 = \left(2 - \sqrt{2}\right) l$$
$$Maxwell: N_1 l_1 + N_2 l_2 + N_3 l_3 = \frac{1}{2}\sqrt{2} q l^2 \approx 0.70710\, q l^2$$
$$l_s = 4 - 2\sqrt{2}\, l \approx 1.17157\, l$$
$$f^* = \frac{\sqrt{2}-1}{2} l \approx 0.20710\, l$$

In the next example the same total load *∑F* will be split into four equal point loads. Also this conventionally results in a discretised version of a parabola in which the arch segments are the tangents of the parabola.

Again the segments of the arch halfway the loads and the supports are exactly equal. If the point loads with evenly distributed along these segments we get a constant load along the axis of the arch, in other words we have the shape of a catenary. The total load path is lower than the parabolic solution with approximately the same total length. Again the horizontal thrust *H* is constant and arc segments have the same angles as their equivalent rays in the force polygon.

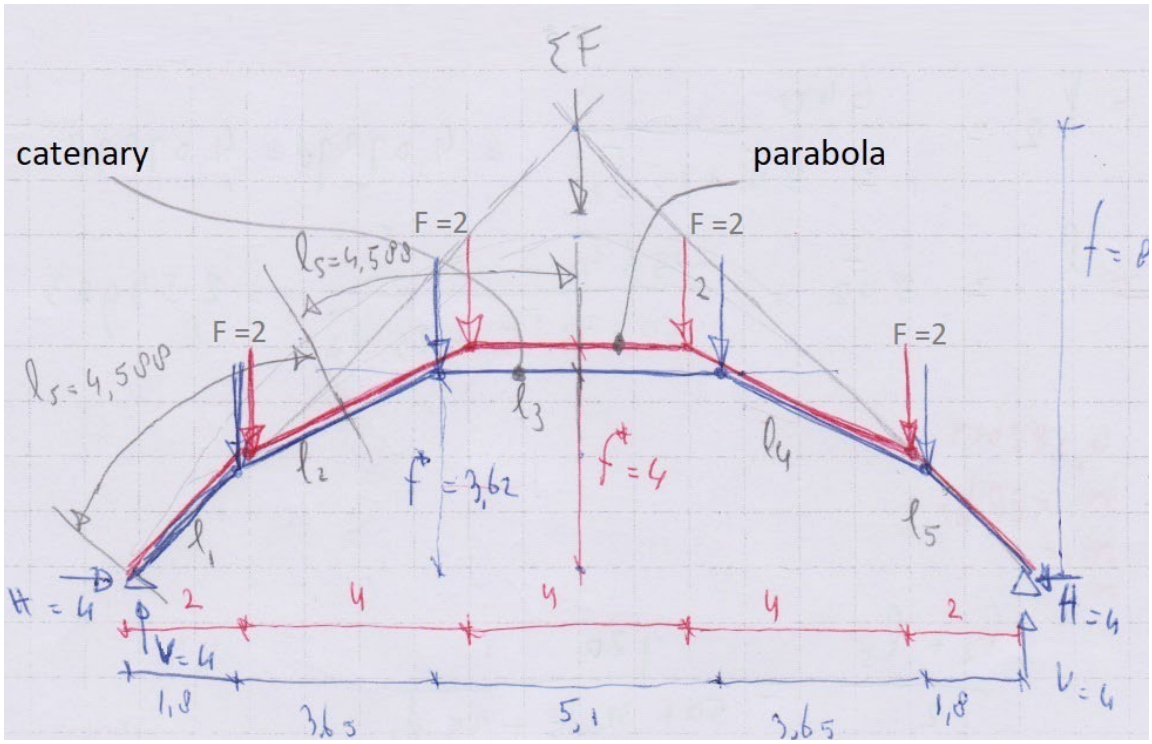

$$E_{pot,tot} = \sum_i l_i^2 N_i \rightarrow minimum$$

$$E_{pot,tot} = l_1^2 2\sqrt{2} + l_2^2 2\sqrt{5} + l_3^2 4 + l_4^2 2\sqrt{5} + l_5^2 4\sqrt{2} \rightarrow min$$

with compatability:

$$l - (x_1 + x_2 + x_3 + x_4 + x_1) = 0 \Rightarrow 16 - \left(\frac{1}{2}\sqrt{2}l_1 + \frac{2}{5}\sqrt{5}l_2 + l_3 + \frac{2}{5}\sqrt{5}l_4 + \frac{1}{2}\sqrt{2}l_5\right) = 0$$

with symmetry: $l_1 = l_5 : l_2 = l_4$

$$\Rightarrow l_1 = 8\sqrt{2} - \frac{2}{5}\sqrt{10}l_2 - \frac{1}{2}\sqrt{2}l_3$$

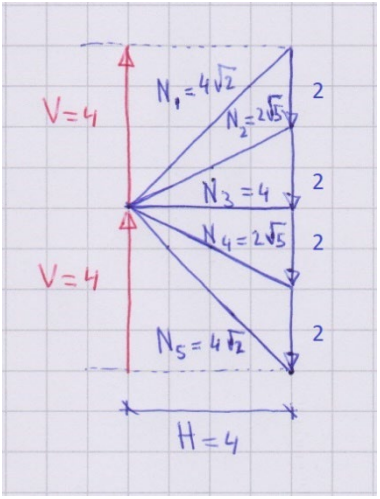

$$\sum \frac{\partial E_{pot,tot}}{\partial l_2} = 0 \Rightarrow l_3 = 16 - \frac{4}{5}\sqrt{5}l_2 - \frac{5}{8}\sqrt{2}l_2$$

$$\sum \frac{\partial E_{pot,tot}}{\partial l_3} = 0 \Rightarrow l_2 = 40\sqrt{5} - \frac{5}{2}\sqrt{5}l_3 - \frac{5}{4}\sqrt{10}l_3$$

$$\Rightarrow l_1 = l_5 = \frac{400}{50 + 32\sqrt{5} + 25\sqrt{2}} : l_2 = l_4 = \frac{640}{50 + 32\sqrt{5} + 25\sqrt{2}} : l_3 = \frac{800}{50 + 32\sqrt{5} + 25\sqrt{2}}$$

$$l_1 + \frac{1}{2}l_2 = \frac{l_1 + l_2}{2} = \frac{720}{50 + 32\sqrt{5} + 25\sqrt{2}} \approx 4.588$$

From these examples and the rules of reciprocity we can conclude the following for this method. It provides for an arch (or cable) the thrust line with the most evenly "distributed" load along its axis with the lowest total load path with the longest possible total length, the catenary.
In other words: if there are more modes of displacement kinematically admissible whilst considering the arch as flexible (cable or thrust line), the shape with the minimum potential energy will prevail.
The catenary is the revolved curve that forms the catenoid. The loads of the catenary are actually the resolved components of the hoop forces, and can therefore be considered as the in-plane tension and not as out-of-plane loads.

Maxwell's method in these cases with fixed internal axial forces N_i would produce a near flat thrust line, yet it can be used to find the optimal span – rise ratio.

$N_1 = N_5 = 4\sqrt{2}: N_2 = N_4 = 2\sqrt{5}: N_3 = 4$

"$parabola$"
$l_1 = l_5 = 2\sqrt{2}: l_2 = l_4 = 2\sqrt{5}: l_3 = 4$

$Maxwell: N_1 l_1 + N_2 l_2 + N_3 l_3 + N_4 l_4 + N_5 l_5 = 88$

$l_s = 4\sqrt{2} + 4\sqrt{5} + 4 \approx 18.60112$
$f^* = \frac{1}{2}\sqrt{2} l_1 + \frac{1}{5}\sqrt{5} l_2 = 4$

"$catenary$" / $discretized\ catenary$
$l_1 = l_5 = \frac{400}{50 + 32\sqrt{5} + 25\sqrt{2}}: l_2 = l_4 = \frac{640}{50 + 32\sqrt{5} + 25\sqrt{2}}: l_3 = \frac{800}{50 + 32\sqrt{5} + 25\sqrt{2}}$

$Maxwell: N_1 l_1 + N_2 l_2 + N_3 l_3 + N_4 l_4 + N_5 l_5 = \frac{3200\sqrt{2} + 2560\sqrt{5} + 2880}{50 + 32\sqrt{5} + 25\sqrt{2}} \approx 85.71702$

$l_s = \frac{2880}{50 + 32\sqrt{5} + 25\sqrt{2}} \approx 18.35452$
$f^* = \frac{1}{2}\sqrt{2} l_1 + \frac{1}{5}\sqrt{5} l_2 \approx 3.62667$

If the discretized catenary, the result of the minimization of the potential energy, is compared with the analytical solution it can be concluded that the segments have the same tangents of the catenary function like with the parabola as the result of truncation, see section 2.5. The energy solution is an approximation, the finer the discretization the higher the rise will be and the closer to the analytical solution the result will be.

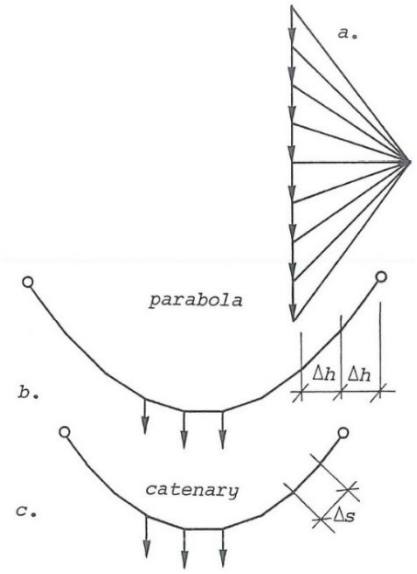

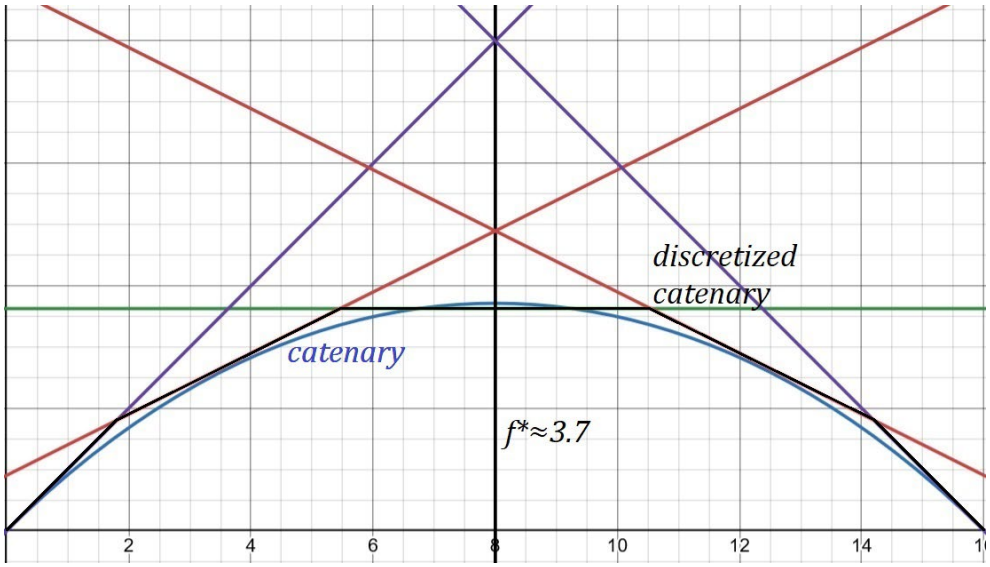

Comparing the results of the catenary function to those for the discretized catenary the fit is very close.
A last remark in this section, the force polygon for the discretized parabola and catenary is the same, due to the differing distance of the applied loads along their axis the two form diagrams are achieved.

$$catenary$$

$$q = \frac{F \cdot 4}{l_s} = \frac{2 \cdot 4}{18.35452} \approx 0.43586 \colon H = 4 \colon l = 16$$

$$z(x) = \frac{H}{q}\left(\cosh\frac{q(x - l/2)}{H} - \cosh\frac{ql/2}{H}\right)$$

$$\Rightarrow z(x) = \frac{4}{0.43586}\left(\cosh\frac{0.43586\left(x - \frac{16}{2}\right)}{4} - \cosh\frac{0.43586 \cdot \frac{16}{2}}{4}\right)$$

$$= 9.17726\left(\cosh\frac{0.43586(x - 8)}{4} - \cosh(0.87172)\right)$$

$$l_s = \int_0^{16}\left(1 + \left(\frac{dz}{dx}\right)^2\right)^{\frac{1}{2}} dx = \int_0^{16}\cosh\left(\frac{x - 8}{9.17726}\right) dx \approx 18.10478$$

$$f^* = z(8) \approx 3.71335$$

3.8 Overview of variational principles

Short overview of the variational principle as given in this chapter, with their respective characteristics and applications.

- variational principle of the force density:

$$\overline{\Pi} = \sum_i l_i^2 \, q_i \rightarrow minimum$$

  - use to find the equilibrium geometry for an unloaded network
  - the length and the angles of the bars of the network are not fixed (nodes of network are free)

- variational principle of complementary energy:

$$E_{compl,tot} = \sum_i N_i^2 \, l_i \rightarrow minimum$$

  - to solve the redundancies of a loaded truss or network in equilibrium, to find the correct force polygon
  - the length and the angles of the bars of the network are fixed, the form diagram is fixed
    (nodes are fixed)

- variational principle of potential energy:

$$E_{pot,tot} = \sum_i l_i^2 \, N_i \rightarrow minimum$$

  - to optimize the form diagram by minimizing its developed length or surface area (N_i = constant) or total load path ($N_i \neq$ constant)
  - angles of forces and bars are fixed, the force polygon is fixed (nodes of network are free but with conditions)

3.9 Similarities of methods for examining extrema

In section 3.7 the variational method of minimizing the potential energy was used. This method has a similarity to other methods for examining extremes of a function, such as the method of least squares and the stretched grid method. These methods have in common a quadratic function which reaches its minimum of maximum value when its derivative is equal to zero.

$$\overline{\Pi} = \sum_i l_i^2 \, q_i \rightarrow minimum$$

$$\sum_{i=1} \frac{\partial \overline{\Pi}}{\partial l_i} = 0$$

The method of least squares minimizes the sum of squared residuals *R*, or explained in another more visualising way it expresses the sum of the areas of the squares minimized [53]. This method is used to find a compression only thrust network that is as close as possible, “best-fit”, to a given surface, such as a gothic vault [54].

$$R(a,b) = \sum_{n=1}^{N} \left(y_n - (ax_n + b)\right)^2 \rightarrow minimum$$

$$\frac{\partial R}{\partial a} = 0: \frac{\partial R}{\partial b} = 0:$$

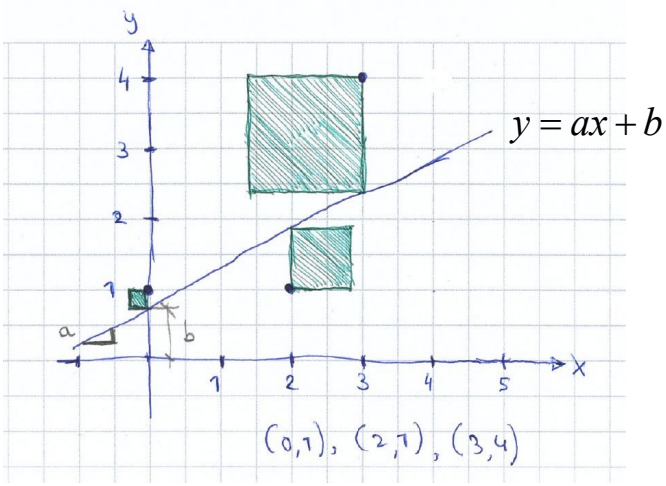

The stretched grid method [55] is equivalent to the variational method of minimizing the potential energy (*Π*), and is related to elastic grids. This method is used to find a minimum surface, based on the total energy balance of a nodal network. Similar to the example in section 3.7 regarding the catenoid and the catenary.

As a very simple example of the stretched grid method an asymmetric grid cell (quad) with the mid node (5) displaced from the centre of the cell. By minimizing the total potential energy of the system this becomes symmetric.

$$\Pi = D \sum_{i=1}^{n} l_i^2 \rightarrow minimum$$

$$\rightarrow \sum_{i=1} \frac{\partial \Pi}{\partial \Delta x_{kj}} = 0$$

$with$:
$D = an\ arbitrary\ constant$
$n = total\ number\ of\ segments\ in\ the\ network$
$l_i = length\ of\ segment$
$\Delta x = displacement\ of\ a\ node$
$j = the\ number\ of\ interior\ node\ of\ the\ area$
$k = the\ number\ of\ the\ axis$

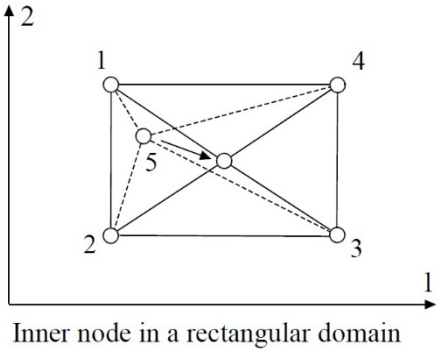

Inner node in a rectangular domain

Figure 28 "tightening up" a node [image 55]

The formation of the minimal surface the catenoid by means of the stretched grid method results, thus minimizing the total potential energy, result in a solution equal to the example in section 3.7.

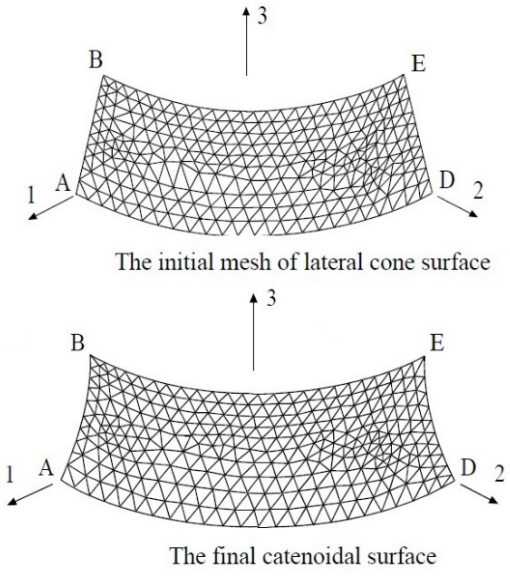

Figure 29 minimizing a surface [images 55]

The topology of the mesh of grids is also of important. For the example of section 3.7 the total surface area, bounded by two closed circles, is minimized resulting in a catenoid. The topology of this mesh was orthogonal. The catenoid with a triangular mesh and also found by minimizing the total potential energy, which is proportional to the surface area, allows non-planar quads on the surface to be approximated by triangles. This should result in smoother surfaces [56].

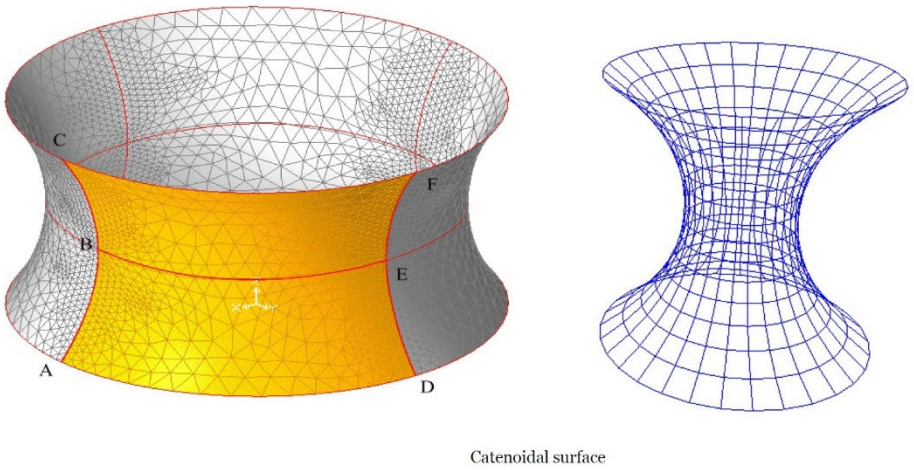

Figure 30 influence mesh topology on smoothness of surface [image left 56]

The choice of topology for the grid of a thrust network is of significance. Four sided surface (quads) grids are unable to contain shear forces as the members of the network are extension only. Thus the load can only be carried by axial forces. When a quad thrust network is used as a simulation of a shell structure, thus neglecting its in-plane shear forces, the result is a compression only thrust network. Thus negating the possible tension membrane forces of the shell which are a result of its shear forces. In order to be able to transfer shear forces, diagonals have to be added to the quads. This holds for all networks which have no in-plane form stability. More in detail see section 8.2.

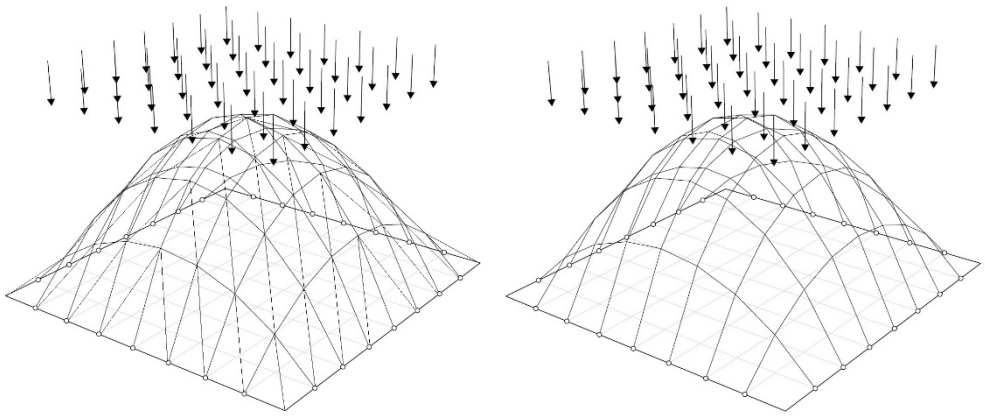

Figure 31 thrust network: left in-plane form stable, right not form stable

4 Indeterminate 3D graphic statics

4.1 Introduction

In chapter 2 formulas were derived to quantify the relations of and between form diagrams and force polygons of funicular structures, such as cables and arches in 2D. The structures from chapter 2 are statically determinate. Their vertical support reactions are obtained by solving equations of equilibrium or by using graphic statics, in the same way as for beams.

Funicular structures in 3D are an enigma, statically indeterminate in respect of their support reactions and their load transfer. If the vertical reactions are known then the relations of chapter 2 and 3 can be used to construct the 3D form diagram and force polygon. In this chapter an approach will be set out to determine the vertical reactions and the forces in the 3D network using the energy method of variation.

4.2 Statically (in)determinate 3D trusses

In section 3.3 statically indeterminate trusses in 2D were solved by using the variational method of the lowest complementary energy. This can be expanded to statically indeterminate trusses in 3D [57].

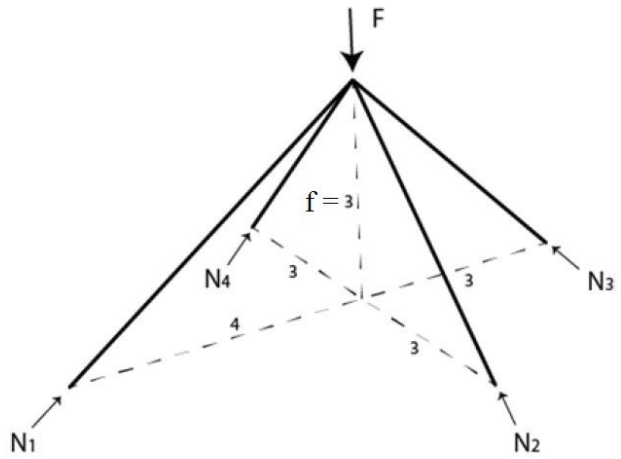

Figure 32 indeterminate 3D truss [image 57]

Although the truss has a form diagram which is reciprocal to the force polygon of a funicular structure (section 3.5), its form diagram has a similar shape if the funicular structure has only one point load, see section 2.3. For this structure the product of the horizontal force *H* and the rise of the cable *f* is constant. This is not so for the truss. For the funicular structures the relation between the

form diagram and the force polygon are only based on equilibrium and are statically determinate in 2D. For the truss structure the stiffness has to be taken into account due to its indeterminate state, as well as its equilibrium. So when its rise *f* is altered the horizontal support reactions *H* do not change in the same reciprocal way like with the funicular structures.
Funicular structures in 3D are usually not statically determinate. Based on the variational method of the lowest complementary energy and the reciprocity between funicular and truss structures the alternate method to determine their support reactions is derived.

$$E_{compl,N} = \sum_i N_i^2 l_i \rightarrow minimum$$
$$E_{compl,N} = N_1^2 5 + N_2^2 3\sqrt{2} + N_3^2 3\sqrt{2} + N_4^2 3\sqrt{2} \rightarrow min$$

$with\ equilibrium$:
$\Sigma F_x = 0$
$$N_3 \frac{1}{2}\sqrt{2} - N_1 \frac{4}{5} = 0$$

$\Sigma F_y = 0$
$$N_2 \frac{1}{2}\sqrt{2} - N_4 \frac{1}{2}\sqrt{2} = 0$$

$\Sigma F_z = 0$
$$N_1 \frac{3}{5} + N_2 \frac{1}{2}\sqrt{2} + N_3 \frac{1}{2}\sqrt{2} + N_4 \frac{1}{2}\sqrt{2} = \Sigma F$$

$$\Rightarrow E_{compl,N} = \frac{243\sqrt{2}}{25} N_1^2 + 5N_1^2 - \frac{42\sqrt{2}}{5} F N_1 + 3\sqrt{2}F^2 = 0$$
$$\sum_i \frac{\partial E_{compl,N}}{\partial N_i} = \frac{486\sqrt{2}}{25} N_1 + 10N_1 - \frac{42\sqrt{2}}{5} F = 0$$

$$\Rightarrow N_1 = \frac{14580 - 3750\sqrt{2}}{29278} F \approx 0.31684\ F$$
$$N_2 = N_4 = \frac{5250 + 4433\sqrt{2}}{29278} F \approx 0.39344\ F$$
$$N_3 = \frac{11664\sqrt{2} - 6000}{29278} F \approx 0.35847\ F \Rightarrow$$

$$V_1 = \frac{3}{5} N_1 \approx 0{,}190F$$
$$V_2 = \frac{1}{2}\sqrt{2}\, N_2 \approx 0{,}278F$$
$$V_3 = \frac{1}{2}\sqrt{2}\, N_3 \approx 0{,}253F$$
$$V_4 = \frac{1}{2}\sqrt{2}\, N_4 \approx 0{,}278F$$

4.3 An alternative method to determine vertical support reactions

The axial force N_i is used in the variational method of the lowest complementary energy for the truss. The axial force can be resolved into the vertical component V_i and the horizontal thrust H. Consider the rise f of the truss with two bars and one point load being lowered downwards until it approaches zero. The horizontal thrust H and the complementary energy will go to infinity because the load can no longer by carried by the axial force. The load is carried by a shear force equal to the vertical component V_i , similar to a beam.

The form diagram of a funicular structure has no physical properties because its topology represents the lines of action of the forces and thus has no stiffness, thereby it is assumed that the axial forces do not result in strains which have an influence on the distribution of the internal forces. Only the state of equilibrium is represented in the force polygon which determines this distribution.
The load distribution of a funicular structure is equivalent to that of a beam, which was explained in section 2.3. The constant product of the funicular structure Hf represents the maximum moment in the beam as a result of the total load ΣF. And the support reactions of the two systems are equal. This principle will be used to determine the support reactions of a 3D form diagram with an equivalent grid.
Additionally in order to solve the support reactions of a 3D funicular structure it has to be presumed that is has no physical properties. But it is again a collection of intersecting lines of action which form a network in equilibrium. The equivalent grid needs to have the same relation to the 3D network as the beam to the 2D funicular structure. This means the equivalent grid also has no physical properties. Thus let's assume the beam has no strains (curvature), this implies it has an infinite (bending) stiffness.

Returning to the total equation of the complementary energy the first two parts have to be omitted. The energy as result of the axial forces disappears because a beam or grid is a truss with rise f is equal to zero. The second part relating to the bending moments in the beam or grid also disappears because it has an infinite bending stiffness. The last part regarding the vertical forces and thus also the vertical support reactions remains.
In other words a truss with a rise of "zero" results in a beam so that the H and f fall out of the energy of the axial force N_i and only the part relating to the vertical force V_i and span a_i are left.

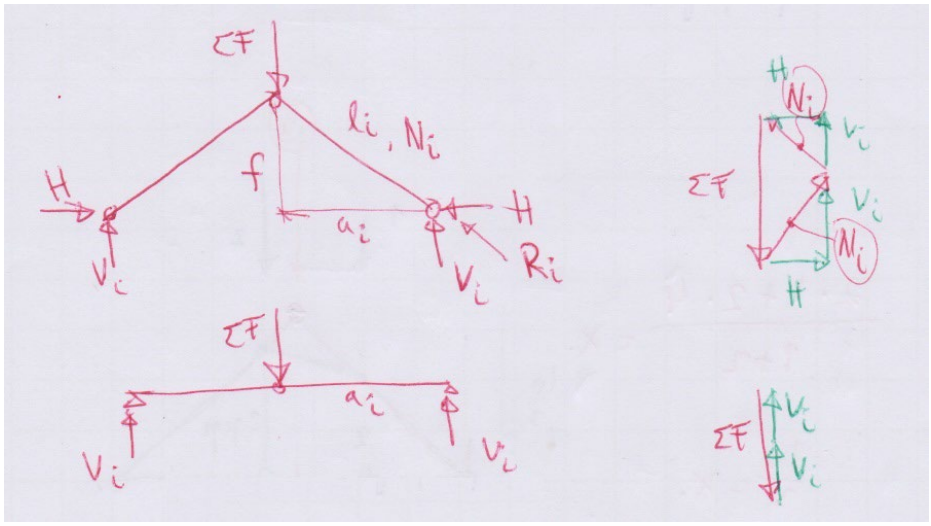

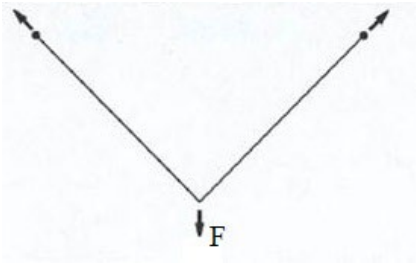

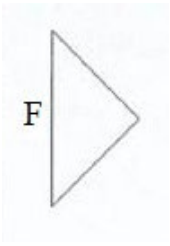

The variational method of the lowest complementary energy with respect to the shear forces is used to determine the vertical support reactions.

$$E_{compl,N} = \int_0^{l_i} \frac{1}{2EA} N_i^2 dx + \int_0^{l_i} \frac{1}{2EI} M_i^2 dx + \int_0^{l_i} \frac{1}{2GA_{sh}} V_i^2 dx \rightarrow minimum$$

$$E_{compl,N} = \sum_i N_i^2 l_i = \sum_i \left(V_i^2 + H^2\right)\left(a_i^2 + f^2\right)^{1/2} \rightarrow min$$

$$f \rightarrow 0: N_i \rightarrow \infty: H \rightarrow \infty \Rightarrow E_{compl,N} \rightarrow \infty$$

$$with: EI = \infty \Rightarrow E_{compl,V} = \sum_i V_i^2 l_i \longrightarrow min$$

In the next section some examples will be used to explain the method, and test it for suitability and accuracy. This will first be done on statically determinate beams and grid and then statically indeterminate grids.

4.4 Determinate and indeterminate examples

a. *statically determinate examples*
The first example is a beam with a point load. The proposed method results in the exact solution.
The next example is a grid in three directions with one central load and with one axis of symmetry. For grids in addition to the equilibrium of the forces also the rotational equilibrium around both axis out of plane are needed. This also produces the exact result.
This is followed by another grid in three directions with a central load but without an axis of symmetry. The result is nearly exact, there is a small error. For statically determinate examples this method is redundant because the equations of equilibrium are sufficient. These examples are included to show the general application of the proposed method, but it is mainly intended for use solving statically indeterminate 3D funicular networks.

example 1

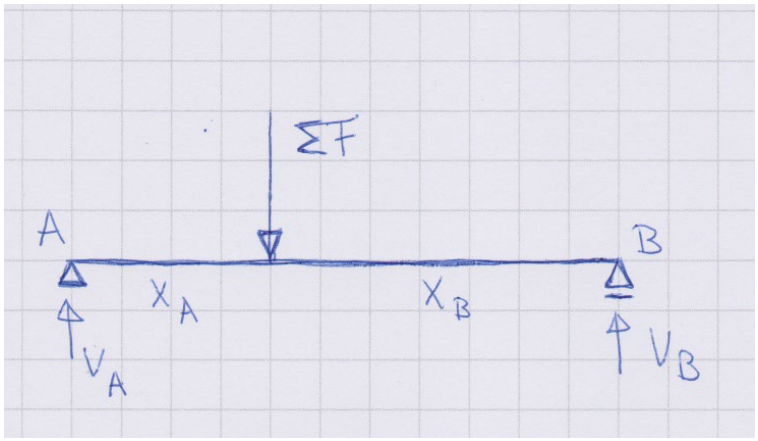

$$E_{compl,V} = \sum_i V_i^2 l_i \longrightarrow min$$

$$V_A^2 x_A + V_B^2 x_B \longrightarrow min$$

$$with: x_A = \alpha x_B : x_A + x_B = l$$

$$equilibrium:$$
$$V_A + V_B = \Sigma F \Rightarrow V_B = \Sigma F - V_A$$

$$V_A^2 \alpha x_B + (\Sigma F - 2\Sigma F V_A + V_A^2) x_B \longrightarrow min$$

$$\sum \frac{\partial E_{compl,V}}{\partial V_A} = \alpha V_A + V_A - \Sigma F = 0 \Rightarrow V_A = \frac{\Sigma F}{1+\alpha} = \frac{x_B}{l}\Sigma F$$

$$V_B = \frac{\alpha \Sigma F}{1+\alpha} = \frac{x_A}{l}\Sigma F$$

example 2

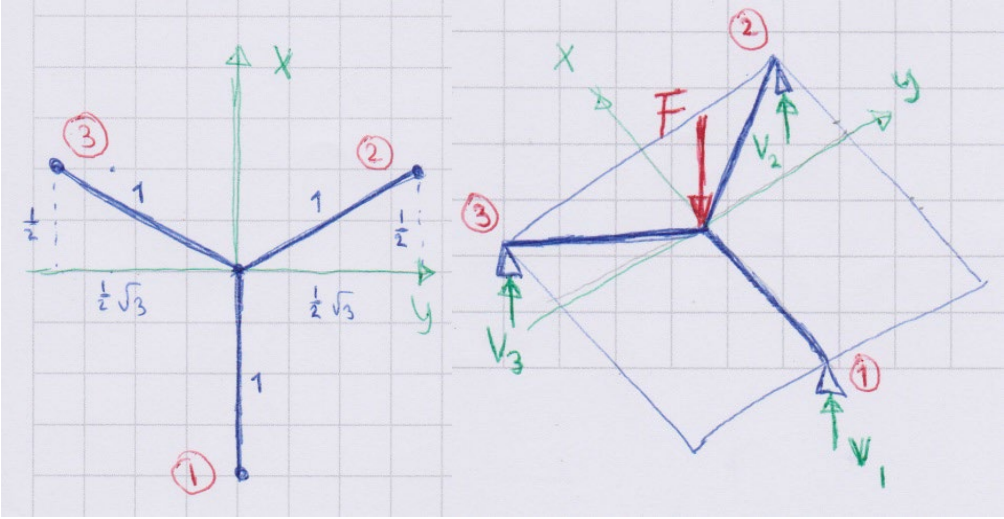

$$E_{compl,V} = \sum_i V_i^2 l_i \longrightarrow min$$
$$V_1^2 l_1 + V_2^2 l_2 + V_3^2 l_3 \longrightarrow min$$
$$V_1^2 1 + V_2^2 1 + V_3^2 1 \longrightarrow min$$

$equilibrium$:
$$\Sigma M_x = 0$$
$$V_2 \frac{1}{2}\sqrt{3} - V_3 \frac{1}{2}\sqrt{3} = 0 \Rightarrow V_2 = V_3$$

$$\Sigma M_y = 0$$
$$V_1 1 - V_2 \frac{1}{2} - V_3 \frac{1}{2} = 0 \Rightarrow V_2 = 2V_1 - V_3$$

$$\Sigma F_z = 0$$
$$V_1 + V_2 + V_3 = \Sigma F \Rightarrow V_3 = \Sigma F - 2V_1$$

$$E_{compl,V} = (\Sigma F)^2 - 2\Sigma F V_1 + 3V_1^2 \longrightarrow min$$

$$\sum \frac{\partial E_{compl,V}}{\partial V_1} = -\Sigma F + 3V_1 = 0 \Rightarrow V_1 = \frac{1}{3}\Sigma F$$
$$V_2 = \frac{1}{3}\Sigma F : V_3 = \frac{1}{3}\Sigma F$$

example 3

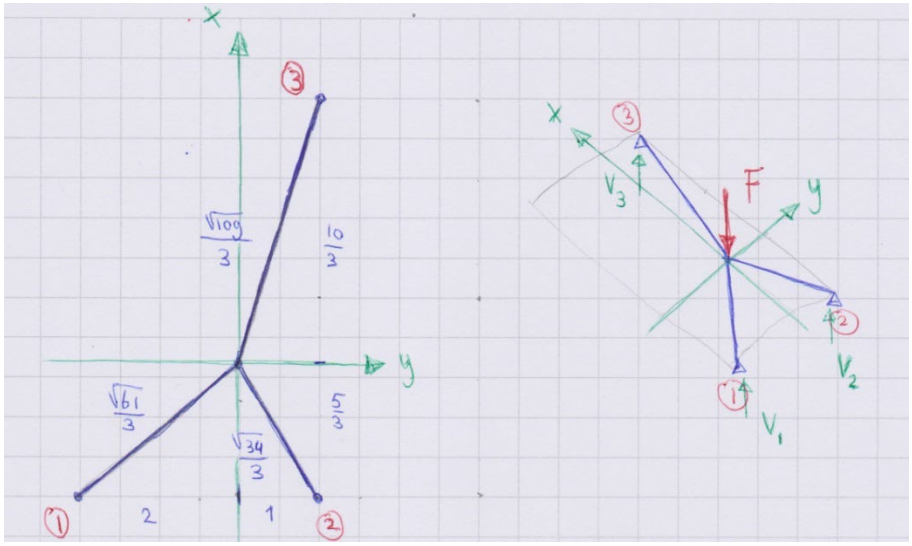

$$E_{compl,V} = \sum_i V_i^2 l_i \longrightarrow min$$
$$V_1^2 l_1 + V_2^2 l_2 + V_3^2 l_3 \longrightarrow min$$

$$V_1^2 \frac{\sqrt{61}}{3} + V_2^2 \frac{\sqrt{34}}{3} + V_3^2 \frac{\sqrt{109}}{3} \longrightarrow min$$

equilibrium:

$$\left.\begin{array}{l} \Sigma M_x = 0 \\ V_2 + V_3 - 2V_1 = 0 \\ \Sigma M_y = 0 \\ V_1 + V_2 - 2V_3 = 0 \end{array}\right\} V_2 = V_3$$

$$\Sigma F_z = 0$$
$$V_1 + V_2 + V_3 = \Sigma F$$

using direct equilibrium:

$$\sum M_y = 0$$
$$V_3 \cdot \frac{10}{3} - V_2 \cdot \frac{5}{3} - V_1 \cdot \frac{5}{3} = 0$$
$$\sum M_x = 0$$
$$V_3 \cdot 1 + V_2 \cdot 1 - V_1 \cdot 2 = 0$$
$$\sum F_z = 0$$
$$V_3 + V_2 + V_1 - \Sigma F = 0$$
$$\rightarrow V_1 = V_2 = V_3 = \frac{1}{3}\Sigma F \approx 0.333\ \Sigma F$$

$$E_{compl,V} = \frac{\sqrt{61}}{3}\Sigma F - \frac{4\sqrt{61}}{3}\Sigma F V_3 + \frac{4\sqrt{61}}{3}V_3^2 + \frac{\sqrt{34}}{3}V_3^2 + \frac{\sqrt{109}}{3}V_3^2 \longrightarrow min$$

$$\sum \frac{\partial E_{compl,V}}{\partial V_3} = -\frac{4\sqrt{61}}{3}\Sigma F + \frac{8\sqrt{61}}{3}V_3 + \frac{2\sqrt{34}}{3}V_3 + \frac{2\sqrt{109}}{3}V_3 = 0$$
$$\Rightarrow V_3 = \frac{4\sqrt{61}}{8\sqrt{61} + 2\sqrt{34} + 2\sqrt{109}}\Sigma F \approx 0.32876\ \Sigma F$$
$$V_2 = \frac{4\sqrt{61}}{8\sqrt{61} + 2\sqrt{34} + 2\sqrt{109}}\Sigma F \approx 0.32876\ \Sigma F$$
$$V_1 = \frac{2\sqrt{34} + 2\sqrt{109}}{8\sqrt{61} + 2\sqrt{34} + 2\sqrt{109}}\Sigma F \approx 0.34246\ \Sigma F$$

b. statically indeterminate examples

The first example is a grid in four directions with no axis of symmetry and a central load. The results obtained are in good agreement with those obtained from finite element analysis.

example 1

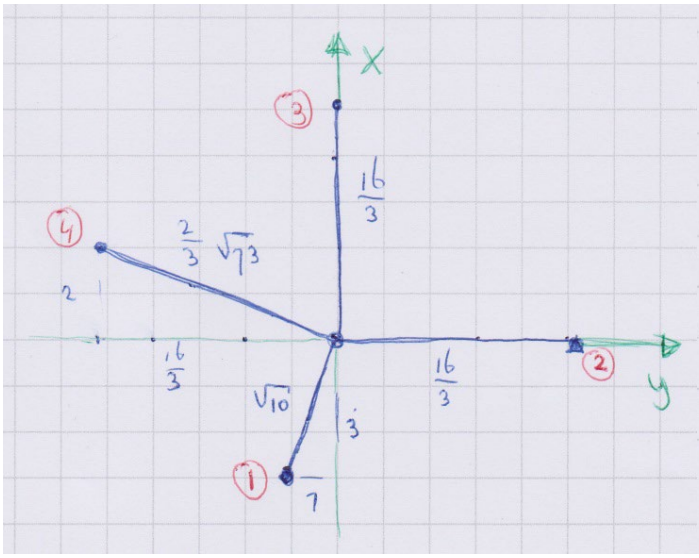

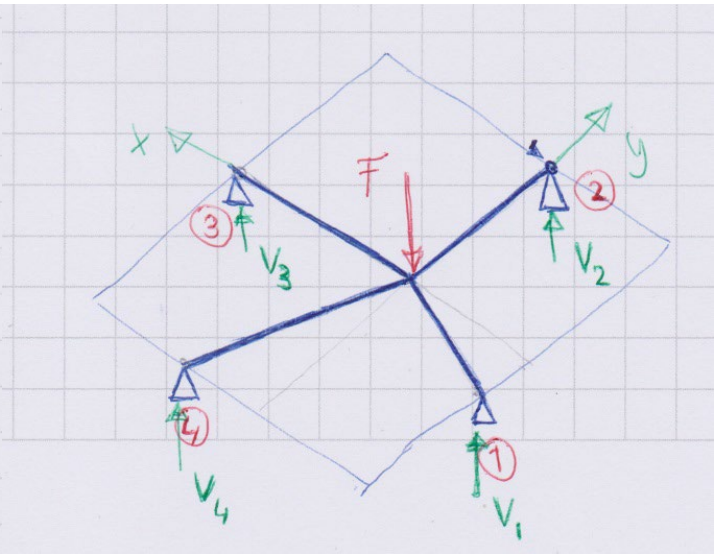

$$E_{compl,V} = \sum_i V_i^2 l_i \longrightarrow min$$

$$V_1^2 l_1 + V_2^2 l_2 + V_3^2 l_3 + V_4^2 l_4 \longrightarrow min$$

$$V_1^2\sqrt{10} + V_2^2\frac{16}{3} + V_3^2\frac{16}{3} + V_4^2\frac{2\sqrt{73}}{3} \longrightarrow min$$

equilibrium:

$$\Sigma M_x = 0$$

$$V_1\,1 + V_4\frac{16}{3} - V_2\frac{16}{3} = 0 \Rightarrow V_4 = V_2 - \frac{3}{16}V_1$$

$$\Sigma M_y = 0$$

$$V_4\,2 + V_3\frac{16}{3} - V_1 3 = 0 \Rightarrow V_3 = \frac{9}{16}V_1 - \frac{6}{16}V_4$$

$$\Sigma F_z = 0$$

$$V_1 + V_2 + V_3 + V_4 = \Sigma F \Rightarrow V_2 = \frac{8}{13}\Sigma F - \frac{185}{208}V_1$$

$$E_{compl,V} = \sqrt{10}V_1^2 + \frac{1024}{507}(\Sigma F)^2 - \frac{2960}{507}\Sigma F V_1 + \frac{34225}{8112}V_1^2 + \frac{13467}{2704}V_1^2 - \frac{402}{169}\Sigma F V_1 + \frac{48}{169}(\Sigma F)^2 + \frac{128\sqrt{73}}{507}(\Sigma F)^2 - \frac{448\sqrt{73}}{507}\Sigma F V_1 + \frac{392\sqrt{73}}{507}V_1^2 \longrightarrow min$$

$$\sum \frac{\partial E_{compl,V}}{\partial V_1} = \frac{37313}{2028} V_1 + 2\sqrt{10} V_1 + \frac{784\sqrt{73}}{507} V_1 - \frac{448\sqrt{73}}{507} \Sigma F - \frac{4166}{507} \Sigma F = 0$$

$$\Rightarrow V_1 = \frac{33328 + 3584\sqrt{73}}{74626 + 8112\sqrt{10} + 6272\sqrt{73}} \Sigma F \approx 0.41561\, \Sigma F$$

$$V_2 = \frac{16281 + 4992\sqrt{10} + 672\sqrt{73}}{74626 + 8112\sqrt{10} + 6272\sqrt{73}} \Sigma F \approx 0.24572\, \Sigma F$$

$$V_3 = \frac{14985 - 1872\sqrt{10} + 2016\sqrt{73}}{74626 + 8112\sqrt{10} + 6272\sqrt{73}} \Sigma F \approx 0.17086\, \Sigma F$$

$$V_4 = \frac{10032 + 4992\sqrt{10}}{74626 + 8112\sqrt{10} + 6272\sqrt{73}} \Sigma F \approx 0.16779\, \Sigma F$$

$for\ \Sigma F = 1000$:	$FEM\ results\ for\ \Sigma F = 1000\ (with\ EI = \infty)$:
$V_1 = 415.61$	415.9
$V_2 = 245.72$	245.5
$V_3 = 170.86$	171.1
$V_4 = 167.79$	167.5

The next example refers back to section 4.2. The grid is the horizontal projection of this truss, so the rise *f* is zero. The difference is that the truss is composed of bars whose bar lengths determines their axial stiffness ratios (*EA* is presumed constant) and thus the load distribution and that the grid has infinitely stiff beams.

The results for the vertical support reactions are compared with a finite element calculation (GSA) and corresponds closely. Compared to the vertical support reactions of the truss of section 4.2, there is a small difference of about 5 percent.

example 2

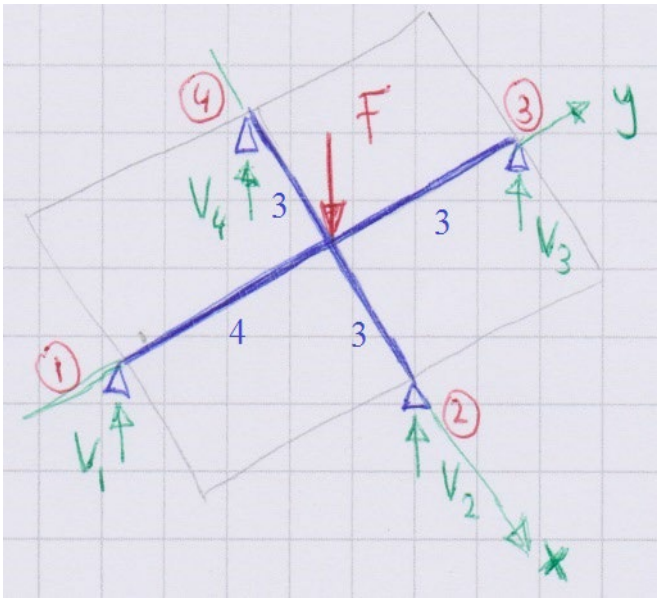

$$E_{compl,V} = \sum_i V_i^2 l_i \rightarrow minimum$$

$V_1^2 l_1 + V_2^2 l_2 + V_3^2 l_3 + V_4^2 l_4 \rightarrow min$
$V_1^2 4 + V_2^2 3 + V_3^2 3 + V_4^2 3 \rightarrow min$

with equilibrium:
$\Sigma M_x = 0$
$V_1 4 - V_3 3 = 0$

$\Sigma M_y = 0$
$V_2 3 - V_4 3 = 0$

$\Sigma F_z = 0$
$V_1 + V_2 + V_3 + V_4 = \Sigma F$

$\frac{35}{2} V_1^2 - 7\,\Sigma F V_1 \rightarrow min$

$\sum \frac{\partial E_{compl,V}}{\partial V_1} = 35 V_1 - 7\,\Sigma F = 0$ *FEM results (with* $EI = \infty$*)*:

$\Rightarrow V_1 = \frac{1}{5}\,\Sigma F = 0.2\,\Sigma F$ $0.1999\,\Sigma F$

$V_2 = V_3 = V_4 = \frac{4}{15}\,\Sigma F \approx 0.2666\,\Sigma F$ $0.2667\,\Sigma F$

compare with results of equivalent 3D truss from section 4.2:
$V_1 \approx 0{,}190F$
$V_2 \approx 0{,}278F$
$V_3 \approx 0{,}253F$
$V_4 \approx 0{,}278F$

4.5 Form diagrams, networks in 3D

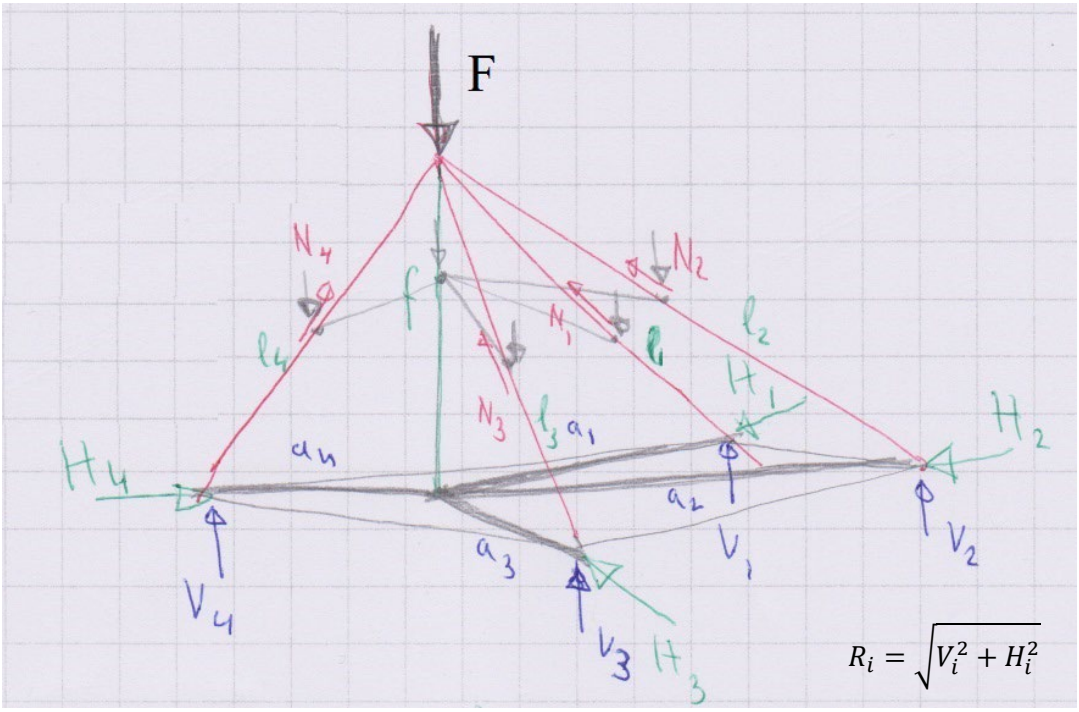

Constructing 2D form diagrams using force polygons are not difficult as they are statically determinate. 3D networks or form diagrams are more difficult to construct as they are in nearly all cases statically indeterminate. The problems that need to be solved are the determination of the vertical support reactions and the shape and topology of the network, the discretized thrust surface. Together they determine the load path and multiple solutions could are possible. For a 3D funicular network the vertical support reactions can be calculated by using the proposed method in this chapter. Hereby the global load transfer is determined, the next step is find the correct shape and topology of the network (see also section 3.8).
A 3D funicular network can be treated like the 2D version, which means that the relations and methods derived in section 4.4 can be used.

$$H_i f = V_i a_i \Rightarrow f \sum_i H_i = \sum_i V_i a_i = constant = M_{tot}$$

$example$:
$M_{tot} = V_1 a_1 + V_2 a_2 + V_3 a_3 + V_4 a_4$
$M_{tot} = (H_1 + H_2 + H_3 + H_4) f$

$with$:
$V_i = \frac{f}{l_i} N_i : H_i = \frac{a_i}{l_i} N_i : with\ force\ density : q_i = \frac{N_i}{l_i}$
$\Sigma F = \sum_i V_i = \sum_i N_i \frac{f}{l_i} = f \sum_i q_i \Rightarrow Q = \frac{1}{f} \Sigma F$
$M_{tot} = \sum_i V_i a_i = \sum_i N_i \frac{f}{l_i} a_i = f \sum_i a_i\, q_i$

According to the membrane shell theory, which disregards the shells material properties, equilibrium with the loads can be achieved taking into account of the correct boundary conditions. That means the problem becomes statically determinate. A distinct example is a spherical dome, loaded by self-weight or a uniformly distributed load. This can be solved using the membrane equations or graphic statics [58] [59]. Due to the axis of symmetry the dome can be regarded as a pseudo 2D problem, similar to the catenary which is the 2D cross section of the catenoid. The hoop forces in a dome act like additional loads on the arch-like wedge shaped cross section to ensure equilibrium. There is only one possible load path which excludes eccentricities and thus moments and the system is statically determinate. The difference with the catenoid is that the axis of catenary coincides with the thrust line of the load, as a result the force polygon of the catenary has a pole. In the case of the dome the axis of the dome is not equal to the thrust line of the load. The resolved components of the hoop force guarantees that the rays of the force polygon follow the axis of the dome, its force polygon does not have one pole, but results in a membrane state of equilibrium.

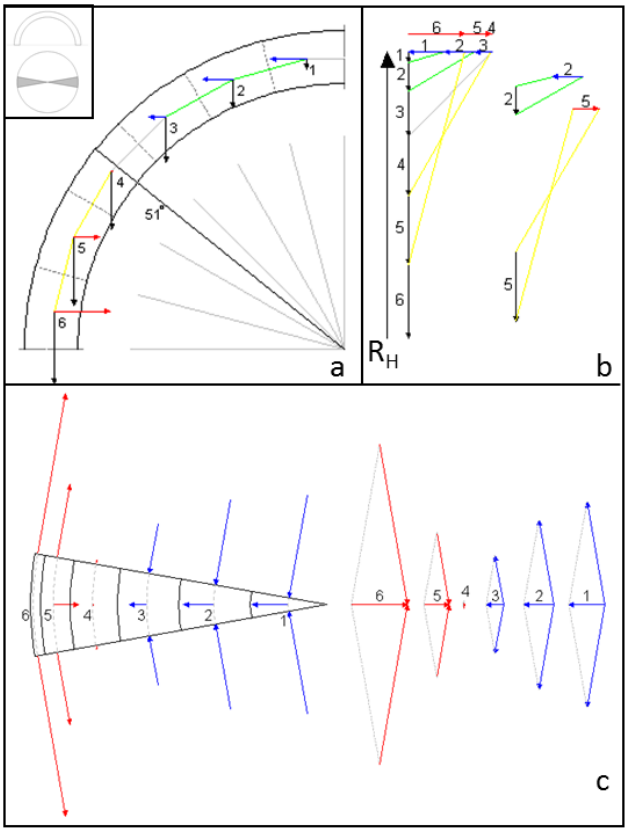

Figure 33 meridian and hoop forces of dome [image 59]

$$membrane\ equation:$$

$$\frac{n_{xx}}{r_x} + 2\frac{n_{xy}}{r_{xy}} + \frac{n_{yy}}{r_y} = -p_z$$

From the previous two examples a fundamental distinction has to be made between the thrust line or surface of the load and the shape of the cable, arch or shell. This will be discussed in the chapter 7 in more detail in relation to shell

structures. The thrust line and thrust surface can always be determined. They represent the lines of action of the loads and the internal forces of the 2D and 3D form diagrams which have no material properties. The problem for 3D cases is finding which thrust surface is the correct one. As there are multiple admissible load paths, hence shapes and topologies of the thrust surface that ensure equilibrium given its loads and support conditions, there will always be a solution with the lowest complementary energy. As is the case with soap films and bubbles.

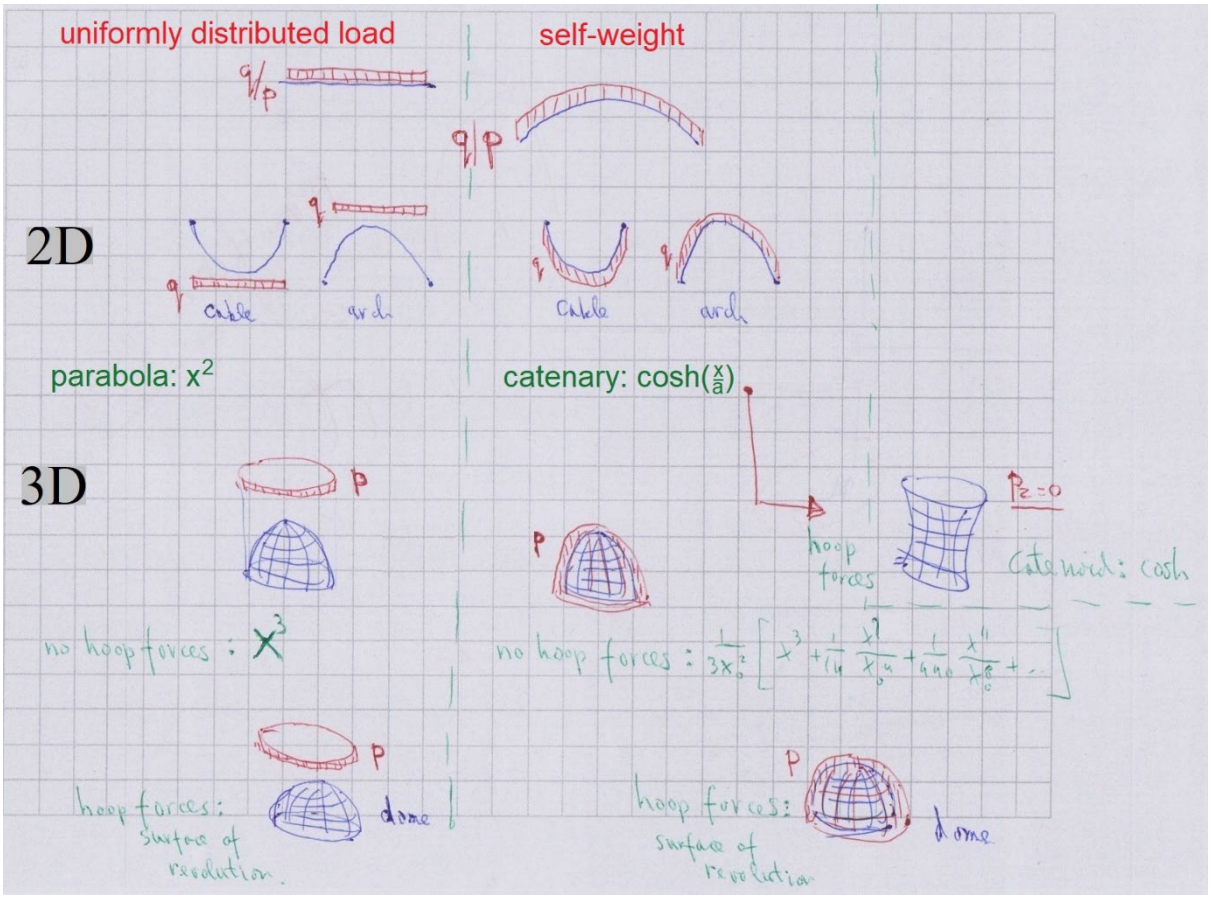

An elliptic paraboloid on semi-rigid edges with a uniform load has a membrane solution. There is an Airy stress function solution of the partial second order differential equation (Pucher's equation) [60], which only takes into account equilibrium and not the shells material properties. This makes the problem statically determinate, there is one admissible load path given the load and boundary conditions. As in the case of the dome the thrust surface of the load and the surface of the shell do not coincide, corrective hoop forces similar to the dome provide the moment free membrane solution.

In the case of the same shell but different support conditions, namely on four corner points, and with free edges, bending moments and shear forces are

needed to ensure equilibrium. This problem therefore now becomes statically indeterminate. Obviously the membrane or Pucher's equation do not suffice in these cases, due to being both based on equilibrium only.

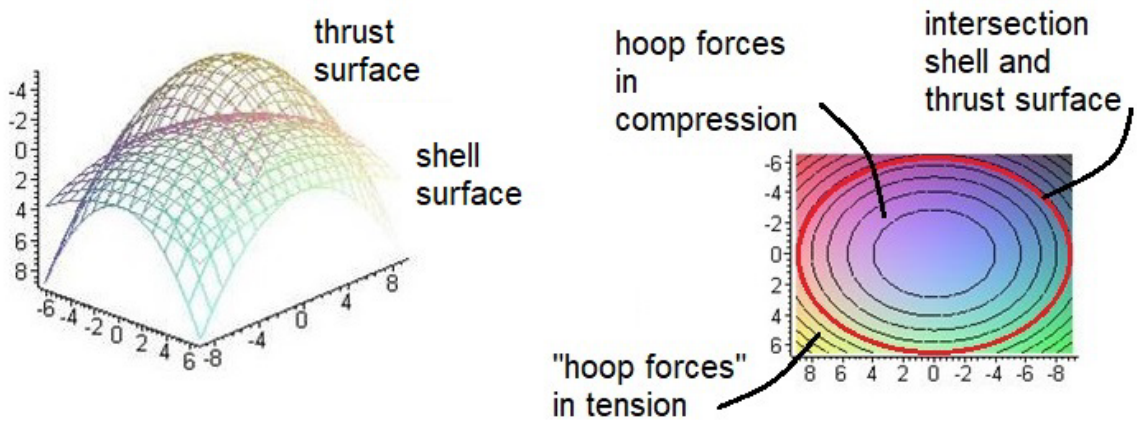

Figure 34 elliptic paraboloid [image 11]

In section 2.5 a total load was subdivided into a uniformly distributed load, if this is done with sufficient steps the discretized result converges to a parabola, where the rays of the force polygon are the tangents of the parabola. In section 4.3 it was explained that a 3D form diagram, like the 2D example of the uniformly distributed load, has no physical properties. Its topology represents the lines of action of the forces.

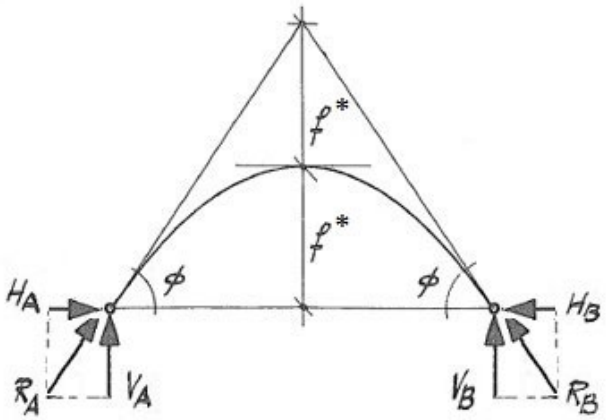

$$2D: parabola$$

$$V = \int q\, dx = qx + c \ldots$$

$$M = \int qx\, dx = \frac{1}{2}qx^2 + c \ldots$$

$$point\ of\ application\ of\ total\ load:$$

$$f = 2f^*$$

To solve a 3D statically indeterminate case such as described above, the following method is proposed. But first we have to distinguish between statically determinate and indeterminate cases.

A triangular based shell on three supports with free edges and a square based shell on four supports with four edges are statically determinate (two axis of symmetry). In both cases the point of application of the total load, which

represents a uniformly distributed load, is to be found in the centroid of both horizontal planes. The 3D form diagram can be truncated in the same way as the 2D case of the uniformly distributed load (section 2.5).

For the 2D case this result in a parabolic shaped form diagram, for a 3D surface of revolution in a parabolic or cubic one, parabolic if the position of subdivided loads are set at an equal horizontal distance, cubic if the position of subdivided loads are free to "relax" in the horizontal plane like in the examples of section 3.7. The first truncation result in the horizontal tangent plan. For the parabolic cases this is half from the base to the point of application of the total load [61] and for the cubic case this one third.

$3D: cubic$

$$v = \int qx\,dx = \frac{1}{2}qx^2 + c \ldots$$

$$m = \int \frac{1}{2}qx^2 dx = \frac{1}{6}qx^3 + c \ldots$$

$point\ of\ application\ of\ total\ load$:

$f = 3f^*$

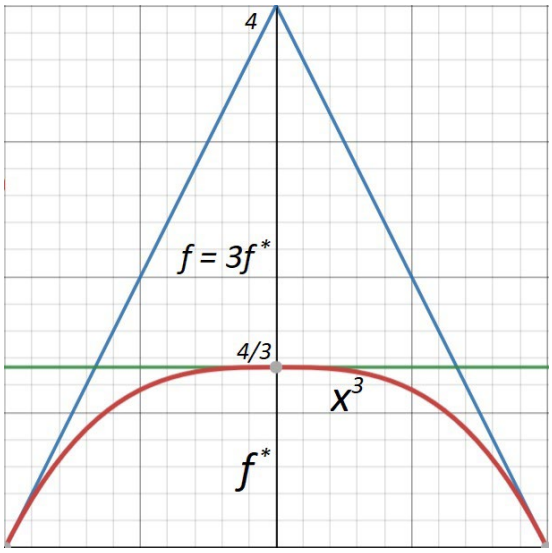

The load transfer is in two directions for the 3D case, that explains why the form diagram is parabolic or cubic. With the triangular, especially an equilateral one, and square based examples it can be observed that load transfer is in two directions and that the central part of the form diagram, thrust surface, is parabolic or cubic. The free edges will need to be funicular "arch" shaped to ensure moment free edges.

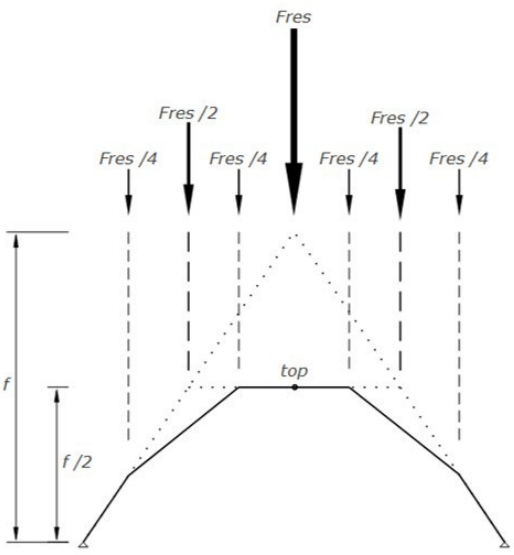

Figure 35 parabola by subdividing load [image 61]

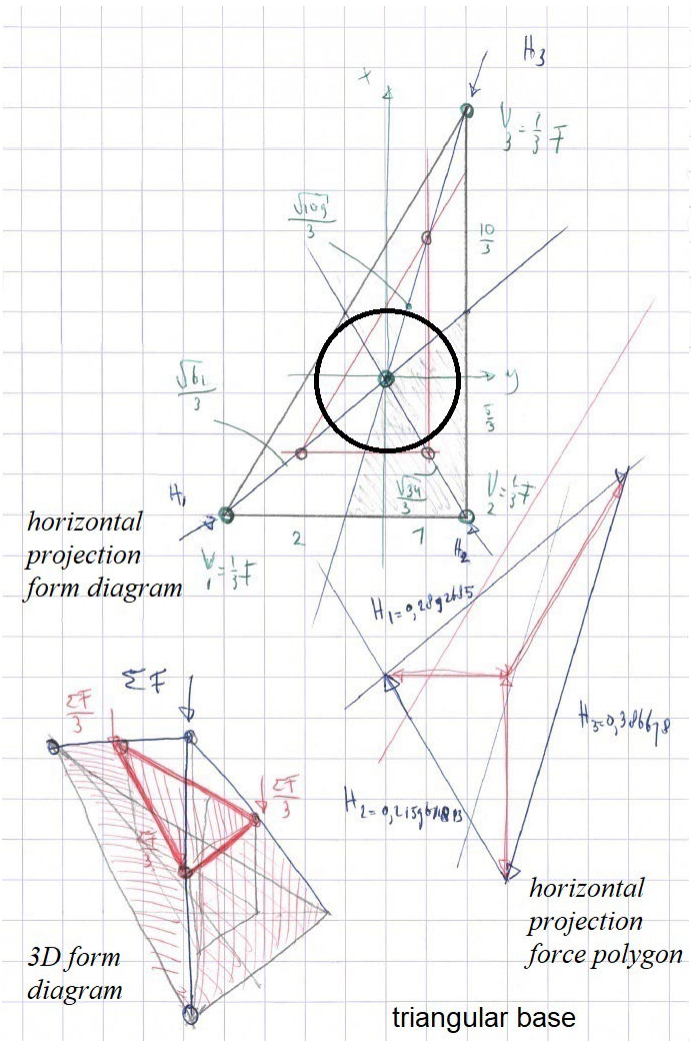

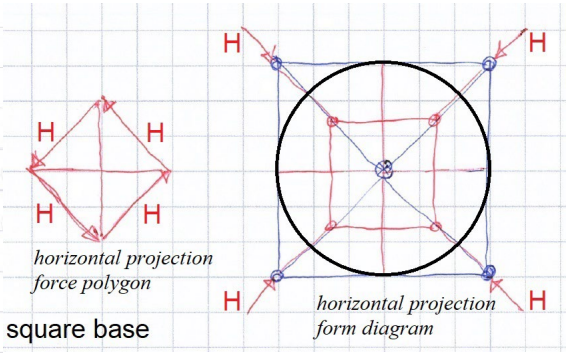

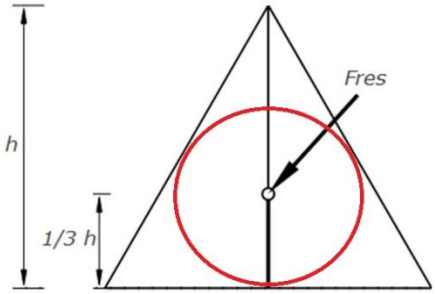

Shells on four and more supports with free edges which have a non-symmetric floor plan and a uniformly distributed load are statically indeterminate.
The correct form diagram or funicular network can be found by following the procedure listed below. The topology of the network grid is important, see section 3.9.

- Calculate the vertical support reactions, as described in section 4.3 and 4.4.
- Determine the position of the total load with respect to the positions of the supports in the horizontal plane, which for a uniformly distributed load is the same position of the centroid of the area of the load.
- Assume a rise *f* from the horizontal plane for the point of application of the total load, see beginning of this section.
- Determine the horizontal support reactions, using the method given at the beginning of this section.

- Subdivide the total uniform load by making a first truncation of the parabolic or cubic envelop into as many subdivided loads as there are supports. Place the subdivided loads in the nodes of the network.
    - This involves setting the position of the subdivided loads in the centroid of the area of the uniformly distributed load it represents in the horizontal plane (parabolic). Use the force density equations to arrive at an arbitrary equilibrium network by setting a value for the force density and taking into account the angles of the support reactions R_i. Iteratively minimising the total complementary energy of the network by varying the force densities, and thus the heights of the network nodes.
    - As a possible second step let the position of the subdivided loads free in the horizontal plane (cubic), then minimise the total potential energy of the network, keeping the support reactions constant. This results in a more compact network, the load is now uniform along the surface arc lengths instead of projected, similar to that of self-weight.

- The sum of the product of the horizontal reactions and the rise f is constant with constant vertical support reactions, so the overall height of the funicular network can be altered (scaled, see section 2.5).
- Further refining the network ‘s mesh by more subdivisions of the load and truncation leads to a better approximation of the network, minimising the complementary or potential energy again as described in previous steps.

The correct form diagram or funicular network can also be achieved without first estimating the vertical and horizontal support reactions, as is done at the beginning of this section. It would also be possible to start with a horizontal projection of the form diagram (section 2.9) of an initial trial network, use the force density equations to arrive at an arbitrary equilibrium network by setting a value for the force density and then minimising its total complementary and potentially the potential energy.

Note that if the shell's ground base is non-symmetric the tangent plane will no longer be horizontal as for the case of the symmetric based shell. The horizontally projected forces of the truncation must be in equilibrium by forming a closed force polygon. This could mean that as result of the first trial truncation by subdividing the total load $\sum F$ into loads they are different to their corresponding vertical support reactions. By tilting the tangent plane to ensure equilibrium the subdivided loads will re-distribute whilst keeping the vertical support reaction constant. This is automatically the result of minimising the complementary or potential energy.

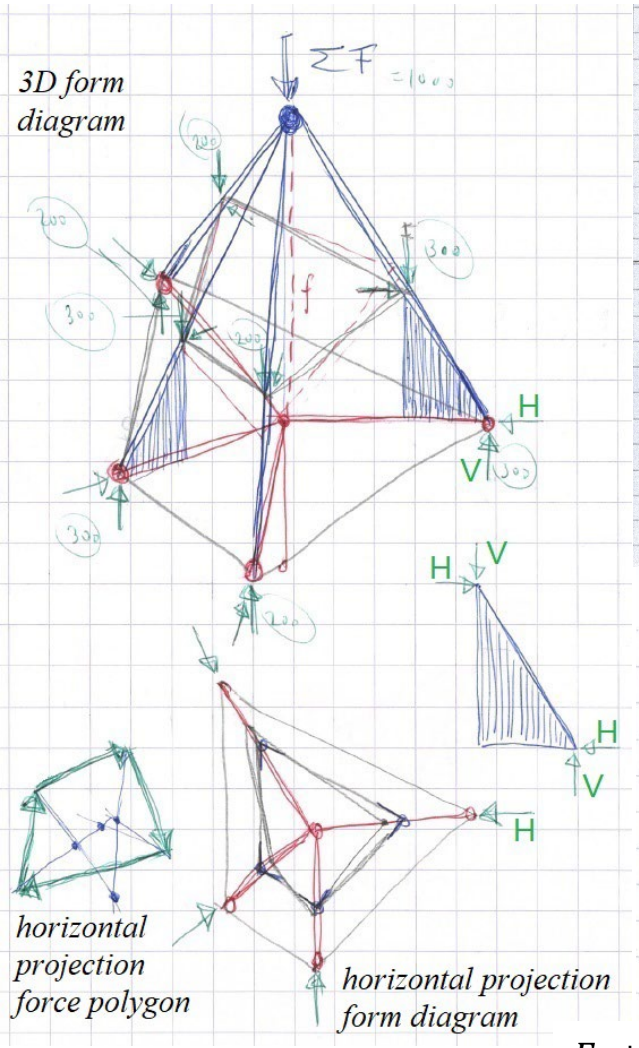

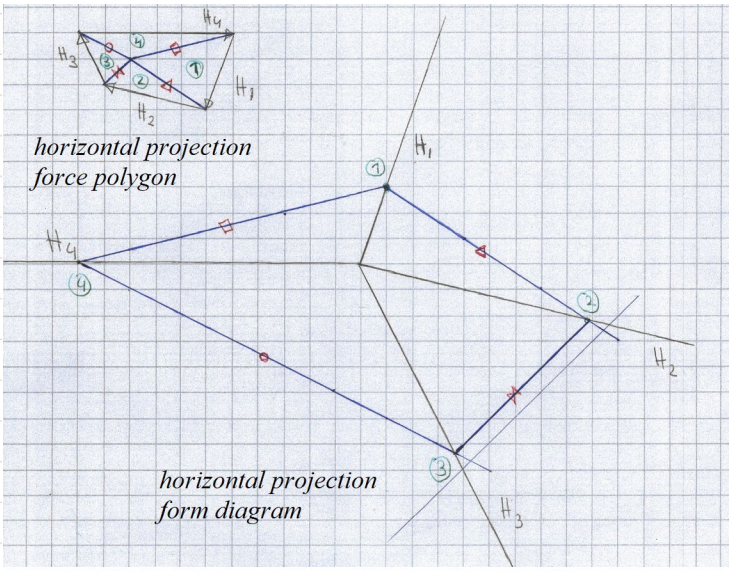

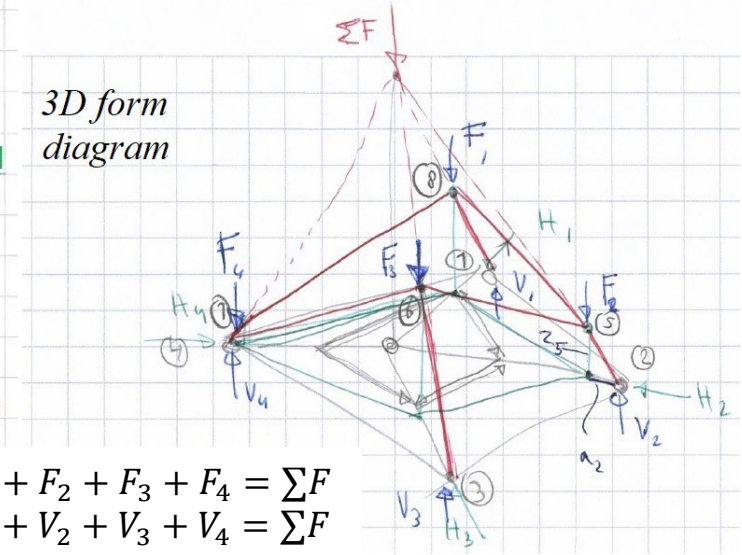

$$F_1 + F_2 + F_3 + F_4 = \sum F$$
$$V_1 + V_2 + V_3 + V_4 = \sum F$$

4.6 The degree of accuracy of energy approximations

With the example of section 3.7 the degree of the accuracy of energy principles will be discussed. The force density is in this case not constant for all lines of action, the top two lines of action now only have half of the value.

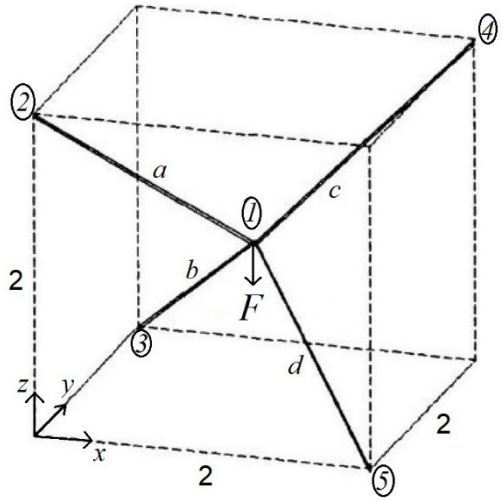

After the equilibrium geometry has been found via the variational principle of the force density, which is equivalent to solving the force density equation for an unloaded case, the network will be loaded with a point load *F* in node 1.

$$\overline{\Pi} = \sum_i l_i^2 \, q_i \rightarrow minimum$$

$$q_i(l_a^2 + l_b^2 + l_c^2 + l_d^2) \rightarrow minimum$$

$$with: q_{a,c} = \frac{N_a}{l_a} = \frac{N_c}{l_c} = 1 \; and \; q_{b,d} = \frac{N_b}{l_b} = \frac{N_d}{l_d} = 2$$

$$l_a^2 = (x_1 - 0)^2 + (y_1 - 0)^2 + (z_1 - 2)^2$$
$$l_b^2 = (x_1 - 0)^2 + (y_1 - 2)^2 + (z_1 - 0)^2$$
$$l_c^2 = (x_1 - 2)^2 + (y_1 - 2)^2 + (z_1 - 2)^2$$
$$l_d^2 = (x_1 - 2)^2 + (y_1 - 0)^2 + (z_1 - 0)^2$$

$$\rightarrow (6x_1^2 + 6y_1^2 + 6z_1^2 - 12x_1 - 12y_1 - 8z_1 + 32) \rightarrow minimum$$
$$\frac{\partial}{\partial x_1} = 12x_1 - 12 = 0 \rightarrow x_1 = 1$$
$$\frac{\partial}{\partial y_1} = 12y_1 - 12 = 0 \rightarrow y_1 = 1$$
$$\frac{\partial}{\partial z_1} = 12z_1 - 8 = 0 \rightarrow z_1 = \frac{2}{3}$$

As seen in section 3.7, using the force density equations leads to the same results.

$$\frac{N_a}{l_a}(x_1 - x_2) + \frac{N_b}{l_b}(x_1 - x_3) + \frac{N_c}{l_c}(x_1 - x_4) + \frac{N_d}{l_d}(x_1 - x_5) = 0$$
$$\frac{N_a}{l_a}(y_1 - y_2) + \frac{N_b}{l_b}(y_1 - y_3) + \frac{N_c}{l_c}(y_1 - y_4) + \frac{N_d}{l_d}(y_1 - y_5) = 0$$
$$\frac{N_a}{l_a}(z_1 - z_2) + \frac{N_b}{l_b}(z_1 - z_3) + \frac{N_c}{l_c}(z_1 - z_4) + \frac{N_d}{l_d}(z_1 - z_5) = 0$$

$$with: q_{a,c} = \frac{N_a}{l_a} = \frac{N_c}{l_c} = 1 \; and \; q_{b,d} = \frac{N_b}{l_b} = \frac{N_d}{l_d} = 2$$

$$and: x_2 = x_3 = y_2 = y_5 = z_3 = z_5 = 0$$
$$x_4 = x_5 = y_3 = y_4 = z_2 = z_4 = 2$$

$$\rightarrow solve: x_1 = y_1 = 1\,, z_1 = \frac{2}{3}$$

The forces of the network will be determined by the variational principle of complementary energy. Note this network is not comprised of physical bars, but constitutes a network of lines of action of forces in equilibrium. Thus a 3D form diagram, a thrust network, is formed.

$$E_{compl,tot} = \sum_i N_i^2 \, l_i \rightarrow minimum$$

$symmerty$:

$$l_a = l_c = \left[1^2 + 1^2 + \left(\frac{4}{3}\right)^2\right]^{\frac{1}{2}} = \frac{1}{3}\sqrt{34}$$

$$l_b = l_d = \left[1^2 + 1^2 + \left(\frac{2}{3}\right)^2\right]^{\frac{1}{2}} = \frac{1}{3}\sqrt{22}$$

$$N_a = N_c \; and \; N_b = N_d$$

$$V_{a,c} = \frac{2\sqrt{2}}{\sqrt{17}} N_{a,c} \; and \; V_{b,d} = \frac{\sqrt{2}}{\sqrt{11}} N_{b,d}$$

$$equilibrium: F - (V_a + V_b + V_c + V_d) = 0$$

$$N_a^2 l_a + N_b^2 l_b + N_c^2 l_c + N_d^2 l_d \rightarrow minimum$$

$$\frac{\partial}{\partial N_b} = \frac{\left(4\left(17\sqrt{17} + 44\sqrt{11}\right)N_b - 17\sqrt{374}F\right)}{66\sqrt{2}} = 0$$

$$\rightarrow \; N_b = N_d = -\frac{17\sqrt{187}\left(17\sqrt{17} - 44\sqrt{11}\right)}{32766\sqrt{2}} F \approx 0.38047 \; F$$

By means of symmetry the l_a & l_b – and l_c & l_d – part can be considered as being statically determinate, each loaded by $F/2$. Compared with their vertical component of the force N, or the vertical support reaction, the result of the variational principle will have a small margin of error of the order of 3%.

$$V_b = V_d = \frac{\sqrt{2}}{\sqrt{11}} N_b \approx 0.16223\ F$$
$$V_a = V_c \approx 0.33777\ F$$

$$correct\ solution\ on\ the\ basis\ of\ symmetry:$$

$$ratio\ of\ slope\ l_b / l_a = {}^{1}/_{2} \rightarrow$$
$$V_b = V_d = 0.16666\ F$$
$$V_a = V_c = 0.33333\ F$$

Although this example is not a thrust network it does exemplify the use of complementary energy. The solutions for 3D graphic statics are always an approximation, also by means of variational principles, but they do provide the lowest energy solutions.

5 Thrust line of statically indeterminate arches

5.1 Introduction

There is only one unambiguous solution for the thrust line of a statistically determinate arch and it can be determined easily. Because of the statically determinacy of the arch we know that the thrust line must pass through the point where the moments are equal to zero, such as the hinges. The thrust line thus can be drawn using a force polygon, which is its reciprocal figure.

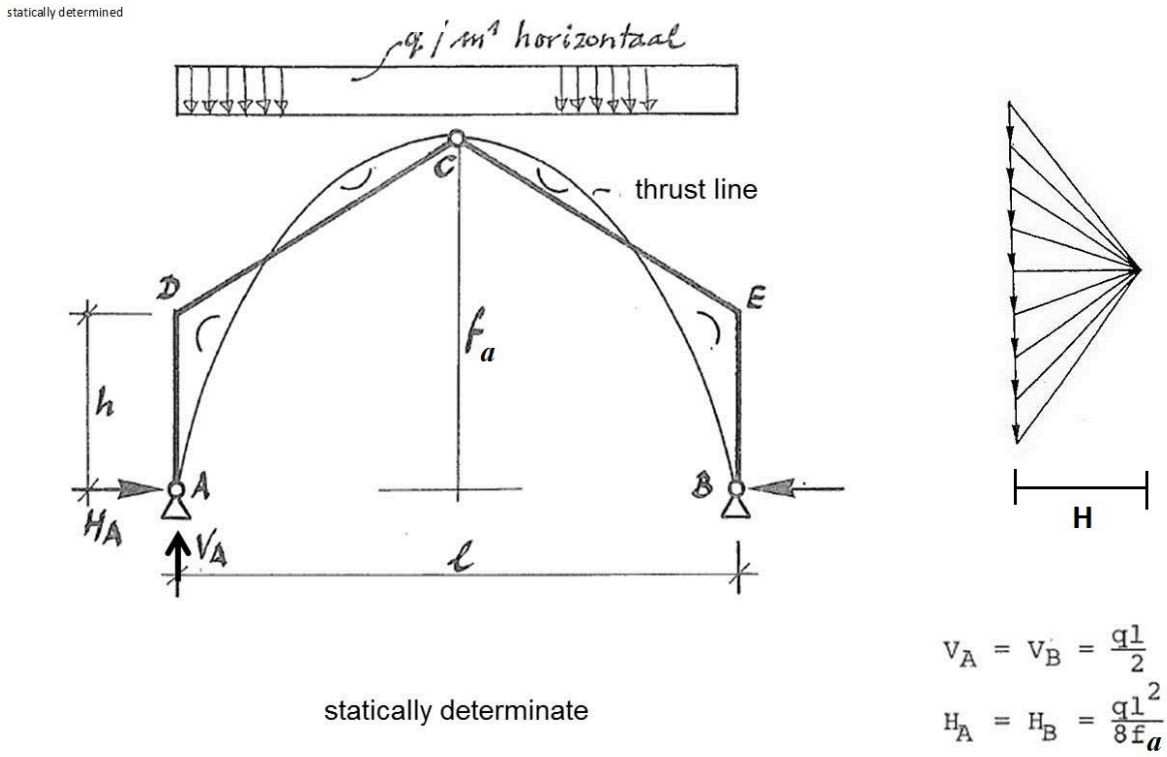

This is not the case for statically indeterminate arches with hinged supports, which degree of indeterminacy is: $s = 1$. A range of possible solutions exist that satisfy equilibrium, consequently each solution is viable. To be able to determine the correct solution, several analytical and numerical methods can be used, such as a FEM or the finite difference method. The correct solution is the one in which the statically indeterminacy, which determines the support reaction and the internal forces of the system, is solved. In the case of the arch the rise *f* of the thrust line or the horizontal reaction force *H* can be solved. The method used here is analogous to that in the previous chapters. To determine the value of the redundant is to minimize the complementary energy of the system [62] [63].

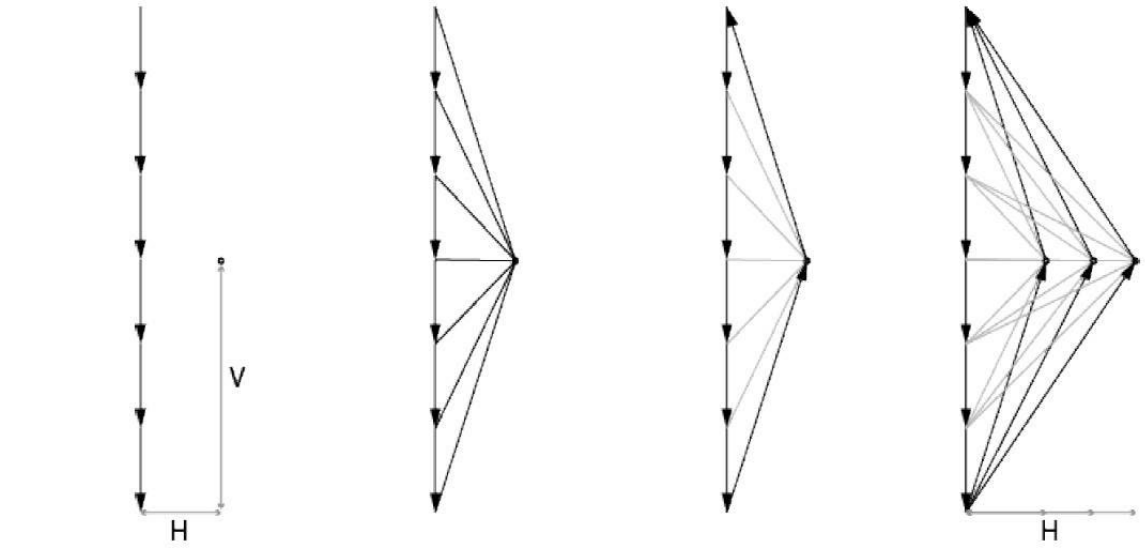

Figure 36 relation of arch and force polygon [images 62]

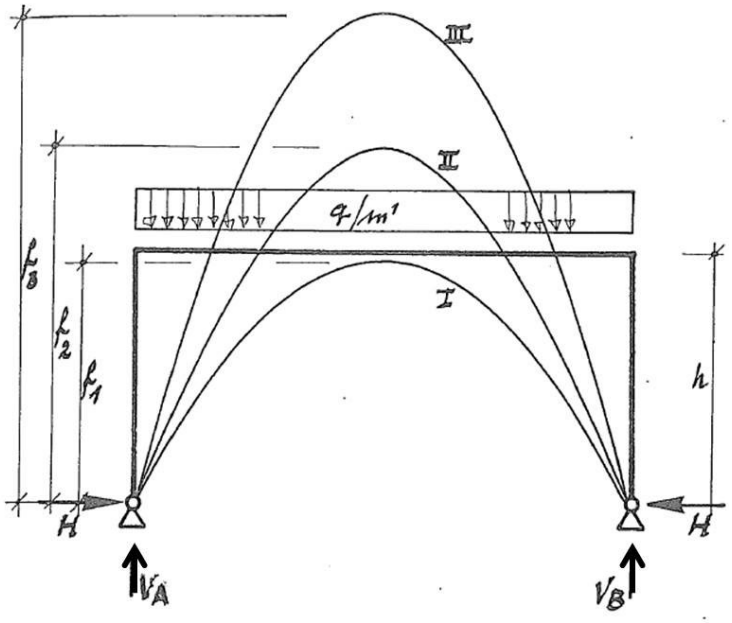

The total complementary energy of a system exists out of two parts, one due to extension (*N*) and the other due to bending (*M*).

$$E_{compl,N\&M} = \frac{1}{2}\frac{N^2 l_s}{EA} + \frac{1}{2}\frac{M^2 l_s}{EI}$$

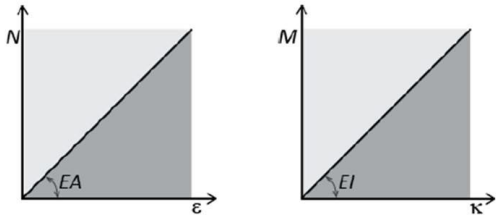

$l_s = arc\ lenght\ of\ the\ arch$

$with\ for\ rectangular\ cross\ section$:

$A = bt : I = \frac{1}{12}bt^2$

Because we are only concerned with the minimum complementary energy we can simplify this formula for the case of an arch with a uniform (prismatic) cross section.

$$E_{compl,N\&M} = N^2 l_s + \frac{12}{t^2} M^2 l_s$$

For most arches and shells the thickness *t* is much smaller than the arc length of the arch/shell l_s. In section 5.6 it will be shown that the energy due to extension (*N*) is much smaller than the bending energy and can therefore be neglected. The equation for the complementary energy reduces to.

$$E_{compl,M} = \frac{12}{t^2} M^2 l_s$$

In section 5.5 the procedure will be explained in detail and will be demonstrated with an example and an analytical proof of this theorem [64].

5.2 Relation between the thrust line and the axis of the arch

We will use an example in the next section to elaborate on the method of solving the redundant (*H* or *f*) by using the full expression to determine the complementary energy and minimizing this for the system. This will be done by varying the magnitude of the horizontal reaction force *H* until the minimum value has been reached.
For this procedure we need information from both the actual arch and a - for now assumed - course of the thrust line. The force polygon of the thrust line gives a direct relation between the loads in the arch or thrust line and the internal axial of the thrust line. The axis of the arch and the thrust line will probably not coincide, which means the axial force of the thrust line has an

eccentricity to the axis of the arch thus resulting in bending moments in the arch. It must be noted for completeness that it is entirely possible that the thrust line and the axis of the arch coincide, forming a funicular arch thus without bending moments.

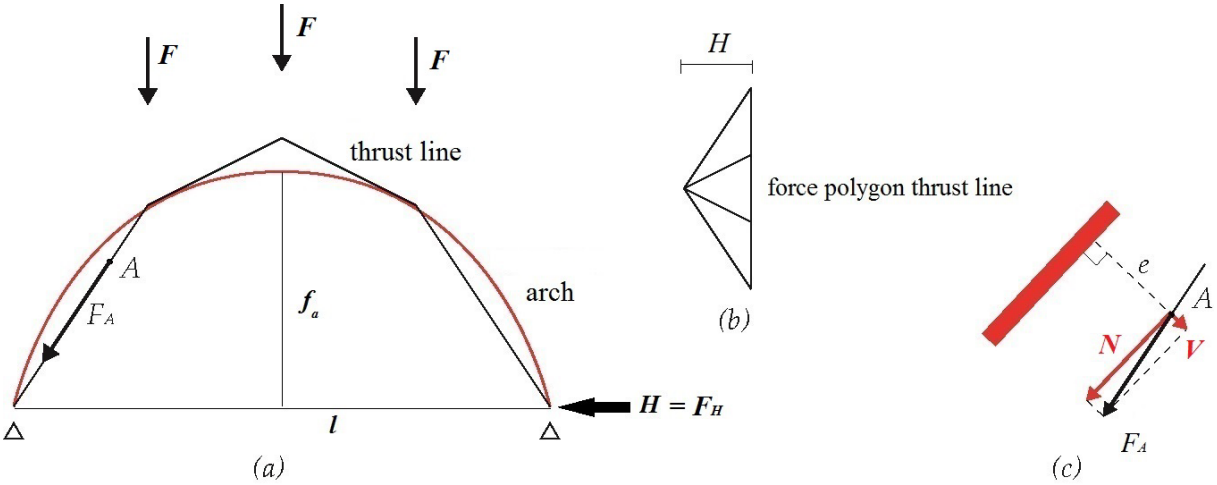

The information required from the arch concerns its geometry, the applied loads and the support conditions, which we will limit in this text to hinges. By assuming a magnitude for the horizontal thrust *H* together with the applied loads *F* a force polygon can be constructed. This force polygon has a reciprocal diagram which forms the thrust line of the arch.
Because of the discrepancy between the axis of the arch and the thrust line, the internal axial forces (N_i , V_i , M_i) of the structure can be related to the force F_i of the thrust line. The bending moment M_i depends on the distance (eccentricity *e*) between the axis and the thrust line. There are several ways to determine this, but because horizontal reaction force *H* ($=F_H$) is the redundant, the bending moment will be determined by multiplying F_H with the vertical eccentricity e_v. In this way we can set up an equation for the complementary energy of the system with only one parameter or unknown, the redundancy F_H.

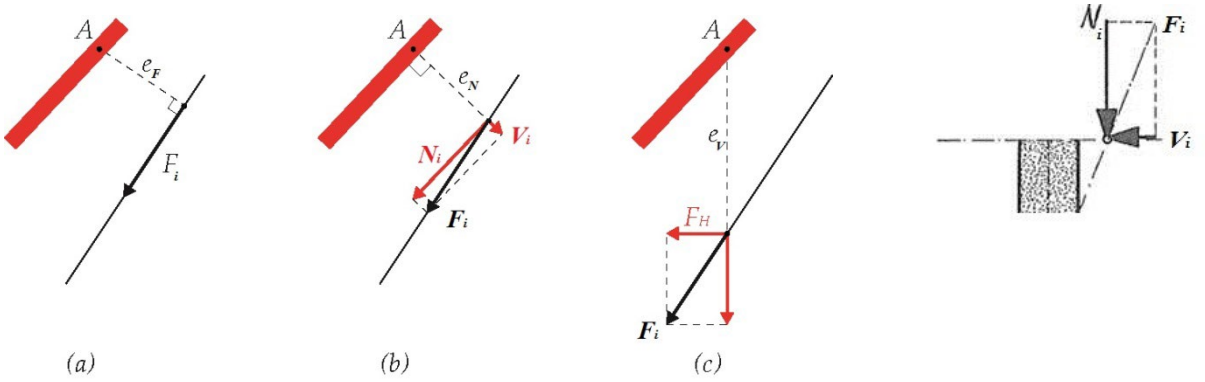

$$M_i = F_i e_F \qquad M_i = N_i e_N \qquad M_i = F_H e_V$$

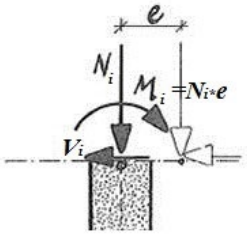

Figure 37 relation eccentricity with axis arch [images 63]

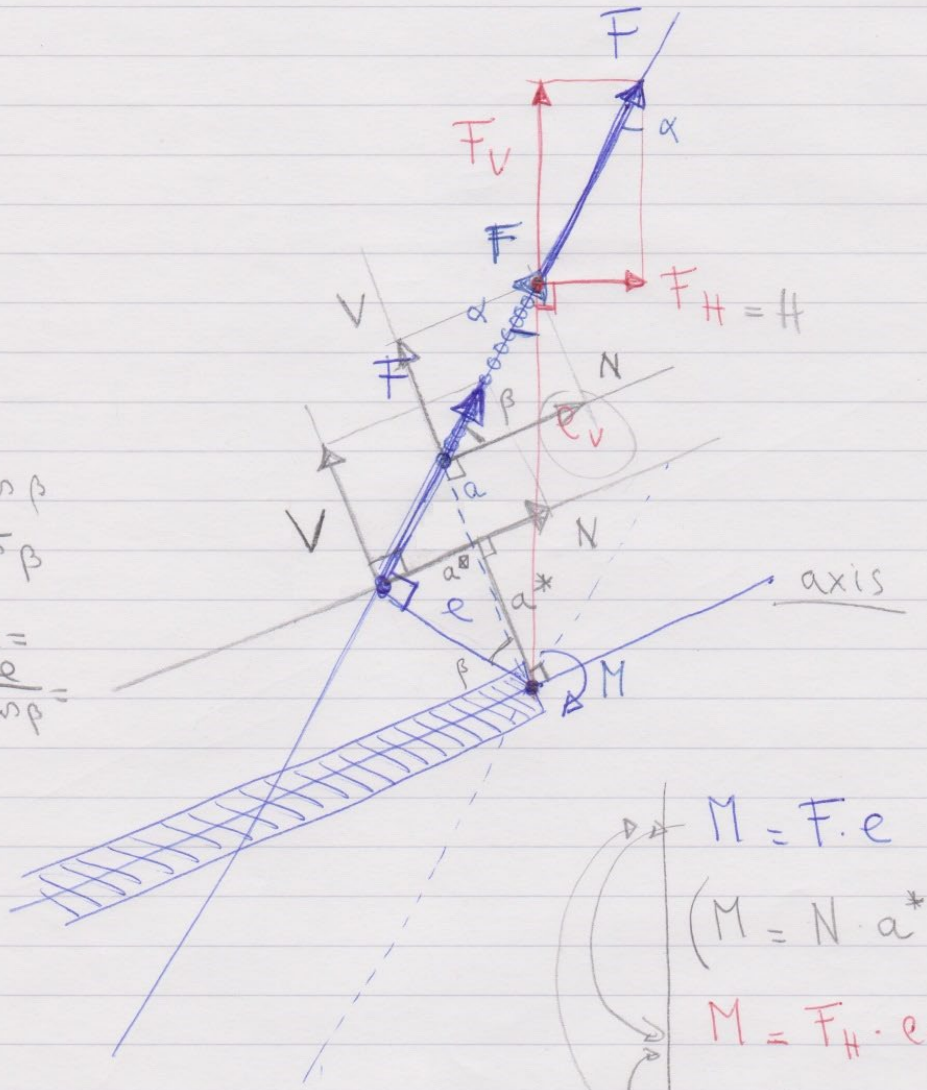

$N = F \cos\beta$

$a = \frac{e}{\cos\beta}$

$M = N\,a =$

$F \cos\beta \cdot \frac{e}{\cos\beta} =$

$F \cdot e$

$M = F \cdot e$

$(M = N \cdot a^* + V a^{**})$

$M = F_H \cdot e_V \quad (e_H = 0)$

$M = N\,a$

$F_H = F \sin\alpha$

$e_V = \frac{e}{\sin\alpha}$

$M = F_H \cdot e_V = F \sin\alpha \cdot \frac{e}{\sin\alpha} = F \cdot e$

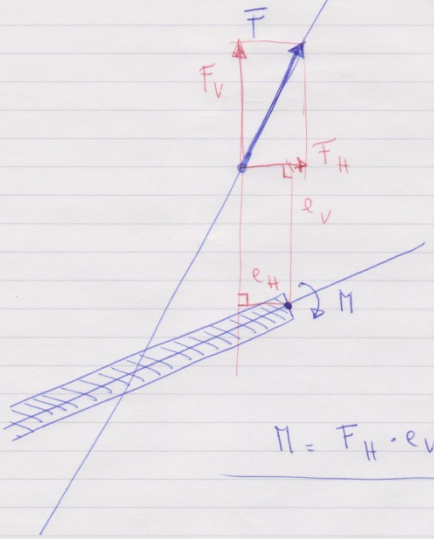

$M = F_H \cdot e_V + F_V \cdot e_H.$

We can graphically represent the relation between the force polygon of the thrust line and the structure (axis) in one force polygon. The classical force polygon shows the forces F_i of the thrust line, and by decomposing these forces according to the slope of the respective segments into which the arch is discretised, we get the internal forces (N_i , V_i) of the structure, we can represent these in the same diagram.

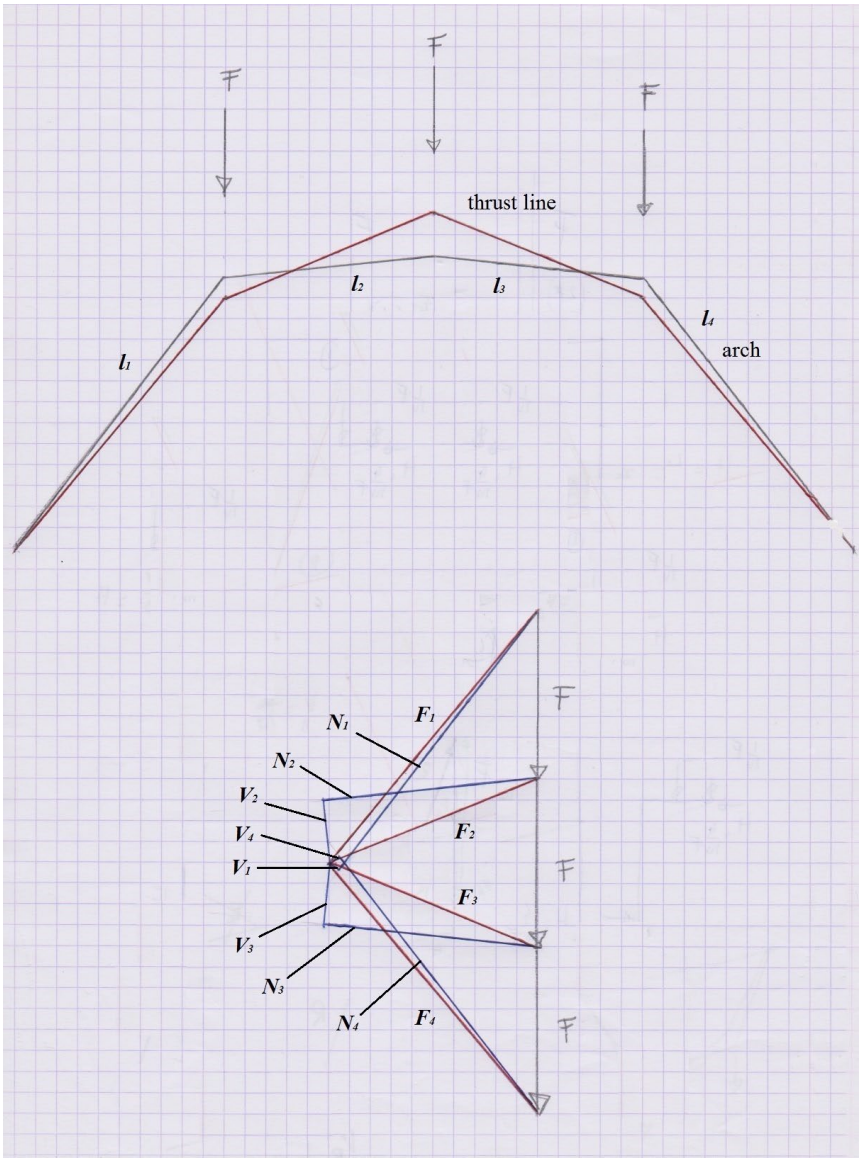

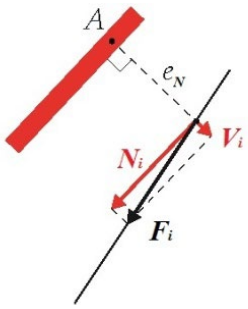

5.3 Solving the indeterminate horizontal thrust

As an example the structure can be discretised into straight segments with the loads (*F*) applied to the folds between the segments and their local coordinate system defined. The redundant F_H (*H*) will be solved by minimizing the complementary energy due to bending of the system. It is acceptable to neglect the energy due to extension, as will be shown in section 5.6.

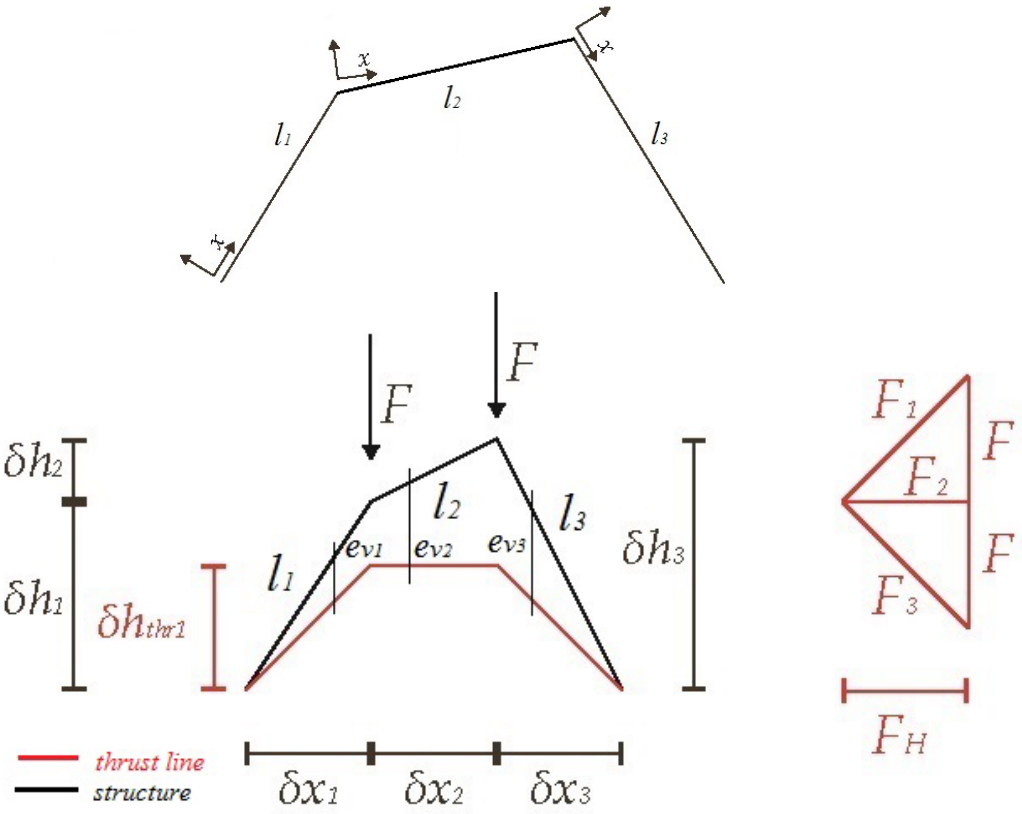

Figure 38 relation trust line with axis arch [images 63]

For the above three bar arch the total complementary energy will be analytically determined and minimized. For this example the spacing between the loads is equal.

$$\delta x_1 = \delta x_2 = \delta x_3 = \delta x$$

First equations are set-up to quantify the vertical distance between the arch and the assumed thrust line (excentricity e_v) based on a viable presupposed force polygon (ensure equilibrium). With the help of these, the moments in the structure will be determined expressed as a function of the redundancy F_H. The squared moments will be integrated over the arc length of the arch, for each segment, which results in the total complementary energy of the structure, and is minimized to ascertain the exact solution for F_H.

$$e_{v1} = (\delta h_1 - \delta h_{t1})\frac{x}{l_1}$$
$$e_{v1} = (\delta h_1 - \delta h_{t2})\frac{x}{l_2} + (\delta h_1 - \delta h_{t1})$$
$$e_{v1} = (\delta h_3 - \delta h_{t3})\frac{-x + l_3}{l_3}$$

The goal is to express the outcome for F_H in terms only pertaining to parameters of the geometry of the arch; the horizontal and vertical projected distance of each segment (δx_i , δh_i) and the segment length (l_i). For this it is necessary to replace in the expression for the eccentricities the rise of each segment of the thrust line δht_i . This is also takes care of the necessity to include the vertical component of the axial force in each segment F_{iv} which is related to the load (F) of the structure.

$$\delta h_{t1} = \frac{F_{1v}}{F_H}\delta x$$
$$\delta h_{t2} = \frac{F_{2v}}{F_H}\delta x$$
$$\delta h_{t3} = \frac{F_{3v}}{F_H}\delta x$$

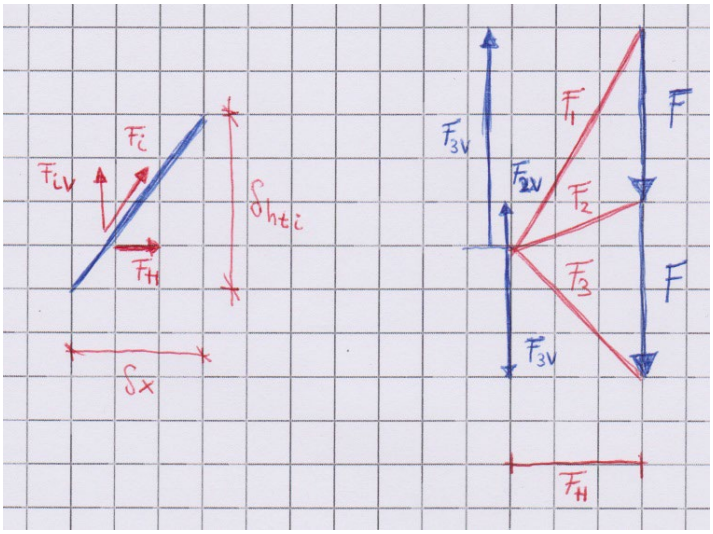

The expressions for the eccentricities can be multiplied with the redundancy F_H to determine the bending moments in each segment.

$$M_1 = F_H e_{v1} = F_H\left(\frac{\delta h_1}{l_1} - \frac{F_{1v}}{F_H}\frac{\delta x}{l_1}\right)x$$
$$M_2 = F_H e_{v2} = F_H\left(\frac{\delta h_2}{l_2} - \frac{F_{2v}}{F_H}\frac{\delta x}{l_2}\right)x - F_{1v}\delta x + F_H\delta h_1$$
$$M_3 = F_H e_{v3} = F_H\left(-\frac{\delta h_3}{l_3} + \frac{F_{3v}}{F_H}\frac{\delta x}{l_3}\right)x - F_{3v}\delta x + F_H\delta h_3$$

By integrating these moments over the length of each segment, we arrive at the total complementary energy of the structure, where the last five terms are not a funtion of F_h. In the next section it will be shown that these relate to the transfer of the load.

$$E_{compl,M} = \int_0^{l_1} M_1^2\,dx + \int_0^{l_2} M_2^2\,dx + \int_0^{l_3} M_3^2\,dx =$$
$$\frac{1}{3}\delta h_1^2 l_1 F_H^2 + \left(\frac{1}{3}\delta h_2^2 + \delta h_1 \delta h_2 + \delta h_1^2\right) l_2 F_H^2 + \frac{1}{3}\delta h_3^2 l_3 F_H^2 -$$
$$\frac{2}{3}F_{1v}\,\delta h_1 \delta x l_1 F_H - \left[F_{1v}(2\delta h_1 + \delta h_2) + F_{2v}\left(\delta h_1 + \frac{2}{3}\delta h_2\right)\right]\delta x l_2 F_H - \frac{2}{3}F_{3v}\delta h_3 \delta x l_3 F_H +$$
$$\underbrace{\frac{1}{3}F_{1v}^2\delta x^2 l_1 + \frac{1}{3}F_{2v}^2\delta x^2 l_2 + \frac{1}{3}F_{3v}^2\delta x^2 l_3 + F_{1v}^2\delta x^2 l_2 + F_{1v}F_{2v}\delta x^2 l_2}_{load\ transfer}$$

By minimizing this we get an exact solution for the redundant F_H.

$$\frac{dE_{compl,M}}{dF_H} = 0 \Rightarrow$$

$$F_H = \frac{F_{1v}\delta x\left(\frac{2}{3}\delta h_1 l_1 + 2\delta h_1 l_2 + \delta h_2 l_2\right) + F_{2v}\delta x\left(\delta h_1 l_2 + \frac{2}{3}\delta h_2 l_2\right) + F_{3v}\delta x\left(\frac{2}{3}\delta h_3 l_3\right)}{\frac{2}{3}\delta h_1^2 l_1 + \frac{2}{3}\delta h_2^2 l_2 + \frac{2}{3}\delta h_3^2 l_3 + 2\delta h_1^2 l_2 + 2\delta h_1 \delta h_2 l_2}$$

The images below provide a visual overview of the process. Figure (*e*) shows the area that has been integrated to get the structures total complementary (bending) energy.

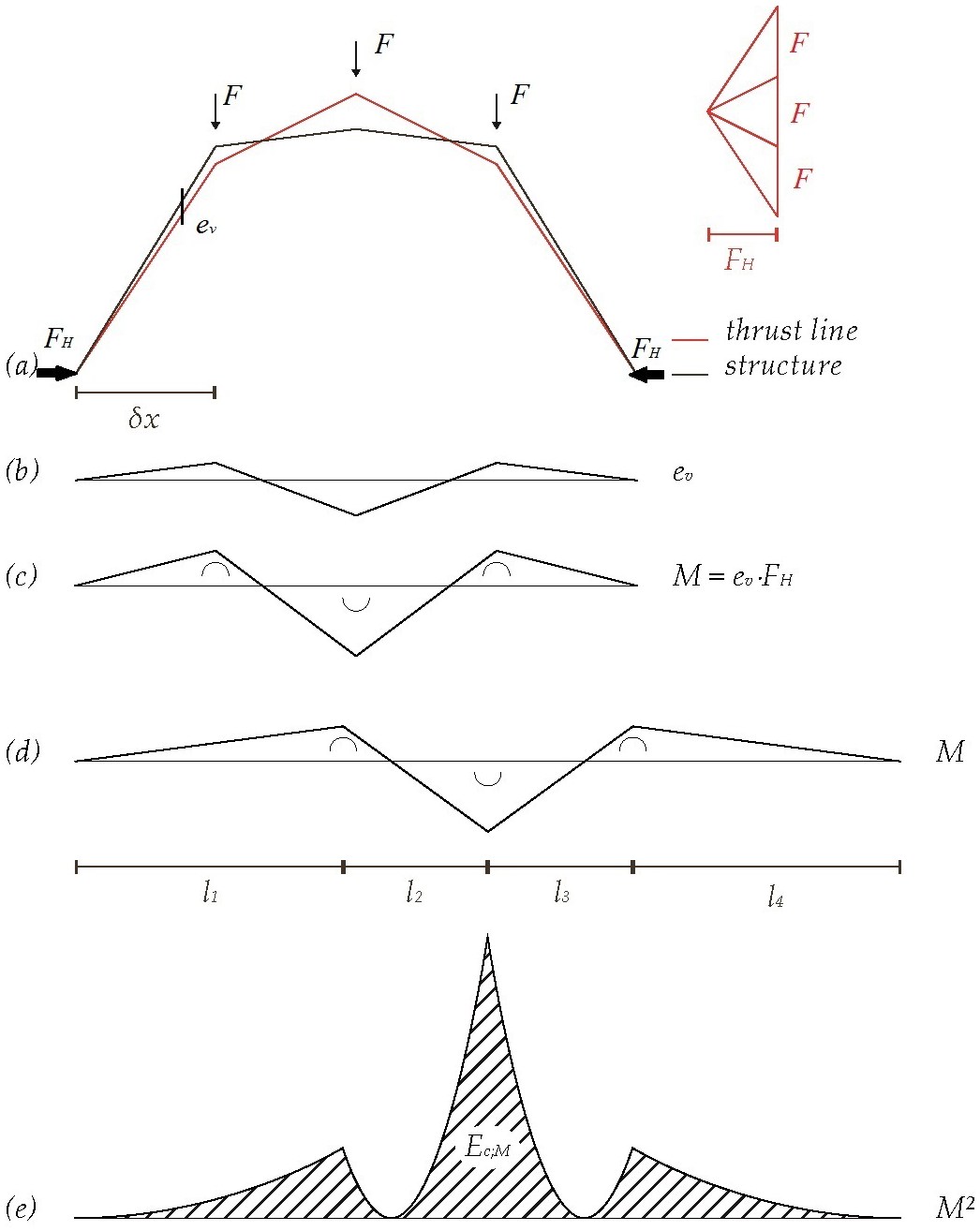

Figure 39 graphic representation of the complementary energy arch [images 63]

This section will be concluded with a numerical elaboration. For this we need to make an initial assumption of the force polygon and thus the thrust line.
The value for F_H calculated by minimizing the total complementary (bending) energy is 3375 N. The value obtained from a FEM (GSA) calculation, in which of course the energy due to extension is not neglected, is 3374 N, that is an error of 0.03%. When the value of F_H has been calculated, the correct force polygon and thrust line can be drawn.

$$F_H = \frac{5000*3\left(\frac{2}{3}*4*5+2*4*3+0\right)-1000*3\left(0+4*3\right)+4000*3\left(\frac{2}{3}*4*5\right)}{\frac{2}{3}*4^2*5+0+\frac{2}{3}*4^2*5+2*4^2*3+0} = 3375\ N$$

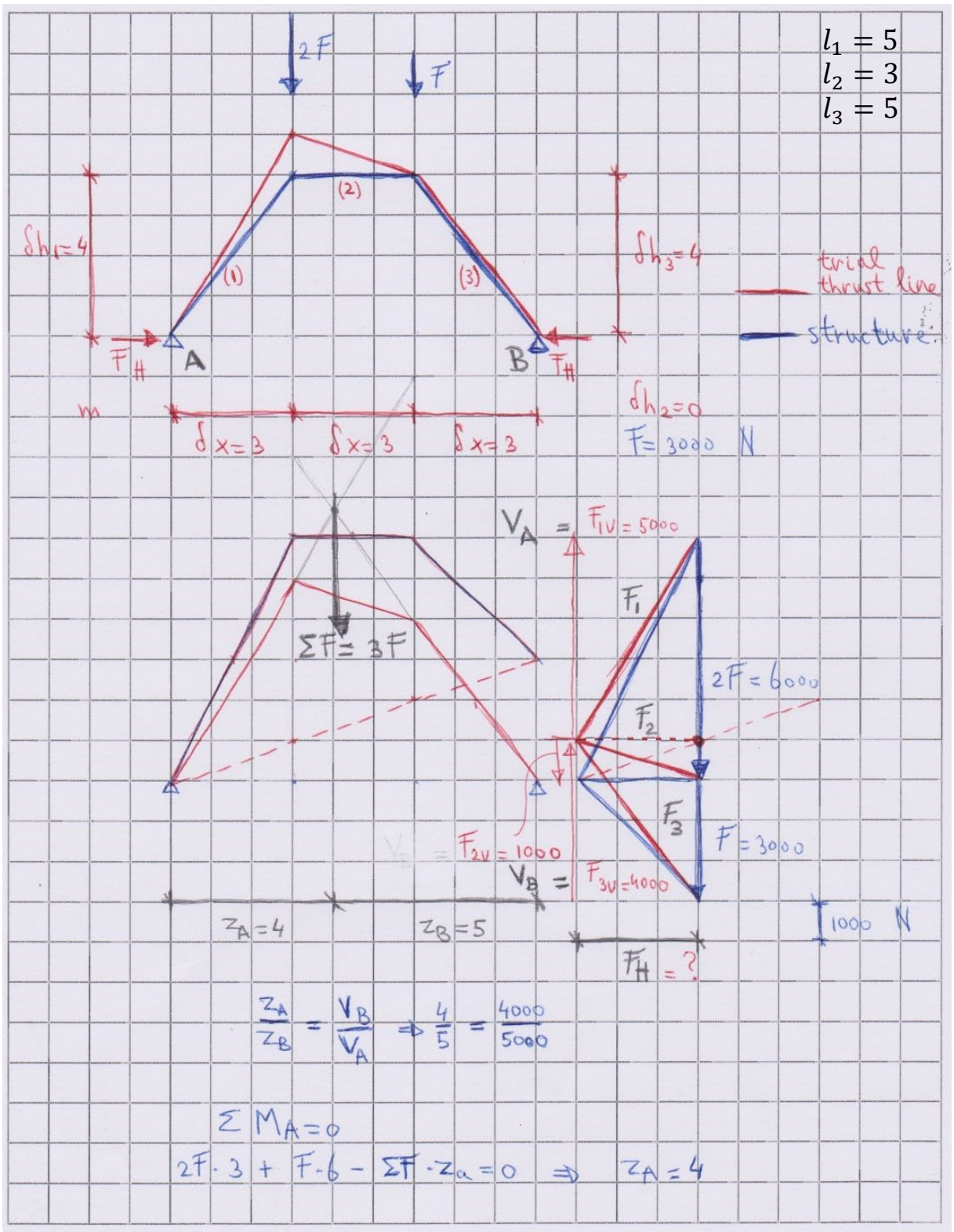

5.4 The two load cases and Maxwell's load path for indeterminate arches

The total complementary energy due to bending has two parts. The first part is a function of the horizontal thrust *H*, the second part is only related to the vertical forces in the system. This part remains constant if the horizontal thrust changes by scaling the force polygon. It relates to the load transfer and is equivalent to the load transfer of a beam with the same load and span. In fact there are two load cases each with their own energy. We further elaborate using the example of the previous section.

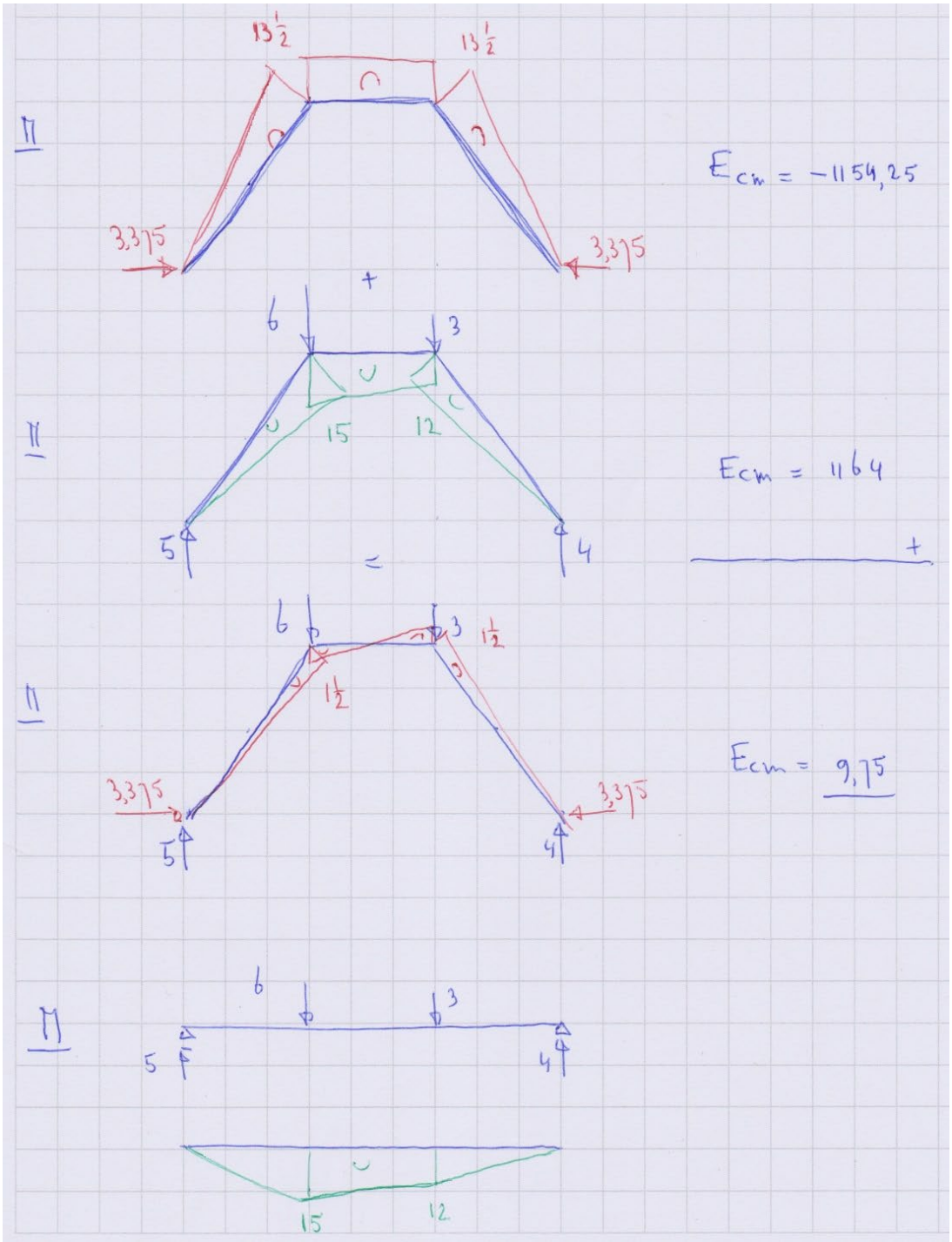

When the static indeterminacy, the horizontal thrust, is solved the resulting total energy has the smallest possible difference between the energy of the two load cases.

$$E_{compl,M:H} = \frac{1}{3}\delta h_1^2 l_1 F_H^2 + \left(\frac{1}{3}\delta h_2^2 + \delta h_1 \delta h_2 + \delta h_1^2\right) l_2 F_H^2 + \frac{1}{3}\delta h_3^2 l_3 F_H^2 - \frac{2}{3}F_{1v}\,\delta h_1 \delta x l_1 F_H$$
$$- \left[F_{1v}(2\delta h_1 + \delta h_2) + F_{2v}\left(\delta h_1 + \frac{2}{3}\delta h_2\right)\right]\delta x l_2 F_H - \frac{2}{3}F_{3v}\delta h_3 \delta x l_3 F_H = -1154.25$$

$$E_{compl,M:V} = \frac{1}{3}F_{1v}^2 \delta x^2 l_1 + \frac{1}{3}F_{2v}^2 \delta x^2 l_2 + \frac{1}{3}F_{3v}^2 \delta x^2 l_3 + F_{1v}^2 \delta x^2 l_2 + F_{1v}F_{2v}\delta x^2 l_2 = 1164$$

$$E_{compl,M} = E_{compl,M:V} - E_{compl,M:H} = 1164 - 1154.25 = 9.75$$

Another way of solving the statical indeterminacy is thus minimizing the difference between the two energy parts.

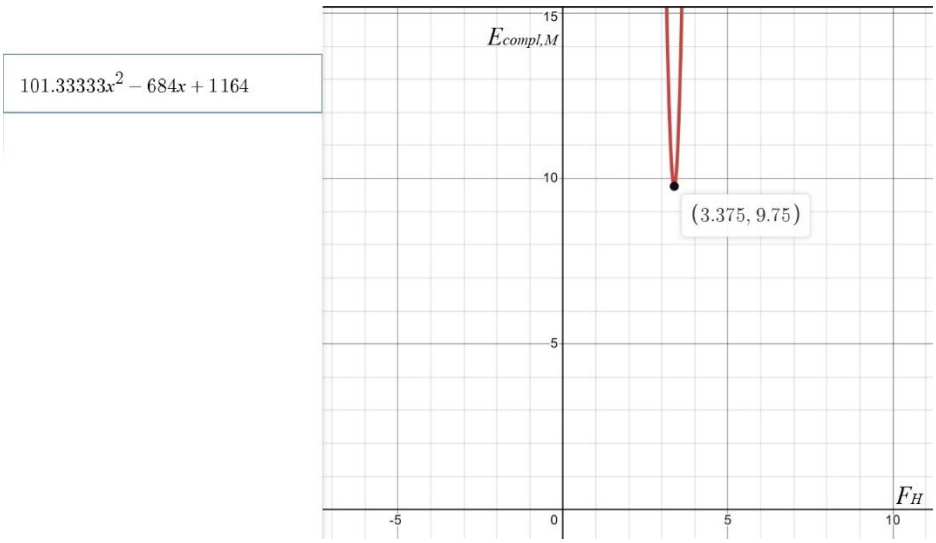

This result is the same solution for the horizontal thrust.

$$E_{compl,M:H} = 101\frac{1}{3}F_H^2 - 684F_H$$
$$E_{compl,M:V} = 1164$$

$$E_{compl,M} = 101\frac{1}{3}F_H^2 - 684F_H + 1164 \rightarrow min \Rightarrow F_H = 3.375$$
$$E_{compl,M} = 101\frac{1}{3}(3.375)^2 - 684(3.375) + 1164 = 9.75$$

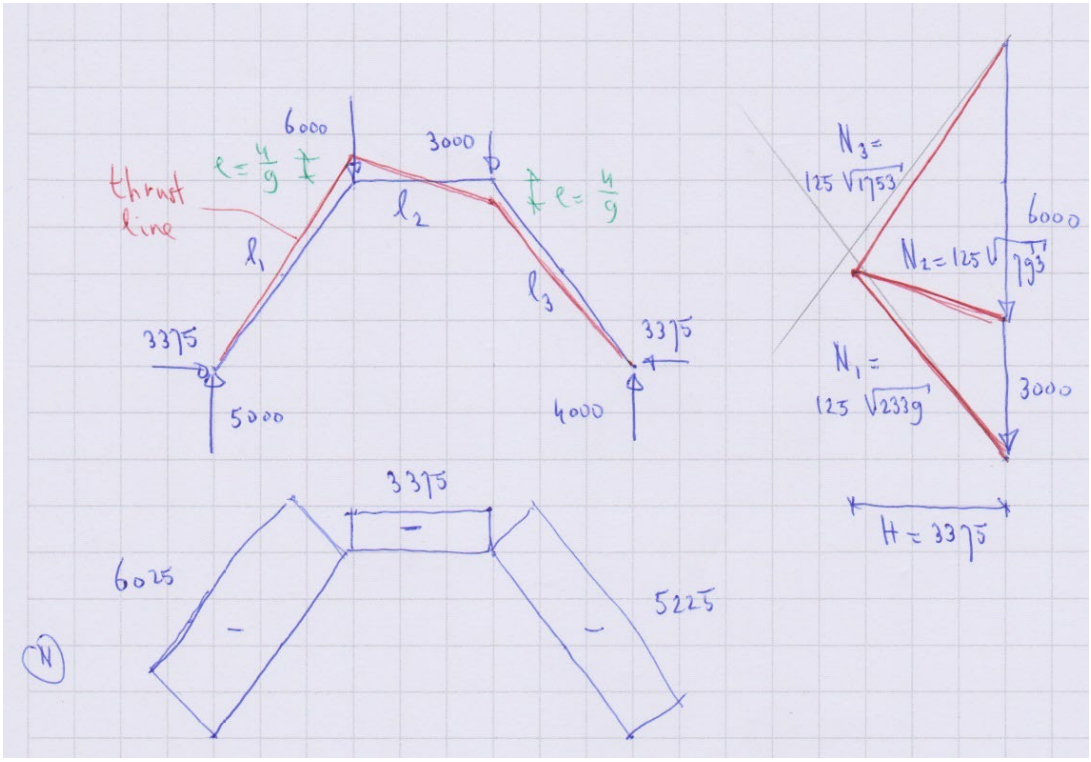

To-date, Maxwell's load path theorem is has only been used for statically determinate structures.

$$\textit{Maxwell load path}: \underbrace{\sum_i N_{t_i} l_{t_i} - \sum_i N_{c_i} l_{c_i}}_{internal\ forces} = \underbrace{\sum_i \vec{F}_i \cdot \vec{r}_i}_{loads,\ reactions}$$

But this theorem is also applicable for statically indeterminate arches. The reason for this is that the summation of the work done by the shear forces over all members is always zero. The work done by bending in each cross section is also zero, the tension is equal to the compression in each cross section. The load path for the arch is slightly lower than for the thrust line.

$l_1 = 5$
$l_2 = 3$
$l_3 = 5$

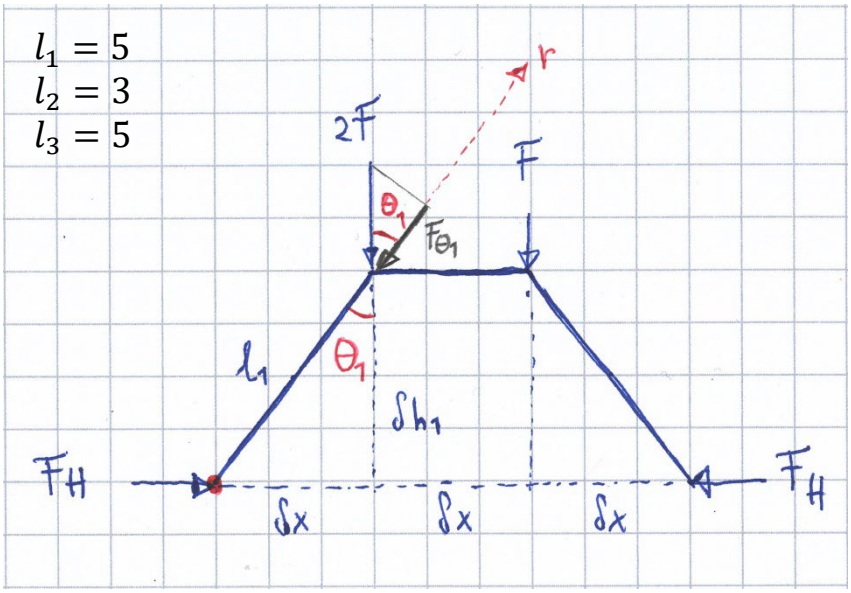

$$\cos\theta_1 = \frac{F_{\theta_1}}{2F} = \frac{\delta h_1}{l_1}$$
$$\Rightarrow F_{\theta_1} l_1 = 2F \cdot \delta h_1$$

$Maxwell\ load\ path$:

$arch$:
$2F\ \delta h_1 + F\ \delta h_3 + F_H 3\delta x = 24000 + 12000 + 30375 = 66375$
$N_1 l_1 + N_2 l_2 + N_3 l_3 = 30125 + 10125 + 26174 = 66375$

$thrustline$:
$2F\frac{40}{9} + F\frac{32}{9} + F_H\ 9 = \frac{80000}{3} + \frac{32000}{3} + 30375 = 67708\frac{1}{3}$
$N_1 l_1 + N_2 l_2 + N_3 l_3 = \frac{291125}{9} + \frac{99125}{9} + \frac{219125}{9} = 67708\frac{1}{3}$

5.5 Procedure of the method

The hand calculation of a relatively simple example in the previous section is cumbersome. With more complex examples the complexity will increase rapidly. This makes a computational procedure attractive to solve the redundant F_H.

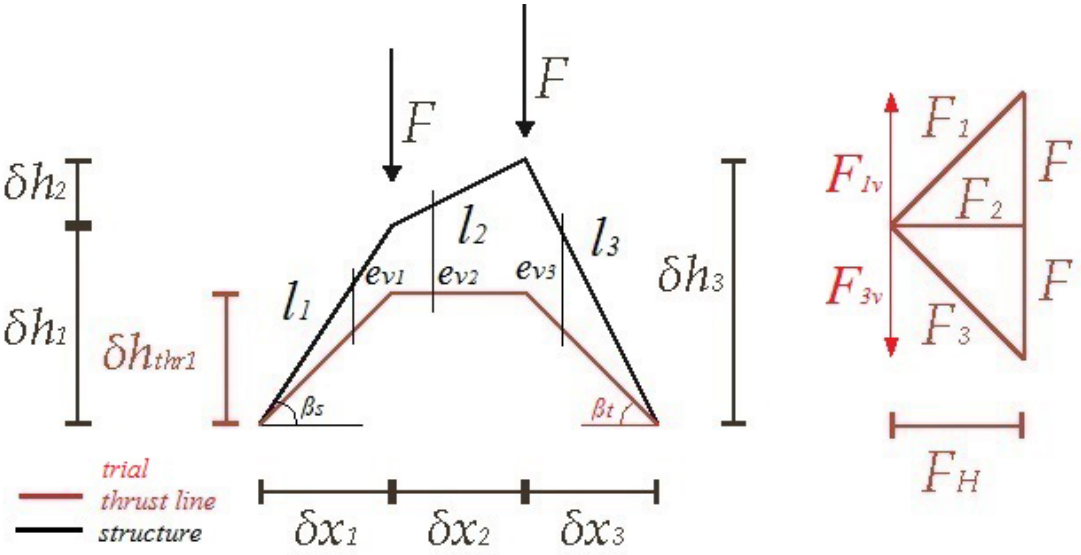

A parametric platform makes a good design tool and is advised as a basis for the computational procedure, allowing a real-time feedback and to be able to present the results of the process visually. Some parameters are fixed, for example relating to the geometry of the arch, or the given loads. Other parameters depend on the redundant F_H which is the unknown to be solved. We will denote the two types of parameter with: fixed ***f*** and dependant ***d***.

The following parameters are needed.

- geometry of the arch:
    a) the horizontal projected distance of each segment (δx_i) ***f***
    b) the vertical projected distance of each segment (δh_i) ***f***
    c) the segments length (l_i) ***f***
    d) the angle of each segment with the horizontal axis (β_{si}) ***f***

- draw a force polygon (***d***) based on the loads (***f***) which ensures equilibrium

- geometry of the thrust line (based on viable presupposed force polygon):
    a) the horizontal projected distance of each segment (δx_i), equal to arch ***f***
    b) the vertical projected distance of each segment (δh_{ti}) ***d***

c) the angle of each segment with the horizontal axis (β_{ti}) ***d***

- calculate the total complementary energy of the system:
  a) determine the internal axial force arch ***d***:

$$\gamma_i = \beta_{si} - \beta_{ti}$$

$$N_i = F_i \cos\gamma_i$$

  b) calculate the eccentricities along the arc length (local coordinate system) ***d***: e_{vi}

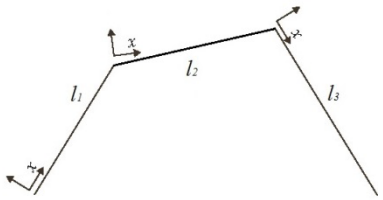

  c) calculate the total extension complementary energy ***d***

$$E_{c,n} = \Sigma N_i^2 l_i$$

$$if\ t << \delta_x, \delta h_i, l_i\ then\ compl.energy\ N\ can\ be\ neglected$$

  d) calculate the total bending complementary energy ***d***

$$E_{c,m} = \Sigma \frac{12}{t^2} \left(F_H e_{vi}\right)^2 l_i$$

This can be done by numerically integrating the area of $(M_i)^2$ along the arc length.

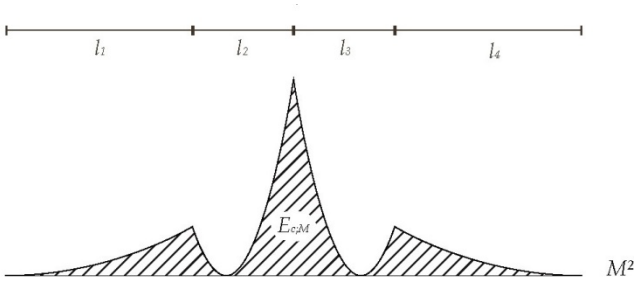

  e) vary the value of F_H until the total complementary $E_{c,nm}$ energy is at a minimum to attain its correct value.

An alternative procedure is to square the difference of the area's under the arch and the thrust line of the load, the eccentricity, and minimized these to solve the redundancy *f* and *H*.

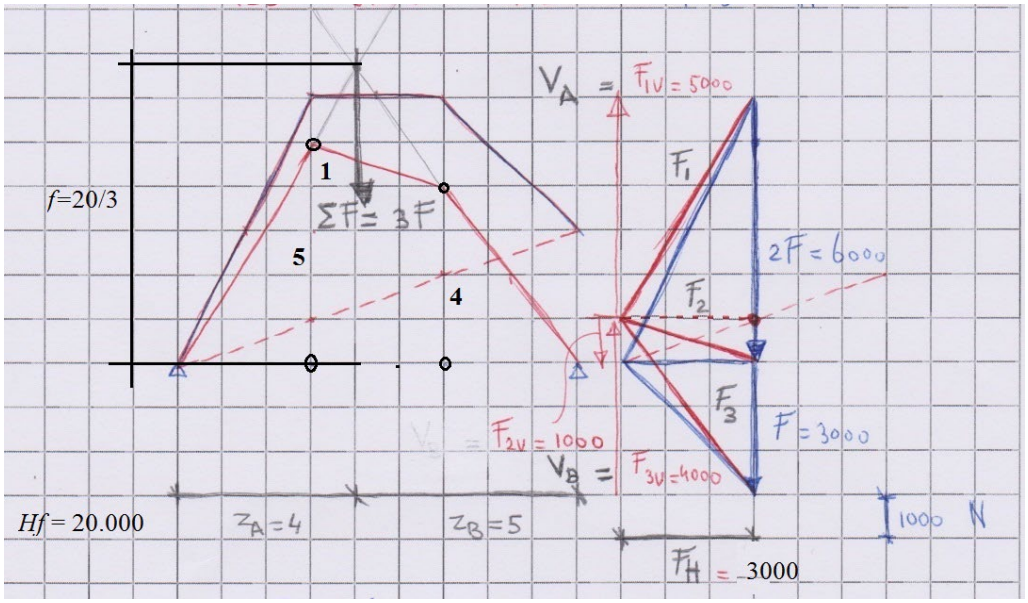

$$F_H f = 3000\frac{20}{3} = 20000$$

$$with: \delta h_{ti} = \alpha_i f$$
$$\alpha_1 = \frac{50}{\frac{20}{3}} = \frac{3}{4}: \alpha_2 = \frac{1}{\frac{20}{3}} = \frac{3}{20}: \alpha_3 = \frac{4}{\frac{20}{3}} = \frac{3}{5}$$

$$area\ under\ arch:$$
$$A_{arch} = \delta x\left(\frac{1}{2}\delta h_1 + \delta h_1 + \frac{1}{2}\delta h_3\right) = 3\left(\frac{1}{2}4 + 4 + \frac{1}{2}4\right) = 24$$

$$area\ under\ thrust\ line:$$
$$A_{thrust} = \frac{1}{2}\delta h_{t1}\delta x + \left(\delta h_{t1} - \frac{1}{2}\delta h_{t2}\right)\delta x + \frac{1}{2}\delta h_{t3}\delta x$$
$$= \frac{1}{2}\frac{3}{4}f\,3 + \left(\frac{3}{4}f - \frac{1}{2}\frac{3}{20}f\right)3 + \frac{1}{2}\frac{3}{5}f\,3 = \frac{81}{20}f$$

$$e_v = A_{thrust} - A_{arch} = \frac{81}{20}f - 24$$

$$E_{compl,M} = M^2 = F_H^2 e_v^2 = F_H^2\left(\frac{6561f^2}{400} - \frac{972f}{5} + 576\right) \rightarrow min$$
$$\frac{d\,E_{compl,M}}{df} = 0 \Rightarrow \frac{6561}{200}f - \frac{972}{5} = 0 \Rightarrow f = \frac{160}{27}$$
$$F_H f = 20000 \Rightarrow F_H = 20000\frac{27}{160} = 3375$$

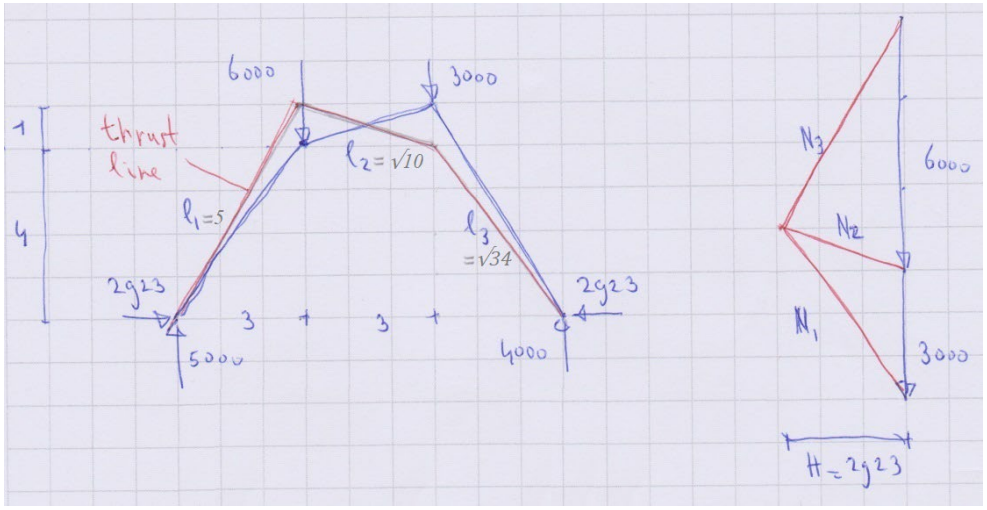

The simplified procedure with only the equivalent area's gives an exact solution if the arch and the loads are symmetric. By numerically subtracting the area's under the arch and the thrust line of the load the information on the distribution of the eccentricity along the axis is lost. This results in a small error in this example due to the arch's asymmetry. But this method gives a sufficiently good result for design purposes.

$$F_H f = 3000\frac{20}{3} = 20000$$

$$with: \delta h_{ti} = \alpha_i f$$
$$\alpha_1 = \frac{3}{4}: \alpha_2 = \frac{3}{20}: \alpha_3 = \frac{3}{5}$$

$$area\ under\ arch:$$
$$A_{arch} = 3\left(\frac{1}{2}4 + 4 + \frac{1}{2}1 + \frac{1}{2}5\right) = 27$$

$$area\ under\ thrust\ line:$$
$$A_{thrust} = \frac{81}{20}f$$

$$e_v = A_{thrust} - A_{arch} = \frac{81}{20}f - 27$$

$$E_{compl,M} = M^2 = F_H^2 e_v^2 = F_H^2\left(\frac{6561f^2}{400} - \frac{2187f}{10} + 729\right) \rightarrow min$$
$$\frac{d\,E_{compl,M}}{df} = 0 \Rightarrow \frac{6561}{200}f - \frac{2187}{10} = 0 \Rightarrow f = \frac{20}{3}$$
$$F_H f = 20000 \Rightarrow F_H = 20000\frac{3}{200} = 3000 \quad (error\ 2.57\%)$$
$$exact: F_H = 2923$$

5.6 Contribution of extension to complementary energy

The complementary energy is taken into account as a result of the axial force, extension.

$$E_{compl,N} = N_i^2 l_i = (F_i \cos\gamma_i)^2 l_i$$
$$with: F_i^2 = F_H^2 + F_{iV}^2$$

$$E_{compl,M} + E_{compl,N} =$$
$$\frac{12}{t^2}\begin{bmatrix} \frac{1}{3}\delta h_1^2 l_1 F_H^2 + \left(\frac{1}{3}\delta h_2^2 + \delta h_1 \delta h_2 + \delta h_1^2\right) l_2 F_H^2 + \frac{1}{3}\delta h_3^2 l_3 F_H^2 \\ -\frac{2}{3}F_{1v}\,\delta h_1 \delta x l_1 F_H - \left[F_{1v}(2\delta h_1 + \delta h_2) + F_{2v}\left(\delta h_1 + \frac{2}{3}\delta h_2\right)\right]\delta x l_2 F_H \\ -\frac{2}{3}F_{3v}\delta h_3 \delta x l_3 F_H \end{bmatrix}$$
$$+(F_H^2 + F_{1V}^2) l_1 \cos^2\gamma_1 + (F_H^2 + F_{2V}^2) l_2 \cos^2\gamma_2 + (F_H^2 + F_{3V}^2) l_3 \cos^2\gamma_3$$

In the expression for the horizontal thrust the contribution due to the axial force can be neglected if the height of the arch is of an order smaller than the dimensions related to the height and span of the arch. Basically the extension of the members is neglected.

$$\frac{dE_{compl,M\&N}}{dF_H} = 0 \Rightarrow$$

$$and\ with\ maximum\ value\ for \cos^2\gamma_i = 1:$$
$$F_H = \frac{12\left[F_{1v}\delta x\left(\frac{2}{3}\delta h_1 l_1 + 2\delta h_1 l_2 + \delta h_2 l_2\right) + F_{2v}\delta x\left(\delta h_1 l_2 + \frac{2}{3}\delta h_2 l_2\right) + F_{3v}\delta x\left(\frac{2}{3}\delta h_3 l_3\right)\right]}{12\left[\frac{2}{3}\delta h_1^2 l_1 + \frac{2}{3}\delta h_2^2 l_2 + \frac{2}{3}\delta h_3^2 l_3 + 2\delta h_1^2 l_2 + 2\delta h_1 \delta h_2 l_2\right] + \underbrace{t^2[2l_1 + 2l_2 + 2l_3]}_{compl\ energy\ N}}$$
$$if\ t \ll \delta x, \delta h_i, l_i\ then\ complementary\ energy\ N\ can\ be\ neglected$$

5.7 Example semi-circular arch

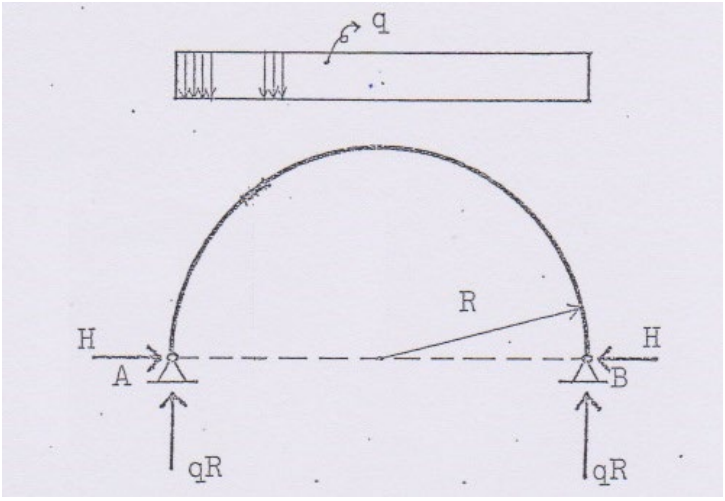

$$R = \frac{1}{2}l$$

The method of this chapter will be demonstrated by the next two examples. For a semi-circular statically indeterminate arch with a uniformly distributed load the horizontal thrust is determined by minimizing the complementary energy, this results in a near exact solution.

$semi-circular\ arch$:
$y_{arch} = (xl - x^2)^{1/2}$

$thrust\ line\ uniform\ distributed\ load\ (parabola)$:
$with: f = \frac{ql^2}{8F_H}$

$$y_{thrust} = f - \frac{f(x-R)^2}{R^2} = \frac{q}{F_H}\frac{xl-x^2}{2}$$

$$e_v = y_{arch} - y_{arch} = \left((xl-x^2)^{1/2} - \left(\frac{q}{F_H}\frac{xl-x^2}{2}\right)\right)$$

$$M^2 = F_H^2 e_v^2$$

$$E_{compl,M} = \int_0^l M^2 dx = F_H^2 \int_0^l \left((xl-x^2)^{1/2} - \left(\frac{q}{F_H}\frac{xl-x^2}{2}\right)\right)^2 dx \rightarrow min$$

$$E_{compl,M} = \frac{l^3}{6}F_H^2 - \frac{3\pi l^4}{128}qF_H + \frac{l^5}{120}q^2 \rightarrow min$$

$$\frac{dE_{compl,M\&N}}{dF_H} = 0 \Rightarrow \frac{l^3}{3}F_H - \frac{3\pi l^4}{128}q = 0$$

$$\Rightarrow F_H = \frac{9\pi}{128}ql \approx 0.221\ ql \quad (error\ 4.1\%)$$

$$exact: F_H = \frac{2}{3\pi}ql \approx 0.212\ ql$$

Here is shown the solution using the squared difference of the areas under the arch and the thrust line of the load, minimising these to solve the redundancy *f*, which results in the exact solution, with the contribution of the extension being neglected. The result with this method is more exact if, apart from an approximately symmetric geometry, there are multiple loads or a distributed load.

$$semi-circular\ arch:$$
$$y = (2Rx - x^2)^{1/2}$$

$$thrust\ line\ uniform\ distributed\ load\ (parabola):$$
$$with: F_H = \frac{ql^2}{8f} = \frac{qR^2}{2f}$$
$$y = f - \frac{f(x-R)^2}{R^2}$$

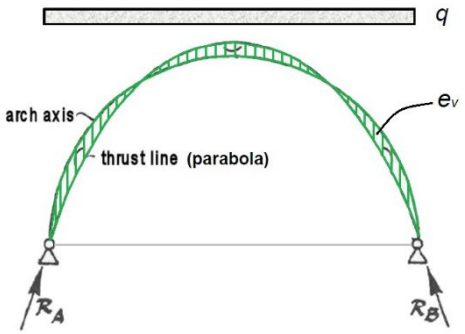

$$area\ under\ arch:$$
$$A_{arch} = \frac{1}{2}\pi R^2$$
$$area\ under\ thrust\ line:$$
$$A_{thrust} = \frac{4}{3}fR$$

$$e_v = A_{thrust} - A_{arch} = \frac{4}{3}fR - \frac{1}{2}\pi R^2 = \frac{8fR - 3\pi R^2}{6}$$

$$E_{compl,M} = M^2 = F_H^2 e_v^2 = F_H^2\left(\frac{16f^2R^2}{9} - \frac{4\pi fR^3}{3} + \frac{\pi^2R^2}{4}\right) \rightarrow min$$
$$\frac{dE_{compl,M}}{dF_f} = 0 \Rightarrow \frac{32R^2}{9}f - \frac{4\pi R^3}{3} = 0$$
$$\Rightarrow f = \frac{3\pi}{8}R$$
$$F_H = \frac{qR^2}{2f} \Rightarrow f = \frac{qR^2}{2F_H} = \frac{3\pi}{8}R$$
$$\Rightarrow F_H = \frac{4}{3\pi}qR$$

Now the redundancy *f* is solved, and the precise rise of the thrust line is known, the horizontal thrust F_h is also fixed. The moments in the arch can now be determined, this is done be considering the arch as a superposition of two load cases; the beam loaded by the uniformly distributed load *q* and the curved arch loaded by the horizontal thrust F_h [65].

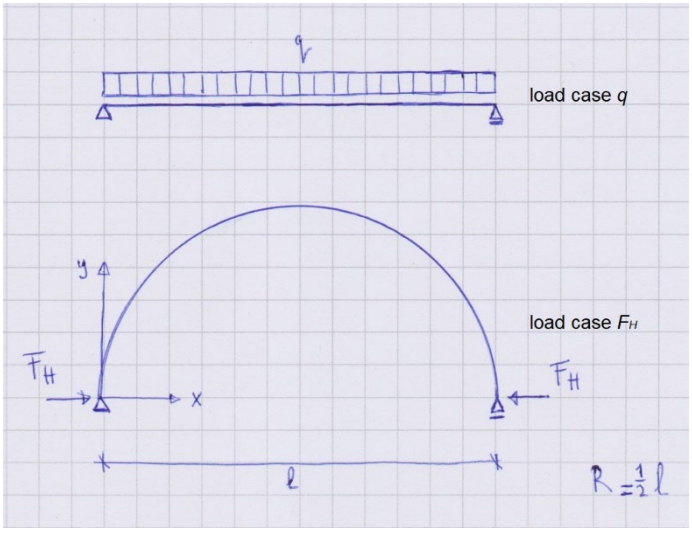

$$M_{arch} = M_q + F_H \cdot y_{arch}$$

Bending moments should be avoided as much as possible when designing an arch. A well designed arch should carry its load efficiently mainly through axial forces instead of bending moments. It is important to assess the structural behavior and to analyze the load-transfer mechanism of an arch during the design process.

$$with: F_H = \frac{4}{3\pi} qR = \frac{2}{3\pi} ql$$

$$\Rightarrow y_{thrust} = \frac{3\pi(xl - x^2)}{4l}$$

$$M_{F_H} = F_H \cdot y_{arch} = \frac{2}{3\pi} ql \cdot (xl - x^2)^{\frac{1}{2}} = \frac{2ql(xl - x^2)^{\frac{1}{2}}}{3\pi}$$

$$M_q = -\frac{qx}{2}(l - x)$$

$$M_{arch} = M_q + M_{F_H} = \frac{-3\pi x(l - x) + 4l(xl - x^2)^{\frac{1}{2}}}{6\pi} q$$

Two methods to assess the efficiency of the arch will be presented here; one on the stress level with the ratio between the axial (σ_n) and bending (σ_m) stresses and via the strain-energy with the ratio of the axial (E_n) and bending (E_m) strain-energy [66, 67].

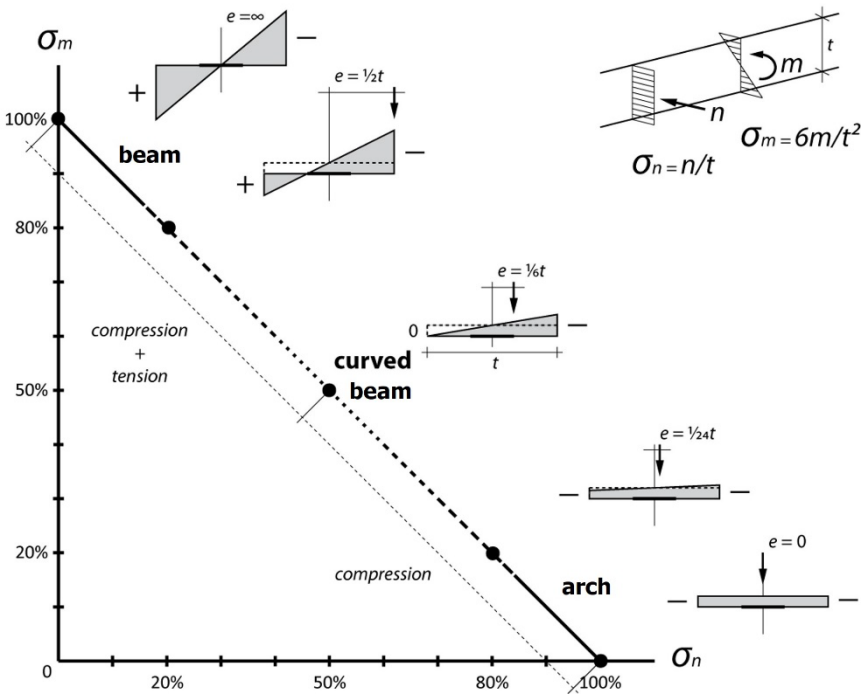

$$for\ b = 1:$$

$$\left.\begin{aligned}\sigma_n &= \frac{n}{t}\\ \sigma_m &= \frac{6m}{t^2}\end{aligned}\right\} Stress\ ratio: \frac{\sigma_n}{\sigma_m + \sigma_n} = \frac{n}{\frac{6m}{t} + n} \cdot 100\%$$

When the ratios are close to 1, the load transfer is primarily done by the axial force. The more the ratio moves to zero, bending will become predominate. With the results of a finite element analysis of the arch an assessment has been performed with both methods. In each point along the arc length the assessment has been determined and is represented in the graph.

$$for\ b = 1:$$

$$with:$$

$$\varepsilon = \frac{n}{Et}\ and\ \kappa = \frac{m}{E\frac{1}{12}t^3}$$

$$\left.\begin{aligned}E_n &= \frac{1}{2}\frac{n^2}{Et}\\ E_m &= \frac{1}{2}\frac{m^2}{E\frac{1}{12}t^3}\end{aligned}\right\} Strain\ energy\ ratio: \frac{E_n}{E_m + E_n} = \frac{n^2}{\frac{12m^2}{t^2} + n^2} \cdot 100\%$$

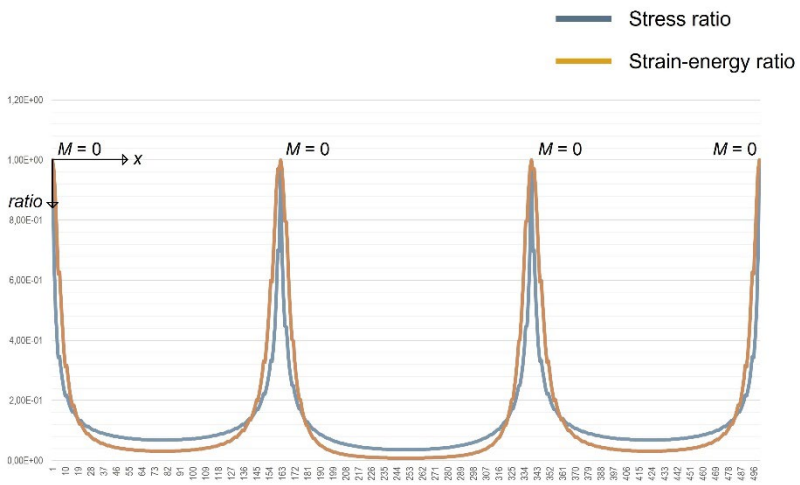

Figure 40 stress and strain energy ratio's along the axis of the arch[image 66]

In the next example the semi-circular arch is loaded by four point loads. The loads have a value and are placed in such a way that the areas under the arch and the thrust line are equal, the force polygon and accompanying thrust line are thus given. This results immediately in the correct solution; $E_{compl,M} = 0$, thus demonstrating the equivalent areas method. The eccentricity of the thrust line, which is the difference between the areas under the arch and the thrust line, can be used to extend Pucher's equation to include bending, see section 6.3.

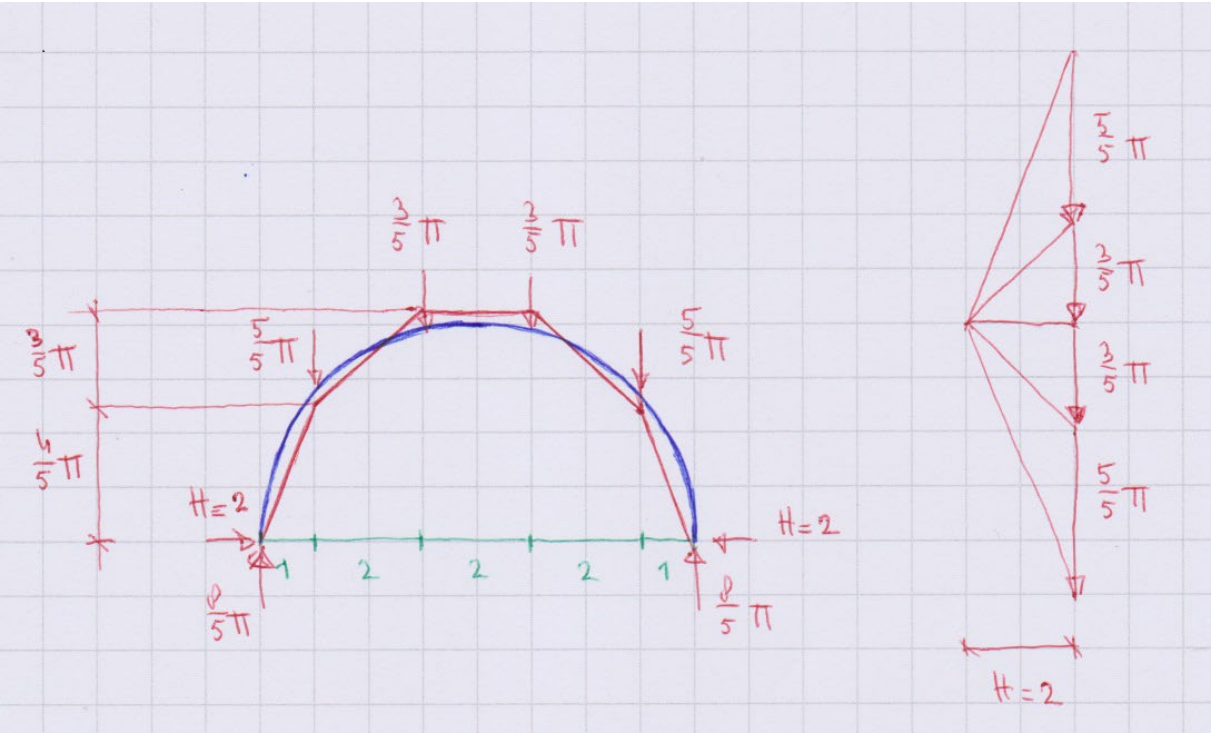

$semi-circular\ arch$:
$y = (2Rx - x^2)^{1/2}$
$with$:
$R = 4$: $\delta x = 2$

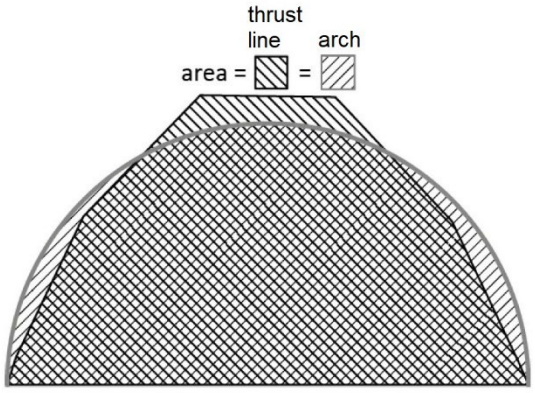

$area\ under\ arch$:
$A_{arch} = \frac{1}{2}\pi R^2 = 8\pi$

$area\ under\ thrust\ line$:
$A_{thrust} = 2\left(\frac{1}{2}\cdot\frac{1}{2}\delta h_{t1}\delta x\right) + 2\left(\delta h_{t1}\delta x + \frac{1}{2}\delta h_{t2}\delta x\right) + (\delta h_{t1} + \delta h_{t2})\delta x = 8\pi$
$e_v = A_{thrust} - A_{arch} = 8\pi - 8\pi = 0$
$E_{compl,M} = M^2 = F_H^2 e_v^2 = 0$

$with\ F_H = 2$: $\Sigma M_{thrust,apex} = 0 \Rightarrow$
$\frac{3}{5}\pi 1 + \frac{5}{5}\pi 3 + 2\frac{7}{5}\pi - \frac{8}{5}\pi 4 = 0$

6 The stress function of arches

6.1 Introduction

There are two expressions using stress functions for internal forces which are relevant for arches, the 4th order in-plane stress equation which includes the condition of compatibility, and the 2nd order Pucher's equation which is only based on equilibrium.
Because the plane stress equation also concerns compatibility it is suited to solve statically indeterminate problems depending on the support conditions. Pucher's equation is used for membrane solutions, which disregard bending moments [68]. In fact Pucher's equation is closely related to the membrane and cable equations.

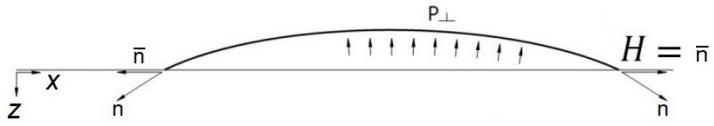

shallow membrane:

$$n\left(\frac{\partial^2 z}{\partial x^2}+\frac{\partial^2 z}{\partial y^2}\right)=-p_z \approx p_\perp$$

$$p_z \neq p_\perp$$
$$H \neq n$$

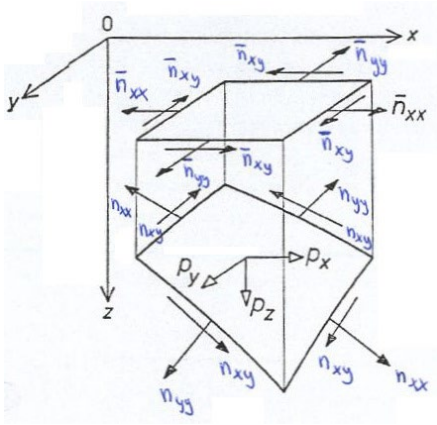

$plane\ stress\ equation$:

$$\frac{\partial^4 \phi}{\partial x^4}+2\frac{\partial^4 \phi}{\partial x^2 \partial y^2}+\frac{\partial^4 \phi}{\partial y^4}=0$$

$with$:

$$n_{xx}=\frac{\partial^2 \phi}{\partial y^2}, n_{xy}=-\frac{\partial^2 \phi}{\partial x \partial y}, n_{yy}=\frac{\partial^2 \phi}{\partial x^2}$$

$Pucher's\ equation$:

$$\frac{\partial^2 \phi}{\partial y^2}\frac{\partial^2 z}{\partial x^2}-2\frac{\partial^2 \phi}{\partial x \partial y}\frac{\partial^2 z}{\partial x \partial y}+\frac{\partial^2 \phi}{\partial x^2}\frac{\partial^2 z}{\partial y^2}=-p_z$$

$with$:

$$\bar{n}_{xx}=\frac{\partial^2 \phi}{\partial y^2}, \bar{n}_{xx}=-\frac{\partial^2 \phi}{\partial x \partial y}, \bar{n}_{yy}=\frac{\partial^2 \phi}{\partial x^2}$$

$membrane\ equation$:

$$n_{xx}\frac{\partial^2 z}{\partial x^2}+2n_{xy}\frac{\partial^2 z}{\partial x \partial y}+n_{yy}\frac{\partial^2 z}{\partial y^2}=-p_z$$

$cable\ equation$:

$$H_x\frac{\partial^2 z}{\partial x^2}+2H_{xy}\frac{\partial^2 z}{\partial x \partial y}+H_y\frac{\partial^2 z}{\partial y^2}=-p_z$$

The plane stress equation does not contain geometric information about curved structures. The other three equations incorporate the shape of the curved surface by means of the shape function. The cable equation and Pucher's equation, in contrast to the membrane equation, is concerned with the horizontal projection of the internal forces and the horizontal support reactions respectively. If the curved surface is very shallow, then the three 2nd

order equations are practically similar, where the cable equation as given here represents a discretised surface, such as cable nets. But the horizontal support reactions can also be represented as a uniformly distributed force.

6.2 Funicular arches

In chapter 2 it was explained that the form diagram (shape function) of a cable or arch, which in these cases was the funicular line, is similar to the bending moment diagram for a beam with the same load, span and support conditions. Here an explanation is given using the stress and shape functions, and Pucher's equation.

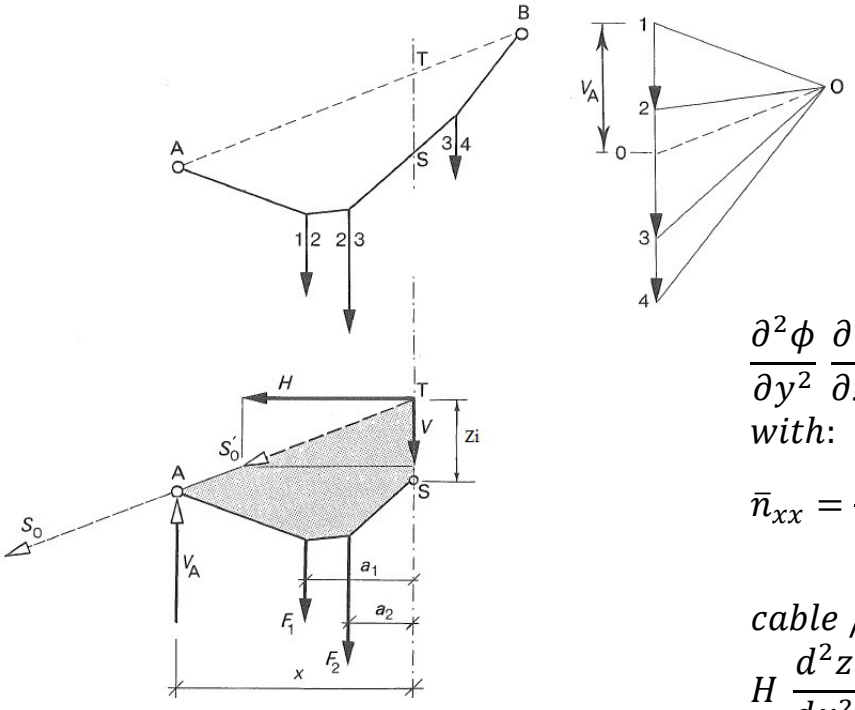

$$\sum M_s = 0:$$

$$\underbrace{V_A x - F_1 a_1 - F_2 a_2}_{M_x} - H \cdot z_i = 0$$

$$M_x = H \cdot z_i$$

$$\frac{\partial^2 \phi}{\partial y^2}\,\frac{\partial^2 z}{\partial x^2} = -p_z$$

$$with:$$

$$\bar{n}_{xx} = \frac{\partial^2 \phi}{\partial y^2}$$

$$cable\ /\ arch:$$

$$H\,\frac{d^2 z}{dx^2} = -q \Rightarrow V = H\frac{dz}{dx}$$

$$beam:$$

$$\frac{d^2 M}{dx^2} = -q \Rightarrow V = \frac{dM}{dx}$$

Two examples will be used, one with a uniformly distributed load and one with a linear distributed load. For both cases a shape function based on the load transfer can be derived, the arch will have the same exact shape. For the uniformly distributed load this results in the parabolic form diagram and the linear distributed load in a cubic form diagram.

Pucher's equation will be used for both examples to derive the stress function.

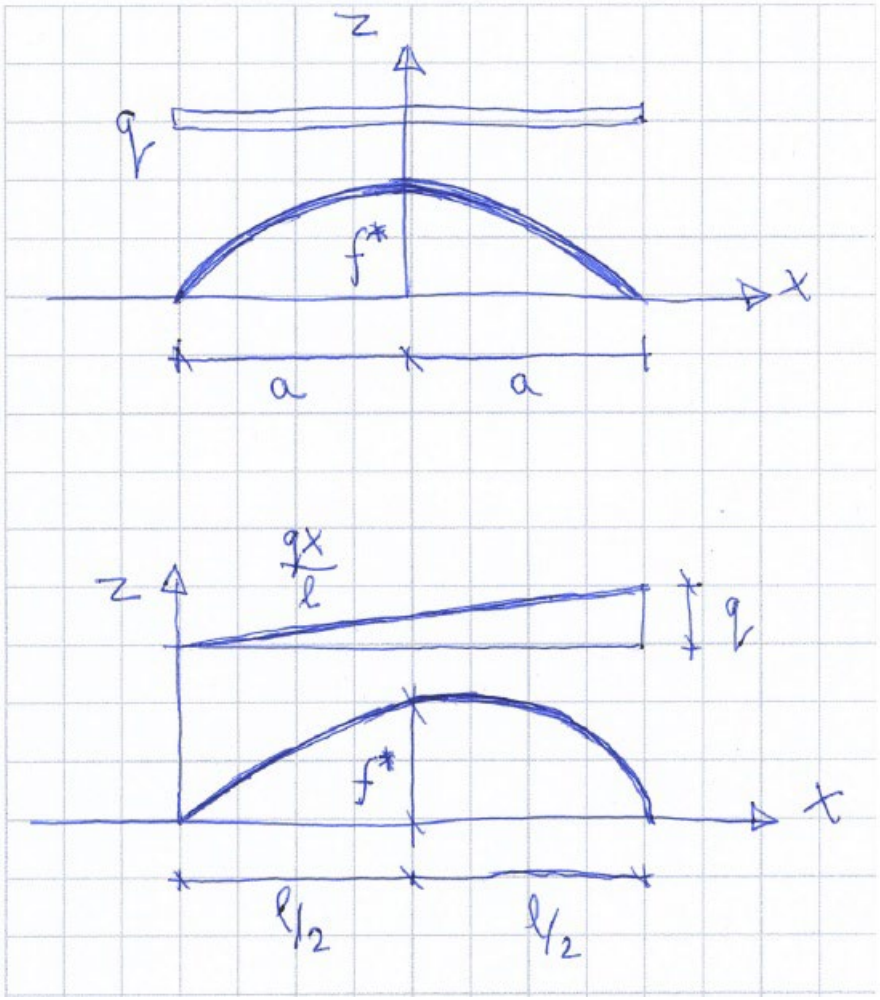

$$shape\ function\ load:$$
$$z(x) = -c_1 x^2 + c_2$$
$$z(0) = -c_1 0^2 + c_2 = f^*$$
$$z(a) = -c_1 a^2 + c_2 = 0$$
$$\Rightarrow c_1 = \frac{f^*}{a^2};\ c_2 = f^*$$
$$z(x) = f^*\left(1 - \frac{x^2}{a^2}\right)$$

$$shape\ function\ load:$$
$$z(x) = -c_1 x^3 + c_2 x$$
$$z\left(l/2\right) = -c_1\left(l/2\right)^3 + c_2 x = f^*$$
$$z(l) = -c_1 l^3 + c_2 x = 0$$
$$\Rightarrow c_1 = \frac{8f^*}{3l^3};\ c_2 = \frac{8f^*}{3l}$$
$$z(x) = \frac{8f^*}{3l^3}\left(lx - \frac{x^3}{l}\right)$$

Interestingly the second derivatives of the shape function (load / arch) and of the stress function are reciprocal and their product is equal to the load.

$$\frac{\partial^2\phi}{\partial y^2}\frac{\partial^2 z}{\partial x^2} = q$$
$$z_{arch}(x) = f^*\left(1 - \frac{x^2}{a^2}\right) \Rightarrow \frac{\partial^2 z}{\partial x^2} = -\frac{2f^*}{a^2}$$
$$\phi = \iint \frac{q}{-\frac{2f^*}{a^2}}dy \Rightarrow \phi = -\frac{qa^2}{4f^*}y^2 + \cdots$$
$$\frac{\partial^2\phi}{\partial y^2} = -\frac{qa^2}{2f^*} = H$$
$$\frac{\partial^2\phi}{\partial y^2}\frac{\partial^2 z}{\partial x^2} = q \Rightarrow \underbrace{\left(\underbrace{-\frac{a^2}{2f^*}}_{reciprocal}\ \underbrace{q}_{load}\right)}_{H} \cdot \underbrace{-\frac{2f^*}{a^2}}_{reciprocal} = q$$
$$M_{equiv}(x) = \frac{\partial^2\phi}{\partial y^2} z_{arch}(x) = \frac{qa^2}{2f^*} \cdot f^*\left(1 - \frac{x^2}{a^2}\right) = \frac{q(a^2 - x^2)}{2}$$

The diagram of the equivalent moment, the product of the horizontal thrust *H* and the shape function, is the mirror image of the shape function.

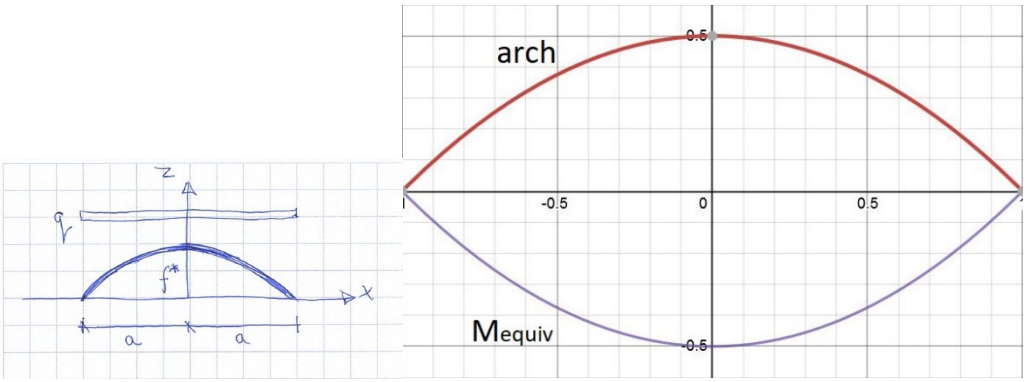

It can be observed this holds for both examples.

$$\frac{\partial^2\phi}{\partial y^2}\frac{\partial^2 z}{\partial x^2} = \frac{qx}{l}$$

$$z_{arch}(x) = \frac{8f^*}{3l^2}\left(lx - \frac{x^3}{l}\right) \Rightarrow \frac{\partial^2 z}{\partial x^2} = -\frac{16f^*x}{l^3}$$

$$\phi = \iint \frac{\frac{qx}{l}}{-\frac{16f^*x}{l^3}}\,dy \Rightarrow \phi = -\frac{ql^2}{4f^*}y^2 + \cdots$$

$$\frac{\partial^2\phi}{\partial y^2} = -\frac{ql^2}{16f^*} = H$$

$$\frac{\partial^2\phi}{\partial y^2}\frac{\partial^2 z}{\partial x^2} = \frac{qx}{l} \Rightarrow \underbrace{\left(\underbrace{-\frac{l^3}{16f^*x}}_{reciprocal}\underbrace{\frac{qx}{l}}_{load}\right)}_{H} \cdot \underbrace{-\frac{16f^*x}{l^3}}_{reciprocal} = \frac{qx}{l}$$

$$M_{equiv}(x) = \frac{\partial^2\phi}{\partial y^2}z_{arch}(x) = \frac{ql^2}{16f^*}\cdot\frac{8f^*}{3l^2}\left(lx - \frac{x^3}{l}\right) = \frac{q(l^2x - x^3)}{6l}$$

Note that the apex of both the equivalent moment and the shape function is eccentric.

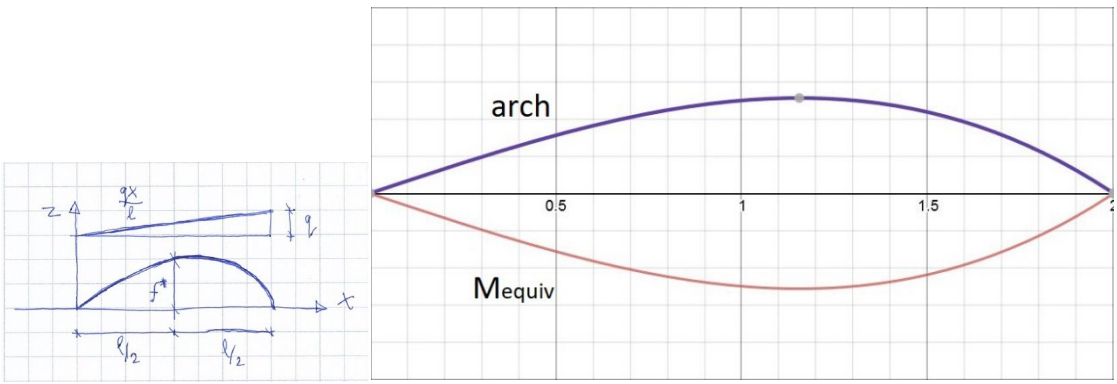

The consequence of this is that the form diagram, the shape function, is equal to the thrust line of the load and thus equal to the equivalent bending moment diagram.

The distribution of the shear force of the equivalent beam and the transfer of the vertical load of the arch or cable are equal and produce the already derived horizontal thrust.

$$f^* = \frac{qa^2}{2H} \Leftarrow \begin{cases} V = \dfrac{dM}{dx} = -qx \\ V = H\dfrac{dz}{dx} = -H\dfrac{2f^*}{a^2}x \end{cases}$$

$$f^* = \frac{ql^2}{16H} \Leftarrow \begin{cases} V = \dfrac{dM}{dx} = \dfrac{ql}{6} - \dfrac{q}{2l}x^2 \\ V = H\dfrac{dz}{dx} = H\left(\dfrac{8f^*}{3l} - \dfrac{8f^*}{l^3}x^2\right) \end{cases}$$

This example looks trivial, but it is important as it shows that if the shape function of the arch is exactly the same as the thrust line, the form diagram, it is equal to the moment diagram of the equivalent beam.

If the parabolic arch is rotated around the z-axis to form a shell of revolution with a uniformly distributed load there will be hoop forces besides meridian forces, see chapter 7.

Both the shape function and the stress function are parabolic. If the arch is a 2D structure in a plane surface then the horizontal thrust is a discrete force. But it can be observed that both functions are in fact a 3D surface. Which are mono-clastic surfaces along an axis in perpendicular directions.

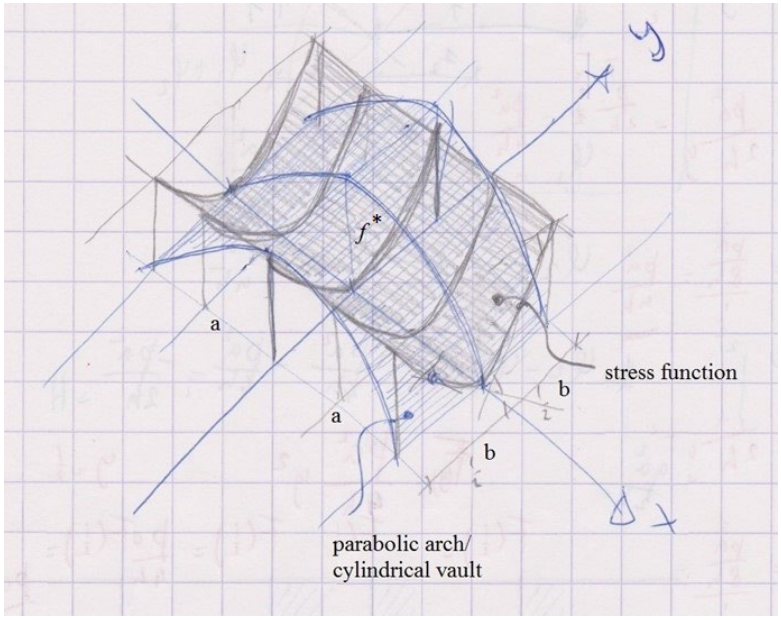

The thrust is therefore uniformly distributed, *h* [N/m]. The discrete value of the thrust *H* [N] / *h* [N/m] is the difference in slope of the stress function.

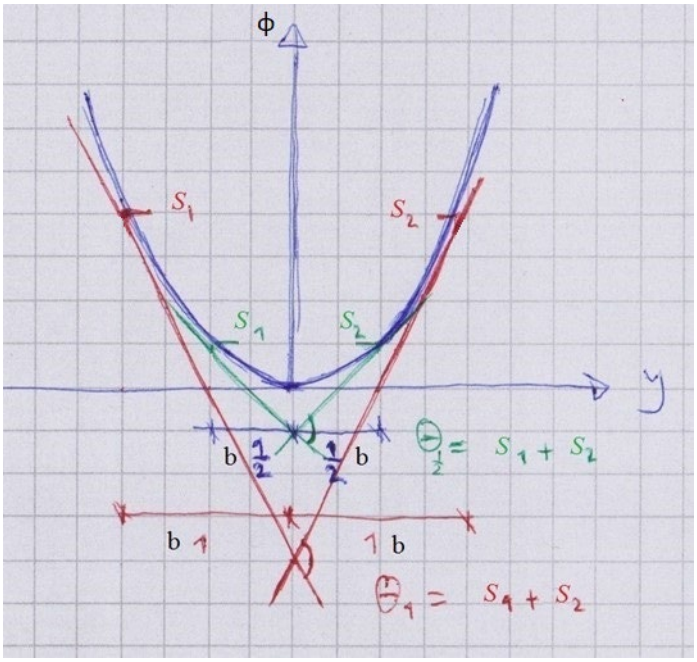

$$\phi(y) = \frac{pa^2}{4f^*}y^2$$

$$s = \frac{\partial\phi}{\partial y} = \frac{pa^2}{2f^*}y^2$$

$$H = h \cdot 2b = \left(\frac{\partial\phi}{\partial y}\right)_2 - \left(\frac{\partial\phi}{\partial y}\right)_1 = \theta$$

$$for: b = \frac{1}{2}, y = \frac{1}{2}\ and\ y = -\frac{1}{2}$$

$$s_1 = s_2 = \frac{pa^2}{4f^*} \Rightarrow \theta_{1/2} = s_1 + s_2 = \frac{pa^2}{2f^*} \Rightarrow h = \frac{pa^2}{2f^*}$$

$$for: b = 1, y = 1\ and\ y = -1$$

$$s_1 = s_2 = \frac{pa^2}{2f^*} \Rightarrow \theta_1 = s_1 + s_2 = \frac{pa^2}{f^*} \Rightarrow h = \frac{pa^2}{2f^*}$$

6.3 Non funicular arches

In this example the load and the arch have different functions. The load being a linear distributed load has a cubic shape function and the arch shape is parabolic.

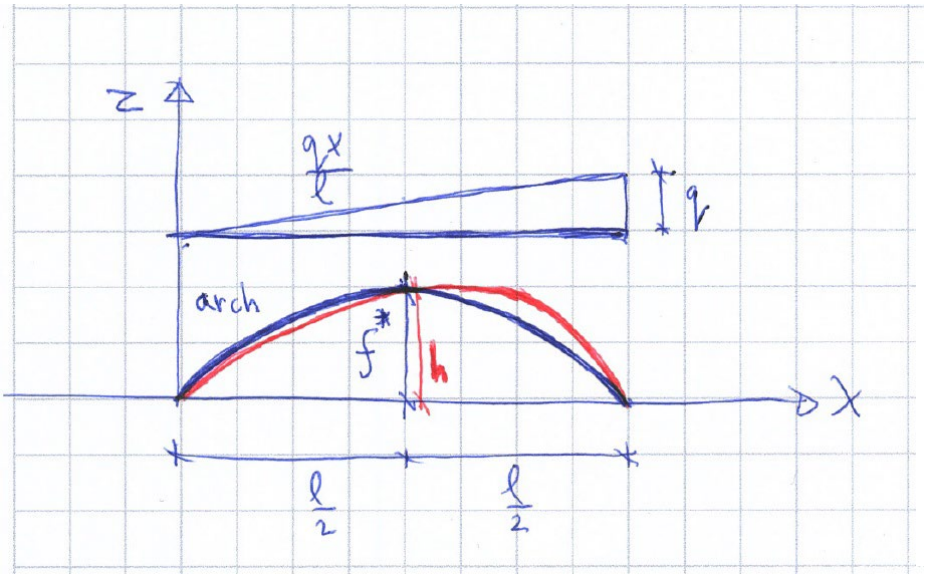

$$shape\ function\ arch:$$

$$z(x) = -c_1\left(x - {}^{l}/_{2}\right)^2 + c_2$$

$$z(0) = -c_1\left(0 - {}^{l}/_{2}\right)^2 + c_2 = 0$$

$$z\left({}^{l}/_{2}\right) = -c_1\left({}^{l}/_{2} - {}^{l}/_{2}\right)^2 + c_2 = f^*$$

$$\Rightarrow c_1 = -\frac{4f^*}{l^2};\ c_2 = f^*$$

$$z(x) = \frac{4f^*(lx - x^2)}{l^2}$$

First the relation has to be established between the two functions. This is done by minimising the complementary energy, as shown in chapter 5. It seems the rise mid span of both functions is equal. Because the thrust line and the axis of the arch do not coincide, bending moments in the arch are expected.

$$shape\ function\ arch:$$

$$z_{arch}(x) = \frac{4f^*(lx - x^2)}{l^2}$$

$$thrust\ line\ load:$$

$$\tilde{z}_{load}(x) = \frac{8h}{3l^2}\left(lx - \frac{x^3}{l}\right)$$

$$area\ under\ arch:$$

$$A_{arch} = \int_0^l \frac{4f^*(lx - x^2)}{l^2}\,dx = \frac{2lf^*}{3}$$

$$area\ under\ load:$$

$$A_{load} = \int_0^l \frac{8h}{3l^2}\left(lx - \frac{x^3}{l}\right)dx = \frac{2lh}{3}$$

$$E_{compl,M} = M^2 = F_H^2 e_v^2 = F_H^2\left(\frac{2lf^*}{3} - \frac{2lh}{3}\right) \rightarrow min$$

$$\Rightarrow f^* = h$$

For this case Pucher's equation will be extended by adding the second order differential equation (M-hill) of the beam that concerns equilibrium. The stress function will be derived, and again the second derivatives of the functions for the thrust line and the stress function are reciprocal but its product is no longer equal to the load but is only a part of it. The difference of load is carried by bending and shear forces in the arch. The moment distribution can be derived from this difference.

$$extending\ Pucher's\ equation:$$
$$\underbrace{\frac{d^2\phi}{dy^2}\frac{d^2z}{dx^2}}_{Pucher's\ equation} + \underbrace{\frac{d^2M}{dx^2}}_{beam\ equation} = -q$$

It can also be concluded that the symmetric part of the linear distributed load for which the thrust line is parabolic is carried by the symmetric and parabolic arch. The antisymmetric part of the load results in bending in the arch.

$$\frac{d^2M}{dx^2} + \frac{d^2\phi}{dy^2}\frac{d^2z}{dx^2} = \frac{qx}{l}$$
$$q\left(\frac{x}{l} - \frac{1}{2}\right) + \Big(\underbrace{-\frac{l^2}{8f^*}}_{reciprocal} \quad \underbrace{\frac{q}{2}}_{load} \Big) \cdot \underbrace{-\frac{8f^*}{l^2}}_{reciprocal} = \frac{qx}{l}$$
$$\Rightarrow q\left(\frac{x}{l} - \frac{1}{2}\right) + \frac{q}{2} = \frac{qx}{l}$$

$$\underbrace{\frac{d^2\phi}{dy^2}\frac{d^2z}{dx^2}}_{Pucher's\ equation} = \frac{q}{2}$$

$$\underbrace{\frac{d^2M}{dx^2}}_{beam\ equation} = q\left(\frac{x}{l} - \frac{1}{2}\right)$$

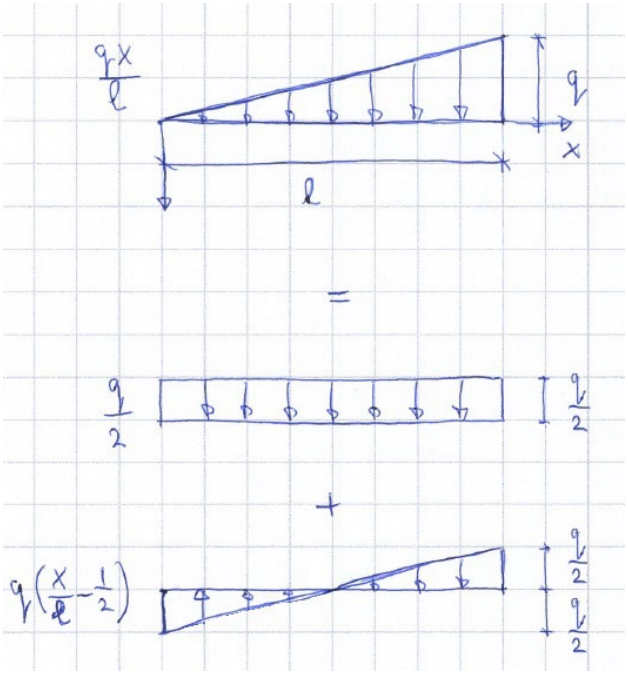

The cubic thrust line of the linear distributed load is "split" into a parabolic one, which is the axis of the arch, and for the symmetric load and bending of the arch for the antisymmetric load.

The mechanics of the load transfer is partly by the moment hill (slope of the moment diagram / shear force) and partly by the slope on the shape of the arch (“arch action”).

$$\frac{d^2M}{dx^2}+\frac{d^2\phi}{dy^2}\frac{d^2z}{dx^2}=\frac{qx}{l}$$

$$z_{arch}(x)=\frac{4f^*(lx-x^2)}{l^2}\Rightarrow\frac{d^2z}{dx^2}=-\frac{8f^*}{l^2}:\ \tilde{z}_{load}(x)=\frac{8h}{3l^2}\left(lx-\frac{x^3}{l}\right)\Rightarrow\frac{d^2\tilde{z}}{dx^2}=-\frac{16hx}{l^3}$$

$$stress\ function\ of\ load:\phi=\iint\frac{\frac{qx}{l}}{\frac{d^2\tilde{z}}{dx^2}}dy=\iint\frac{\frac{qx}{l}}{-\frac{16hx}{l^3}}dy\Rightarrow\phi=-\frac{ql^2}{32h}y^2+..$$

$$\frac{d^2\phi}{dy^2}=-\frac{ql^2}{16h}=-\frac{ql^2}{16f^*}=H$$

$$\frac{d^2M}{dx^2}+\frac{d^2\phi}{dy^2}\frac{d^2z}{dx^2}=\frac{qx}{l}\Rightarrow\frac{d^2M}{dx^2}+\underbrace{\left(\underbrace{-\frac{l^2}{8f^*}}_{reciprocal}\ \underbrace{\frac{q}{2}}_{load}\right)}_{H}\cdot\underbrace{-\frac{8f^*}{l^2}}_{reciprocal}=\frac{qx}{l}$$

$$\Rightarrow\frac{d^2M}{dx^2}=q\left(\frac{x}{l}-\frac{1}{2}\right)$$

$$M(x)=\iint q\left(\frac{x}{l}-\frac{1}{2}\right)dx=q\left(\frac{x^3}{6l}-\frac{x^2}{4}\right)+C_1x+C_2$$

$with$:

$$M(0)=M(l)=0\Rightarrow C_1=\frac{ql}{12};C_2=0$$

$$M(x)=\frac{q(2x^3-3lx^2+l^2x)}{12l}$$

The first part is accompanied by bending moments and the second part by an axial force.

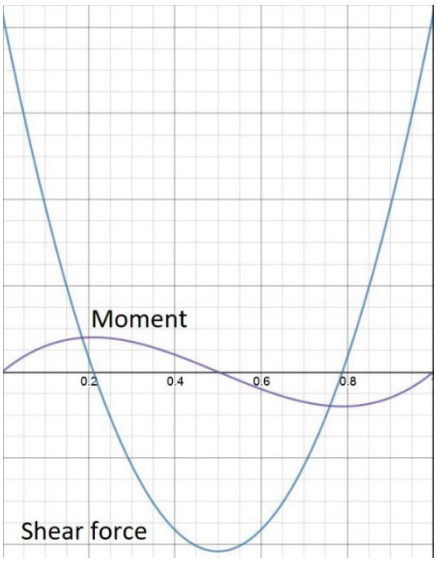

$$M(x)=\frac{q(2x^3-3lx^2+l^2x)}{12l}$$

$$V(x)=\frac{dM}{dx}=\frac{q(6x^2-6lx+l^2)}{12l}$$

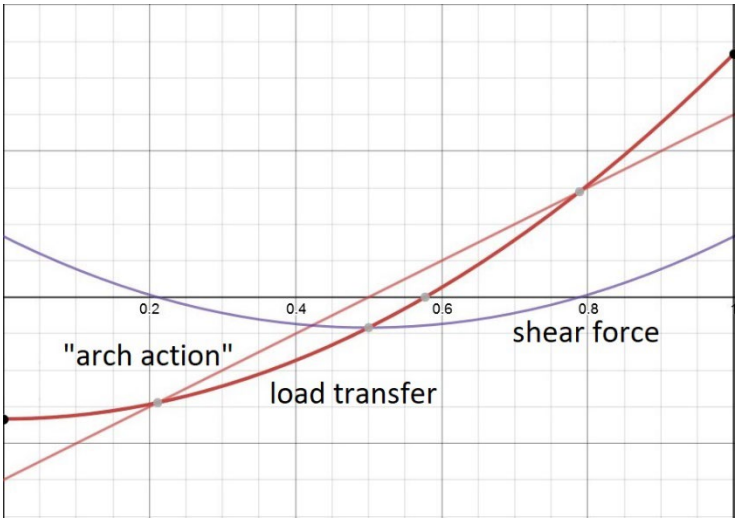

$$load\ transfer:$$

$$V = \underbrace{H\frac{dz}{dx}}_{\text{"arch action"}} + \underbrace{\frac{dM}{dx}}_{\substack{\text{shear force /} \\ \text{moment hill}}}$$

$$= -\frac{ql^2}{16f^*}\frac{4f^*(l-2x)}{l^2} + \frac{dM}{dx}$$

$$V = -\frac{q(l-2x)}{4} + \frac{q(6x^2-6lx+l^2)}{12l}$$

$$= \frac{q(3x^2-l^2)}{6l}$$

The moment diagram of the equivalent beam is no longer equal to the shape function of the arch, but it is still equal to the thrust line of the linear distributed load.

$$M_{equiv}(x) = \frac{d^2\phi}{dy^2}\cdot\tilde{z}_{load}(x) = \frac{ql^2}{16f^*}\cdot\frac{8f^*}{3l^2}\left(lx - \frac{x^3}{l}\right) = \frac{q(l^2x-x^3)}{6l}$$

$$M_{equiv}(x) = H\cdot z_{arch}(x) - M(x) = \frac{ql^2}{16f^*}\cdot\frac{4f^*(lx-x^2)}{l^2} - \frac{q(2x^3-3l^2x+l^2x)}{12l} = \frac{q(l^2x-x^3)}{6l}$$

If this example is revolved around the vertical axis at mid span the load will be carried by membrane forces only; meridian, hoop and shear forces.

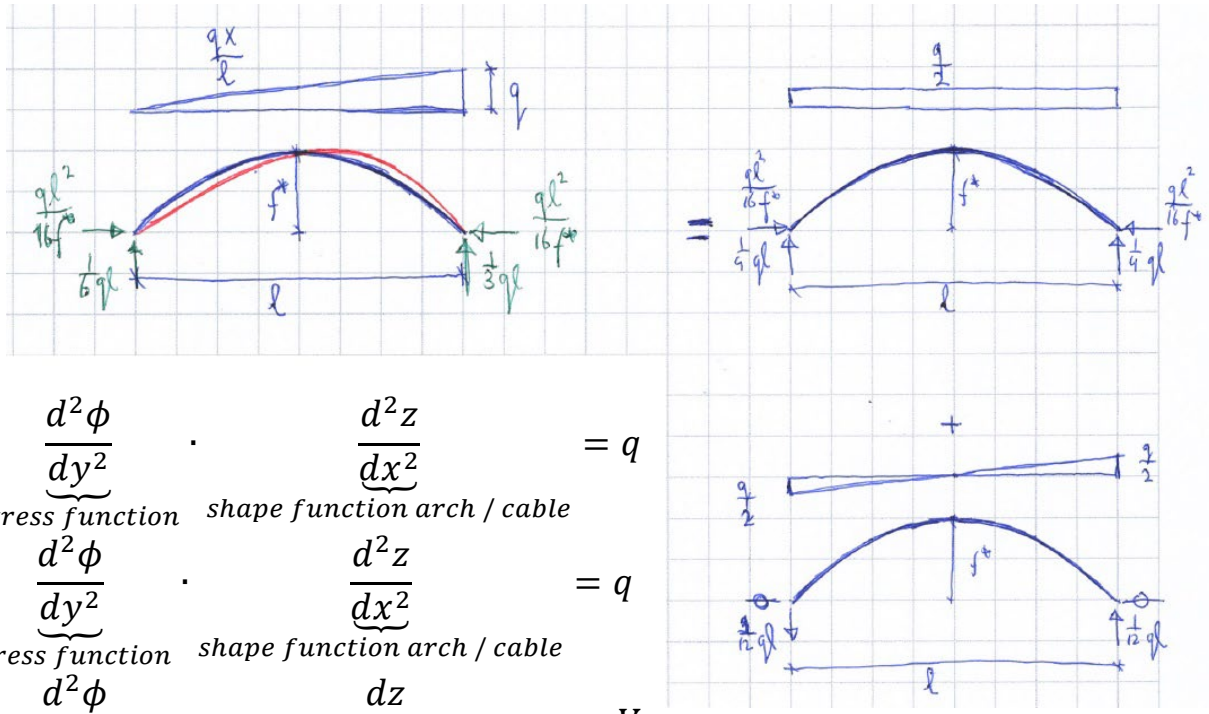

$$\underbrace{\frac{d^2\phi}{dy^2}}_{stress\ function}\cdot\underbrace{\frac{d^2z}{dx^2}}_{shape\ function\ arch\ /\ cable} = q$$

$$\underbrace{\frac{d^2M}{dx^2}}_{beam\ equation} + \underbrace{\frac{d^2\phi}{dy^2}}_{stress\ function}\cdot\underbrace{\frac{d^2z}{dx^2}}_{shape\ function\ arch\ /\ cable} = q$$

$$\underbrace{\frac{dM}{dx}}_{moment\ hill} + \underbrace{\frac{d^2\phi}{dy^2}}_{stress\ function}\cdot\underbrace{\frac{dz}{dx}}_{shape\ function\ arch\ /\ cable} = V$$

The purpose of these examples is to distinguish between the moment hill, stress function, function of the load (thrust line, form diagram) and the shape function of the structure (arch, cable).
These different functions can be expanded from arches and cables to shells and membranes, as shown in chapters 7 and 8.

In chapter 5 the moment in the arch was determined by multiplying the horizontal thrust with the eccentricity e_v of the thrust line in respect to the axis of the arch. The eccentricity is obtained by subtracting the function of the thrust line from the shape function of the arch.

By using the eccentricity the 2nd order differential equation, thus Pucher's equation including bending, in one direction can be reformulated as a function of the stress function, the shape function and the eccentricity with the thrust line.

$$Pucher's\ equation\ in\ one\ direction:$$
$$-p_z = \frac{\partial^2 \phi}{\partial y^2}\frac{\partial^2 z}{\partial x^2}$$
$$reformulated\ Pucher's\ equation:$$
$$-q = \frac{d^2\phi}{dy^2}\left(\frac{d^2 z}{dx^2} + \frac{d^2 e_v}{dx^2}\right)$$

The reformulated equation of Pucher is applicable to arches, for shell structures the relationship between the stress function and the shape function is more complex, see chapter 8. With arches deviations of the thrust line from its axis results in bending moments. For shell structures this is not always the case, additional internal forces (e.g. the hoop forces in domes) can alter the shape of the thrust surface of the load so that it does coincides with the shells centroidal plane and thus avoiding bending moment, see chapter 7. But if additional internal forces are not sufficient to ensure a membrane state of stress in a shell, bending moment and shear forces will be needed, see sections 8.9 and 8.10.

Using the reformulated Pucher's equation results in the same equations for the bending moment *M*, the load transfer *V* and the load *q*.

$$e_v(x) = \tilde{z}_{load}(x) - z_{arch}(x)$$
$$with:$$
$$e_v = \frac{8f^*}{3l^2}\left(lx - \frac{x^3}{l}\right) - \frac{4f^*(lx - x^2)}{l^2} = -\frac{8f^*x^3 - 12lf^*x^2 + 4l^2f^*x}{3l^3}$$

$$M(x) = H \cdot e_v(x) = \frac{d^2\phi}{dy^2} \cdot e_v(x) = -\frac{ql^2}{16f^*}\left(-\frac{8f^*x^3 - 12lf^*x^2 + 4l^2f^*x}{3l^3}\right)$$
$$= \frac{q(2x^3 - 3lx^2 + l^2x)}{12l}$$

$$V = \frac{d^2\phi}{dy^2}\frac{dz}{dx} + \frac{dM}{dx} \Rightarrow V = \frac{d^2\phi}{dy^2}\left(\frac{dz}{dx} + \frac{de_v}{dx}\right)$$
$$q = \frac{d^2\phi}{dy^2}\frac{d^2z}{dx^2} + \frac{d^2M}{dx^2} \Rightarrow q = \frac{d^2\phi}{dy^2}\left(\frac{d^2z}{dx^2} + \frac{d^2e_v}{dx^2}\right)$$

$$V = \frac{d^2\phi}{dy^2}\left(\frac{dz}{dx} + \frac{de_v}{dx}\right) = -\frac{ql^2}{16f^*}\left(\frac{4f^*(l - 2x)}{l^2} - \frac{24f^*x^2 - 24lf^*x + 4l^2f^*}{3l^3}\right) = \frac{q(3x^2 - l^2)}{6l}$$
$$q = \frac{d^2\phi}{dy^2}\left(\frac{d^2z}{dx^2} + \frac{d^2e_v}{dx^2}\right) = -\frac{ql^2}{16f^*}\left(-\frac{8f^*}{l^2} - \frac{8f^*(2x - l)}{l^3}\right) = \frac{qx}{l}$$

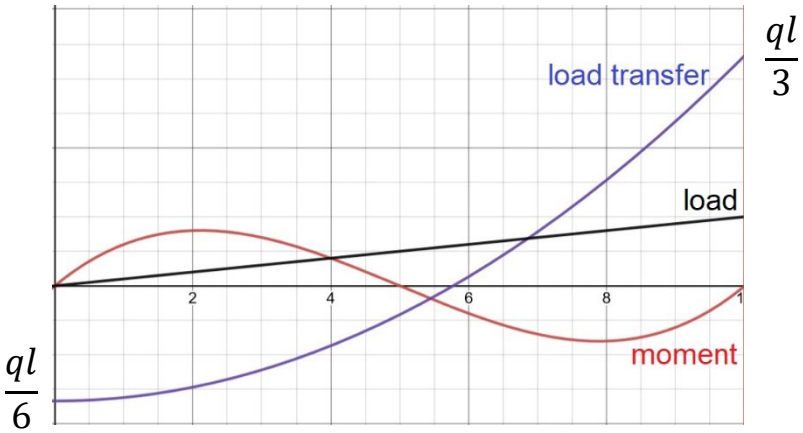

$\frac{ql}{3}$

$\frac{ql}{6}$

6.4 General properties of stress functions

In this section the static-geometric analogy in the equations of thin shell structures [69] will be generalized to beams, this extends to the application of the first and second moment-area theorem's of Mohr.
A general solution to the plane stress equation will be presented for beams and the solution for an arch by means of the plane stress equation will be compared to the solution of Pucher's equation.

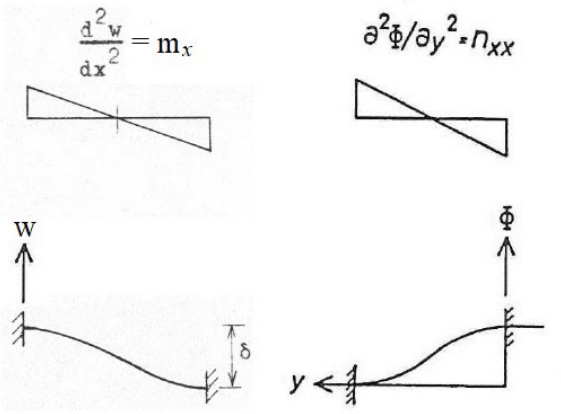

$$static - geometric\ analogy\ for\ beams$$

$$q = EI\frac{d^4w}{dx^4} \qquad k_G = \frac{1}{Et}\frac{\partial^4\phi}{\partial y^4}$$

$$V = -EI\frac{d^3w}{dx^3}$$

$$M = -EI\frac{d^2w}{dx^2}, \kappa = \frac{d^2w}{dx^2} \qquad n = \frac{\partial^2\phi}{\partial y^2}$$

$$\varphi = \frac{dw}{dx} \qquad s = \frac{\partial\phi}{\partial x}$$

$$w \qquad \phi$$

For beams the parameters that are covered by the differential equation range from the load *q* to the displacement *w*, in the static-geometric analogy this ranges from the Gaussian curvature k_G to the stress function ϕ.
For this purpose a beam is compared to the cross section of a stress function of a slab-like beam. Here is a duality, the beam is a line element where the internal forces are a function of the coordinate along the axis and the slab like beam adheres to the plane stress equation and is thus as a surface element a function of both axis of the surface.

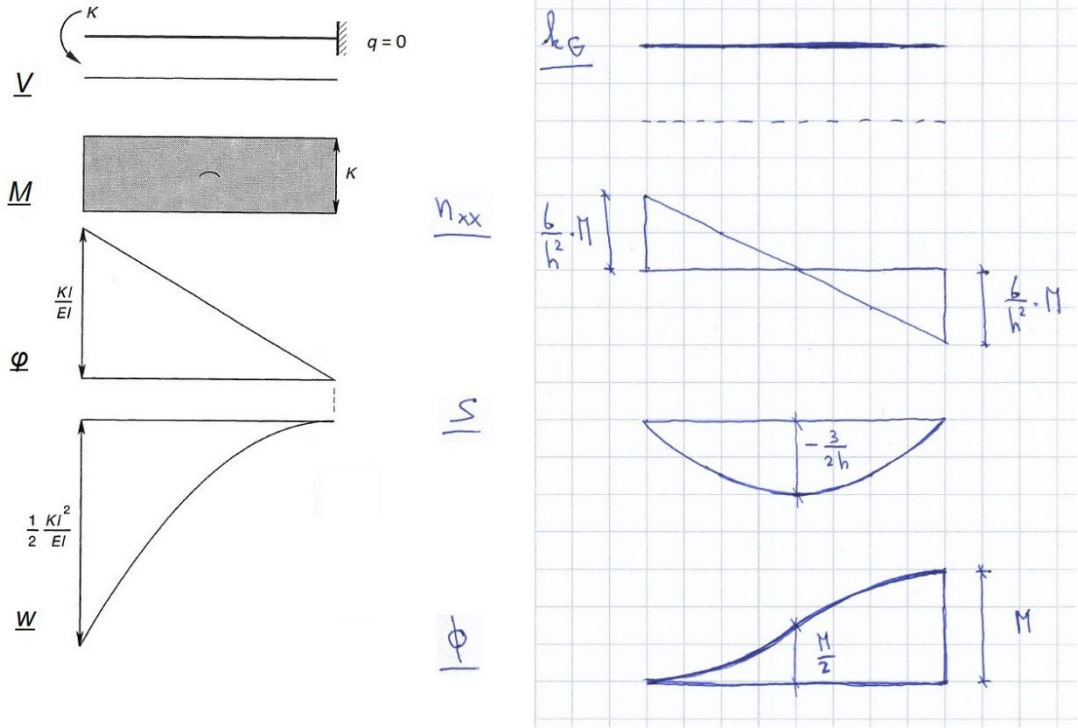

$beam\ equation$:

$$EI\frac{d^4w}{dx^4} = q$$

$plane\ stress\ equation$:

$$\frac{\partial^4\phi}{\partial y^4} = 0$$

$with$:

$$n_{xx} = \frac{\partial^2\phi}{\partial y^2}$$

The internal forces of a beam can be determined using the stress function [70], again here is a duality. The internal forces of a beam are only a function of the coordinate along the axis and the stress functions are a function of a surface, the surface of the beam. In beam theory we assume the beam is just a line element and we reintroduce the second dimension, the height, back when the stresses are calculated.

$$N_x = \int_{y_1}^{y_2} n_{xx}\,dy = \int_{y_1}^{y_2} \frac{\partial^2\phi}{\partial y^2}\,dy = \left(\frac{\partial\phi}{\partial y}\right)_{y_2} - \left(\frac{\partial\phi}{\partial y}\right)_{y_1} = s_2 - s_1 = \left(\frac{\partial\phi}{\partial y}\right)_y$$

$$M = \int_{y_1}^{y_2} (y - y_1) n_{xx}\,dy = \int_{y_1}^{y_2} (y - y_1)\frac{\partial^2\phi}{\partial y^2}\,dy = \left[(y - y_1)\frac{\partial\phi}{\partial y}\right]_{y_1}^{y_2} - \int_{y_1}^{y_2} \frac{\partial\phi}{\partial y}\,dy$$

$$\Rightarrow M = (y_2 - y_1)s_2 - [\phi_2 - \phi_1]$$

Now the static-geometric analogy has been established for beams, it is possible to apply Mohr's moment-area theorems to the stress function [71].
This will be done by a generalisation of Mohr's first and second moment-area theorem:

- the change in rotation (φ) / slope (*s*), the first derivative of the function, over a distance along the axis is equal to the area of the second derivative over that distance
- the intersection of the tangents of the rotations / slopes is in the same position, along the axis, as the centroid of the area of the diagram of the second derivative

$static - geometric\ analogy$

$Mohr's\ first\ theorem$:

$$\varphi_2 - \varphi_1 = \int_{x_1}^{x_2} \frac{M}{EI}\,dx = \int_{x_1}^{x_2} \kappa\,dx = \theta \qquad s_2 - s_1 = \int_{y_1}^{y_2} n dy = N$$

$Mohr's\ second\ theorem$:

$$w_2 - w_1 = \varphi_1(x_2 - x_1) + \int_{x_1}^{x_2} \frac{M}{EI}(x_2 - x)dx \qquad \phi_2 - \phi_1 = s_1(y_2 - y_1) + \int_{y_1}^{y_2} n(y_2 - y)dy$$

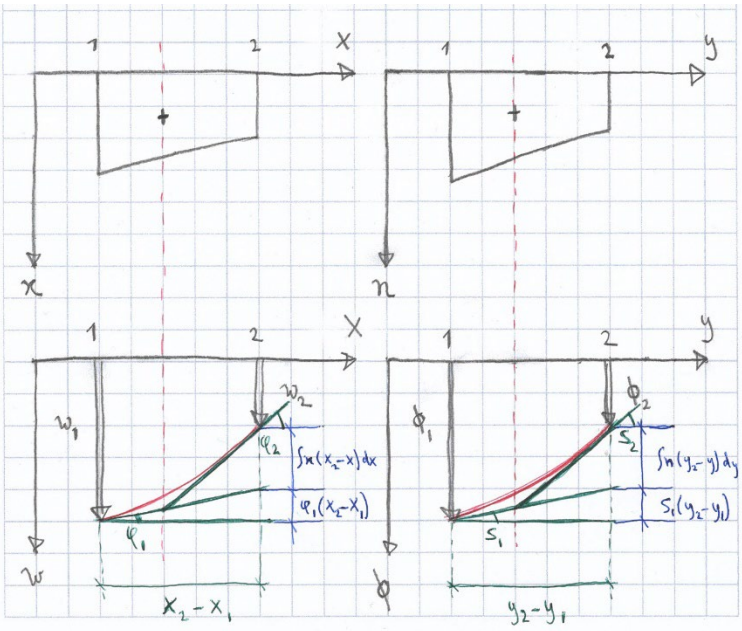

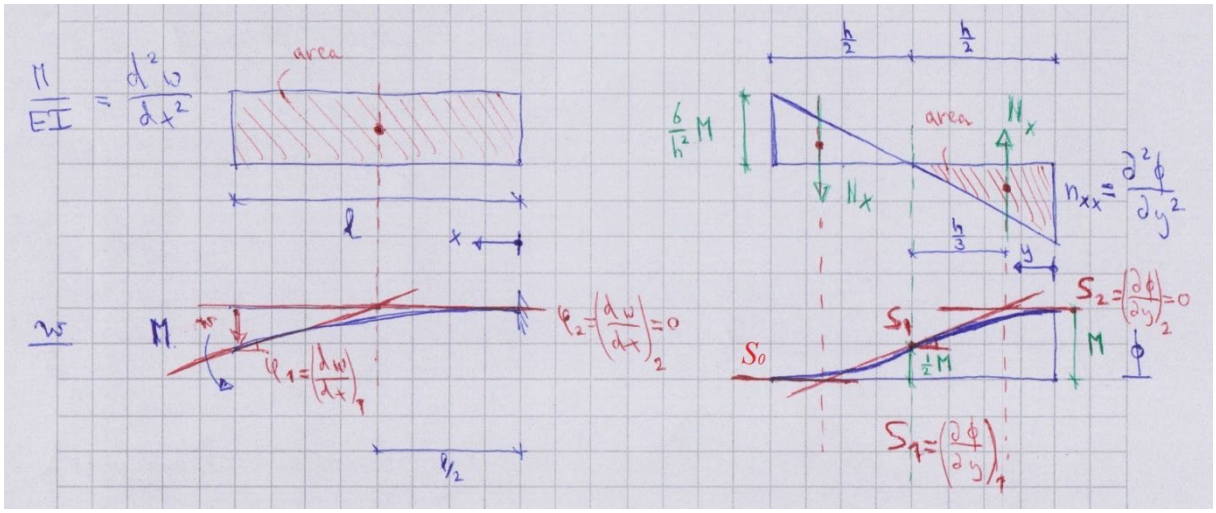

static − geometric analogy

Mohr's first theorem:

$$\varphi_2-\varphi_1=\int_{x_1}^{x_2}\frac{M}{EI}dx=\int_{x_1}^{x_2}\kappa\,dx=\theta \qquad s_2-s_1=\int_{y_1}^{y_2}ndy=N$$

$$\varphi_2-\varphi_1=\frac{M}{EI} \qquad s_2-s_1=0-\frac{1}{2}\frac{h}{2}\cdot\frac{6}{h^2}M=-\frac{h}{4}\frac{6}{h^2}\frac{pl^2}{8}=-\frac{3}{16}\frac{pl^2}{h}=N_x$$

Mohr's second theorem:

$$w_2-w_1=\varphi_1(x_2-x_1)+\int_{x_1}^{x_2}\frac{M}{EI}(x_2-x)dx \qquad \phi_2-\phi_1=s_1(y_2-y_1)+\int_{y_1}^{y_2}n(y_2-y)dy$$

$$w_2-w_1=-\frac{M}{EI}\cdot-l+\frac{M}{EI}\cdot-\frac{l}{2}=\frac{Ml^2}{2EI} \qquad \phi_2-\phi_1=-\frac{3}{16}\frac{pl^2}{h}\cdot-\frac{h}{2}+-\frac{3}{16}\frac{pl^2}{h}\cdot-\frac{h}{6}=\frac{1}{16}pl^2=\frac{1}{2}M$$

$$\Rightarrow\ \phi_0-\phi_1=M$$

6.5 Applications of the stress function to beams

The first application is a bar with a centric axial force. The stress function is parabolic which results in a constant stress distribution [72].

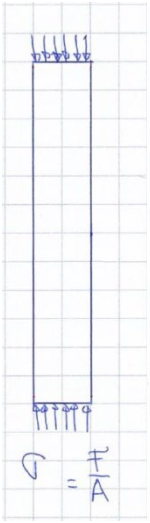

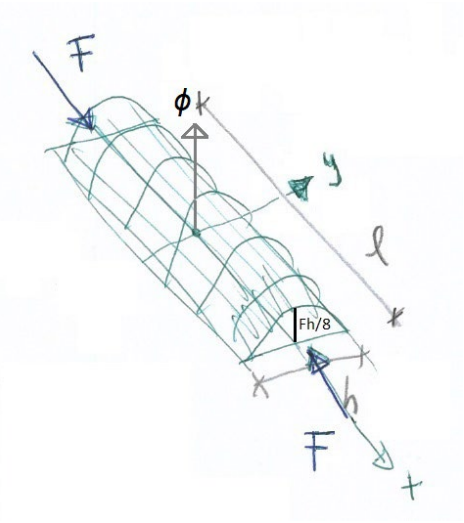

$$n_{xx} = \frac{\partial^2 \phi}{\partial y^2} = -\frac{F}{h}$$

$$\phi = \iint -\frac{F}{h}\, dy = -\frac{F}{h} y^2 + C_1 y + C_2$$

$with$:

$$C_1 = 0$$

$$\phi\left(h/2\right) = -\frac{F}{h}\left(h/2\right)^2 + C_2 = 0$$

$$\Rightarrow C_2 = \frac{Fh}{8}$$

$$\phi = F \cdot \frac{(h^2 - 4y^2)}{8h}$$

The stress function is a product of the force (x-direction) and stress distribution (y-direction). When the stress function is discretized the difference of the slope of the tangents is equal to the axial force.

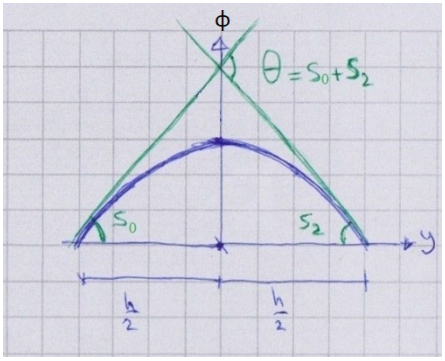

$$s = \frac{\partial \phi}{\partial y} = -\frac{F}{h}\, y$$

$$for: y = \frac{h}{2}\ and\ y\ = -\frac{h}{2}$$

$$s_0 = s_2 = \frac{F}{2} \Rightarrow s_0 + s_2 = F$$

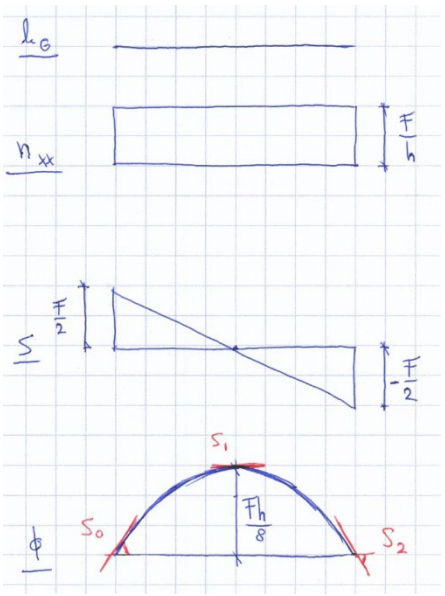

$$Mohr's\ first\ theorem:$$

$$s_2 - s_0 = -\frac{F}{h} - \frac{F}{h} = -F$$

$$Mohr's\ second\ theorem:$$

$$\phi_2 - \phi_0 = \frac{F}{h}\frac{h}{2} - \frac{F}{h}\frac{h}{2}\frac{h}{4} = \frac{Fh}{8}$$

The next example is a classic one, a simply supported beam with a uniformly distributed load [73]. The solution gives the stress distribution in the beam as can be expected from the beam theory, but it does not completely satisfy the plane stress differential equation, although the difference is very small.

$$plane\ stress\ equation:$$
$$\frac{\partial^4\phi}{\partial x^4} + 2\frac{\partial^4\phi}{\partial x^2\partial y^2} + \frac{\partial^4\phi}{\partial y^4} = 0$$
$$with:$$
$$n_{xx} = \frac{\partial^2\phi}{\partial y^2}, n_{xy} = -\frac{\partial^2\phi}{\partial x\partial y}, n_{yy} = \frac{\partial^2\phi}{\partial x^2}$$

In section 6.4 it was shown that the rise along the x-axis of the stress function is equal to the bending moment in the beam *M*. Thus the stress function consists of two parts, the function of the bending moment (x-direction), and a function for the stress distribution (y-direction).

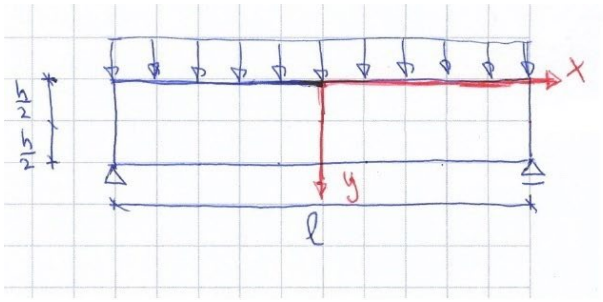

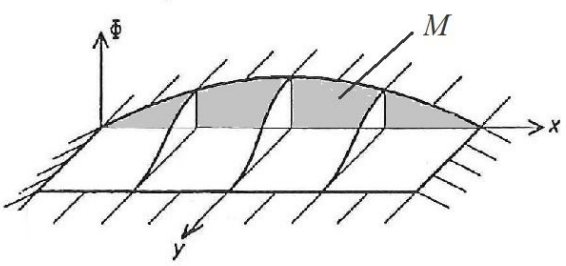

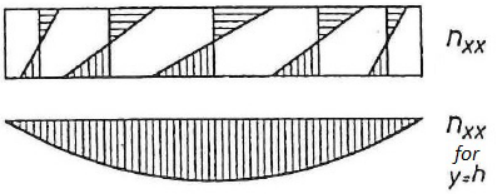

$$\phi = M(x) \cdot \frac{(2y^3 - 3hy^2 + h^3)}{h^3}$$
$$\phi = \underbrace{\frac{q(l^2 - 4x^2)}{8}}_{moment} \cdot \frac{(2y^3 - 3hy^2 + h^3)}{h^3}$$

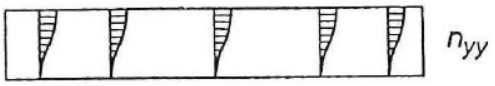

$$n_{xx} = \frac{\partial^2\phi}{\partial y^2} = \frac{q(l^2 - 4x^2)}{8} \cdot \frac{6(2y - h)}{h^3}$$
$$n_{yy} = \frac{\partial^2\phi}{\partial x^2} = -q \cdot \frac{(2y^3 - 3hy^2 + h^3)}{h^3}$$
$$n_{xy} = -\frac{\partial^2\phi}{\partial x\partial y} = -qx \cdot \frac{6y(h - y)}{h^3}$$

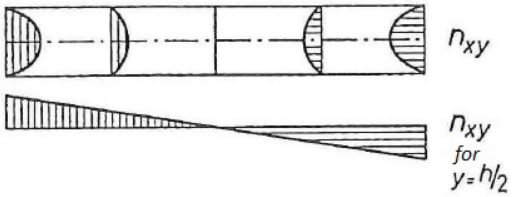

The change of y-slope in y-direction gives the internal compression and tension forces, which are equal, and multiplied with the internal arm gives the internal moment which is in equilibrium with the load.

As observed the difference of slope along the stress function results in discrete internal forces as opposed to distributed internal forces of the stress functions.

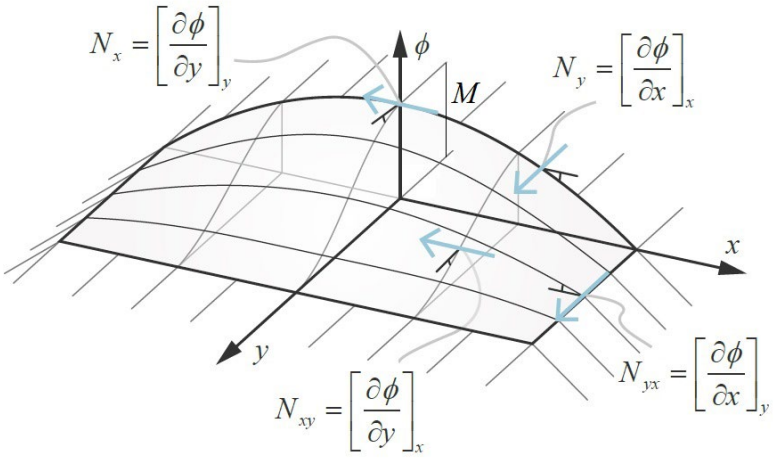

change of y – slope in y – direction :

$$N_x = \left(\frac{\partial \phi}{\partial y}\right)_y$$

change of x – slope in x – direction :

$$N_y = \left(\frac{\partial \phi}{\partial x}\right)_x$$

change of y – slope in x – direction / change of x – slope in y – direction:

$$N_{xy} = \left(\frac{\partial \phi}{\partial y}\right)_x \equiv N_{yx} = \left(\frac{\partial \phi}{\partial x}\right)_y$$

The curvatures of the surface of the stress function represent the stresses [74]. The principle stress trajectories are equivalent to the principle trajectories of the curvatures of the surface. Each meet at an angle of 90 degrees.

$$z = \phi(x, y)$$

$$n_{xx} = \frac{\partial \phi^2}{\partial y^2} \equiv \kappa_{\phi,yy}$$

$$n_{yy} = \frac{\partial \phi^2}{\partial x^2} \equiv \kappa_{\phi,xx}$$

$$n_{xy} = -\frac{\partial \phi^2}{\partial x \partial y} \equiv -\kappa_{\phi,xy}$$

$$n_{1,2} = \frac{n_{xx} + n_{yy}}{2} \pm \sqrt{\left(\frac{n_{xx} - n_{yy}}{2}\right)^2 + {n_{xy}}^2}$$

$$n_{1,2} = \frac{\kappa_{\phi,yy} + \kappa_{\phi,xx}}{2} \pm \sqrt{\left(\frac{\kappa_{\phi,yy} - \kappa_{\phi,xx}}{2}\right)^2 + {\kappa_{\phi,xy}}^2}$$

$$\rightarrow n_1 \equiv \kappa_{\phi,2} \; and \; n_2 \equiv \kappa_{\phi,1}$$

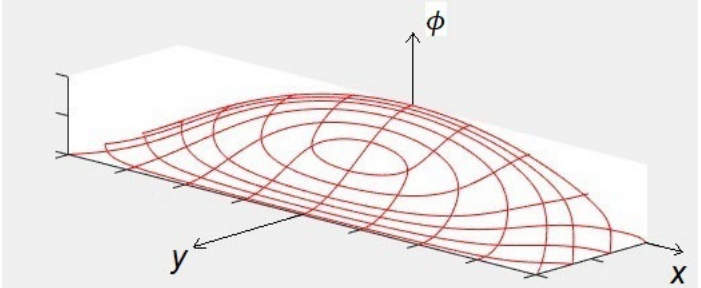

trajectories of stress function

A numerical example of the problem.

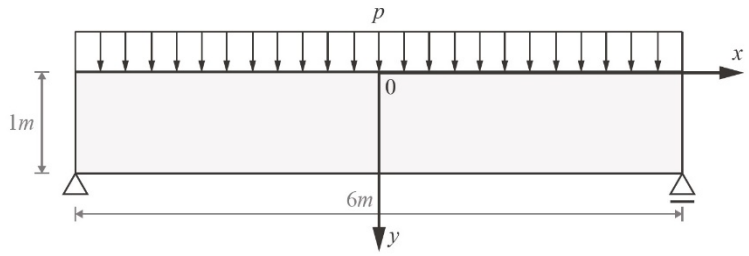

The stress function of the analytic solution, previously discussed, is shown below. The stress function has been discretized, resulting in the polyhedral stress function.

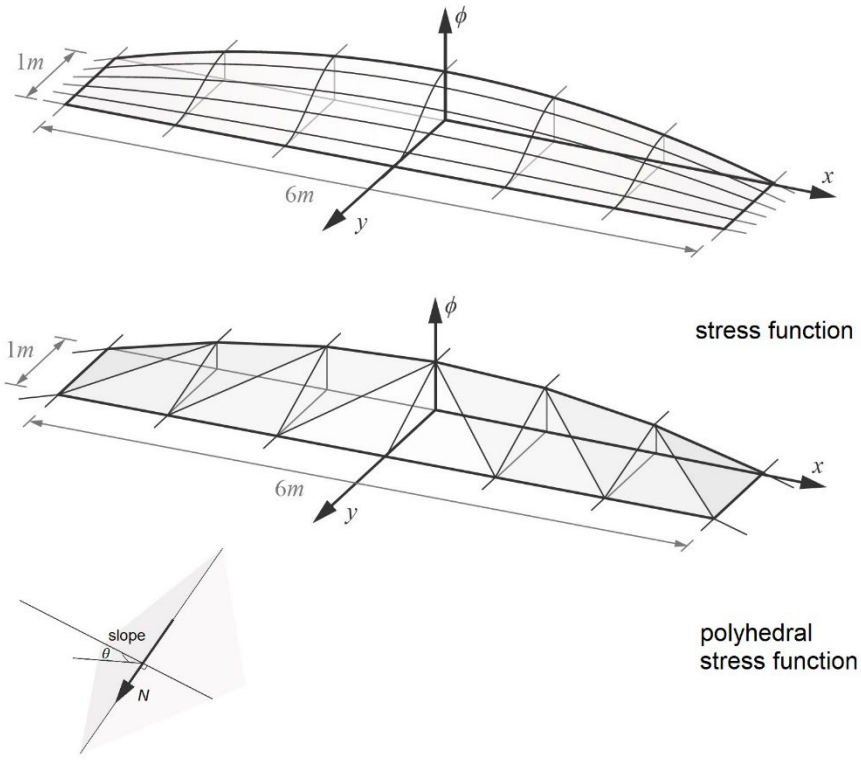

Figure 41 (polyhedral) stress function truss [images 101]

For the smooth stress function the change of slopes gives the discrete internal forces and its curvatures the stresses. The discretized version concentrates the curvature in kinks which are equivalent to the forces in that fold.

The projection onto a horizontal plane serves as the solution of the forces in the bars of a truss with the same loads. Along each fold of the discretized stress function lies a bar. The way the discretization is carried out determines the topology of the truss. The reciprocal figure of the truss, the form diagram, is its force polygon; also known as the Cremona diagram.

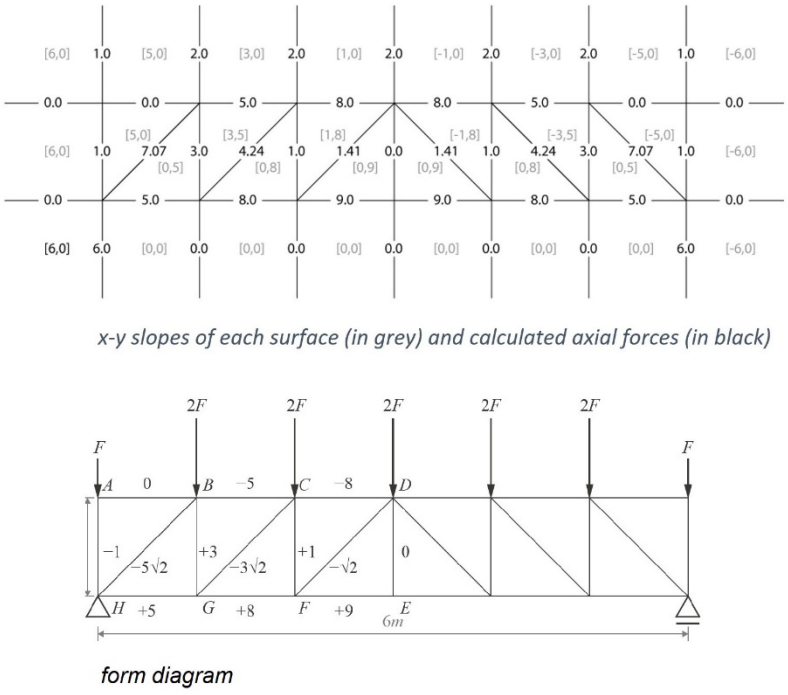

Figure 42 slopes of polyhedral stress function equals bar forces of the truss [images Pim Buskermolen]

Interestingly the way the stress function is discretised to form the polyhedral stress function determines the topology of the truss and the Cremona diagram in the horizontal projection [75] [76]. The support reactions remain equal.

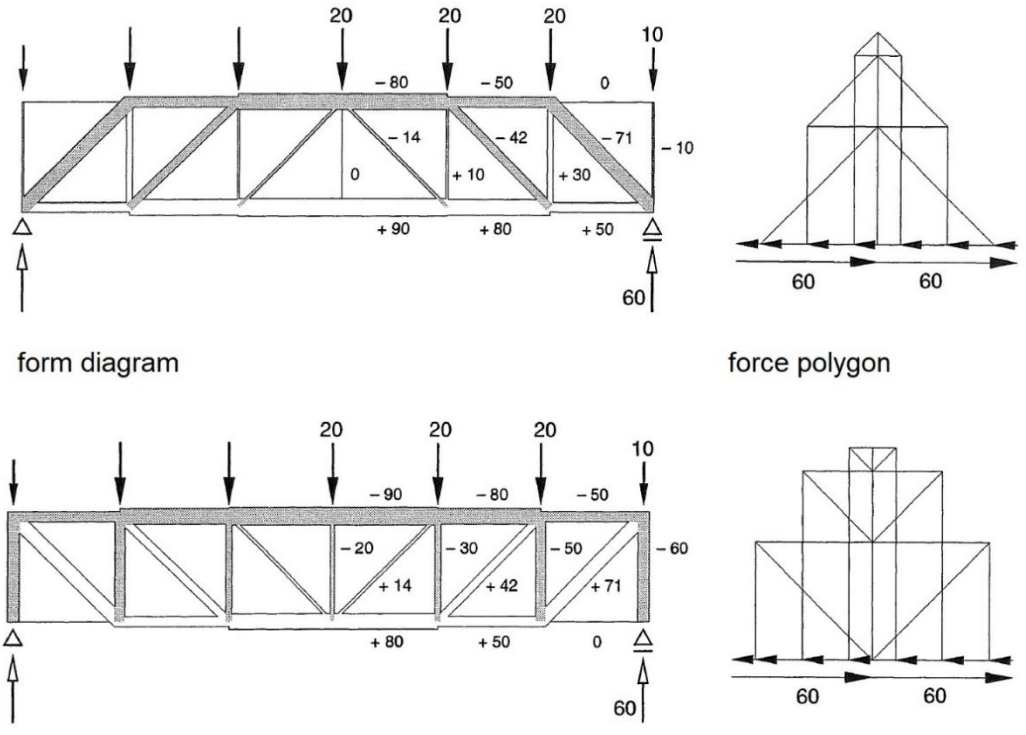

The reciprocal figure of the horizontal projections of the trajectories of the smooth stress surface produces a smooth “force polygon”, which is equivalent to the Cremona diagram, the discretized version of the example.

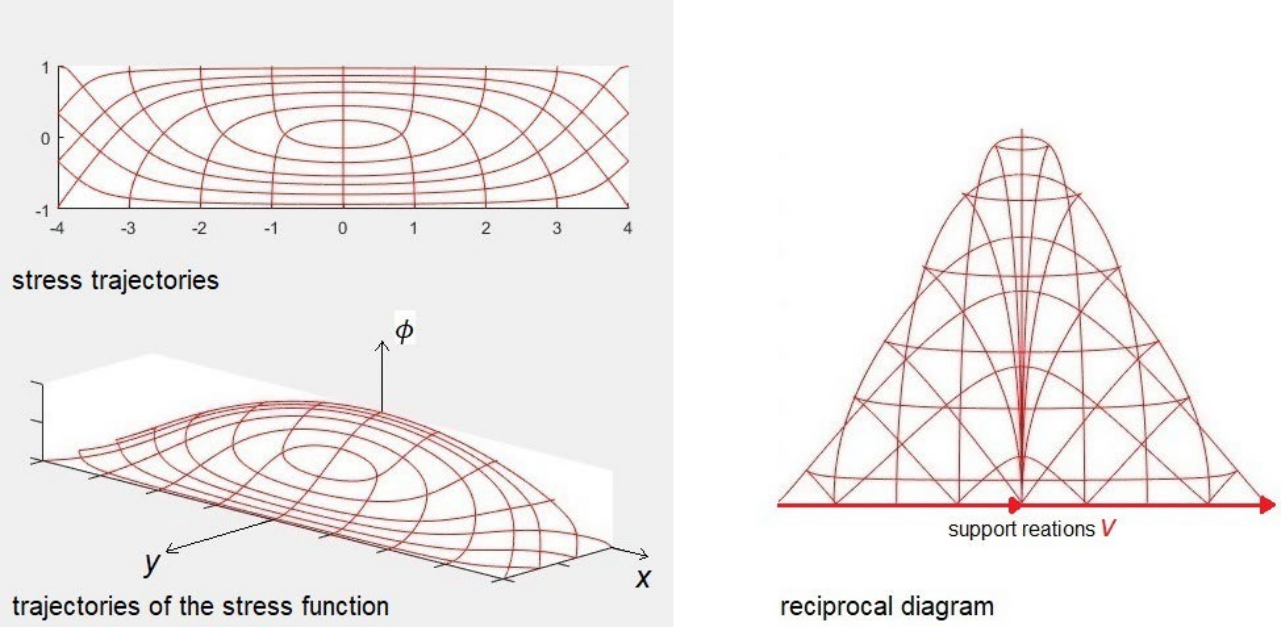

Figure 43 stress trajectories beam and reciprocal diagram [images Yu-Chou Chiang]

A few beams with different loads and different boundary conditions will be examined next.

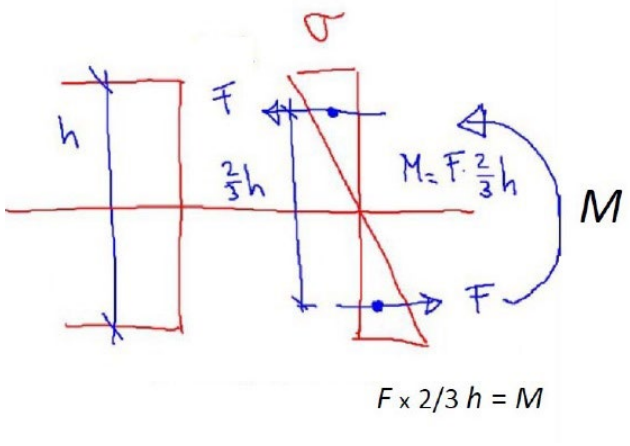

$$for\ x = 0:$$
$$\phi = \frac{ql^2}{8} \cdot \frac{2y^3 - 3hy^2 + h^3}{h^3}$$
$$for\ y = \frac{1}{2}h, y = 0:$$
$$\left(\frac{\partial \phi}{\partial y}\right)_1 = -\frac{3}{16}\frac{ql^2}{h}, \left(\frac{\partial \phi}{\partial y}\right)_2 = 0$$

$$change\ of\ y - slope\ in\ y - dirction:$$
$$\left(\frac{\partial \phi}{\partial y}\right)_2 - \left(\frac{\partial \phi}{\partial y}\right)_1 = \left(\frac{\partial \phi}{\partial y}\right)_y = 0 - -\frac{3}{16}\frac{ql^2}{h} = N_x$$
$$N_x \cdot \frac{2}{3}h = \frac{3}{16}\frac{ql^2}{h}\frac{2}{3}h = \frac{1}{8}ql^2 = M_{max}$$

For a beam with a different boundary condition, in this case fixed outer edges, the stress function is also a product of the bending moment diagram and the 3rd order polynomial needed the obtain the correct stress distribution.

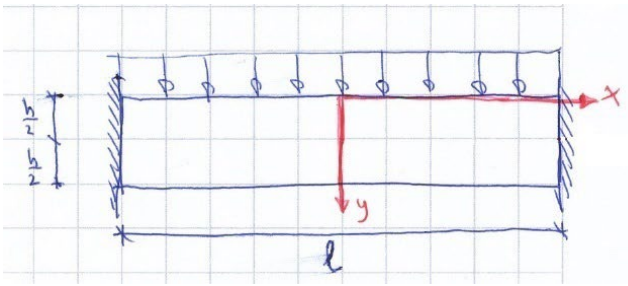

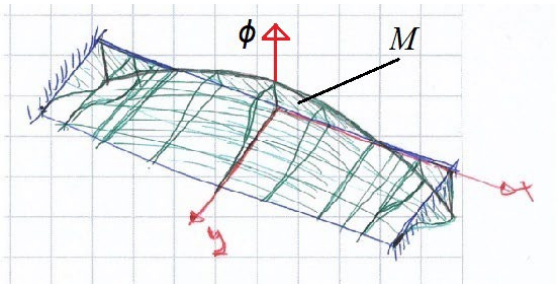

$$\phi = M(x) \cdot \frac{(2y^3 - 3hy^2 + h^3)}{h^3}$$
$$\phi = \underbrace{\frac{q(l^2 - 12x^2)}{24}}_{moment} \cdot \frac{(2y^3 - 3hy^2 + h^3)}{h^3}$$

Two variants of the 3rd order polynomial are used in this chapter, depending on the position of the origin of the coordinate system on the beam surface.

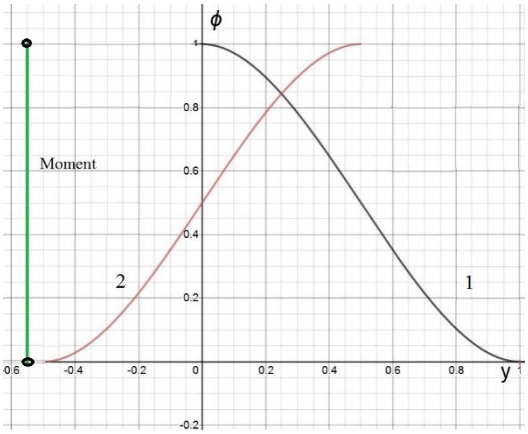

$$\frac{(2y^3 - 3hy^2 + h^3)}{h^3}$$
$$\frac{(3h^2y - 4y^3 + h^3)}{2h^3}$$

We conclude this section with examples of cantilevers with different load cases. Their stress functions all have a same function in the y-direction and thus a similar stress distribution. The moment depends on the load and boundary condition.

$$\phi = \underbrace{M(x)}_{moment} \cdot \underbrace{\frac{(2y^3 - 3hy^2 + h^3)}{h^3}}_{stress\ distribution}$$

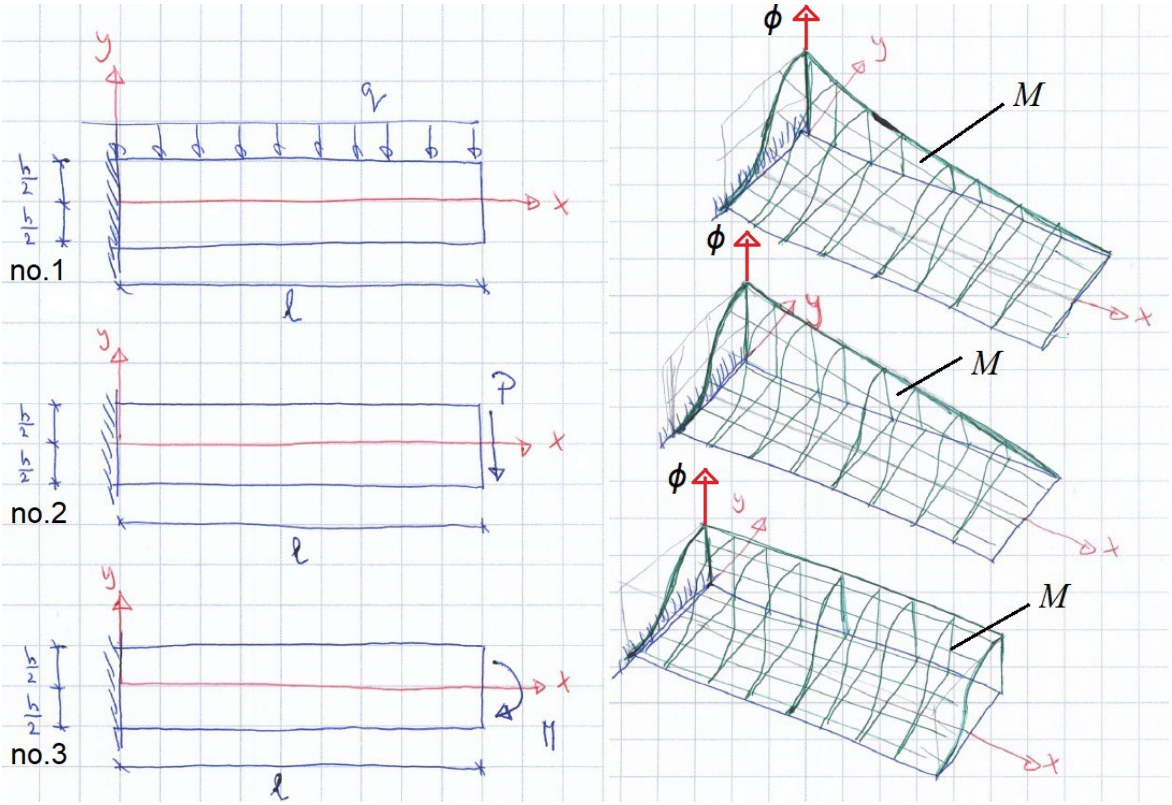

$$\#1. \quad \phi = \underbrace{\frac{q(x^2 - 2xl + l^2)}{24}}_{moment} \cdot \frac{(2y^3 - 3hy^2 + h^3)}{h^3}$$

$$\#2. \quad \phi = \underbrace{P(l - x)}_{moment} \cdot \frac{(2y^3 - 3hy^2 + h^3)}{h^3}$$

$$\#3. \quad \phi = \underbrace{M}_{moment} \cdot \frac{(2y^3 - 3hy^2 + h^3)}{h^3}$$

6.6 Applications of the stress function to arches

Two alternative approaches may be used for deriving the stress function for arches. Pucher's equation can be used, as shown in section 6.2 and 6.3, which would be an obvious choice because it includes the shape function of the curved form of the arch. The other approach is to use the plane stress equation. This equation does not include the shape of the arch, thus its effect needs to be incorporated in the resulting expression.
The problem with Pucher's equation applied to arches is that its result is implicit. It produces the horizontal projection of the axial load in the arch, which for the arch is equal to the horizontal thrust, but not the stress distribution over the height of the cross section of the arch.

If an arch has bending moments due to its shape and the load, the stress function needs to express a combination of stresses as a result of axial forces and bending moments.
With the plane stress equation a combination of stresses can be obtained by the superposition of the cases of the bar with a centric axial force and the simply supported beam with a uniformly distributed load, both separately discussed in section 6.5. The resulting stress function gives the stress distribution of the height of surface area of the beam.

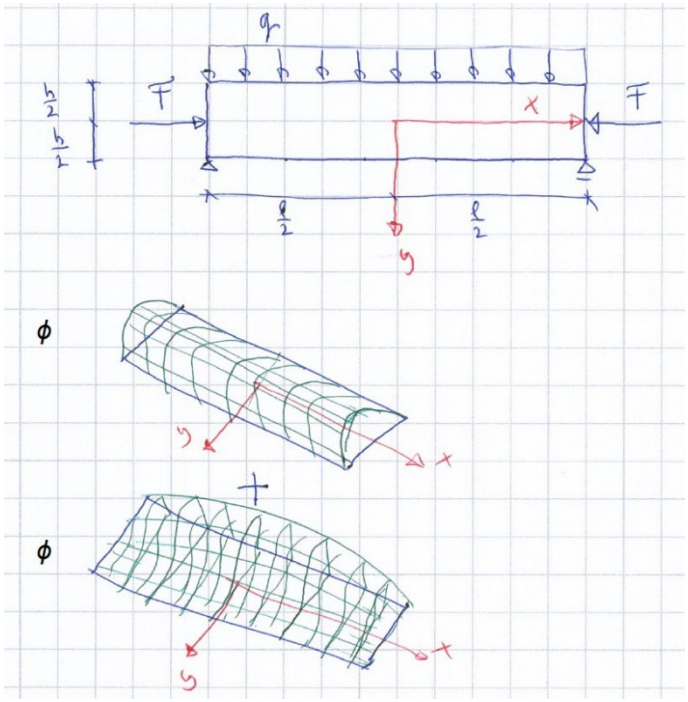

$$\phi = \underbrace{F}_{normal\ force} \cdot \frac{(h^2 - 4y^2)}{8h} + \underbrace{\frac{q(l^2 - 4x^2)}{8}}_{moment} \cdot \frac{(2y^3 - 3hy^2 + h^3)}{h^3}$$

$$n_{xx} = \frac{\partial^2 \phi}{\partial y^2} = -\frac{F}{h} \pm \frac{q(l^2 - 4x^2)}{8} \cdot \frac{6(2y - h)}{h^3}$$

Arches with straight elements, portal frames, can be interpreted as continuous beams on multiple supports with the outer two spans bent inwards to form the portal frame [77].

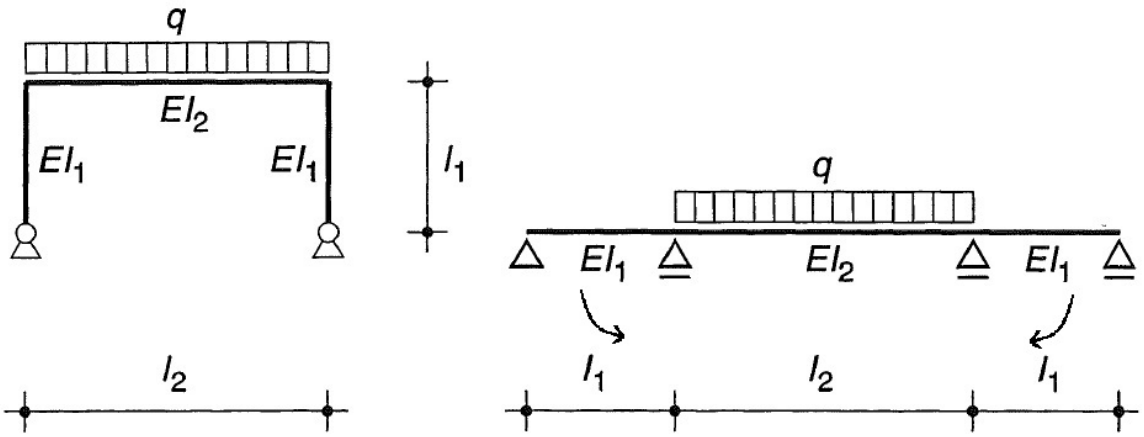

A portal frame, like most arches, has axial forces and bending moments. For this case the combined stress function, presented in the previous paragraph can used. And again the moment distribution can be recognized along the outer boundary of the stress function.

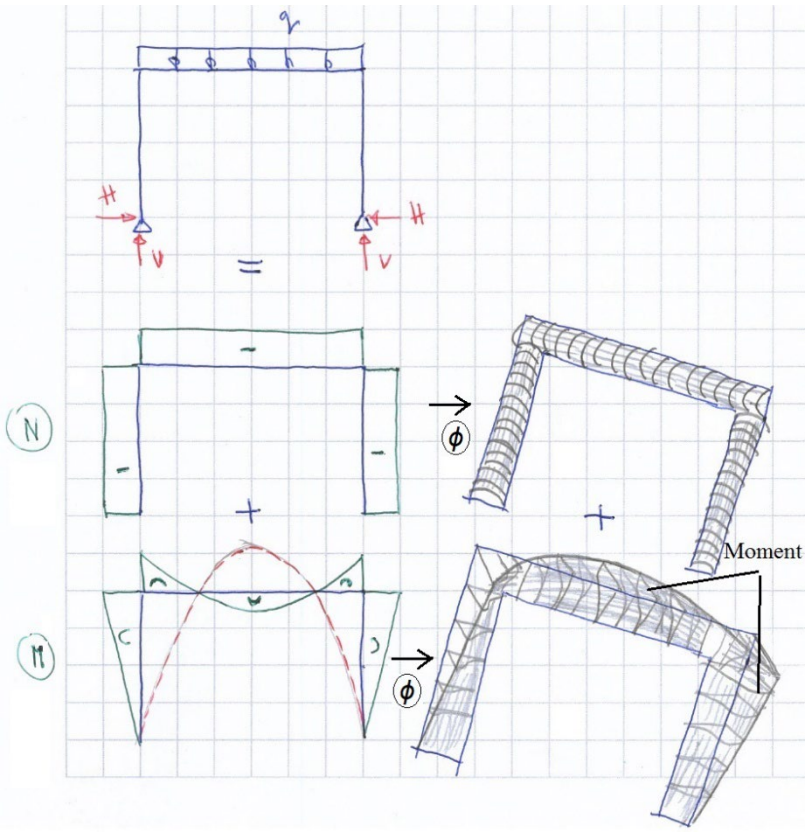

For funicular curved arches, like the parabolic one with a uniformly distributed load, Pucher's equation was used in section 6.2. As mentioned this do not result in a stress distribution over the cross section. A transformation formula has to be used to obtain the axial force in the arch from the projected force, which is the result of the solution of Pucher's equation. From the axial force the stress can be obtained.

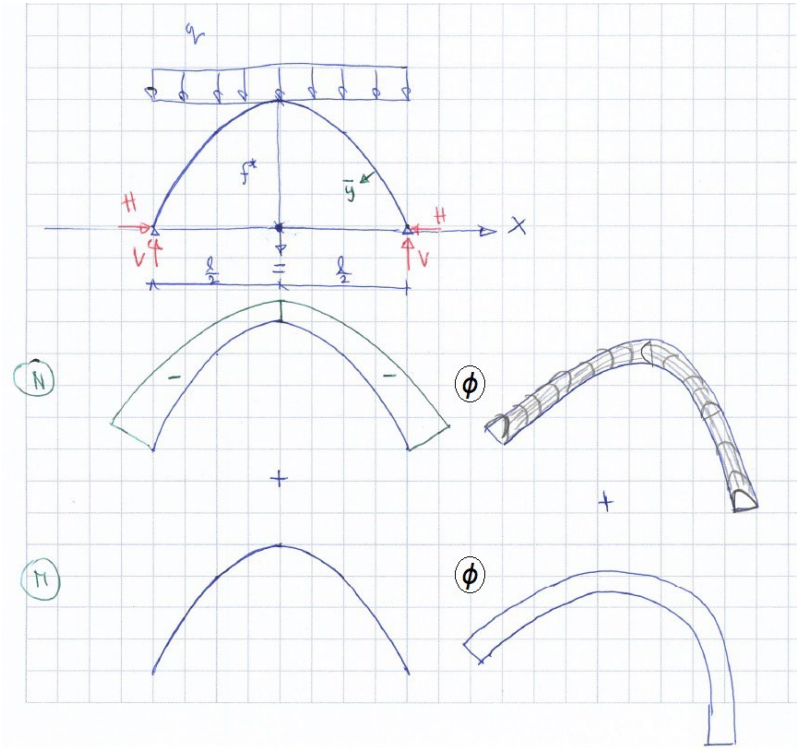

The alternative to the Pucher stress function is the one derived for the bar with a axial force by means of the plane stress equation. This will provide direct information on the stress distribution over the cross section. The stress function needs some adjustment, the first part which concerns the axial force will be in the global coordinate system (*x*-axis) and the second part concerning the stress distribution over the height *h* of the cross section, in the local coordinate ($\bar{y}$-axis) system of the arch.

$plane\ stress\ equation$:

$$\phi = N \cdot \frac{(h^2 - 4\bar{y}^2)}{8h} = \frac{q(l^4 + 64f^{*2}x^2)^{\frac{1}{2}}}{8f^*} \cdot \frac{(h^2 - 4\bar{y}^2)}{8h}$$

$Pucher's\ equation$:

$$\phi = \frac{ql^2}{16f^*}y^2 \Rightarrow H = \frac{\partial^2\phi}{\partial y^2} = \frac{ql^2}{8f^*}, N = H\frac{1}{\cos\varphi}$$

$$N = \frac{ql^2}{8f^*} \cdot \underbrace{\left(1 + \left(\frac{\partial y}{\partial x}\right)^2\right)^{\frac{1}{2}}}_{transformation} = \frac{ql^2}{8f^*} \cdot \left(\frac{(l^4 + 64f^{*2}x^2)^{\frac{1}{2}}}{l^2}\right) = \frac{q(l^4 + 64f^{*2}x^2)^{\frac{1}{2}}}{8f^*}$$

A semi-circular arch with a uniformly distributed load will have bending moments, because the thrust line will not coincide with the axis of the arch resulting in eccentricities and thus bending moments.
In section 5.7 this case was solved and a similar stress function can be used as described in the previous paragraph.

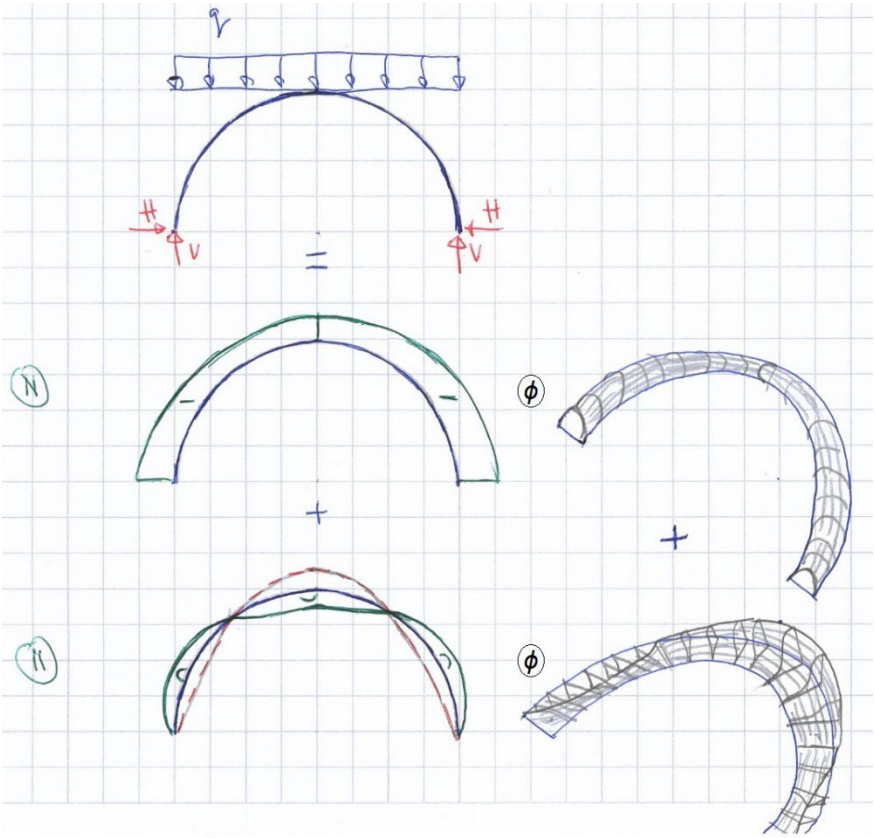

6.7 Graphic statics of stress functions

Now the static-geometric analogy has been established for beams, graphic statics can be used to construct a stress function.

A form diagram and its reciprocal force polygon is the graphical representation of the cable equation. The part of the beam equation that deals with equilibrium is equivalent to the cable equation. It was shown that the shape function of the cable is equivalent to the bending moment diagram. The second part of the beam equation that deals with compatibility and stiffness has the same structure as does the stress function. As a conclusion they can all be represented by means of graphic statics [78] .

$$\begin{cases} H\dfrac{d^2w}{dx^2} = q \\ \dfrac{d^2M}{dx^2} = q \end{cases} \qquad \begin{cases} \dfrac{d^2w}{dx^2} = -\dfrac{M}{EI} \\ \dfrac{d^2\phi}{dy^2} = n \end{cases}$$

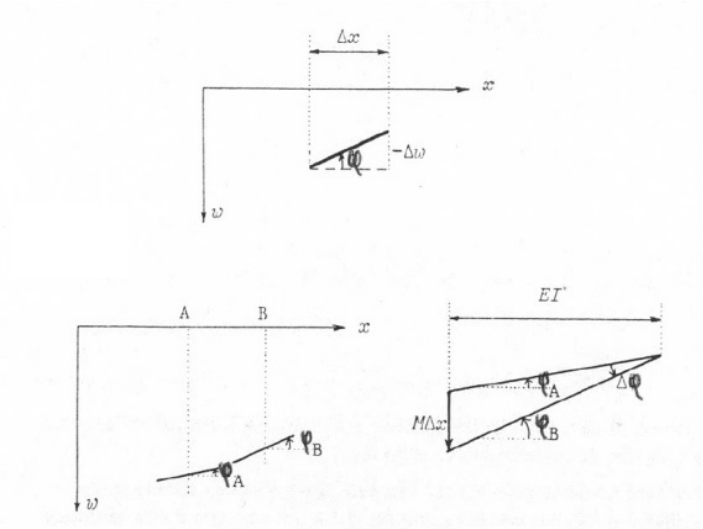

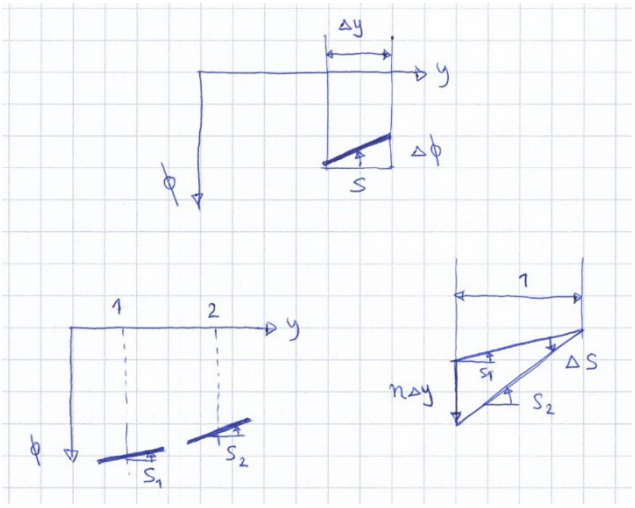

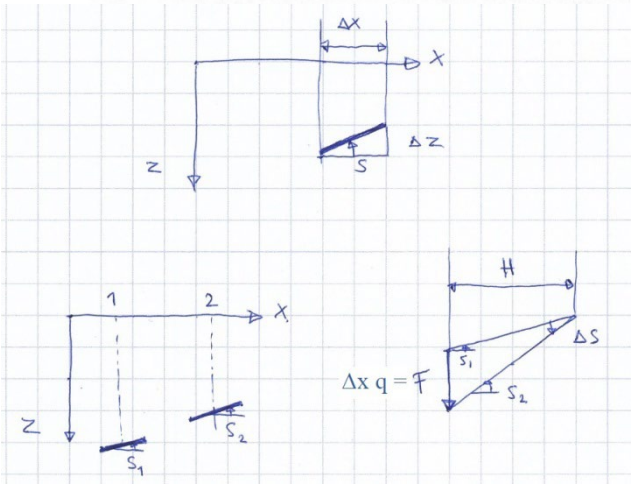

$$\triangle w = \varphi \triangle x \qquad \triangle \phi = s \triangle y$$

$$\triangle \varphi = \frac{M \triangle x}{EI} \qquad \triangle s = \frac{n \triangle y}{1}$$

$$\left.\begin{array}{l} \triangle z = s \triangle x \\ \triangle s = \dfrac{F}{H} \end{array}\right\} \Rightarrow \frac{\triangle z}{\triangle x} = \frac{\triangle xq}{H} \Rightarrow H\frac{\triangle z}{(\triangle x)^2} = q$$

As an example the simply supported beam with a uniformly distributed load and the stress function, from section 6.4, to establish the static-geometric analogy for beams [79] will be used.

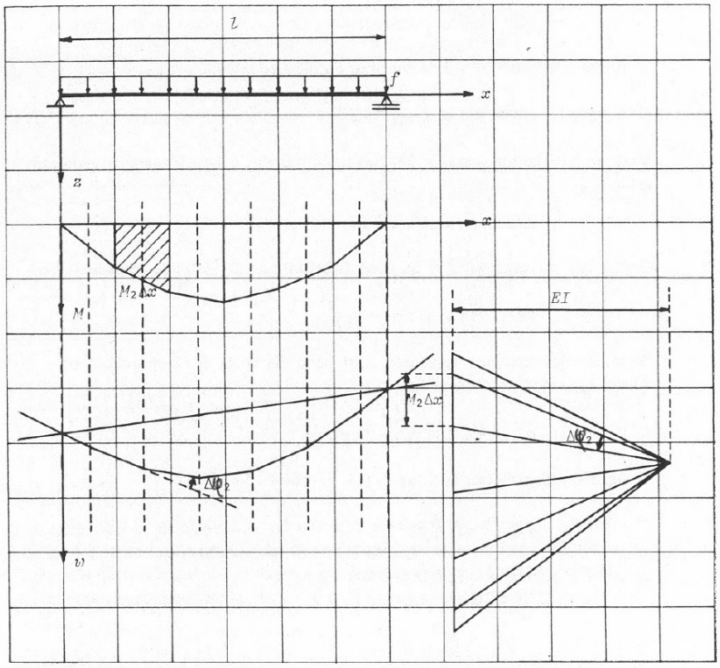

Figure 44 reciprocal diagrams: moment *M* form diagram and deflection *w* polygon [images 79]

For the first example the line of deflection is constructed, for the second example the stress function.

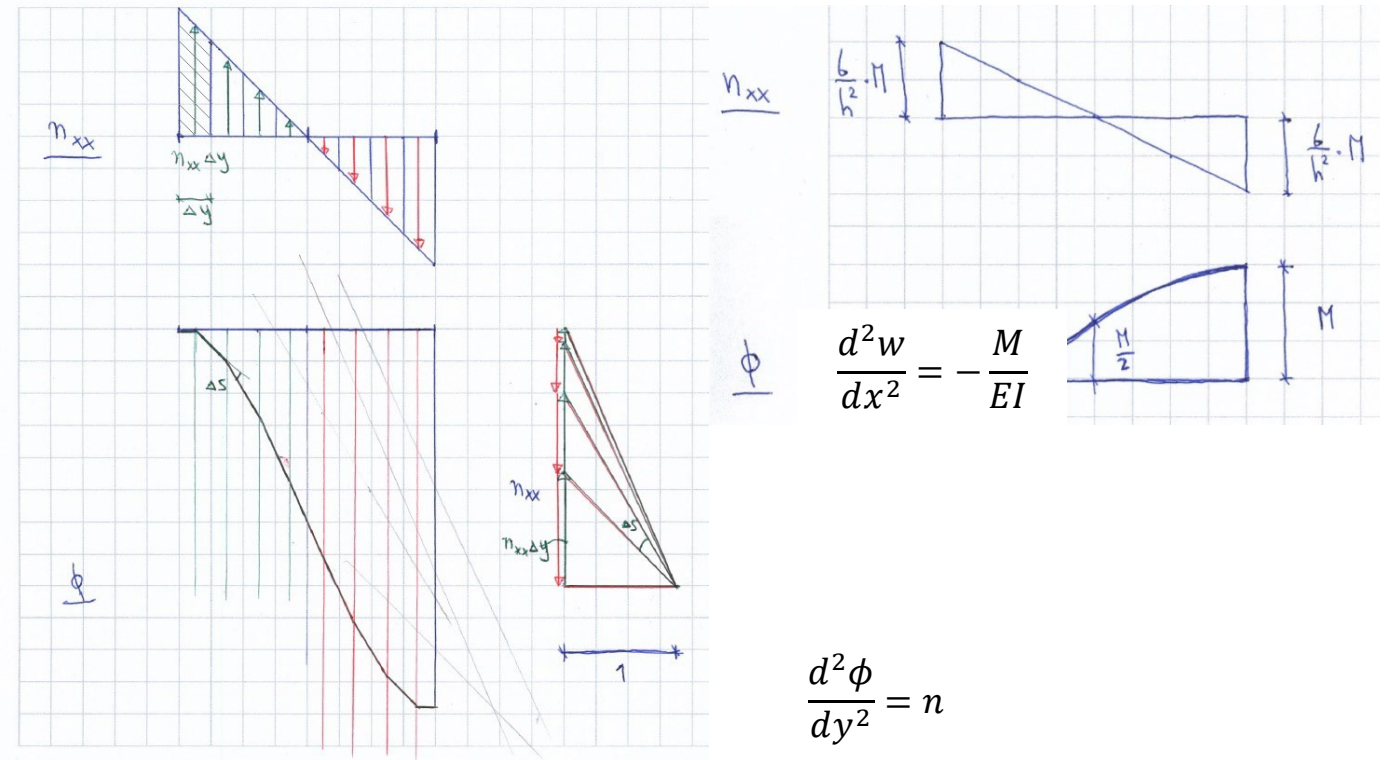

$$\frac{d^2w}{dx^2} = -\frac{M}{EI}$$

$$\frac{d^2\phi}{dy^2} = n$$

Referring back to the example of a uniformly loaded parabolic arch and its accompanying stress function of section 6.2, the stress function will be represented by means of graphic statics.
Both the shape function and the stress function of the arch are a function of the rise of the arch f^*.

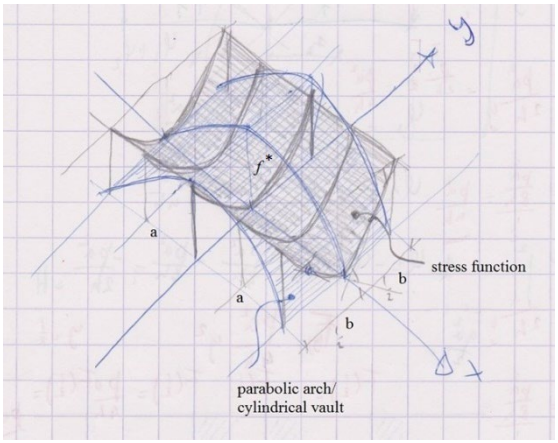

$$z(x) = f^* \left(1 - \frac{x^2}{a^2}\right)$$

$$\phi(y) = \frac{pa^2}{4f^*} y^2$$

$$with: p[N/m^2]$$

If the stress function as a form diagram is discretized it can be represented by a similar polygon as the force polygon of an arch. The slope of the folds (Θ) in the discretized stress function represent summarised forces. Because the polygon represents the slopes of the stress function the horizontal distance of the polygon has unit 1. If the discretized stress function and its reciprocal diagram the polygon is scaled the ratio between slopes of the folds remains constant, the stress function is an isotropic surface [80].

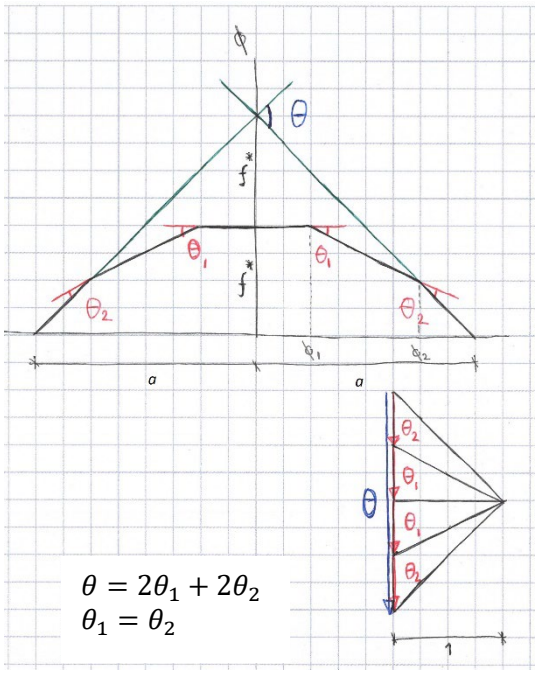

$$scaling\ function: s_{f^*} = \frac{f^*_{+1}}{f^*} = \frac{\phi_{i+1}}{\phi_i}$$

If the rise of the arch *f** is scaled the force polygon and the stress function polygons are scaled accordingly.

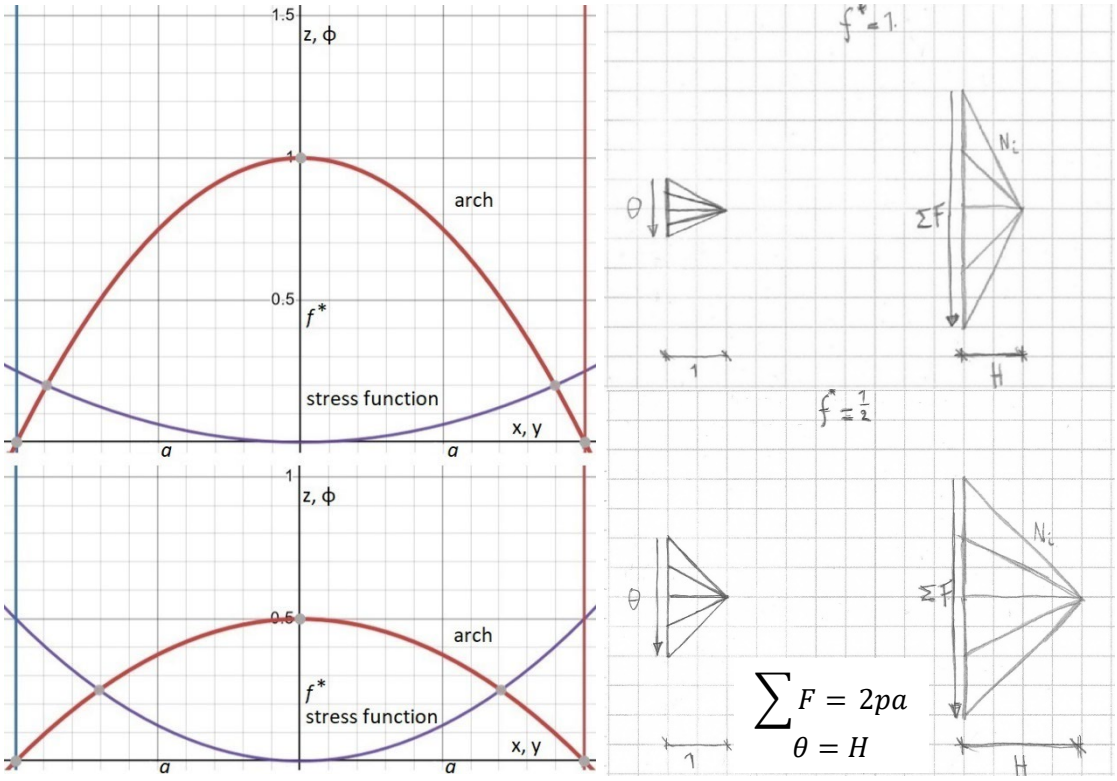

In this chapter the relationship has been explored between the shape function, the stress function, thrust line and the M-hill of the arch. This lays the basis for establishing the relations between these four functions for shell structure. Chapter 7 concerns with membrane shells and in particular axisymmetric ones, and in chapter 8 the general theory of the four functions will be presented.

7 The stress function of membrane shells

7.1 Introduction

In this chapter the relation will be explored between the fundamental characteristics that determine the relation between the geometric and mechanical properties of shells structures. The shell's geometry is described by the shape function. The stress function ensures equilibrium, the thrust surface is equivalent the thrust line of arches. The moment hill associated with slabs has a similar relation to the thrust surface as the moment line of a beam has to the shape of an equivalent arch or cable.
For simplicity this chapter will focus on membrane shells only to introduce the relations, and mainly axisymmetric shells. In the next chapter bending of the shell will be addressed. In chapter 7 and 8 the assumed load is uniformly distributed $p = p_z$ and Poisson's ratio is assumed equal to zero.

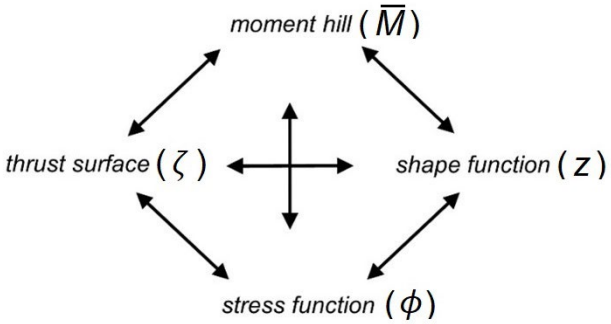

7.2 The cubic funicular arch

To establish the thrust surface of an axisymmetric membrane shell loaded by a uniformly distributed load *p*, first the thrust line of the equivalent arch will be derived.

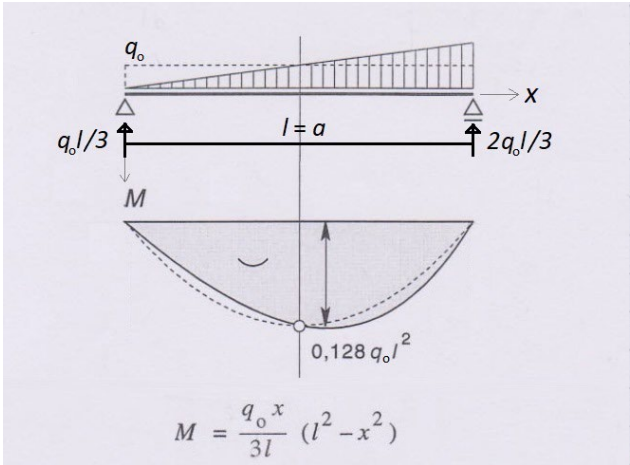

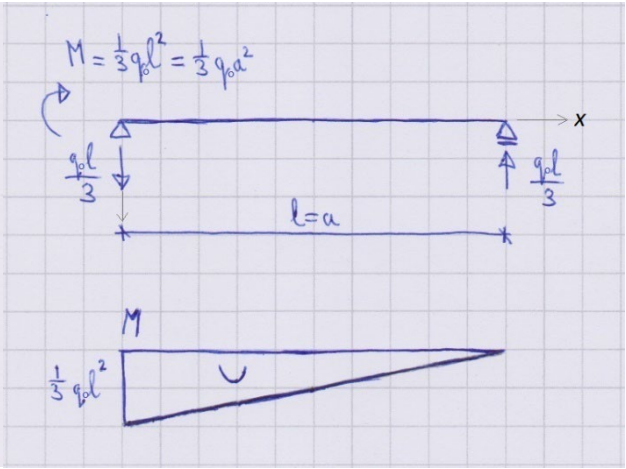

$$q = \frac{2q_0 x}{l}$$

$$M = \frac{q_0 l^2}{3}\left(\frac{l - x}{l}\right)$$

An orange peel part will be taken from an axisymmetric shell and modelled as a beam, which results in a triangular load *q* on the beam. For half of this beam standard formulas can be used to determine the bending moments, and by adding an additional load case to eliminate any support reactions midway this results in the bending moment diagram.

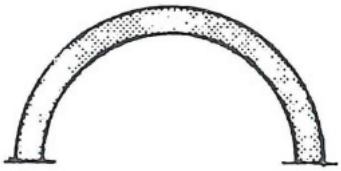

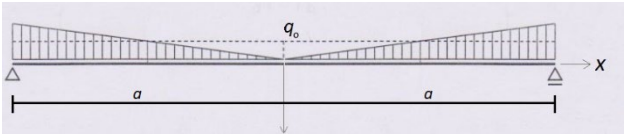

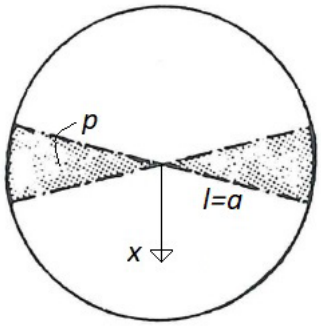

$$P = \pi a^2 p$$
$$q_0 = \frac{P}{2a} = \frac{\pi a p}{2}$$
$$with: l = a$$
$$q = \frac{2q_0 x}{l}$$

By using the analogy between the bending moment diagram and the shape of a cable or its inverse, the arch we arrive at the funicular thrust line for the load case.

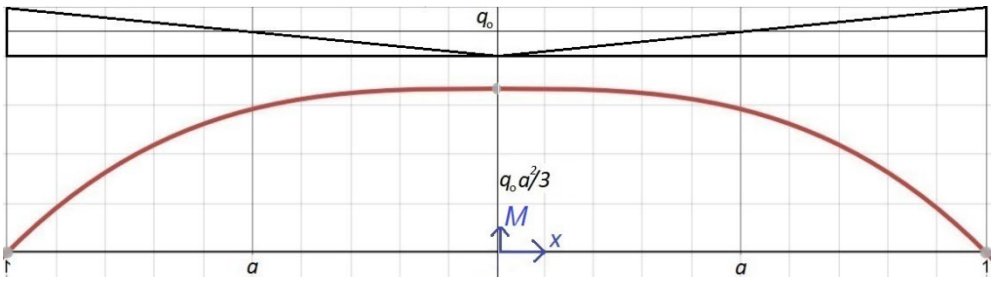

$$M = \left(\frac{q_0 x}{3a}(a^2 - x^2)\right) + \left(\frac{q_0 a^2}{3}\left(\frac{a - x}{a}\right)\right) = \frac{q_0(a^3 - x^3)}{3a}$$

$$M_{max} = \frac{q_0 a^2}{3}$$

$$V = \frac{dM}{dx} = -\frac{q_0 x^2}{a}$$

$$beam - cable/arch\ analogy:$$
$$p = \frac{d^2M}{dx^2} = H\frac{d^2z}{dx^2}$$
$$M = Hz_i\ , with: H = constant$$

The result is a cubic shape function, which can also be determined by using graphic statics. Het horizontal thrust *H* is constant throughout the arch.

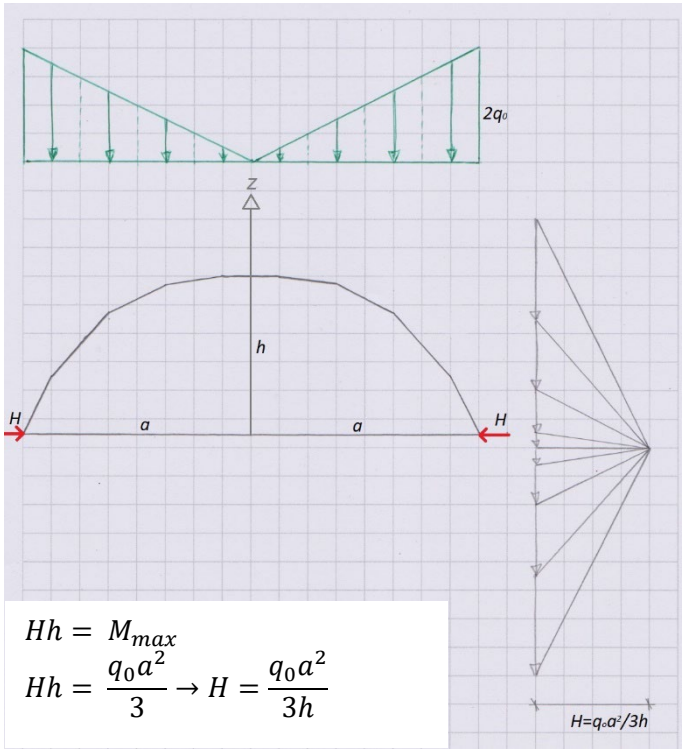

$$Hh = M_{max}$$
$$Hh = \frac{q_0 a^2}{3} \rightarrow H = \frac{q_0 a^2}{3h}$$

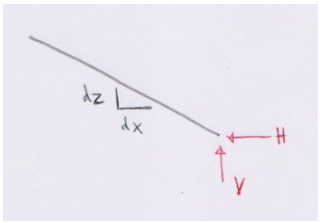

$$\frac{V}{H} = \frac{dz}{dx} \rightarrow V = H\frac{dz}{dx}, H = constant$$
$$M = \int V dx = H\int \frac{dz}{dx}dx = Hz$$
$$M = \frac{q_0(a^3 - x^3)}{3a} = \frac{q_0 a^2}{3h} \cdot z$$
$$\rightarrow z = \frac{h(a^3 - x^3)}{a^3}$$

The shape depends on the ratio of span *a* to rise *h*. Because of the beam analogy Maxwell's load path theorem can be used to obtain the optimum ratio.

$$z = \frac{h(a^3 - x^3)}{a^3}; L_s = \int_{-a}^{a} ds; ds = \left[1 + \left(\frac{dz}{dx}\right)^2\right]^{\frac{1}{2}} dx$$
$$ds = \left[1 + \frac{9h^2x^4}{a^6}\right]^{\frac{1}{2}} dx$$
$$N = [(H)^2 + (V)^2]^{\frac{1}{2}} = \left[\left(\frac{qa^2}{3h}\right)^2 + \left(\frac{qx^2}{a}\right)^2\right]^{\frac{1}{2}} = \frac{q(9h^2x^4 + a^6)^{\frac{1}{2}}}{3ha}$$
$$Nds = \frac{q(9h^2x^4 + a^6)}{3ha^4} dx$$

the total loadpath:
$$V = \frac{1}{\sigma}\int_{-a}^{a} Nds = \frac{1}{\sigma}\int_{-a}^{a} \frac{q(9h^2x^4 + a^6)}{3ha^4} dx = \frac{2aq(5a^2 + 9h^2)}{15h\sigma} = min$$

the lowest value of the loadpath gives the optimal ratio:
$$\Rightarrow \frac{d}{dh} = \frac{2aq(9h^2 - 5a^2)}{15h^2} = 0 \Rightarrow h = \frac{\sqrt{5}}{3}a$$
$$\frac{h}{a} = \frac{\sqrt{5}}{3} \approx 0{,}74535$$

7.3 The cubic funicular shell

In order to obtain the funicular shell [81], equivalent to the funicular arch, with a uniformly distributed load there are no hoop forces which consequently means that the horizontal thrust "*H*" has to be constant, as with the arch [82].

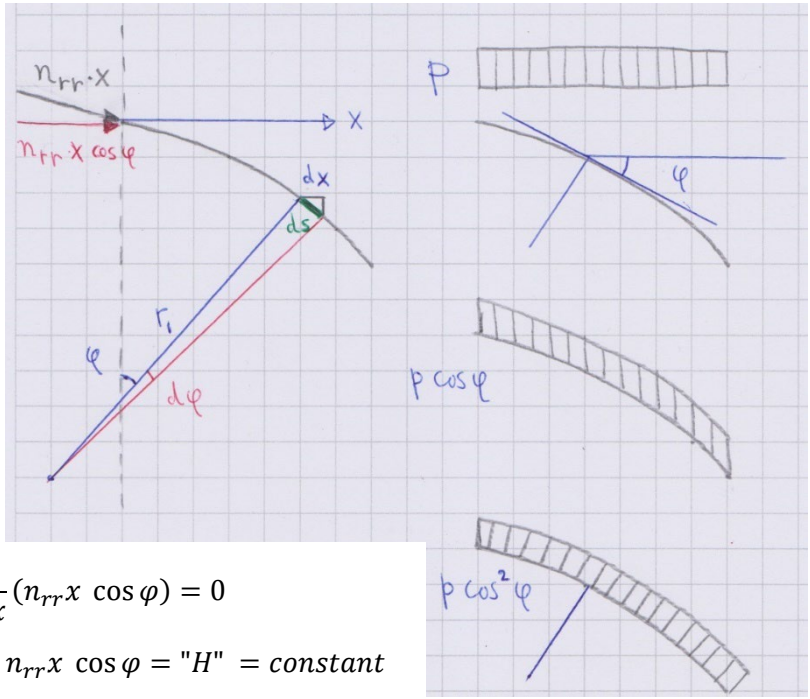

$$\frac{d}{dx}(n_{rr}x\ \cos\varphi) = 0$$

$$\rightarrow n_{rr}x\ \cos\varphi = "H"\ = constant$$

$$with: n_{rr} = r_1 p_{\perp} = r_1 p\cos^2\varphi$$

$$\rightarrow p r_1 x\cos^3\varphi = constant$$

$$with:\ \cos\varphi = \frac{dx}{ds} = \frac{dx}{r_1 d\varphi}$$

$$and: r_1 = \frac{dx}{d\varphi}\frac{1}{\cos\varphi}$$

$$\rightarrow px\frac{dx}{d\varphi}\cos^2\varphi = constant$$

$$px\frac{dx}{d\varphi}\cos^2\varphi = constant$$

$$px\frac{dx}{d\varphi}\cos^2\varphi = \frac{x_0}{2}(supposition)$$

$$\rightarrow x\,dx = \frac{x_0}{2p\cos^2\varphi}\,d\varphi$$

$$\rightarrow \int x\,dx = \int \frac{x_0}{2p\cos^2\varphi}\,d\varphi$$

$$\rightarrow \frac{x^2}{2} + c = \frac{x_0}{2p}\tan\varphi + c$$

$$with: p = 1$$

$$\rightarrow x^2 = x_0\tan\varphi$$

$$\rightarrow \tan\varphi = \frac{x^2}{x_0} = \frac{dz}{dx}$$

$$\rightarrow dz = \frac{x^2}{x_0}\,dx$$

$$\rightarrow z = \int \frac{x^2}{x_0}\,dx$$

$$\rightarrow z = \frac{x^3}{3x_0} + c$$

The result is the same cubic shape function as found for the funicular arch.

$$z = \frac{x^3}{3x_0} + c$$

$$with: x = a\ and\ z = 0$$

$$c = -\frac{a^3}{3x_0}$$

$$with: x = 0\ and\ z = h$$

$$x_0 = \frac{-a^3}{3h}, c = h$$

$$\rightarrow z = \frac{h(a^3 - x^3)}{a^3}$$

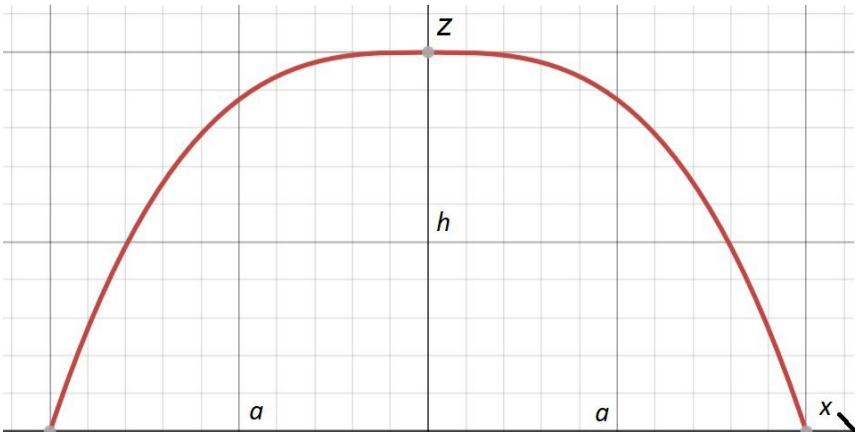

The increment of the horizontal thrust "*H*" has to be equal to zero. Which means that the shape of the dome is determined by the change of slope which is equivalent to the change of the vertical component of the internal force and that carries the load.

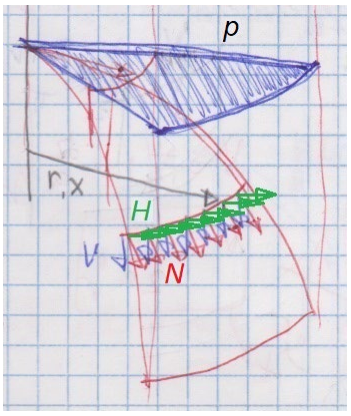

$$"H" = constant \rightarrow V \equiv "H"\frac{dz}{dx}$$
$$the\ increase\ of\ V\ is\ equivalent\ to$$
$$the\ increase\ of\ the\ slope\ \frac{dz}{dx}$$

$$with: "H_{total}" = \bar{n}_{rr} \cdot 2\pi x$$
$$"H" = n_{rr} x \cos\varphi = \bar{n}_{rr} x$$
$$\rightarrow n_{rr} \cos\varphi = \bar{n}_{rr}$$

The horizontal thrust "*H*" is constant but the horizontal projection of the meridian forces $\bar{n}_{rr}$ is not, this is a function of the radius of the dome.

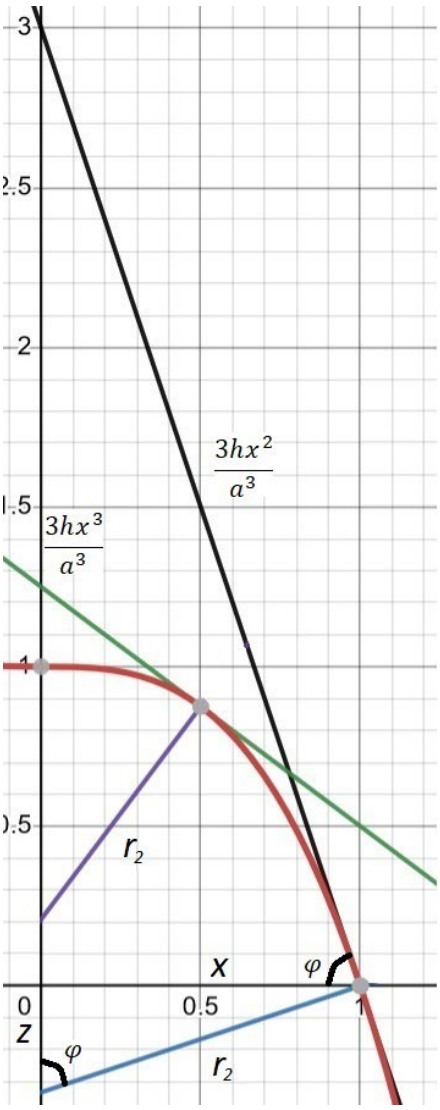

cubic funicular shell

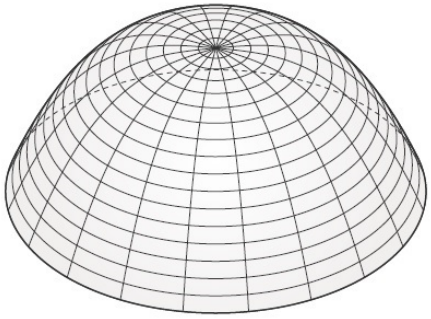

$$z = \frac{h(a^3 - x^3)}{a^3}$$
$$\frac{dz}{dx} = -\frac{3hx^2}{a^3} = -\frac{\frac{3hx^3}{a^3}}{x}$$
$$\frac{x}{z} = \frac{\frac{3hx^3}{a^3}}{x} \rightarrow z = \frac{a^3}{3hx}$$
$$r_2 = (x^2 + (\frac{a^3}{3hx})^2)^{\frac{1}{2}} = \frac{(9x^4h^2 + a^6)^{\frac{1}{2}}}{3hx}$$

The total horizontal thrust "*H*" can also be represented with Dischinger's graphic method [83] to represent the summation of the load and membrane forces. The result is very similar to the arch.

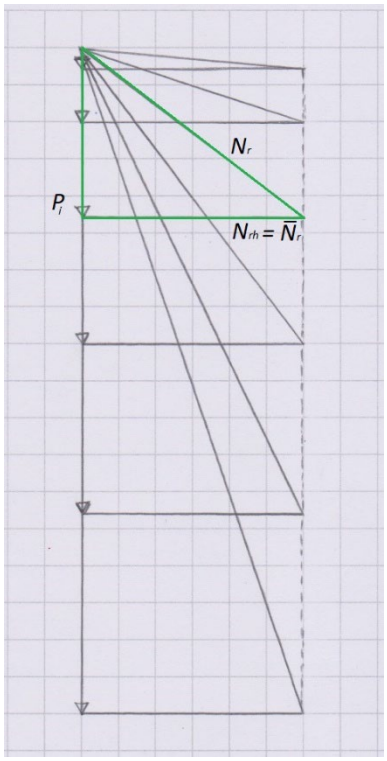

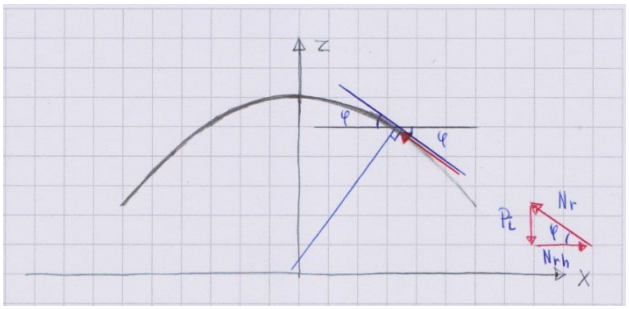

$$P_i = \pi x_i^2 p$$

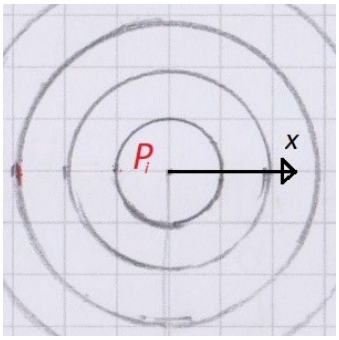

The horizontal component of the membrane force goes to infinity at the axis of revolution of the shell. But to ensure equilibrium and even when there are no membrane hoop forces there must be a force at the summit of the dome.

$$2\pi\, a\, n_{rr} \sin\varphi = \pi a^2 p$$

$$\rightarrow\ n_{rr} = \frac{p r_2}{2}$$

$$with: r_2 = \frac{(9x^4h^2 + a^6)^{\frac{1}{2}}}{3hx}$$

$$\rightarrow\ n_{rr} = \frac{p(9x^4h^2 + a^6)^{\frac{1}{2}}}{6hx}$$

$$with:\ \cos\varphi = \frac{z}{r_2} = \frac{a^3}{(9x^4h^2 + a^6)^{\frac{1}{2}}}$$

$$\bar{n}_{rr} = n_{rr}\cos\alpha = \frac{pa^3}{6hx}$$

$$with: x = a$$

$$\bar{n}_{rr,a} = n_{rr}\cos\alpha = \frac{pa^2}{6h}$$

$$"H" = \bar{n}_{rr} x = \frac{pa^3}{6h}$$

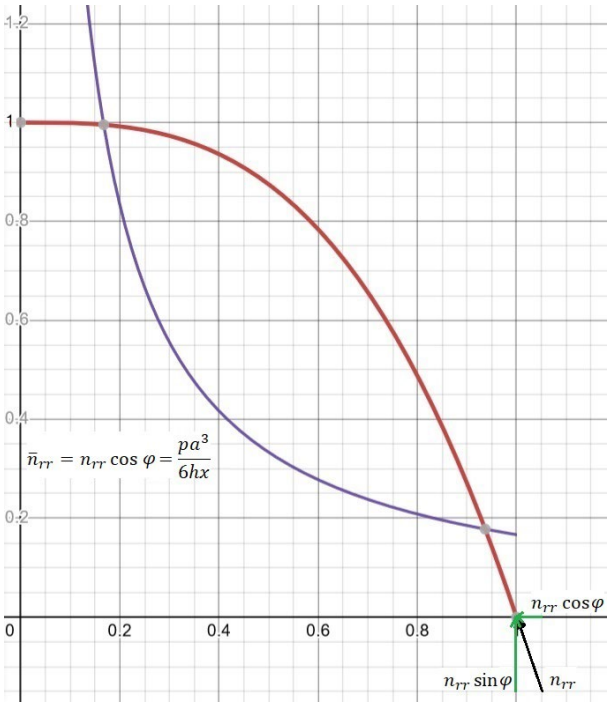

$$"H_{total}" = \bar{n}_{rr,a} \cdot 2\pi a = \frac{\pi a^3 p}{3h}$$

$$with: "H" = N_{rh} = \bar{N}_r$$

By making a cross section through the dome and regarding all the horizontal forces this force can be determined. And by multiplying this with the rise of the dome we arrive at the moment equilibrium. Later it will be shown that this aligns with the moment equilibrium due to the vertical forces.

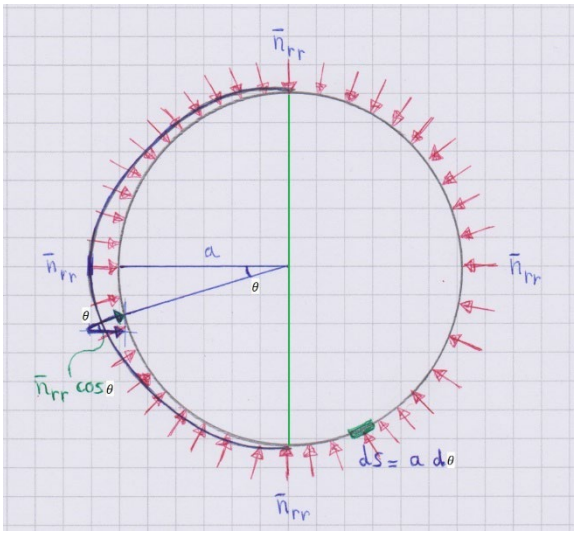

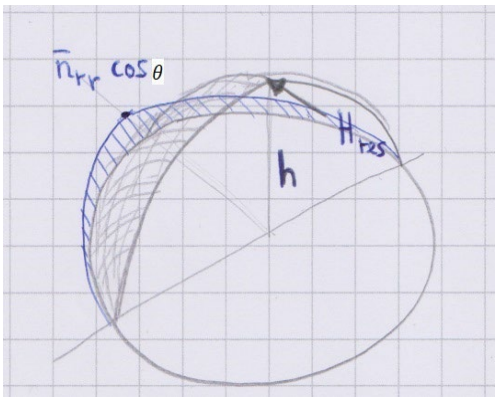

$$H_{res} = \int_{-\frac{\pi}{2}}^{\frac{\pi}{2}} \bar{n}_{rr,a} \cos\theta \, ds = \int_{-\frac{\pi}{2}}^{\frac{\pi}{2}} \bar{n}_{rr,a} \cos\theta \, a \, d\theta = 2a \, \bar{n}_{rr,a}$$

$$with: \bar{n}_{rr,a} = \frac{pa^2}{6h} \rightarrow H_{res} = \frac{pa^3}{3h}$$

$$M_t = H_{res} \cdot h = \frac{pa^3}{3}$$

Because the dome is a surface of revolution Maxwell's load path theorem can be used to obtain the optimum ratio. We arrive at the same result as found for the funicular arch.

$$z = \frac{h(a^3 - x^3)}{a^3}; A_s = \int_0^a \int_0^{2\pi} \left[1 + \left(\frac{dz}{dx}\right)^2\right]^{\frac{1}{2}} x \, dx \, d\theta$$

$$n_{rr} = \frac{p(9x^4h^2 + a^6)^{\frac{1}{2}}}{6hx}$$

the total loadpath:

$$V = \frac{1}{\sigma}\int_0^{2\pi} \int_0^a n_{rr} \left[1 + \left(\frac{dz}{dx}\right)^2\right]^{\frac{1}{2}} x \, dx \, d\theta = \frac{1}{\sigma}\int_0^{2\pi} \int_0^a \frac{(9x^4h^2 + a^6)p}{6ha^6} dx \, d\theta = \frac{\pi p(5a^2 + 9h^2)}{15ah} min$$

the lowest value of the loadpath gives the optimal ratio:

$$\Rightarrow \frac{d}{dh} = \frac{\pi p(9h^2 - 5a^2)}{15ah^2} = 0 \Rightarrow h = \frac{\sqrt{5}}{3}a$$

$$\frac{h}{a} = \frac{\sqrt{5}}{3} \approx 0{,}74535$$

7.4 The spherical dome

The spherical dome loaded by a uniformly distributed load *p* has membrane forces in both directions of the principle curvatures, unlike the funicular dome. The membranes forces in question are the meridian forces n_{rr} and hoop forces $n_{\theta\theta}$, there are no shear membrane forces [84].

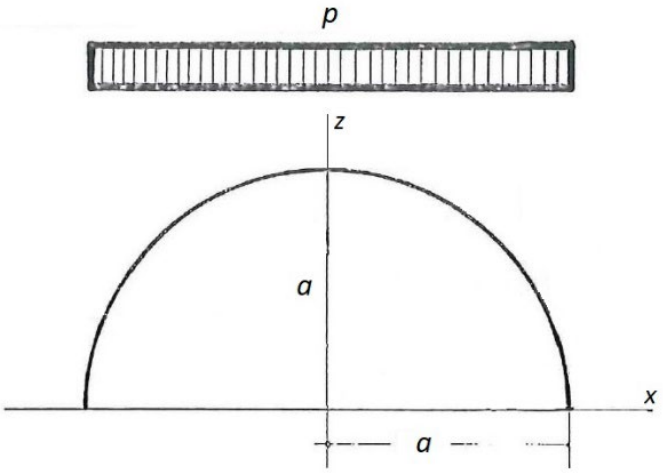

$$z = (a^2 - x^2)^{\frac{1}{2}}$$

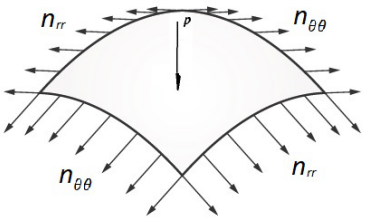

The formulas that describe this problem are well known and can be found in most handbooks on shell structures. The focus here is on the relation between the thrust surface of the load *p* and the dome, similar to that of the thrust line and an arch. Due to the load and the fact that the dome has 3 dimensions there are membrane hoop forces in compression and tension.

The hoop forces has a similar function as the bending moments in an arch if the thrust line does not coincide with the axis of the arch. It corrects the path of the thrust surface so it does coincide with the axis of the dome, so in this case no bending moments are needed. This can be presented by graphic statics.

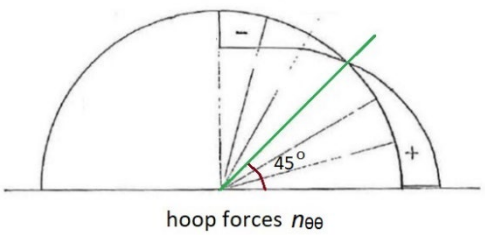

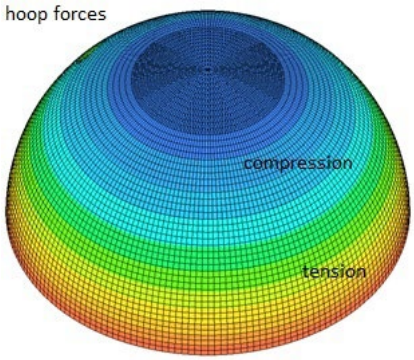

The thrust surface has its own shape function, and for the dome with the uniformly distributed load we can use the shape of the cubic funicular shell for

the accompanying thrust surface. Where the hoop forces are zero in the dome the thrust surface cuts the dome, for this load case under an angle of 45 degrees.

For the thrust surface the correct ratio of rise *h* to span *a** need to be determined in relation to the dome. For this the ratio is used for the optimum load path by using Maxwell's theorem.

It can be observed that the thrust surface of the load falls out- and inside of the span of the dome. Given the fact that the hoop forces are not zero at the spring of the dome this seems reasonable. In fact the membrane forces of the dome are the result of two load cases, the cubic funicular shell (with no hoop forces) and the corrective hoop forces. The result of these two load cases coincides with the axis of the dome.

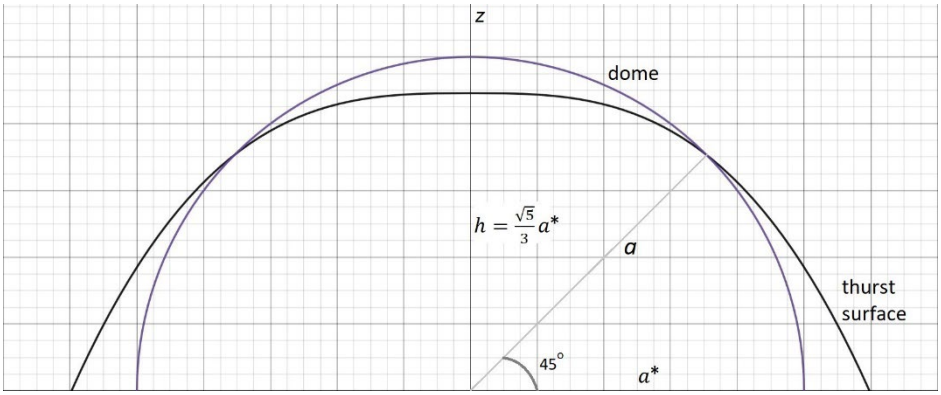

$$shape\ function\ dome: z = (a^2 - x^2)^{\frac{1}{2}}$$
$$thrust\ surface\ dome: \zeta = \frac{h(a^{*3} - x^3)}{a^{*3}} = \frac{\sqrt{5}\, a^*(a^{*3} - x^3)}{3a^{*3}}$$
$$with: a^* \approx 1.19589a$$

Again Dischinger's graphic method can be used including the horizontal component of the hoop forces $\bar{N}_{\theta h}$ in the meridian direction.

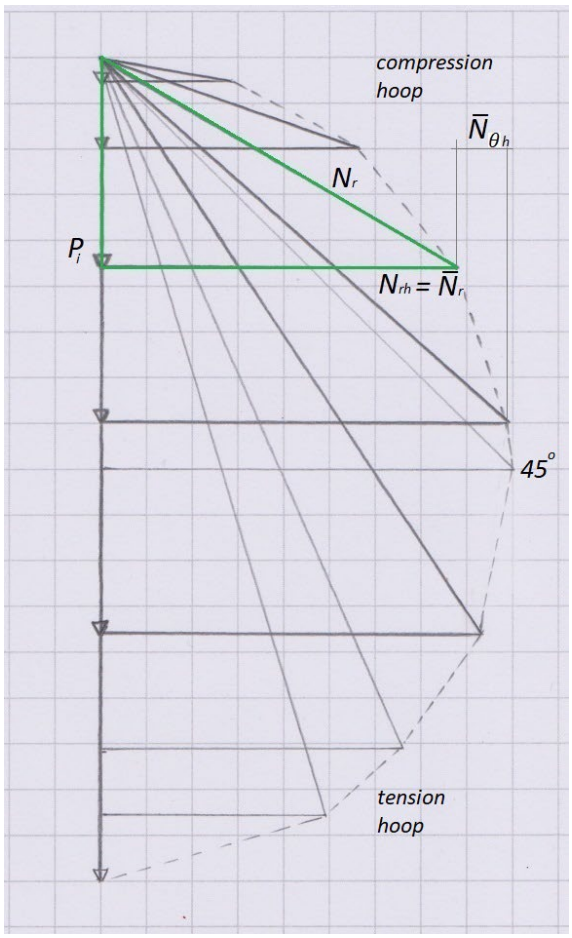

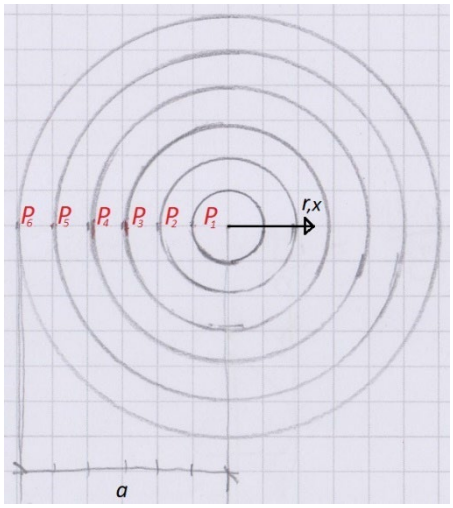

$P = \pi a^2 p$
$P_i = \pi x_i^2 p$

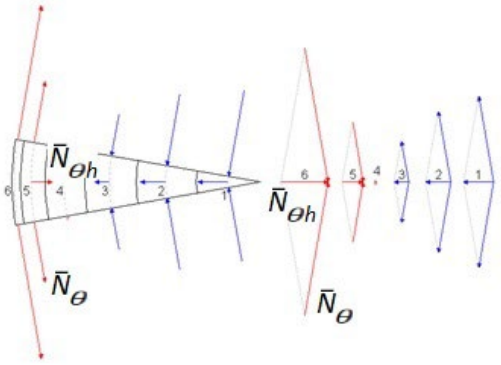

$P = \pi p x^2$
$N_r = n_{rr} 2\pi x$
$N_{rh} = \bar{N}_r = \bar{n}_{rr} 2\pi x$

$H_\theta = \bar{N}_{\theta h}$

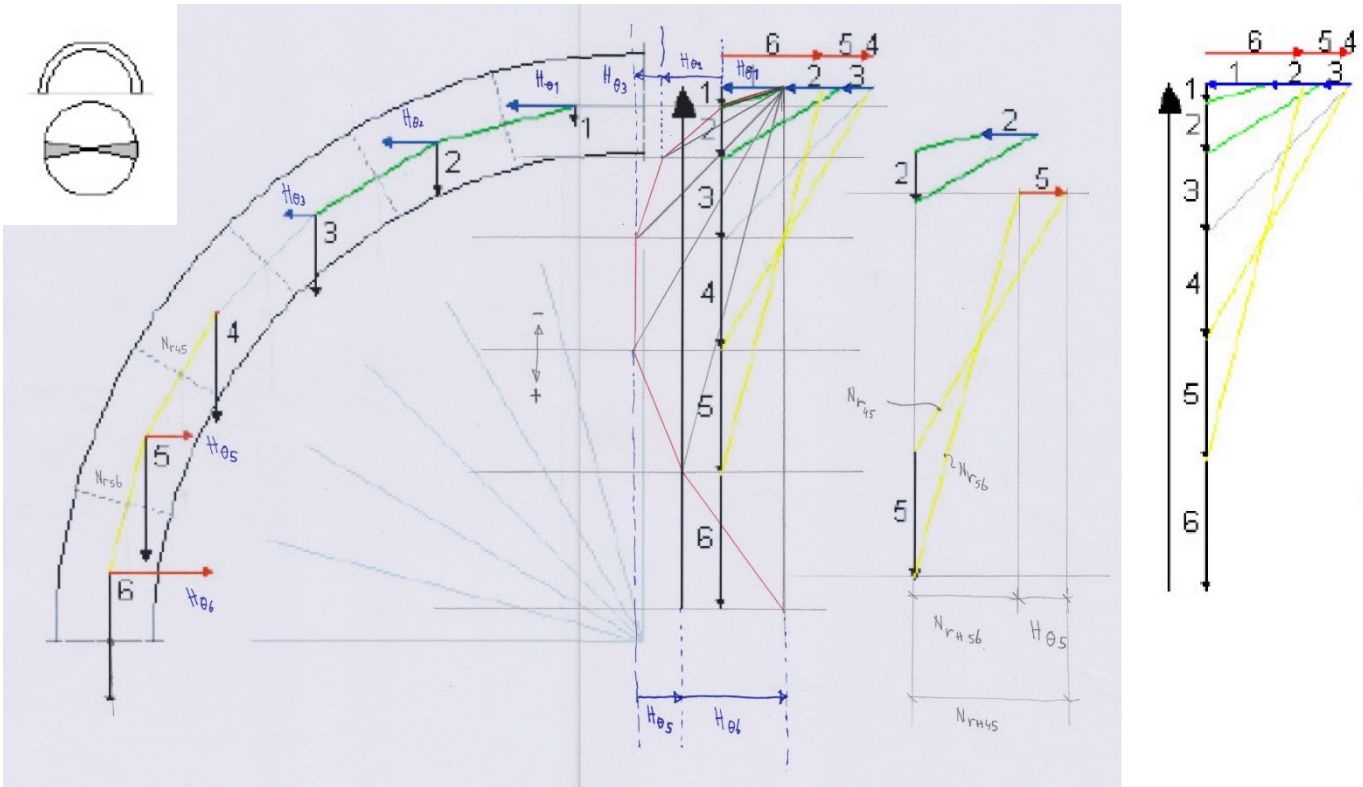

7.5 Deriving the stress function by means of the moment-hill

To establish the relationship between the moment-hill, thrust surface/shape function (for membrane shells these are equal) and the stress function this section starts with considering a mono-clastic shell before the axisymmetric shells will be discussed.

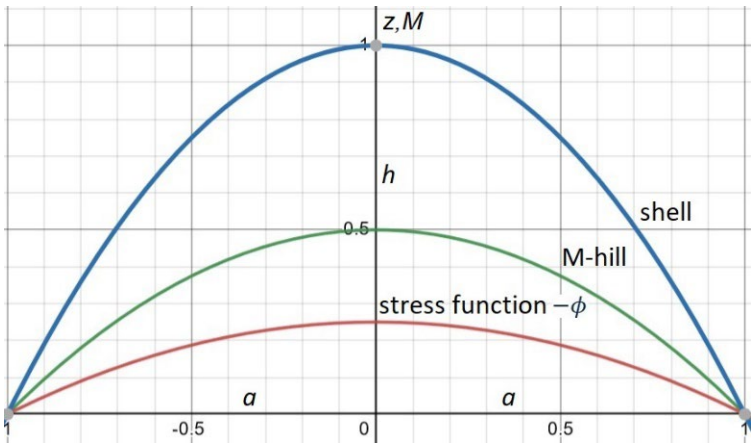

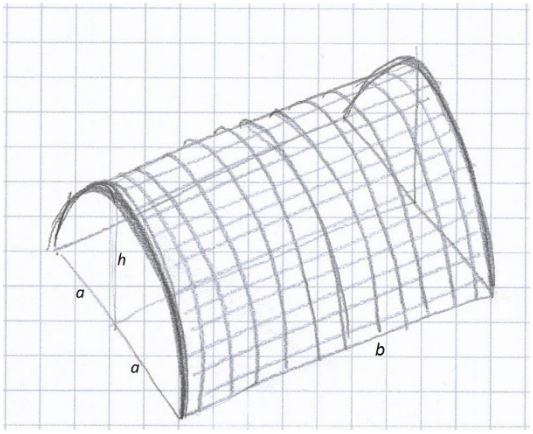

The beam – cable/arch analogy, thus a constant horizontal thrust, will be used in combination with the moment diagram to derive the shape function and the stress function.

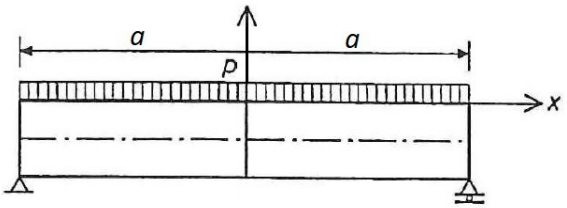

$$\bar{M} = \frac{p(a^2 - x^2)}{2};\ v = \frac{d\bar{M}}{dx} = -xp$$
$$M_{max} = \frac{1}{2}pa^2$$

The result is a parabolic shell. The distributed horizontal thrust $\bar{H}$ is the projected meridian forces $\bar{n}_{xx}$ and constant, which is confirmed with Dischinger's graphic method.

$$\bar{M} = \frac{p(a^2 - x^2)}{2}$$
$$M_{max} = \bar{H}h = \frac{1}{2}pa^2 \rightarrow \bar{H} = \frac{pa^2}{2h}$$

$$M = \bar{H}z \rightarrow z = \frac{h(a^2 - x^2)}{a^2}$$
$$with: \frac{\partial^2 z}{\partial x^2}\frac{\partial^2 \phi}{\partial y^2} + p = 0 \rightarrow \phi = \frac{a^2 p}{4h}\ y^2 + C$$
$$with: z = a\ and\ \phi = 0 \rightarrow C = -\frac{a^4 p}{4h}$$
$$\phi = -\frac{a^2 p}{4h}(a^2 - y^2)$$
$$\bar{n}_{xx} = \frac{\partial^2 \phi}{\partial y^2} = \bar{H} = \frac{a^2 p}{2h} = constant$$

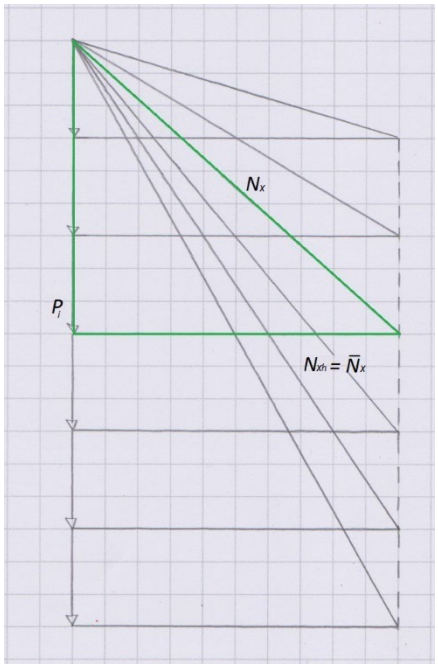

$$P = 2abp$$
$$P_i = 2x_i bp$$
$$with: \bar{N}_x = \bar{n}_{xx} \cdot b$$

The moment-hill, associated with slabs, determines the flow of forces of the loads. The loads flow along the moment-hill's steepest descent toward the supports.

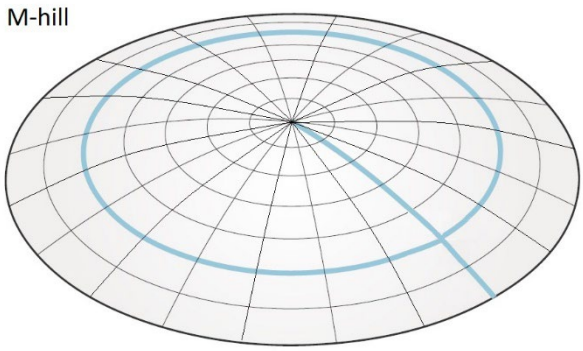

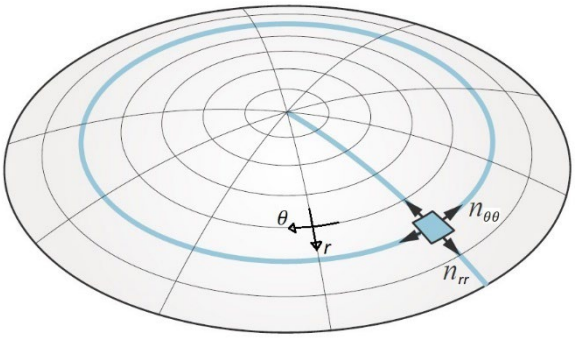

$$v_r = \frac{d\bar{M}}{dr} = max, v_\theta = \frac{d\bar{M}}{d\theta} = 0$$

The moment-hill will be used for a parabolic shell of revolution to determine the stress function. The moment-hill of the previous parabolic shell will be used now because it concerns a shell of revolution, half of the previous moment-hill will be used as the load transfer is in two direction instead of one. It is important to establish that for both example's the distributed horizontal thrust $\bar{H}$, thus the projected meridian forces $\bar{n}_{rr}$ is constant.

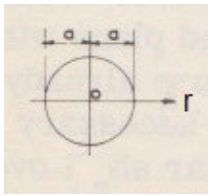

$$parabolic\ shell:\ z = \frac{h(a^2 - r^2)}{a^2}$$

$$take: \bar{M} = \frac{p(a^2 - r^2)}{4} \rightarrow$$

$$M = \bar{H}z \rightarrow \bar{H} = \frac{M}{z} = \bar{n}_{rr} = \frac{pa^2}{4h} = constant$$

$$\frac{\partial^2 z}{\partial x^2}\frac{\partial^2 \phi}{\partial y^2} + \frac{\partial^2 z}{\partial y^2}\frac{\partial^2 \phi}{\partial x^2} + p = 0$$

$$r^2 = x^2 + y^2 \rightarrow \nabla^2 = \frac{\partial^2 z}{\partial x^2} + \frac{\partial^2 z}{\partial y^2} = \frac{\partial^2 z}{\partial r^2} + \frac{1}{r}\frac{\partial z}{\partial r}$$

$$\rightarrow \frac{\partial^2 z}{\partial r^2}\frac{1}{r}\frac{\partial \phi}{\partial r} + \frac{1}{r}\frac{\partial z}{\partial r}\frac{\partial^2 \phi}{\partial r^2} + p = 0, \bar{n}_{rr} = \frac{1}{r}\frac{\partial \phi}{\partial r}, \bar{n}_{\theta\theta} = \frac{\partial^2 \phi}{\partial r^2}$$

$$-\frac{2h}{a^2}\frac{pa^2}{4h} + \frac{1}{r}\cdot -\frac{2hr}{a^2}\frac{\partial^2 \phi}{\partial r^2} + p = 0 \rightarrow \frac{\partial^2 \phi}{\partial r^2} = \frac{pa^2}{4h}$$

$$\phi = \frac{a^2 p}{8h}r^2 + C, with: z = a\ and\ \phi = 0 \rightarrow C = -\frac{a^4 p}{8h}$$

$$\rightarrow \phi = -\frac{a^2 p}{8h}(a^2 - r^2)$$

$$\bar{n}_{rr} = \bar{n}_{\theta\theta} = \frac{pa^2}{4h}$$

$$v_r = \frac{dM}{dr} = -pr$$

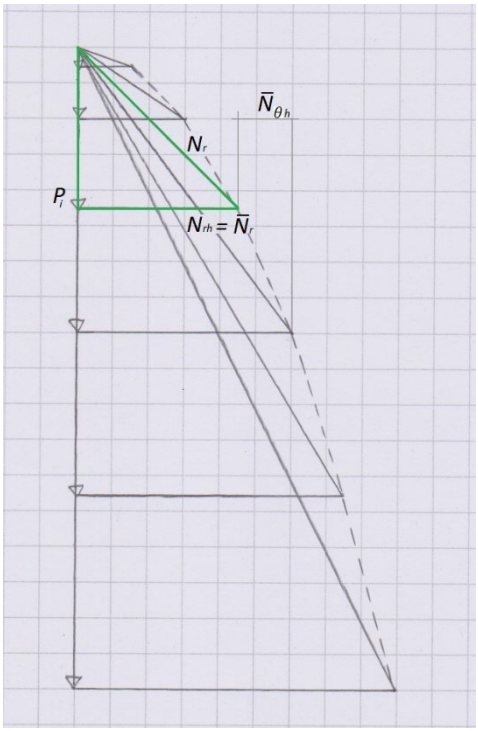

$$P = \pi a^2 p$$
$$P_i = \pi r_i^2 p$$

$$\frac{P_i}{N_{rh}} = \frac{dz}{dx} \quad with: N_{rh} = \bar{n}_{rr} 2\pi r$$
$$\frac{\pi r^2 p}{\bar{n}_{rr} 2\pi r} = \frac{2hr}{a^2} \rightarrow \bar{n}_{rr} = \frac{a^2 p}{4h} = constant$$

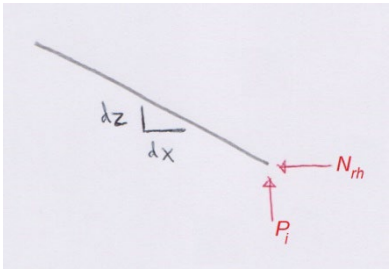

$$alternative:$$
$$\frac{P_i}{N_{rh}} = \frac{dz}{dx} = \frac{v_r}{\bar{n}_{rr}} = \frac{d\bar{M}}{dx}\frac{1}{\bar{n}_{rr}}$$

$$because\ shape\ function\ and\ moment\ hill\ are\ both\ parabolic, \bar{n}_{rr} = constant$$

The parabolic shell of revolution has a relation with an inflated membrane, both principle membrane forces are constant and there are no shear membrane forces [85].

$$membrane\ equation:$$
$$n_{xx}\frac{\partial^2 z}{\partial x^2} + 2n_{xy}\frac{\partial^2 z}{\partial x \partial y} + n_{yy}\frac{\partial^2 z}{\partial y^2} - p = 0$$
$$soap\ bubble, with: n_{xx} = n_{yy} = n\ and\ n_{xy} = 0$$
$$\rightarrow n\left(\frac{\partial^2 z}{\partial x^2} + \frac{\partial^2 z}{\partial y^2}\right) - p = 0$$
$$with: z = \frac{p}{4n}(x^2 + y^2 - a^2)$$
$$\rightarrow\ n\left(\frac{p}{2n} + \frac{p}{2n}\right) - p = 0$$

$$n \approx \bar{n} = \frac{\partial^2 \phi}{\partial x^2} = \frac{\partial^2 \phi}{\partial y^2}$$
$$\rightarrow\ \phi = \frac{\bar{n}}{2}(x^2 + y^2 - a^2) = \frac{\bar{n}}{2}(r^2 - a^2)$$
$$M = \bar{n} \cdot z = \bar{n} \cdot \frac{p}{4\bar{n}}(r^2 - a^2) = \frac{p(a^2 - r^2)}{4}$$

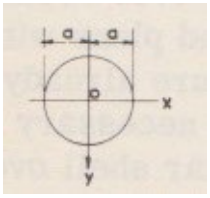

$$x^2 + y^2 = r^2$$

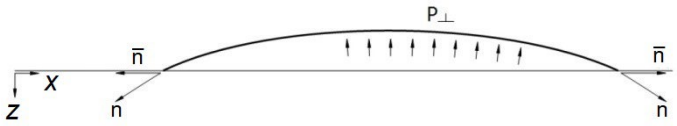

$$n\left(\frac{\partial^2 z}{\partial x^2} + \frac{\partial^2 z}{\partial y^2}\right) = p_\perp$$

Figure 45 photo of soap bubble [image https://creativecommons.org/licenses/by-sa/4.0/]

7.6 Stress function of axisymmetric membrane shells

With the help of the moment-hill the stress function can be derived for different axisymmetric membrane shells with an uniformly distributed load.

$$v_r = \frac{d\bar{M}}{dr} = max, v_\theta = \frac{d\bar{M}}{d\theta} = 0$$
$$\frac{v_r}{\bar{n}_{rr}} = \frac{dz}{dr} \rightarrow \bar{n}_{rr}\frac{dz}{dr} = v_r \rightarrow \frac{1}{r}\frac{\partial\phi}{\partial r}\cdot\frac{dz}{dr} = \frac{d\bar{M}}{dr}$$
$$\bar{M} = \frac{p(a^2 - r^2)}{4} \rightarrow v_r = \frac{d\bar{M}}{dr} = -\frac{pr}{2}$$
$$\frac{1}{r}\frac{\partial\phi}{\partial r}\cdot\frac{dz}{dr} = \frac{d\bar{M}}{dr}$$

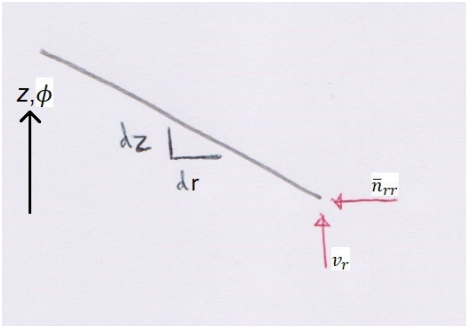

$$conical\ shell: z = \frac{h(a-r)}{a}$$
$$\rightarrow \frac{1}{r}\frac{\partial\phi}{\partial r}\cdot -\frac{h}{a} = \frac{pr}{2} \rightarrow \int\frac{\partial\phi}{\partial r}dr = \int -\frac{pr^2 a}{2h}dr \rightarrow \phi = -\frac{apr^3}{6h} + C$$
$$with: r = a\ and\ \phi = 0 \rightarrow C = \frac{pa^4}{6h}$$
$$\phi = \frac{a(a^3 - r^3)}{6h}p$$

$$parabolic\ shell: z = \frac{h(a^2 - r^2)}{a^2}$$
$$\rightarrow \frac{1}{r}\frac{\partial\phi}{\partial r}\cdot -\frac{2hr}{a^2} = \frac{pr}{2} \rightarrow \phi = \int\frac{\partial\phi}{\partial r}dr = \int -\frac{pra^2}{4h}dr = -\frac{a^2pr^2}{8h} + C$$
$$with: r = a\ and\ \phi = 0 \rightarrow C = \frac{pa^4}{8h}$$
$$\phi = \frac{a^2(a^2 - r^2)}{8h}p$$

$$cubic\ shell: z = \frac{h(a^3 - r^3)}{a^3}$$
$$\rightarrow \frac{1}{r}\frac{\partial\phi}{\partial r}\cdot -\frac{3hr^2}{a^3} = \frac{pr}{2} \rightarrow \phi = \int\frac{\partial\phi}{\partial r}dr = \int -\frac{pa^3}{6h}dr = -\frac{a^3pr}{6h} + C$$
$$with: r = a\ and\ \phi = 0 \rightarrow C = -\frac{pa^4}{6h}$$
$$\phi = \frac{a^3(a - r)}{6h}p$$

$$spherical\ shell: z = (a^2 - r^2)^{\frac{1}{2}}$$
$$\rightarrow \frac{1}{r}\frac{\partial\phi}{\partial r}\cdot -\frac{r}{(a^2 - r^2)^{\frac{1}{2}}} = \frac{pr}{2} \rightarrow \phi = \int\frac{\partial\phi}{\partial r}dr = \int -\frac{pr(a^2 - r^2)^{\frac{1}{2}}}{2}dr = \frac{p(a^2 - r^2)^{\frac{3}{2}}}{6} + C$$
$$with: r = a\ and\ \phi = 0 \rightarrow C = 0$$
$$\phi = \frac{(a^2 - r^2)^{\frac{3}{2}}}{6}p$$

$$all\ above\ solutions\ satisfy\ Pucher's\ equation:$$
$$\frac{\partial^2 z}{\partial r^2}\frac{1}{r}\frac{\partial\phi}{\partial r} + \frac{1}{r}\frac{\partial z}{\partial r}\frac{\partial^2\phi}{\partial r^2} - p = 0$$

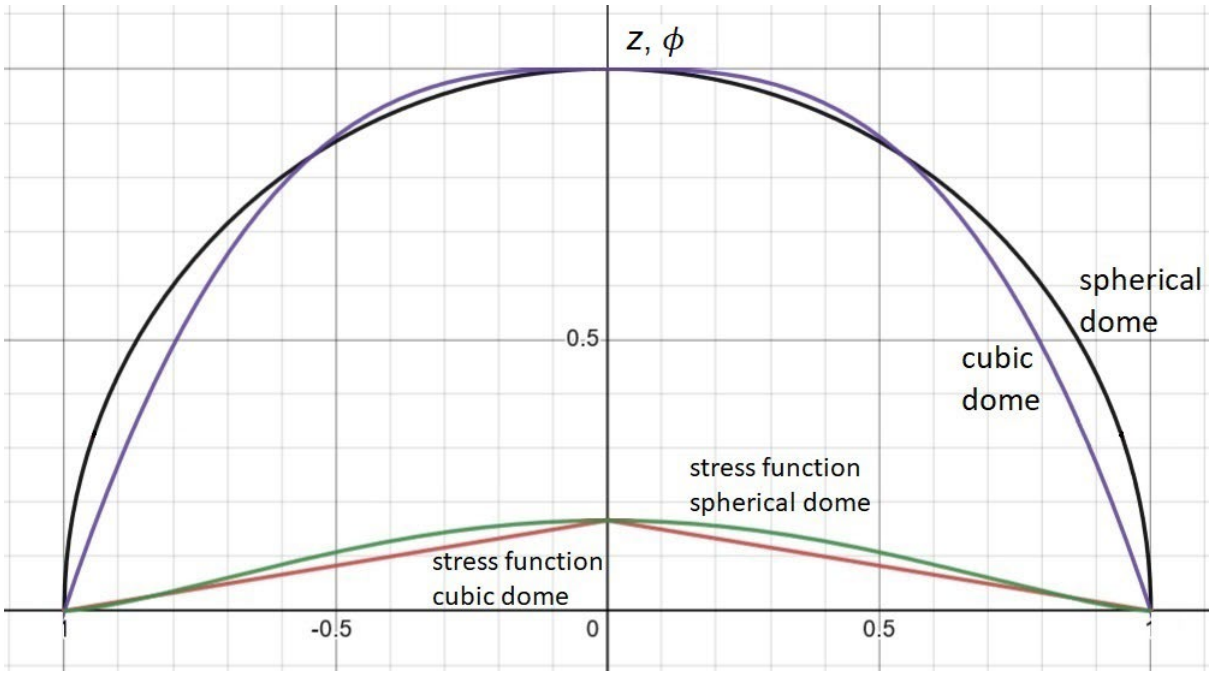

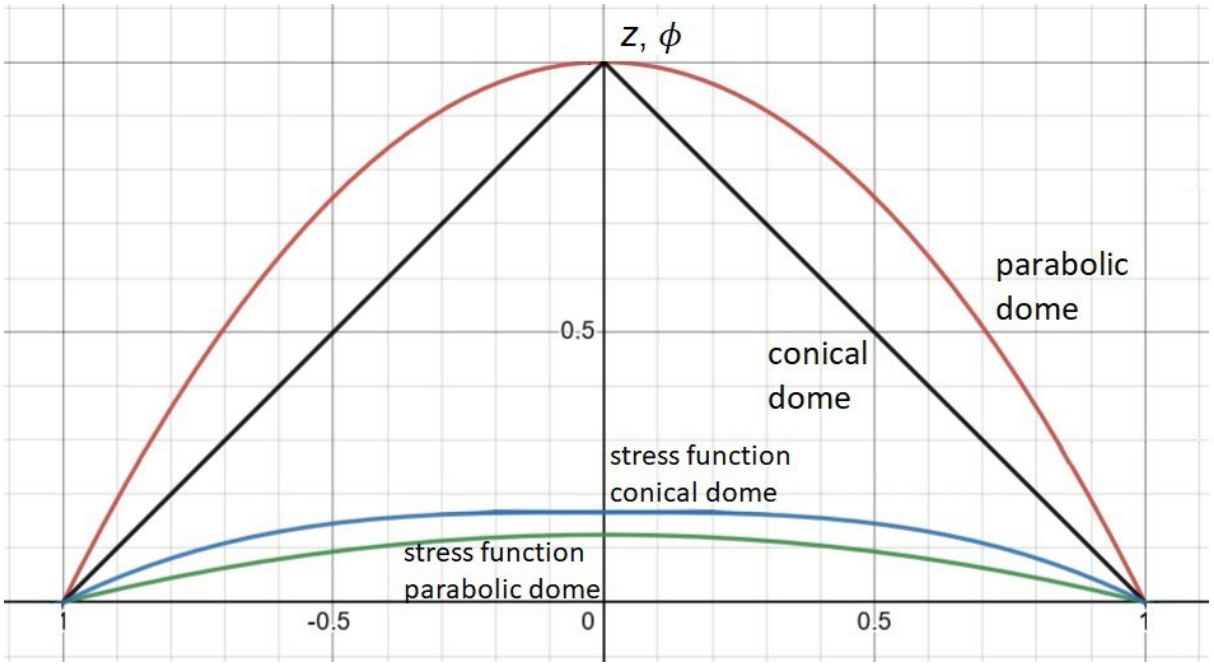

Note that for the different shells the total horizontal thrust $\bar{N}_r$ is not always equal to the projected meridian forces $\bar{n}_{rr}$:

- $conical\ shell$: $\bar{N}_r \neq constant$, $\bar{n}_{rr} \neq constant$
- $parabolic\ shell$: $\bar{N}_r \neq constant$, $\bar{n}_{rr} = constant$
- $cubic\ shell$: $\bar{N}_r = constant$, $\bar{n}_{rr} \neq constant$
- $spherical\ shell$: $\bar{N}_r \neq constant$, $\bar{n}_{rr} \neq constant$

If the horizontal thrust $\bar{N}_r$ is equal to zero then there are no hoop forces in the shell, the cubic shells, and the stress function is a mono-clastic surface like a cone.

When the stress function has been derived the membrane forces can be determined. These correspond with those found in classical shell theory.

$$\bar{n}_{rr} = \frac{1}{r}\frac{\partial \phi}{\partial r}, \bar{n}_{\theta\theta} = \frac{\partial^2 \phi}{\partial r^2}$$

$$n_{rr} = \bar{n}_{rr}\frac{1}{\cos\varphi}, n_{\theta\theta} = \bar{n}_{\theta\theta}\cos\varphi$$

$$\cos\varphi = \left[1 + \left(\frac{\partial z}{\partial r}\right)^2\right]^{-\frac{1}{2}}$$

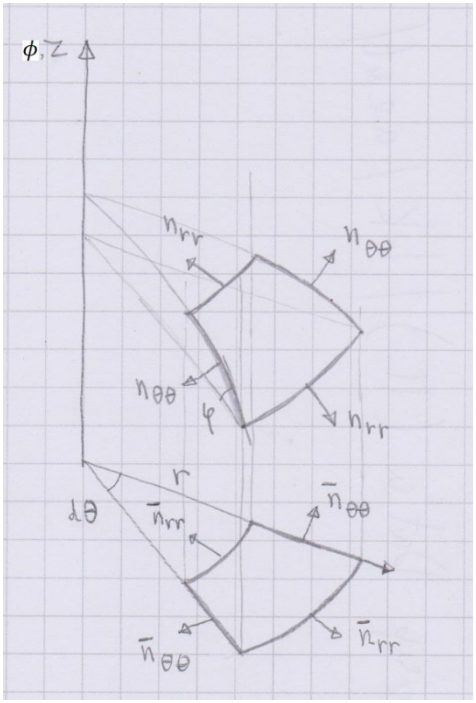

conical shell:

$$\bar{n}_{rr} = -\frac{apr}{2h}, \bar{n}_{\theta\theta} = -\frac{apr}{h}$$

$$n_{rr} = -\frac{pr(a^2+h^2)^{\frac{1}{2}}}{2h}, n_{\theta\theta} = -\frac{a^2 pr}{h(a^2+h^2)^{\frac{1}{2}}}$$

parabolic shell:

$$\bar{n}_{rr} = -\frac{a^2 p}{4h}, \bar{n}_{\theta\theta} = -\frac{a^2 p}{4h}$$

$$n_{rr} = -\frac{p(a^4+4h^2r^2)^{\frac{1}{2}}}{4h}, n_{\theta\theta} = -\frac{a^4 p}{4h(a^4+4h^2r^2)^{\frac{1}{2}}}$$

cubic shell:

$$\bar{n}_{rr} = -\frac{a^3 p}{6hr}, \bar{n}_{\theta\theta} = 0$$

$$n_{rr} = -\frac{p(a^6+9h^2r^4)^{\frac{1}{2}}}{6hr}, n_{\theta\theta} = 0$$

spherical shell:

$$\bar{n}_{rr} = -\frac{p(a^2-r^2)^{\frac{1}{2}}}{2}, \bar{n}_{\theta\theta} = -\frac{p(a^2-2r^2)}{2(a^2-r^2)^{\frac{1}{2}}}$$

$$n_{rr} = -\frac{ap}{2}, n_{\theta\theta} = -\frac{p(a^2-2r^2)}{2a}$$

The membrane forces can be represented with the help of the following diagram.

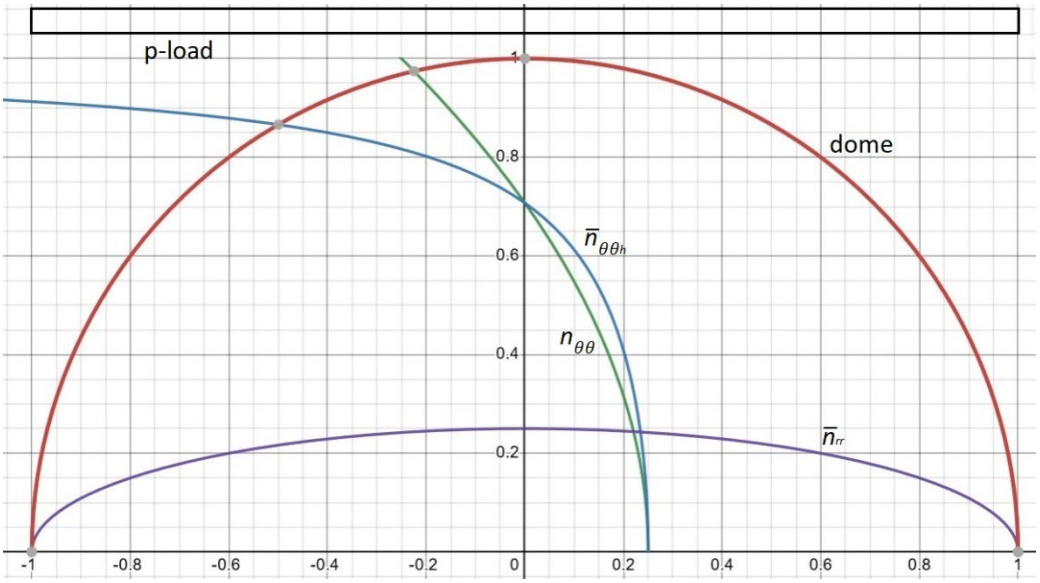

The total load *P* and the total support reactions *V* and are in equilibrium in vertical direction but there is also an internal couple M_t needed for rotational equilibrium. For a circular slab this would result in an internal bending moment, but for a shell the resulting force of internal membrane forces over the internal arm ensures the rotational equilibrium [86].

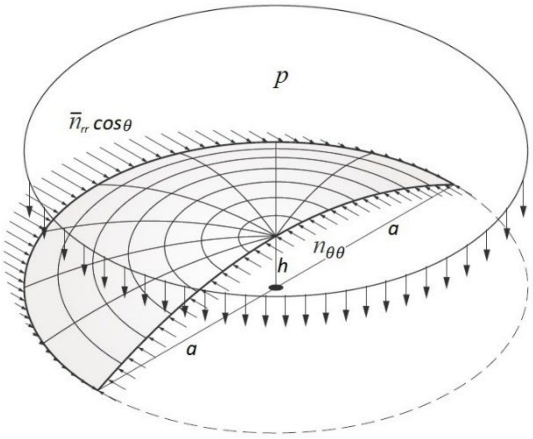

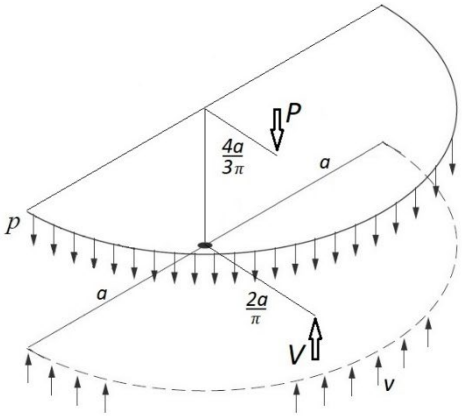

$$V = a\pi\frac{ap}{2} = \frac{a^2\pi}{p}$$

$$P = \frac{a^2\pi}{p}$$

$$e = \frac{2a}{\pi} - \frac{4a}{3\pi} = \frac{2a}{3\pi}$$

$$\rightarrow M_t = Pe = \frac{a^2\pi}{p}\frac{2a}{3\pi} = \frac{a^3 p}{3}$$

This will be demonstrated using the conical shell. As a check for the derived stress function, for this case the classic membrane equation will be used.

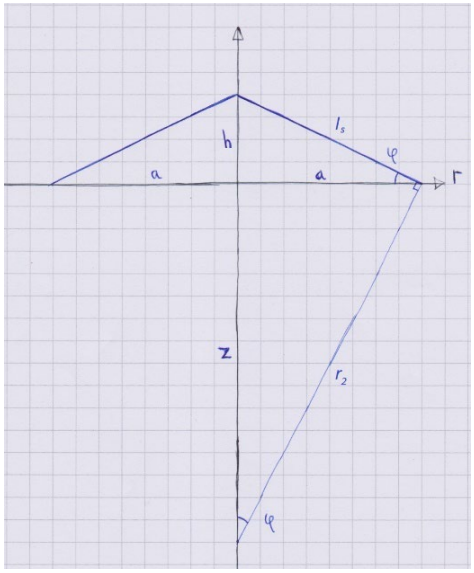

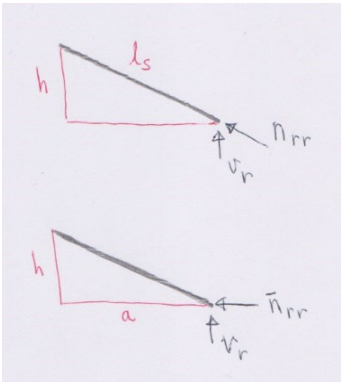

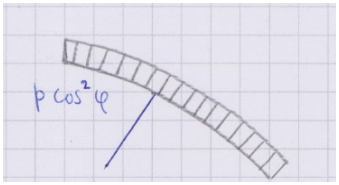

$$\frac{n_{rr}}{r_1} + \frac{n_{\theta\theta}}{r_2} = -p\ \cos^2\varphi$$

$$with: \cos\varphi = \frac{a}{l_s}\ and\ r_1 = \infty$$

$$\frac{r}{z} = \frac{h}{a} \rightarrow z = \frac{ar}{h}$$

$$r_2 = (r^2 + z^2)^{\frac{1}{2}} = \left(r^2 + \left(\frac{ar}{h}\right)^2\right)^{\frac{1}{2}} = \frac{rl_s}{h}$$

$$\rightarrow n_{\theta\theta} = -p\ \cos^2\varphi\, r_2 = p\left(\frac{a}{l_s}\right)^2 \cdot \frac{rl_s}{h} = -\frac{a^2 rp}{hl_s}$$

$$with: l_s = (a^2 + h^2)^{\frac{1}{2}}$$

$$n_{rr} = \frac{r(a^2 + h^2)^{\frac{1}{2}}}{2h}p = \frac{l_s}{2} \cdot -\frac{pr}{2} = \frac{l_s}{2}v_r$$

$$\bar{n}_{rr} = -\frac{apr}{2h} = \frac{a}{h}v_r$$

$$or\ alternatively;$$

$$\frac{n_{rr}}{v_r} = \frac{l_s}{h} \rightarrow n_{rr} = \frac{l_s}{2}v_r$$

$$\frac{\bar{n}_{rr}}{v_r} = \frac{a}{h} \rightarrow \bar{n}_{rr} = \frac{a}{h}v_r$$

The hoop forces in the cross section have a resultant which is equal to the summation of the projected meridian forces in the same direction at the spring of the shell. Mulitplying the resulting force with the internal arm result in the internal couple M_t.

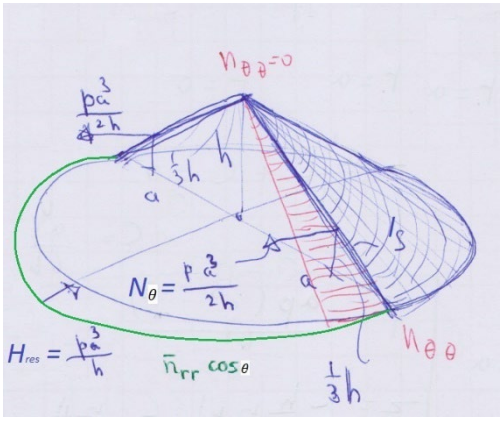

$$n_{\theta\theta} = -\frac{a^2 r}{h(a^2+h^2)^{\frac{1}{2}}} p;\ \bar{n}_{rr,a} = -\frac{ar}{2h} p$$

$$N_\theta = n_{\theta\theta} \cdot \frac{1}{2} l_s = -\frac{a^2 r}{h(a^2+h^2)^{\frac{1}{2}}} p \cdot \frac{1}{2}(a^2+h^2)^{\frac{1}{2}} = -\frac{a^3 p}{2h}$$

$$H_{res} = \int_{-\frac{\pi}{2}}^{\frac{\pi}{2}} \bar{n}_{rr,a} \cos\theta \, ds = \int_{-\frac{\pi}{2}}^{\frac{\pi}{2}} \bar{n}_{rr,a} \cos\theta \, a \, d\theta = 2a \, \bar{n}_{rr,a}$$

$$with: \bar{n}_{rr,a} = -\frac{a^2 p}{2h} \rightarrow H_{res} = -\frac{a^3 p}{h} = 2\, N_\theta$$

$$M_t = H_{res} \cdot \frac{h}{3} = \frac{pa^3}{3}$$

When the summation is taken of the moment hill in the centre cross section we arrive at the same internal couple M_t. Thus there is a direct relation of the moment hill with the thrust surface/shape function (for membrane shells these are equal).

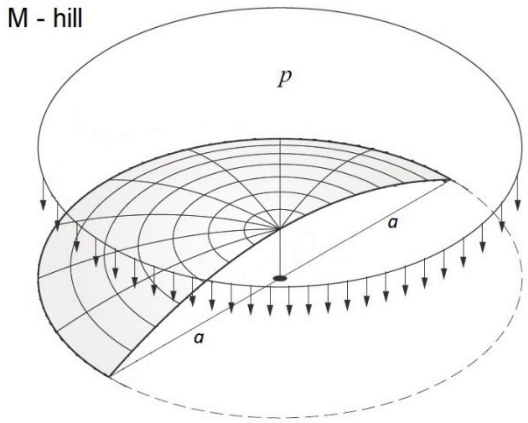

$$M = \frac{p(a^2 - r^2)}{4}$$

$$M_t = \int_{-a}^{a} \frac{p(a^2-r^2)}{4} \, dx = \frac{pa^3}{3}$$

For the parabolic shell the projected meridian forces $\bar{n}_{rr}$, this multiplied with the shape function of the shell we get the moment-hill.

$$\bar{M} = \bar{n}_{rr} \cdot z = \frac{a^2 p}{4h} \cdot \frac{h(a^2 - r^2)}{a^2} = \frac{p(a^2 - r^2)}{4}$$

For the other shells $\bar{n}_{rr}$ is not constant, by integrating $\bar{n}_{rr}$ over the cross section we get for each shell the moment-hill. This outcome confirms the premise for deriving the stress functions.

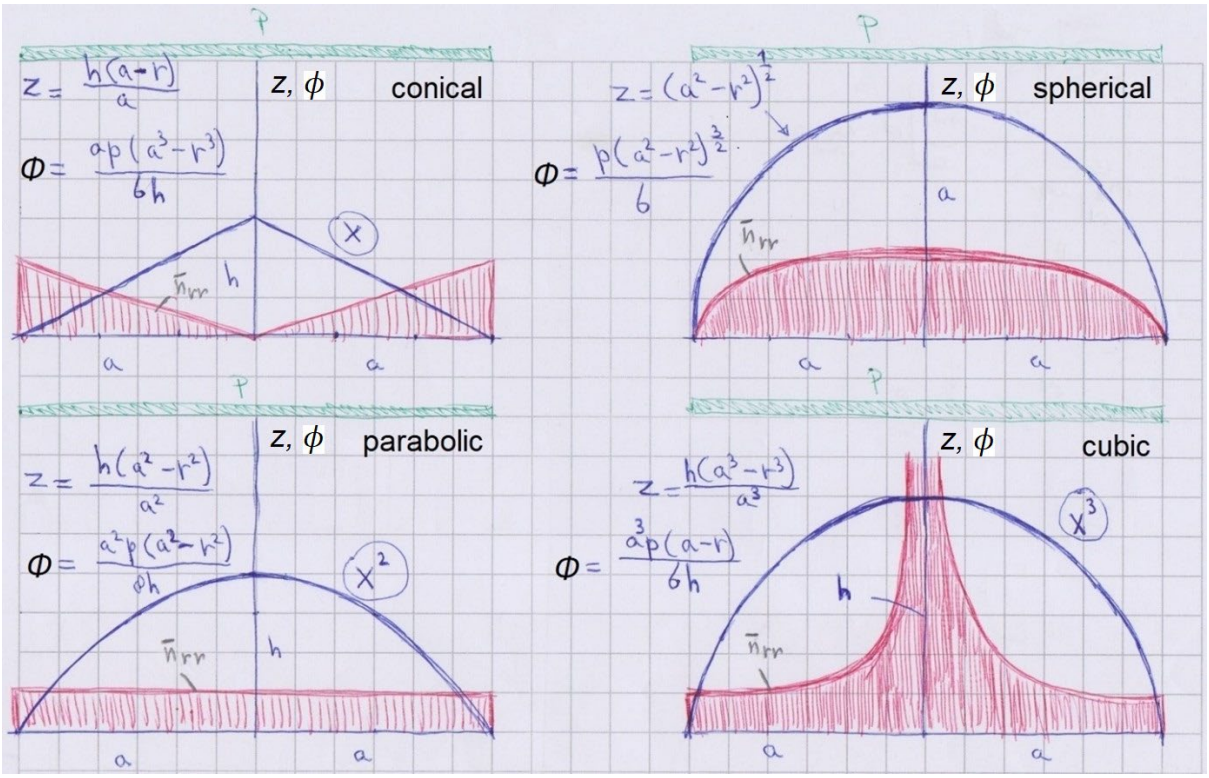

$$\bar{n}_{rr} \cdot \frac{dz}{dr} = v_r \rightarrow \bar{n}_{rr} \cdot \frac{dz}{dr} = \frac{d\bar{M}}{dr} \rightarrow \bar{M} = \int \bar{n}_{rr} \frac{dz}{dr} dr$$

conical shell:

$$\bar{M} = \int -\frac{apr}{2h}\frac{h}{a} dr = \int -\frac{pr}{2} dr = -\frac{px^2}{4} + C$$

$$with: \bar{M} = 0 \; if \; x = a \rightarrow C = \frac{pa^2}{4}$$

$$\rightarrow \bar{M} = \frac{p(a^2 - r^2)}{4}$$

parabolic shell:

$$\bar{M} = \int -\frac{a^2 p}{4h}\frac{2hr}{a^2} dr = \int -\frac{pr}{2} dr \rightarrow \frac{p(a^2 - r^2)}{4}$$

cubic shell:

$$\bar{M} = \int -\frac{a^3 p}{6hr}\frac{3hr^2}{a^3} dr = \int -\frac{pr}{2} dr \rightarrow \frac{p(a^2 - r^2)}{4}$$

spherical shell:

$$\bar{M} = \int -\frac{(a^2 - r^2)^{\frac{1}{2}} p}{2} \frac{r}{(a^2 - r^2)^{\frac{1}{2}}} dr = \int -\frac{pr}{2} dr \rightarrow \frac{p(a^2 - r^2)}{4}$$

It can be observed that there is a reciprocity between the shape function and the stress function of the conical and cubic shell.

$conical\ shell$:

$$z = \frac{h(a-r)}{a}$$

$$\phi = \frac{a(a^3 - r^3)}{6h} p$$

$cubic\ shell$:

$$\phi = \frac{a^3(a-r)}{6h} p$$

$$z = \frac{h(a^3 - r^3)}{a}$$

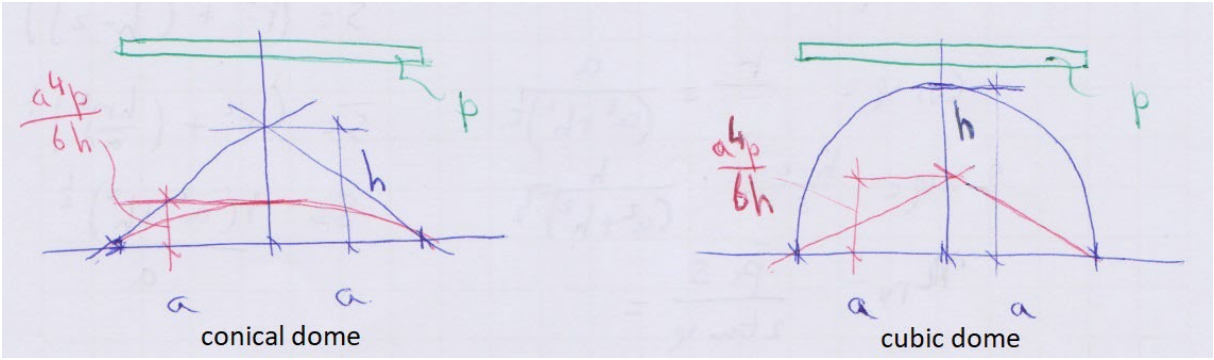

This is in line with the static-geometric analogy if thin shell structures:

$$\frac{\partial^2 z}{\partial r^2}\frac{1}{r}\frac{\partial \phi}{\partial r} + \frac{1}{r}\frac{\partial z}{\partial r}\frac{\partial^2 \phi}{\partial r^2} - p = 0$$

$conical\ shell$:

$$0 \cdot -\frac{apr}{2h} + \frac{1}{r} \cdot -\frac{h}{a} \cdot -\frac{apr}{h} - p = 0 \rightarrow \kappa_{rr} = \frac{\partial^2 z}{\partial r^2} = 0$$

$cubic\ shell$:

$$-\frac{6hr}{a^3} \cdot -\frac{a^3 p}{6hr} + \frac{1}{r} \cdot -\frac{3hr^2}{a^3} \cdot 0 - p = 0 \rightarrow \bar{n}_{\theta\theta} = \frac{\partial^2 \phi}{\partial r^2} = 0$$

$$\bar{n}_{\theta\theta} \leftrightarrow \kappa_{rr}$$

8 The relationship between the shape function, stress function, thrust surface and moment-hill

8.1 Introduction

In this chapter the relation between the fundamental characteristics that determine the relation between the geometric and mechanical properties of shells structures will be further explored. These are the shape function, stress function, thrust surface, and moment-hill. Triangular, rectangular and square based shells will be discussed as their behaviour is more complex than axisymmetric membrane shells. The internal shear and bending forces will have to be taken into account.

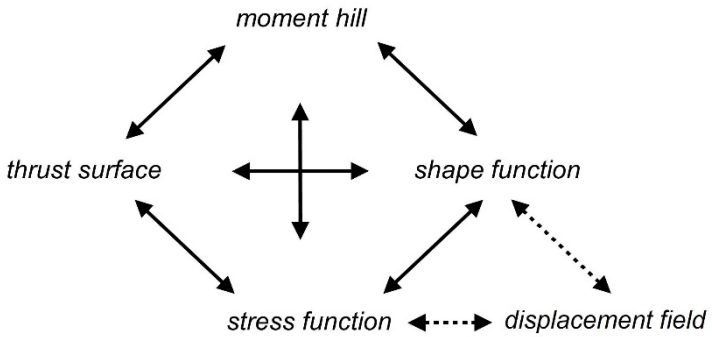

8.2 "Twistless case", moment-hill and thrust network / surface

The twistless case [87] is a phenomenon of slabs in which the flow of forces is independently decoupled in two directions. The strips in these directions are subjected to curvature and bending, but not to twist or torsional moments. Two types can be identified, firstly continuous slabs which deformations fields are due to the their twisless nature translation surfaces. And secondly beam grids in which beams have bending stiffness *K* but no torsional stiffness, these usually do not result in a translation surface [88].

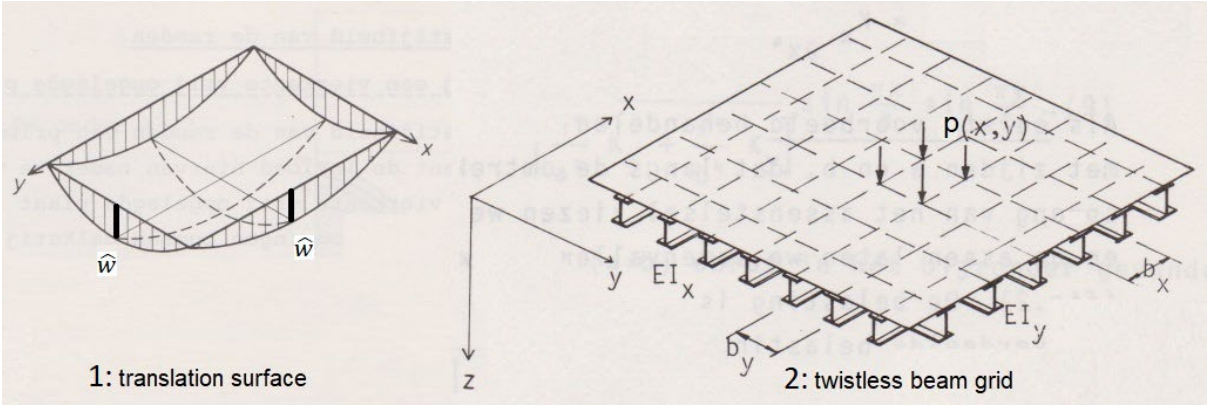

$$w(x,y) = \hat{w}(F(x) + G(y))$$

The first type of twistless case results in a statically determined slab, after the ratio of loads β in the two directions has been chosen. The displacement field is a translation surface, it has curvature in the two directions but no twist. This can be observed in the displacement function *w*, the x- and y-directions are decoupled.

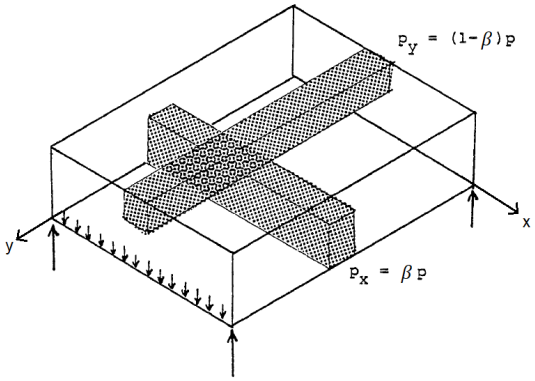

$$\frac{p_x}{p_y} = \frac{\beta}{(1-\beta)} \cdot p$$

For the second type the ratio of loads depends on their respective bending stiffnesses in the two directions. Thus this constitutes a statically indetermined grid.

The moment-hill $\bar{M}$ determines the flow of the shear forces and thus of the load and will always be equal, due to the constant total load. As with most of the loads in this thesis we assume a uniformly distributed load *p* and a Poisson ratio of zero.

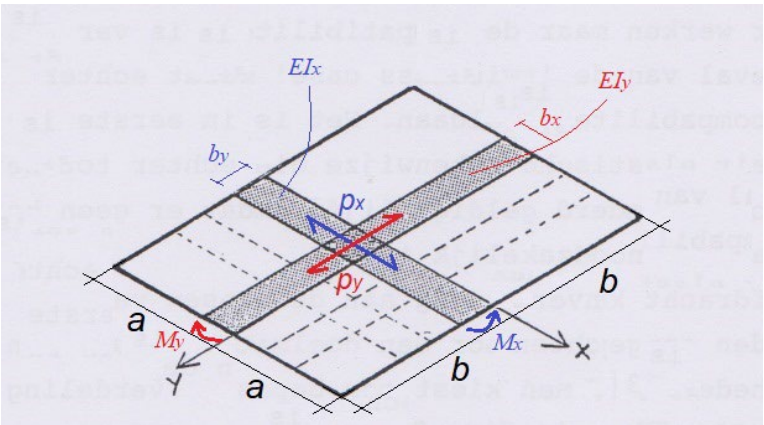

$$p = p_z\,, v = 0$$
$$M_x = \frac{p_x(a^2 - x^2)}{2} \;\; with: p_x = \beta p$$
$$M_y = \frac{p_y(b^2 - y^2)}{2} \;\; with: p_y = (1-\beta)p$$
$$\bar{M} = M_x + M_y = \frac{p}{2}[\beta(a^2 - x^2) + (1-\beta)(b^2 - y^2)]$$
$$v_x = \frac{dM_x}{dx} = -\beta x p$$
$$v_y = \frac{dM_y}{dx} = -(1-\beta) y p$$
$$-p = \frac{\partial v_x}{\partial x} + \frac{\partial v_y}{\partial y} = -\beta p - (1-\beta)p$$
$$if\ a = b \rightarrow \beta = \frac{1}{2}\ and\ \bar{M} = \frac{p(2a^2 - x^2 - y^2)}{4}$$
$$v_x = -\frac{xp}{2}\,, v_y = -\frac{yp}{2}$$

The slopes of the moment-hill represent the shear forces in the two directions.

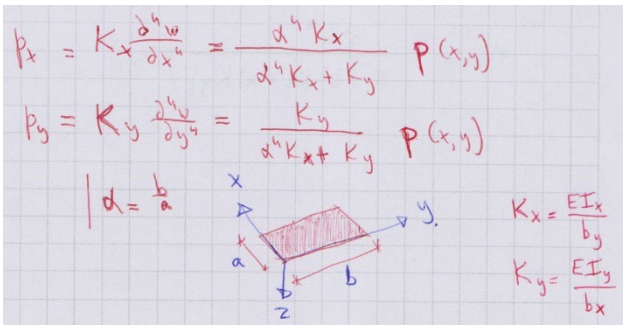

$K = \ strip\ stiffness$
$b = \ width\ of\ strip$
$\alpha = ratio\ of\ strip\ lenght, \alpha = \frac{b}{a}$
$\beta = ratio\ of\ loads$

The second type of twistless case, the torsion-less grid of beams, can be translated to a cable network with no shear panels. For both cases their respective stiffness ratios can be determined with the help of a two-way sine load.

$$p = \check{p}\ \sin\frac{\pi x}{a}\ \sin\frac{\pi y}{b}$$

$$twistless\ case\ beam\ grid: p = K_x\frac{\partial^4 w}{\partial x^4} + \ K_y\frac{\partial^4 w}{\partial y^4}$$

$$with: K_x = \frac{EI_x}{b_y}, K_y = \frac{EI_y}{b_x}$$

$$w = \frac{a^4 b^4}{\pi^4 a^4 K_x + \pi^4 b^4 K_y}\ \check{p}\cdot\sin\frac{\pi x}{a}\ \sin\frac{\pi y}{b}$$

$$with: \alpha = \frac{b}{a} \rightarrow w = \ \frac{\alpha^4 a^4}{\pi^4(\alpha^4 K_x + K_y)}\ \check{p}\cdot\sin\frac{\pi x}{a}\ \sin\frac{\pi y}{b}$$

$$p_x = \ K_x\frac{\partial^4 w}{\partial x^4} = \frac{\alpha^4 K_x}{(\alpha^4 K_x + K_y)}p$$

$$p_y = \ K_y\frac{\partial^4 w}{\partial y^4} = \frac{K_y}{(\alpha^4 K_x + K_y)}p$$

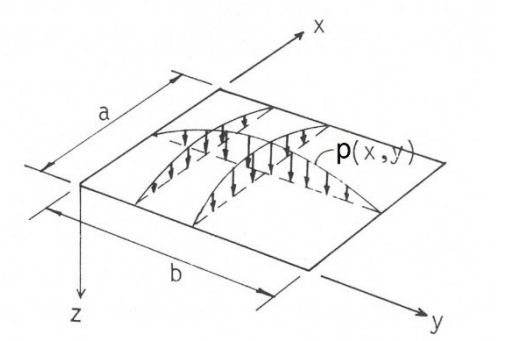

$$cable\ network: p = h_x\frac{\partial^2 z}{\partial x^2} + \ h_y\frac{\partial^2 z}{\partial y^2}\ , with: h_x = \frac{H_x}{b_y}\ , h_y = \frac{H_y}{b_x}$$

$$z = \ \frac{a^2 b^2}{\pi^2 a^2 h_x + \pi^2 b^2 h_y}\check{p}\cdot\sin\frac{\pi x}{a}\ \sin\frac{\pi y}{b}$$

$$p_x = \ h_x\frac{\partial^2 z}{\partial x^2} = \frac{\alpha^2 h_x}{\alpha^2 h_x + h_y}p$$

$$p_y = \ h_y\frac{\partial^2 z}{\partial y^2} = \frac{h_y}{\alpha^2 h_x + h_y}p$$

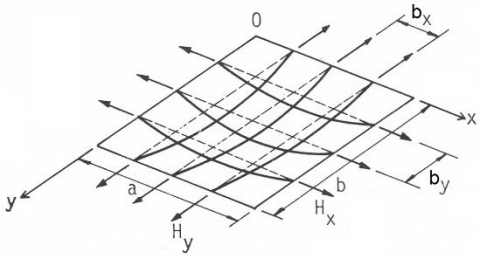

This ratio for the beam grid depends on the respective bending stiffnesses *K* of the two directions, and for the cable network the ratio is fixed by the horizontal thrusts *H*.

$$beam\ grid: \frac{p_x}{p_y} = \frac{\beta p}{(1-\beta)p} = \frac{\alpha^4 K_x}{K_y}p$$

$$cable\ network: \frac{p_x}{p_y} = \frac{\beta p}{(1-\beta)p} = \frac{\alpha^2 h_x}{h_y}p$$

As the gradients of the moment-hill are the shear forces, by changing the curvatures of the moment-hill the ratio of the shear forces changes accordingly. The shape of the $\bar{M}$-hill depends on both ratios α and β.

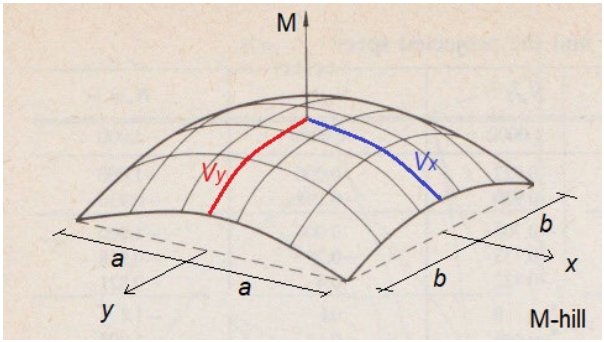

$$\bar{M} = M_x + M_y = \frac{p}{2}[\beta(a^2 - x^2) + (1-\beta)(\alpha^2 a^2 - y^2)]$$

$$if\ x = y = 0:$$

$$\bar{M} = \frac{p}{2}[\beta a^2 + (1-\beta)(\alpha^2 a^2)]$$

$$v_x = \frac{d\bar{M}}{dx}$$

$$v_y = \frac{d\bar{M}}{dy}$$

The step can be made from a twistless slab with “beams” in two directions to “arches” in these directions, again using the beam – cable/arch analogy. Similar as to the cable network. The vertical force *v* act as intermediate, dependant on the $\bar{M}$-hill for the load transfer, and on the shape of the shell.

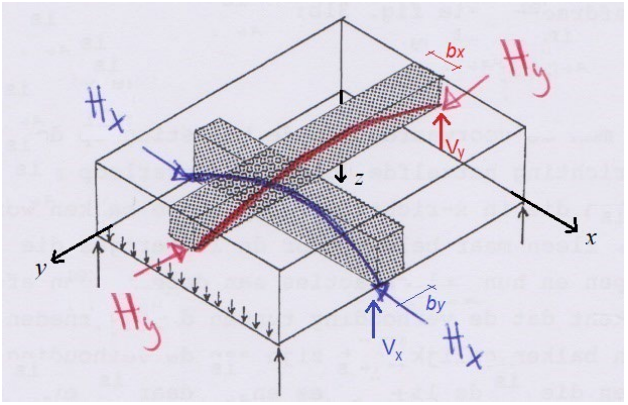

$$h_x = \frac{H_x}{b_y}, h_y = \frac{H_y}{b_x}$$

$$p = p_x + p_y = h_x \frac{d^2 z}{dx^2} + h_y \frac{d^2 z}{dy^2}$$

$$= \beta p + (1-\beta)p$$

$$\frac{v_x}{h_x} = \frac{dz}{dx} \rightarrow v_x = h_x \frac{dz}{dx} = \frac{dM_x}{dx} = -\beta p x$$

$$\frac{v_y}{h_y} = \frac{dz}{dy} \rightarrow v_y = \underbrace{h_y \frac{dz}{dy}}_{\substack{shape \\ function}} = \underbrace{\frac{dM_y}{dy}}_{\substack{moment \\ hill}} = -(1-\beta)py$$

A shell with a translation surface as shape function, depending on its boundary conditions, acts like a “twistless case”. If the shell has semi-rigid edges then the horizontal support reactions will be zero and the loads will be transferred by internal shear forces to the diaphragms, the shell is then not a twistless case. In the situation of a twistless case the ratio of the load transfer will depend, apart from the boundary conditions, on the ratio of the horizontal thrusts. Compared with the twistless slab the ratio of horizontal thrusts is equivalent to the ratio of the bending stiffness.

The next example concerns a shell, pin supported along all sides. Its shape function will be derived.

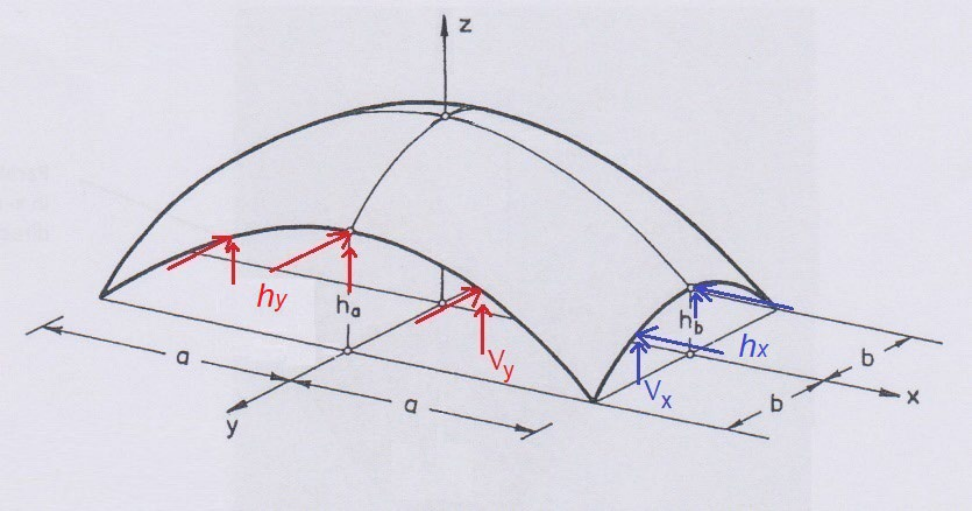

example twistless shell, deriving shape function of shell:

$$h_x = \frac{M_x}{z_x} = \frac{\beta p(a^2 - x^2)}{2z_x}$$

$$h_y = \frac{M_y}{z_y} = \frac{(1-\beta)p\,(b^2 - y^2)}{2z_y}$$

$$M_{x,max} = \frac{\beta p a^2}{2} = h_x \cdot h_a \rightarrow h_x = \frac{\beta p a^2}{2h_a}$$

$$h_x = \frac{\beta p(a^2 - x^2)}{2z_x} = \frac{\beta p a^2}{2h_a} \rightarrow z_x = \frac{h_a(a^2 - x^2)}{a^2}$$

$$M_{y,max} = \frac{(1-\beta)pb^2}{2} = h_y \cdot h_b \rightarrow h_y = \frac{(1-\beta)pb^2}{2h_b}$$

$$h_y = \frac{(1-\beta)p\,(b^2 - y^2)}{2z_y} = \frac{(1-\beta)pb^2}{2h_b} \rightarrow z_y = \frac{h_b(b^2 - y^2)}{b^2}$$

$$\rightarrow z_{shell} = z_x + z_y = h_a\frac{(a^2 - x^2)}{a^2} + h_b\frac{(b^2 - y^2)}{b^2}$$

The $\bar{M}$-hill has been used to derive the shape function of the shell. Due to the pin supports and the twistless case the horizontal thrusts are constant. The stress function of the shell can now be derived, the horizontal thrusts are equal to the projected forces.

$$h_x = \frac{\partial^2\phi}{\partial x^2}, h_y = \frac{\partial^2\phi}{\partial y^2}$$

$$\rightarrow v_x = -\beta p x = \frac{\partial^2\phi}{\partial y^2} \cdot -\frac{2h_a x}{a^2} \rightarrow \frac{\partial^2\phi}{\partial y^2} = \frac{\beta a^2 p}{2h_a}$$

$$\phi_x = \iint \frac{\beta a^2 p}{2h_a}\,dy = \frac{\beta a^2 p}{4h_a}y^2 + C_1$$

$$if\ y = a\ then;\ \phi_x = 0 \rightarrow C_1 = -\frac{\beta a^4 p}{4h_a}$$

$$\rightarrow v_y = -(1-\beta)py = \frac{\partial^2\phi}{\partial x^2} \cdot -\frac{2h_b y}{b^2} \rightarrow \frac{\partial^2\phi}{\partial x^2} = \frac{(1-\beta)b^2 p}{2h_b}$$

$$\phi_y = \iint \frac{(1-\beta)b^2 p}{2h_b}\,dx = \frac{(1-\beta)b^2 p}{4h_b}x^2 + C_2$$

$$if\ x = b\ then: \phi_y = 0 \rightarrow C_2 = -\frac{(1-\beta)b^4 p}{4h_b}$$

$$\phi = -\frac{p}{4}\left[\frac{a^2\beta}{h_a}(a^2 - y^2) + \frac{b^2(1-\beta)}{h_b}(b^2 - x^2)\right]$$

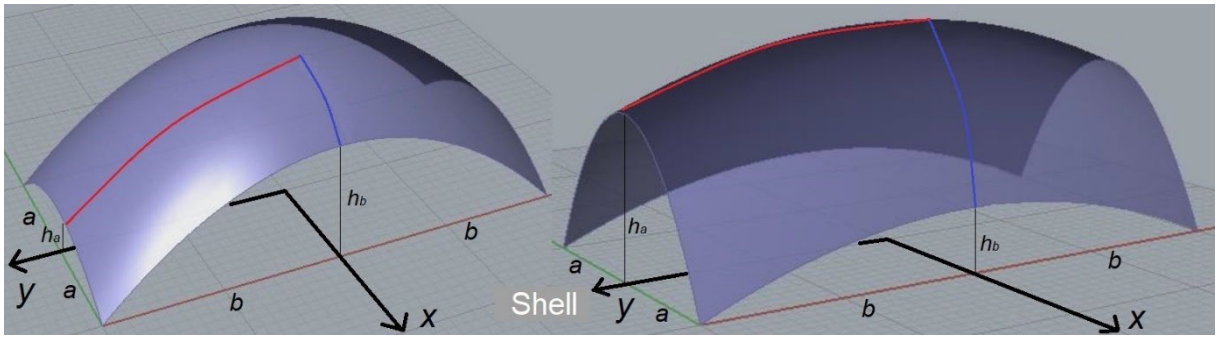

By altering the parameters of the shape function the curvature of the shell changes accordingly. This has an effect on the ratio of the load transfer.

$$p_x = h_x \frac{d^2z}{dx^2} \rightarrow \beta p = \frac{\alpha^2 h_x}{\alpha^2 h_x + h_y} p \rightarrow \beta = \frac{\alpha^2 h_x}{\alpha^2 h_x + h_y}$$

$$p_y = h_y \frac{d^2z}{dy^2} \rightarrow (1-\beta)p = \frac{h_y}{\alpha^2 h_x + h_y} p$$

$$\beta = \frac{\alpha^2 h_x}{\alpha^2 h_x + h_y} \rightarrow \frac{h_x}{h_y} = \frac{\beta}{\alpha^2(1-\beta)}$$

$$h_a \neq h_b \neq 0 \rightarrow \frac{h_x}{h_y} = \frac{\beta p a^2}{2h_a} \cdot \frac{2h_b}{(1-\beta)pb^2} = \frac{h_b}{h_a} \frac{\beta}{\alpha^2(1-\beta)}$$

$$\frac{p_x}{p_y} = \frac{h_x}{h_y} \cdot \frac{\frac{d^2z}{dx^2}}{\frac{d^2z}{dy^2}} \rightarrow \frac{\beta p}{(1-\beta)p} = \frac{h_b}{h_a} \frac{1}{\alpha^2} \frac{\beta}{(1-\beta)} \cdot \frac{k_{xx}}{k_{yy}}$$

$$if\ h = h_x = h_y\ then\colon\ \frac{p_x}{p_y} = \frac{k_{xx}}{k_{yy}}$$

The ratio of the load transfer depends on the shape function and the chosen distribution of the loads. In the next numerical example a different choice of value for β leads to different solutions for the same shape. This should not be possible, each set shape and its accompanying parameters leads to one solution.

$$\frac{p_x}{p_y} = \frac{h_x}{h_y} \cdot \frac{\frac{d^2z}{dx^2}}{\frac{d^2z}{dy^2}} \rightarrow \frac{p_x}{p_y} = \frac{h_b}{h_a} \frac{a^2}{b^2} \frac{\beta}{(1-\beta)} \cdot \frac{k_{xx}}{k_{yy}}$$

$$if\ \alpha = \frac{b}{a} = \frac{2}{1} = 2 \rightarrow \alpha^2 = 4$$

$$shell\ left\colon \frac{h_b}{h_a} = \frac{5}{2}\ ,shell\ right\colon \frac{h_b}{h_a} = \frac{2}{5}$$

$$choose\colon \beta = \frac{1}{2}$$

$$\rightarrow\ shell\ left\colon \frac{p_x}{p_y} = \frac{5}{8} \cdot \frac{k_{xx}}{k_{yy}}\ ,shell\ right\colon \frac{p_x}{p_y} = \frac{1}{10} \cdot \frac{k_{xx}}{k_{yy}}$$

$$choose\colon \beta = \frac{1}{4}$$

$$\rightarrow\ shell\ left\colon \frac{p_x}{p_y} = \frac{5}{24} \cdot \frac{k_{xx}}{k_{yy}}\ ,shell\ right\colon \frac{p_x}{p_y} = \frac{1}{30} \cdot \frac{k_{xx}}{k_{yy}}$$

This is precisely the problem of thrust networks, each load case has an infinite amount of solutions (statically indeterminate). But only one geometry / shape function will be correct.

To solve the problem of multiple possible solutions, the method can be used as described previously in chapter 4 with the help of minimizing the complementary energy in the structure. For this example this will be done in an approximate way, as it is more important to show the principle.

The result is the ratio between the load transfer and the curvatures in both directions.

$$approximate\ arc\ lenght\ parabola: L = l + \frac{8f^2}{3l}$$

$$l_x = 2a + \frac{8h_a^2}{3(2a)} = \frac{6a^2 + 4h_a^2}{3a}$$

$$l_y = \frac{6b^2 + 4h_b^2}{3b}$$

$$N_x^2 = [(h_x)^2 + (v_x)^2] = \left[\left(\frac{\beta p a^2}{2h_a}\right)^2 + (\beta p x)^2\right] = \frac{\beta^2 p^2 (4x^2 h_a^2 + a^4)}{4h_a^2}$$

$$N_y^2 = \left[\left(h_y\right)^2 + \left(v_y\right)^2\right] = \left[\left(\frac{(1-\beta) p b^2}{2h_b}\right)^2 + \left((1-\beta) p y\right)^2\right] = \frac{(1-\beta)^2 p^2 \left(4y^2 h_b^2 + b^4\right)}{4h_b^2}$$

$$N_{x,gem}^2 = \frac{N_{x=0}^2 + N_{x=a}^2}{2}$$

$$E_{compl,N} = l_x \cdot N_{x,gem}^2 + l_y \cdot N_{y,gem}^2 \rightarrow min: \frac{\partial E_{compl,N}}{\partial \beta} = 0$$

$$shell\ left: \frac{\partial E_{compl,N}}{\partial \beta} = \frac{5p^2(6513\beta - 5600)}{4} = 0$$

$$\rightarrow \beta = \frac{5600}{6513} \approx 0.86\,, \quad \frac{k_{xx}}{k_{yy}} = 1.6, \quad \frac{p_x}{p_y} = \frac{3500}{913} \cdot \frac{k_{xx}}{k_{yy}} \approx 3.83 \cdot \frac{k_{xx}}{k_{yy}}$$

$$shell\ right: \frac{\partial E_{compl,N}}{\partial \beta} = \frac{5p^2(5669\beta - 5544)}{4} = 0$$

$$\rightarrow \beta = \frac{5544}{5669} \approx 0.98\,, \quad \frac{k_{xx}}{k_{yy}} = 10, \quad \frac{p_x}{p_y} = \frac{2772}{625} \cdot \frac{k_{xx}}{k_{yy}} \approx 4.44 \cdot \frac{k_{xx}}{k_{yy}}$$

$$k_{xx} = -\frac{2h_a}{a^2}, k_{yy} = -\frac{2h_b}{b^2}$$

$$shell\ left: \frac{k_{xx}}{k_{yy}} = 1.6$$

$$shell\ right: \frac{k_{xx}}{k_{yy}} = 10$$

The previous examples considered a twistless case where there are no shear panels in the model, there are thus no internal shear forces that can contribute to carrying the loads.

If a shape function is used which is not a translation surface, to describe the shell's surface it can still be a twistless case if the twist of the surface is not able to carry loads. This is a hypothetical case, if the shear panels are omitted this will result in a thrust network. A thrust network is a discretized thrust surface without the shear panels and is in fact a twistless case.

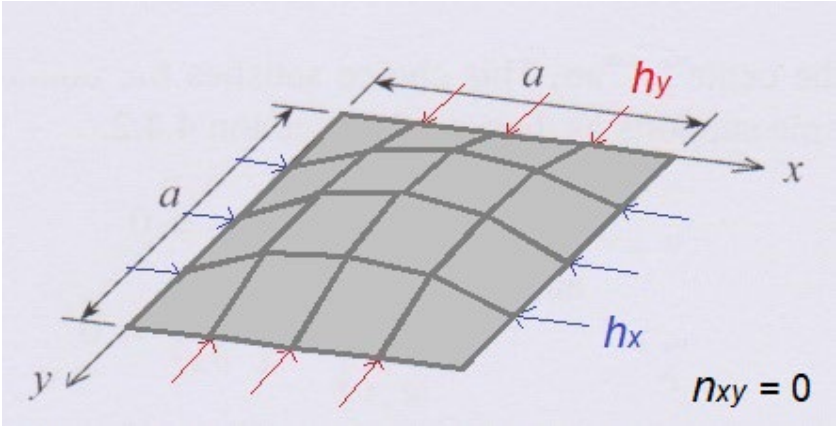

$$square\ base: z_{shell} = \frac{a^4}{2\pi^4} \sin\frac{\pi x}{a} \sin\frac{\pi y}{a}$$
$$with: p = \check{p} \sin\frac{\pi x}{a} \sin\frac{\pi y}{a}$$
$$M_x = M_y = \frac{\check{p}a^2}{2\pi^2} \sin\frac{\pi x}{a} \sin\frac{\pi y}{a}$$
$$v_x = \frac{dM_x}{dx} = \frac{\check{p}a^2}{2\pi^2} \sin\frac{\pi y}{a} \cos\frac{\pi x}{a}$$
$$v_y = \frac{dM_y}{dy} = \frac{\check{p}a^2}{2\pi^2} \sin\frac{\pi x}{a} \cos\frac{\pi y}{a}$$
$$\rightarrow h_x \frac{dz}{dx} = h_x \cdot \frac{a^3 \sin\frac{\pi y}{a} \cos\frac{\pi x}{a}}{2\pi^3} = v_x \rightarrow h_x = \frac{\pi^2 \check{p}}{a^2}$$
$$or\ h_x = \frac{M_x}{z} = \frac{\pi^2 \check{p}}{a^2} = constant$$
$$h_y = h_x$$
$$with: n_{xx}\ and\ n_{yy} \neq 0, n_{xy} = \bar{n}_{xy} = 0$$

The internal forces can be in tension or compression, but there are no shear forces. The load is no longer uniform, but is discretized into forces which are placed in the nodes where the bars meet, similar to the thrust network.

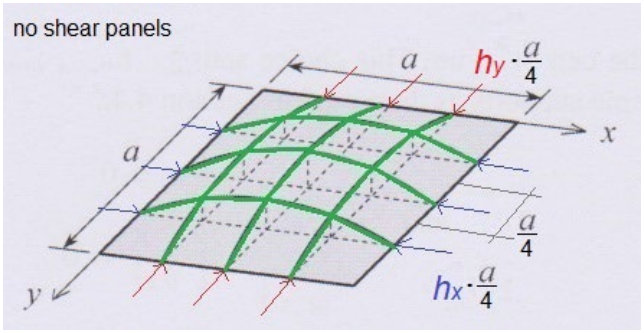

thrust network

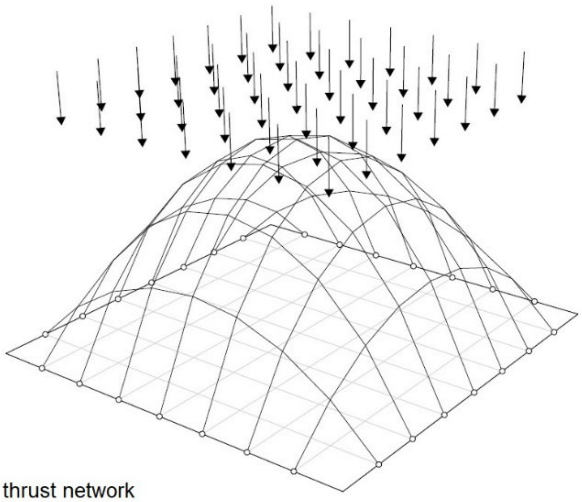

thrust network

In a loaded twisted shear panel, due to its twist, the shear forces have a vertical component which is able to carry part of the load.

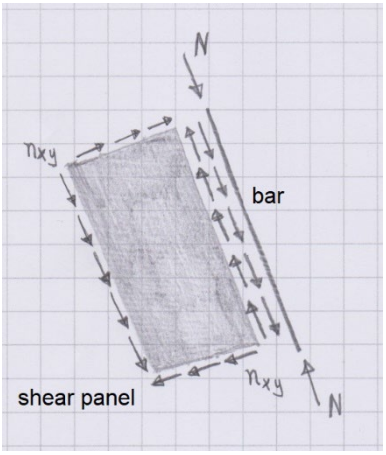

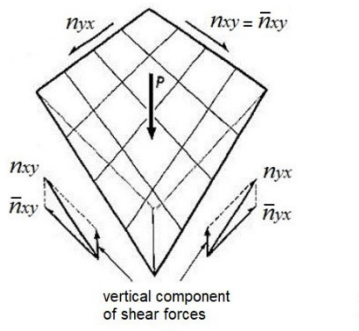

Portion of load carried by shear forces due to twist

A twistless case is statically determinate, once a ratio of the loads (p_x/p_y) has been determined [89]. To begin with there are infinite possibilities for determining this ratio to carry the same total load. This is similar to a thrust network, there are infinite solutions for a network to be able to carry the same load. Each solution, height and topology, which provides equilibrium is a viable option.

The ratio of “curvatures”, or because of the discretized nature of the network the angles, of a chosen network determines the ratio of the load transfer in the different directions.

The geometry of a thrust network is thus dependent on the chosen ratio of the loads. By adding shear panels to a thrust network the problem becomes statically indeterminate, meaning the ratio of the loads can no longer be chosen [90, 91]. For the given shape of the network we get a single solution, the thrust surface.

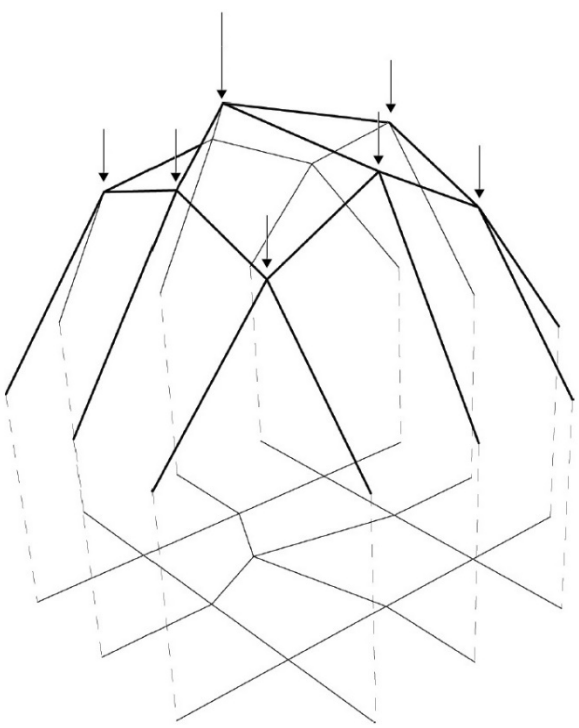

thrust network

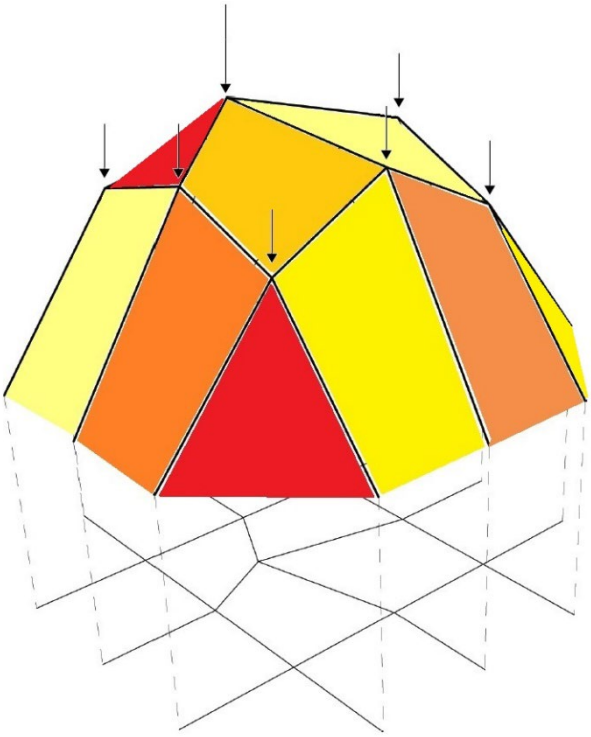

thrust network with shear panels

In the next section the full expression for the thrust network will be derived.

8.3 Shells on a square or rectangular base

This section will discuss the relation between the four basic functions, the shape function, stress function, thrust surface, and moment-hill of shells on a square or rectangular base. Differing from axisymmetric membrane shells this involves some out-of-plane bending, as membrane only solutions are nearly impossible. More in detail on this in the last section.

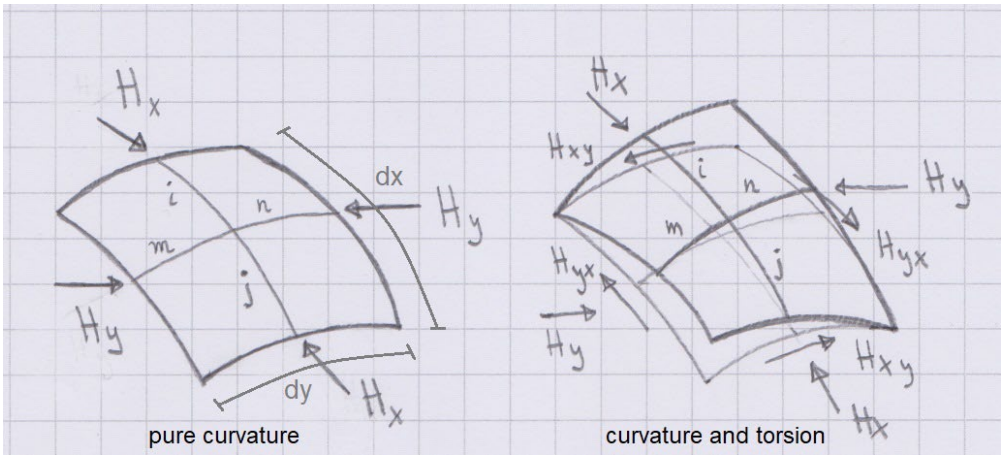

$$H_x = h_x\, dy$$
$$H_y = h_y\, dx$$
$$H_{xy} = h_{xy}\, dy$$
$$H_{yx} = h_{yx}\, dx$$

For square, rectangular and triangular based shells the surface of the four basic functions will not only be curved but also twisted. The consequence of this is that the internal membrane forces and their projected components, will also include shear. Which will contribute in the carrying of the load. In a discretization of these functions the shear panels will need to be added.

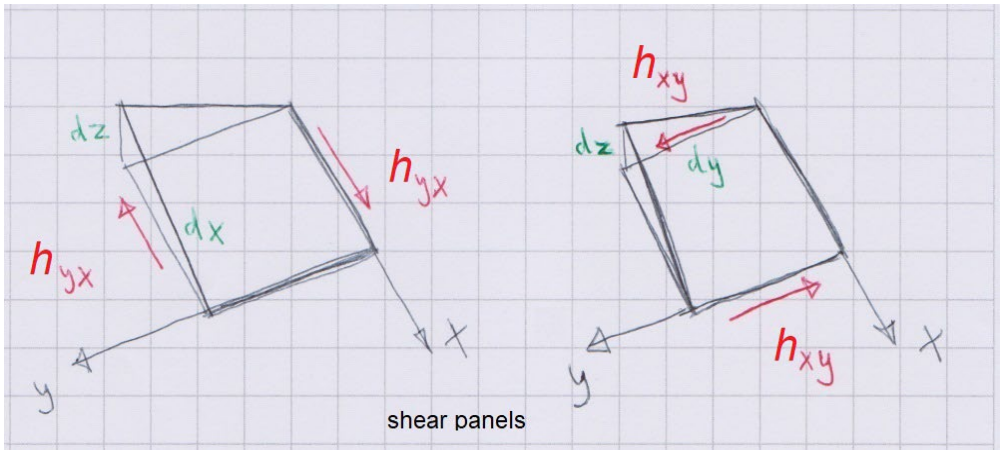

$$v_x = h_x \frac{\partial z}{\partial x} + h_{xy} \frac{\partial z}{\partial y} = \bar{n}_{xx} \frac{\partial z}{\partial x} + \bar{n}_{xy} \frac{\partial z}{\partial y}$$
$$v_y = h_y \frac{\partial z}{\partial y} + h_{yx} \frac{\partial z}{\partial x} = \bar{n}_{yy} \frac{\partial z}{\partial y} + \bar{n}_{xy} \frac{\partial z}{\partial x}$$
$$p = -\left(\frac{\partial v_x}{\partial x} + \frac{\partial v_y}{\partial y}\right) \; with: h_{xy} = h_{yx}$$
$$\rightarrow h_x \frac{\partial^2 z}{\partial x^2} + 2h_{xy} \frac{\partial^2 z}{\partial x \partial y} + h_y \frac{\partial^2 z}{\partial y^2} = -p$$
$$\bar{n}_{xx} \frac{\partial^2 z}{\partial x^2} + 2\bar{n}_{xy} \frac{\partial^2 z}{\partial x \partial y} + \bar{n}_{yy} \frac{\partial^2 z}{\partial y^2} = -p$$

In sections 2.8 and 2.9 it was shown that the discretization used for the force-density method and thrust networks results in a similar expression as the differential scheme of the cable equation with the shear part omitted. By adding the shear panels we get the full differential scheme of the complete cable equation and thrust network [92].

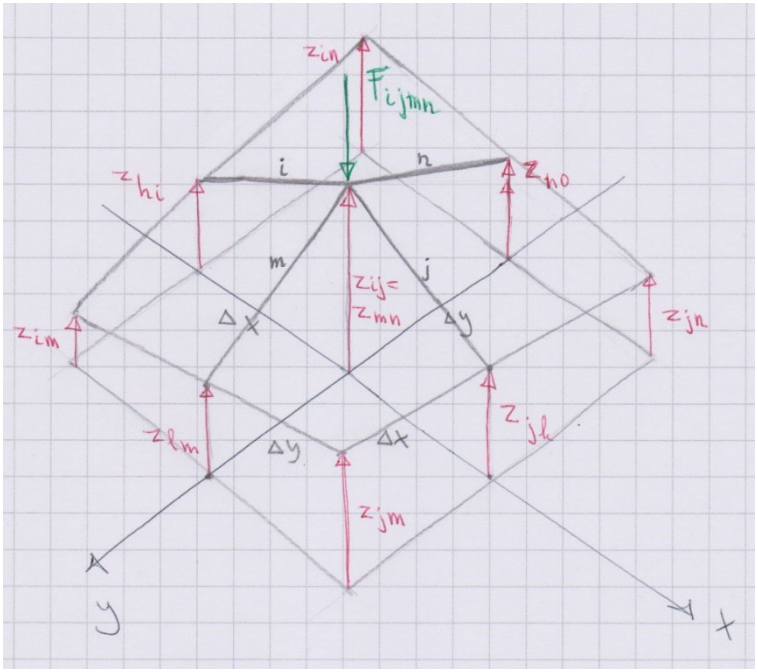

$$H_x \frac{z_{jk} - 2z_{ij} + z_{hi}}{(\triangle x)^2} + 2H_{xy} \frac{z_{jm} - z_{im} + z_{in} - z_{in}}{4 \triangle x \triangle y} + H_y \frac{z_{no} - 2z_{ij} + z_{lm}}{(\triangle y)^2} = p$$

$with: F_{ijmn} = \triangle x \triangle y\, p,$

$z_{mn} = z_{ij}$

$cable\ equation:$

$$\Rightarrow H_x \frac{\partial^2 z}{\partial x^2} + 2H_{xy} \frac{\partial^2 z}{\partial x \partial y} + H_y \frac{\partial^2 z}{\partial y^2} = -p_z$$

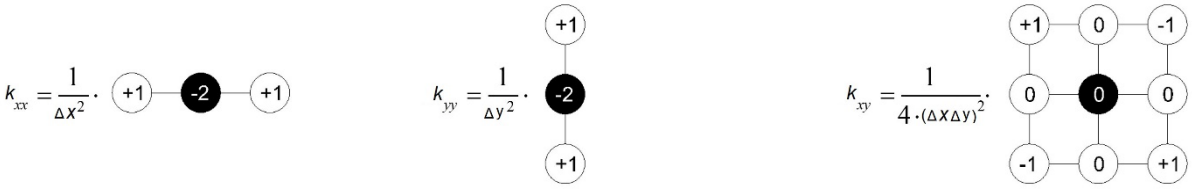

When these equations are solved, a thrust network including shear panels is obtained and thus the thrust surface of the load can be determined. The problem is statically indeterminate, and can be solved by minimizing the complementary energy for the system or by solving the stress function, see section 8.6.

The differential scheme can also be used for a discretization of the stress function and the moment hill, because they are applicable to all second order partial differential equations.

$$2\kappa_{xy} = \frac{\Delta z_i + \Delta z_j + \Delta z_k + \Delta z_k}{xy}$$
$$with: \Delta z_i = z_4 - z_1,$$
$$\Delta z_j = z_4 - z_3,$$
$$\Delta z_k = z_2 - z_3,$$
$$\Delta z_k = z_2 - z_1$$
$$\rightarrow \kappa_{xy} = \frac{-z_1 + z_2 - z_3 + z_4}{xy}$$

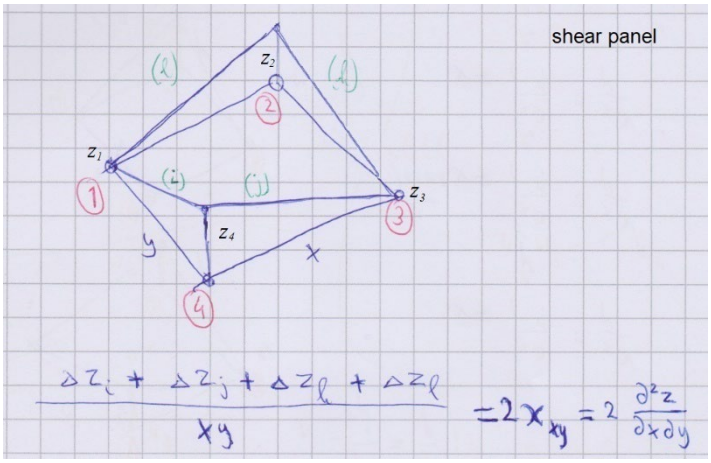

The importance of the equations being second order is that a thrust line of an arch and the thrust surface of a shell are material independent. For the arch this means the problem is mostly statically determinate, depending on the boundary conditions. For some shells the thrust surface is statically determinate, for example of axisymmetric shells, see chapter 7. The analogy between the $\bar{M}$-hill and its equivalent membrane equation will be used to solve the next example, shells on a square or rectangular base with hinge supports along all edges [93]. Its equivalent slab is equally hinge supported along all edges, see section 8.5.

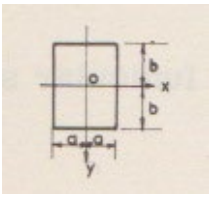

$$soap\ bubble, with: n_{xx} = n_{yy} = n\ and\ n_{xy} = 0$$
$$\rightarrow n\left(\frac{\partial^2 z}{\partial x^2} + \frac{\partial^2 z}{\partial y^2}\right) - p = 0$$
$$for\ rectangle\ slab\ (with\ torsional\ stiffness):$$
$$z = z_{"\bar{M}-hill"} = \frac{16pa^2}{\pi^3 n} \sum_{n=1,3,5\ldots}^{\infty} \frac{1}{n}(-1)^{\frac{n-1}{2}} \left[1 - \frac{cosh\frac{n\pi y}{2a}}{cosh\frac{n\pi b}{2a}}\right] cos\frac{n\pi x}{2a}$$

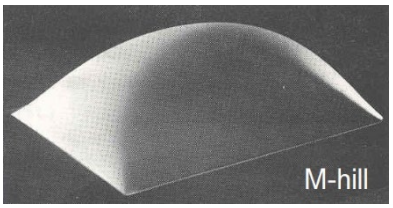

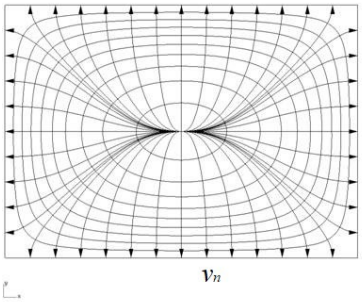

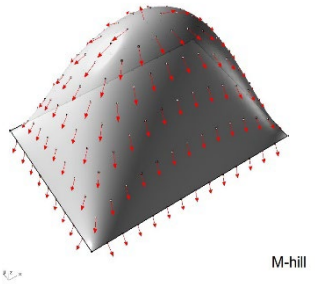

$$\bar{M} - hill:$$
$$\bar{M} = -D\left(\frac{\partial^2 w}{\partial x^2} + \frac{\partial^2 w}{\partial y^2}\right)$$
$$analogous\ to\ soap\ bubble/inflated\ membrane:$$
$$p = n\left(\frac{\partial^2 z}{\partial x^2} + \frac{\partial^2 z}{\partial y^2}\right)$$

$$v_n = \frac{\partial \bar{M}}{\partial n} = max$$
$$v_t = \frac{\partial \bar{M}}{\partial t} = 0$$

The expression for the moment hill of the twistless case adheres to the analogy, and is thus a correct $\bar{M}$-hill. This also holds for the slab with torsional stiffness.

$$moment\ hill\ twistless\ case:$$
$$\bar{M} = \frac{p}{2}[\beta(a^2 - x^2) + (1-\beta)(b^2 - y^2)]$$
$$analogy: \frac{p}{n} = \left(\frac{\partial^2 z}{\partial x^2} + \frac{\partial^2 z}{\partial y^2}\right) \equiv p = -\left(\frac{\partial^2 \bar{M}}{\partial x^2} + \frac{\partial^2 \bar{M}}{\partial y^2}\right)$$
$$z_{"\bar{M}-hill"} = -\frac{p}{2n}[\beta(a^2 - x^2) + (1-\beta)(b^2 - y^2)]$$
$$\rightarrow \left(\frac{\beta p}{n} + \frac{(1-\beta)p}{n}\right) = \frac{p}{n}$$

In this analogy, taken from slab theory, an inflated membrane is equivalent to the moment-hill. The analogy has been used to derive the stress functions in chapter 7 for the axisymmetric shells. For these shells the surface of the moment-hill is curved. For shells on a square or rectangular base the surface is curved and twisted.

$$v_n = \frac{\partial \bar{M}}{\partial n} = max$$
$$v_t = \frac{\partial \bar{M}}{\partial t} = 0$$

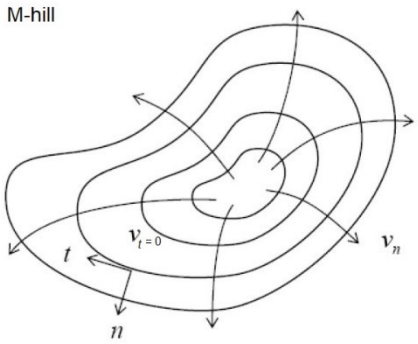

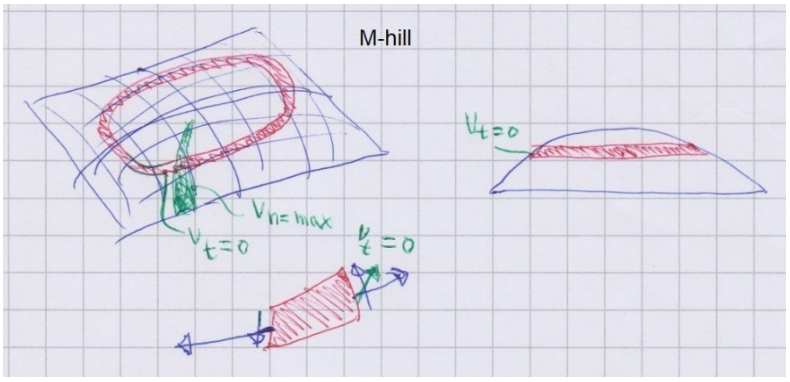

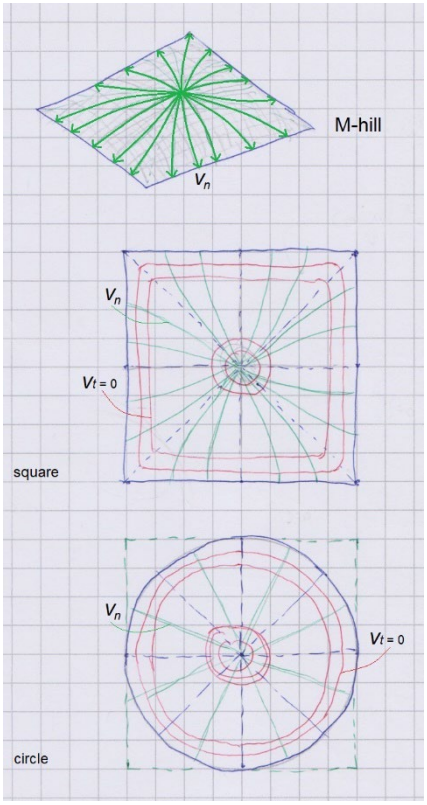

The trajectories of the maximum shear forces v_n in slabs, which are the curves of steepest ascent of the M-hill, are equivalent to the trajectories of the flow of forces of a shell. Comparing the trajectories of a circular or square moment-hill it can be observed that for the latter the lines are skewed outwards like tendons running over an inflated balloon.

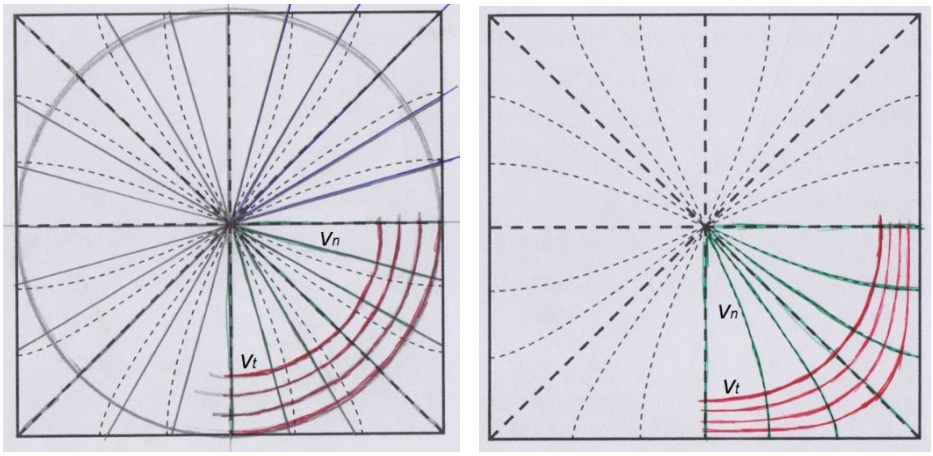

$\bar{M} - hill, round\ versus\ square$

The flow of forces for shells on a square, rectangular and triangular base nearly always involves shear forces in the shell. The strips of the load transfer are, different from the twistless case, not aligned in a orthogonal grid. But the strips do follow the trajectories of the flow of forces.

$M - hill$

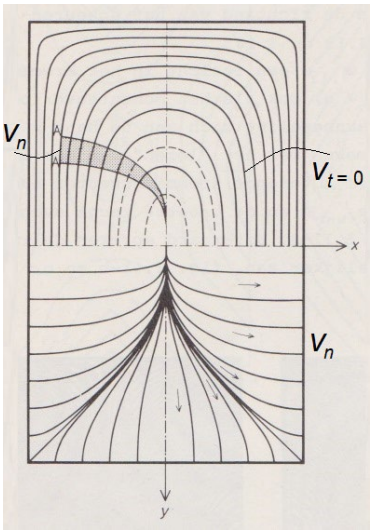

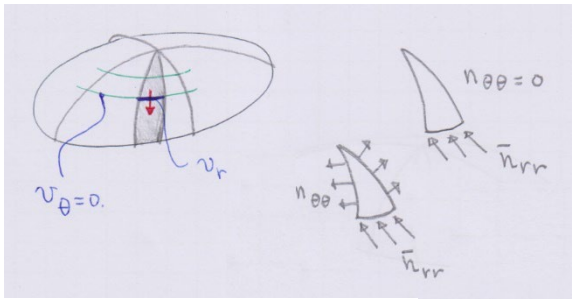

strip is curved

strip is curved and twisted

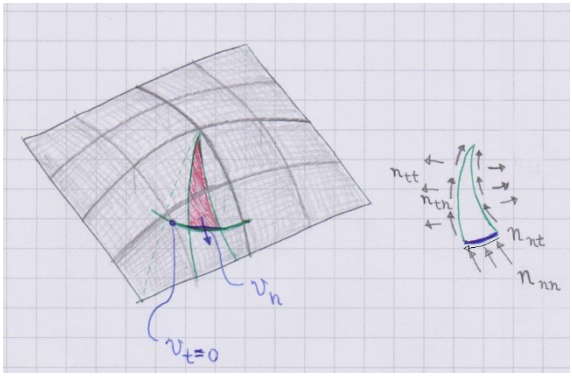

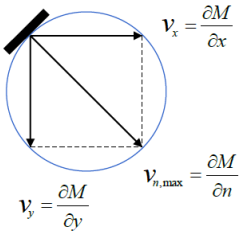

$$v_n = \sqrt{(v_x)^2 + (v_y)^2}$$

$$\bar{n}_{nt} = \bar{n}_{tn}$$

$$v_n = \bar{n}_{nn}\frac{\partial z}{\partial n} + \bar{n}_{nt}\frac{\partial z}{\partial t}$$

$$v_t = \bar{n}_{tt}\frac{\partial z}{\partial t} + \bar{n}_{nt}\frac{\partial z}{\partial n} = 0$$

An example of a shell on a square base is the bubble shell. The shape function of the shell is the same of the inflated membrane. The shell is also subjected to a uniformly distributed load *p*. In order to find the stress function, the approximation of the shape function will be used as found in the “Theory and practice of membrane shells” by Pal Csonka [94].

The example Csonka uses starts from the stress function and derives the accompanying shape function. Because Pucher's equation allows for both functions to be interchanged (see section 8.7), the expression for the stress function will be used as shape function. Thus a useable stress function for this problem is obtained.

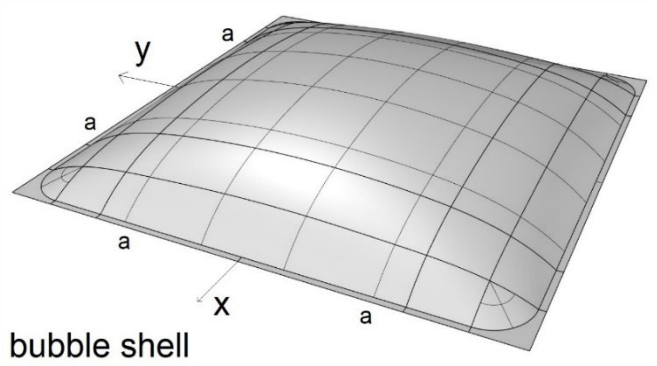

It is impossible for this example to find a fully analytical solution for this example. On the basis of the shape function an analytical solution can be found for the edge of the stress function and for the horizontal thrust $\bar{n}_{yy}$. Using the results of the numerical solution found in Csonka the shear stresses along the edge can be estimated. Because the shell is flat along the edge in the parallel direction the shear force is not able to carry any loads, this results in bending moments and shear forces in the edge zone.

for this example the reciprocal charateristic of Pucher's equation will be used to interchange the shape function z and the stress function ϕ as found in Csonka:

$$z_{shell} = -2K\left(\frac{(a^2-x^2)(a^2-y^2)}{a^4-x^2y^2}\right), \text{with } K \text{ the height of the shell can be chosen.}$$

$$\phi_{,edge} = -\frac{pa^4}{16K}\left(\frac{4}{3}\right)^2\left(\sqrt{3}\frac{x}{a}\,arctan\sqrt{3}\frac{x}{a} - \sqrt{3}arctan\sqrt{3} - \frac{1}{2}ln\frac{3\left(\frac{x}{a}\right)^2+1}{4} + \frac{1}{2}\frac{3-3\left(\frac{x}{a}\right)^2}{4}\right)$$

$$\bar{n}_{yy,edge} = \frac{\partial^2\phi_{,edge}}{\partial x^2} = \frac{pa^4}{K}\cdot\frac{(a^2-x^2)}{4a^2(3x^2+a^2)}$$

$$v_{y,edge} = \bar{n}_{yy}\frac{\partial z}{\partial y} + \bar{n}_{xy}\frac{\partial z}{\partial x}\ with\colon \frac{\partial z}{\partial y} = -\frac{4}{a}\ and\ \frac{\partial z}{\partial x} = 0$$

$$\rightarrow\ v_{y,edge} = \bar{n}_{yy}\cdot -\frac{4}{a}$$

$\rightarrow$ the discrepancy between $v_{y,load}$ and $v_{y,edge}$ has to be carried by out $-$ of $-$ plane internal shear forces and bending moments

stress function

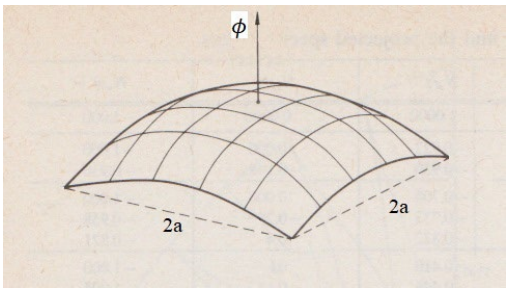

$\bar{M} - hill$

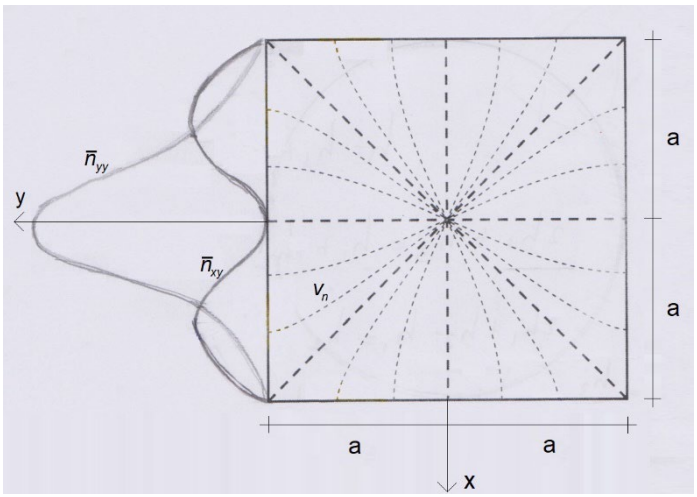

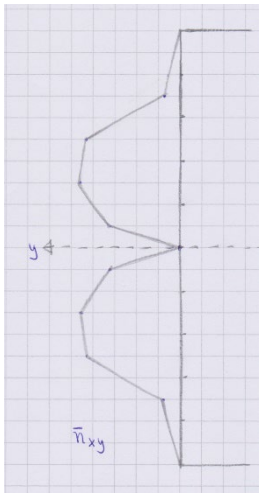

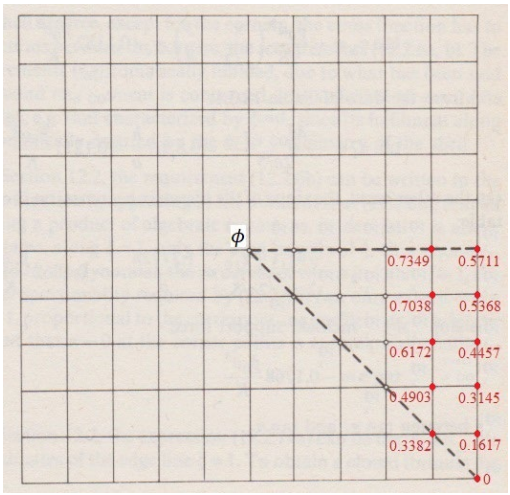

stresses along edge

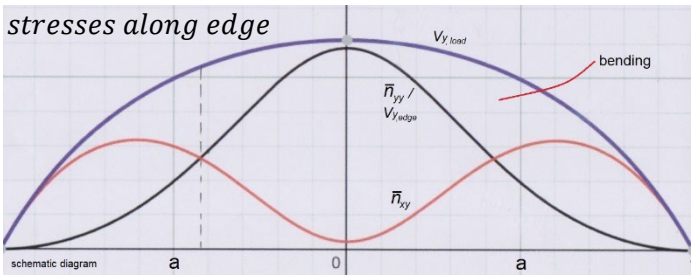

$\bar{n}_{xy}$ *determined by the torsion of the edge of the stress function*

discretized stress function, edge values used for $\bar{n}_{xy}$

FEM calculation

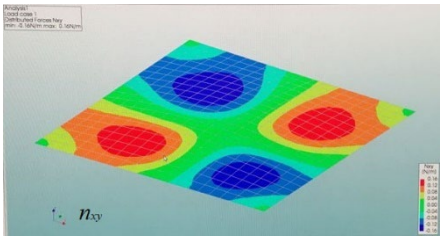

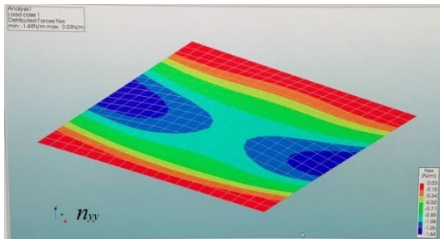

Figure 46 FEM calculation [image by Peter Eigenraam]

The $\bar{M}$-hill shows the flow of forces. The stresses of the bubble shell have been validated by FEM calculations. In the last section it will be outlined how to deal with the bending moments and shear forces.

8.4 Shells on a triangular base

For a shell on a triangular base it is possible to analytically derive the basic functions. The first example is an equilateral triangular shell with pin supports along its edges.

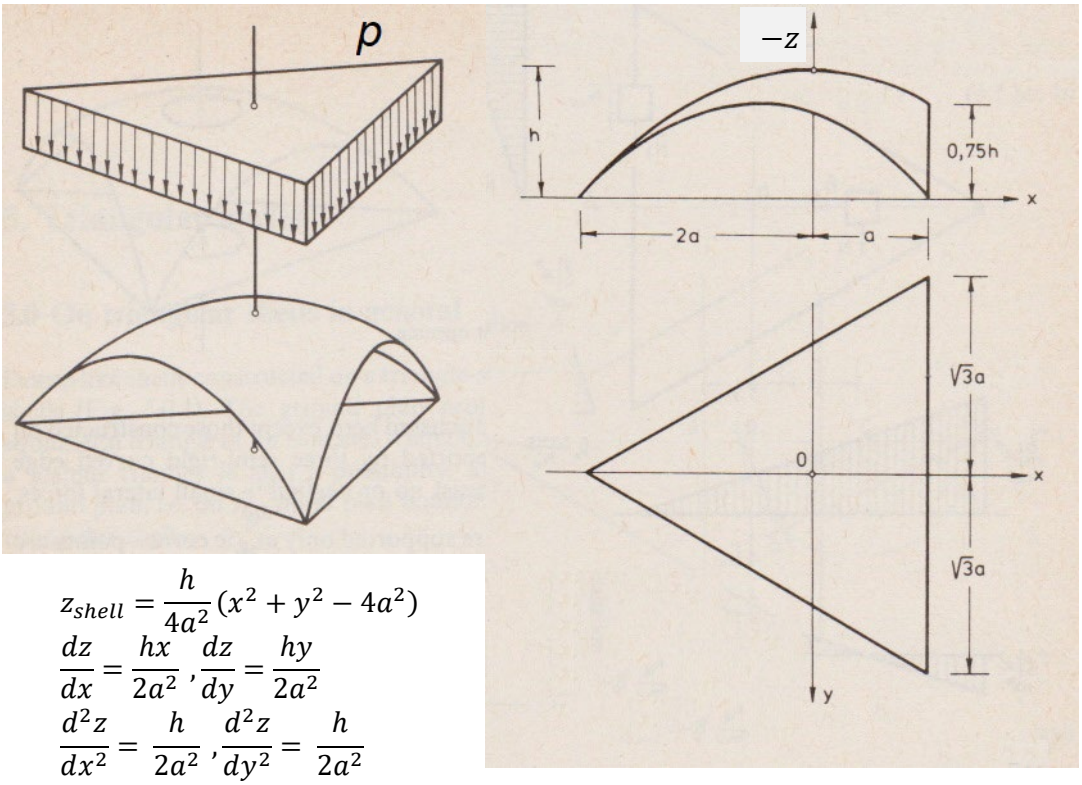

$$z_{shell} = \frac{h}{4a^2}(x^2 + y^2 - 4a^2)$$
$$\frac{dz}{dx} = \frac{hx}{2a^2}, \frac{dz}{dy} = \frac{hy}{2a^2}$$
$$\frac{d^2z}{dx^2} = \frac{h}{2a^2}, \frac{d^2z}{dy^2} = \frac{h}{2a^2}$$

The shape function is given and the $\bar{M}$-hill of the *p*-load will be used to derive the stress function.

$$\bar{M}_{p-load} = -\frac{p(r^2 - a^2)}{4} = -\frac{p(x^2 + y^2 - a^2)}{4}$$
$$v_x = \frac{d\bar{M}}{dx} = -\frac{px}{2}$$
$$v_y = \frac{d\bar{M}}{dy} = -\frac{py}{2}$$
$$v_n = \sqrt{(v_x)^2 + (v_y)^2} = \frac{p}{2}\sqrt{x^2 + y^2} = \frac{p}{2}r$$
$$v_x = \bar{n}_{xx}\frac{dz}{dz} \rightarrow \bar{n}_{xx} = -\frac{px}{2} \cdot \frac{2a^2}{hx} = -\frac{pa^2}{h}$$
$$\bar{n}_{xx} = \bar{n}_{yy} = -\frac{pa^2}{h}, \bar{n}_{xy} = 0$$
$$\left(v_n = \bar{n}_{nn}\frac{dz}{dr} \rightarrow \bar{n}_{nn} = \frac{pr}{2} \cdot \frac{2a^2}{hr} = \frac{pa^2}{h}\right)$$
$$\bar{n}_{xx} = \frac{\partial^2\phi}{\partial y^2} = -\frac{pa^2}{h} \rightarrow \phi_x = -\frac{pa^2}{2h}\, y^2 + C$$
$$\bar{n}_{yy} = \frac{\partial^2\phi}{\partial x^2} = -\frac{pa^2}{h} \rightarrow \phi_y = -\frac{pa^2}{2h}\, x^2 + C$$
$$\phi = \phi_x + \phi_y = -\frac{pa^2}{2h}(x^2 + y^2 + C)$$
$for\ x = -2a\ and\ y = 0\ and\ for\ x = a\ and\ y = \sqrt{3}a$:
$\phi = 0 \rightarrow C = -4a^2$

vault like pinned edge conditions:
$\bar{n}_{xy} = \bar{n}_{nt} = 0$

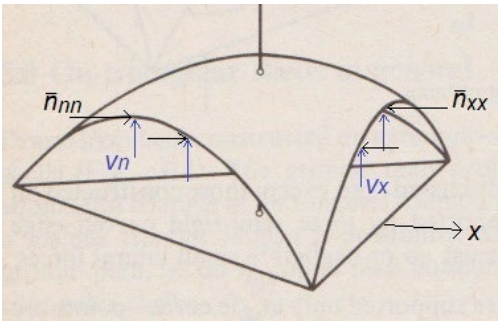

The solution is very similar to the twistless case shell from section 8.2.

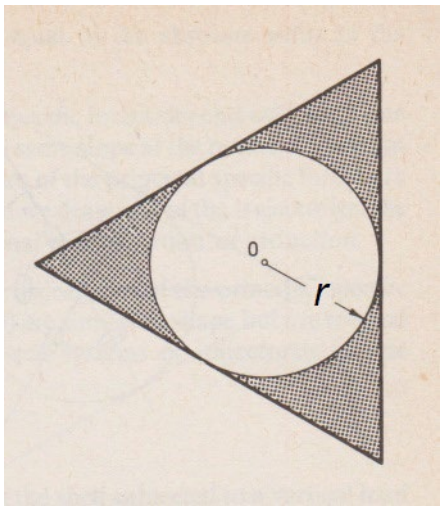

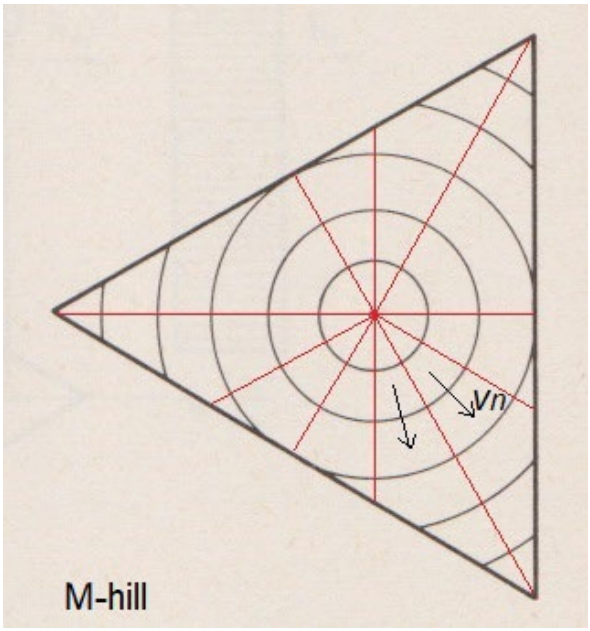

For the same shell the boundary conditions will be changed. The vault like pin supported edge will become a semi-rigid one. This means that the edge can no longer take up thrust perpendicular to the edge, only shear forces can be taken. Structurally the edge will include a diaphragm.
The derivation below of the stress function for the semi-rigid edges is taken from the forementioned book by Csonka. It is based on the premise that the stress function is equal to zero along the edges, as a consequence of the boundary conditions.

$$\frac{\partial^2 z}{\partial x^2}\frac{\partial^2 \phi}{\partial y^2} - 2\frac{\partial^2 z}{\partial x \partial y}\frac{\partial^2 \phi}{\partial x \partial y} + \frac{\partial^2 z}{\partial y^2}\frac{\partial^2 \phi}{\partial x^2} + p = 0$$

$$\rightarrow \frac{h}{2a^2}\left(\frac{\partial^2 \phi}{\partial x^2} + \frac{\partial^2 \phi}{\partial y^2}\right) + p = 0$$

$$to\ satify\ bounday\ condation \rightarrow \phi = 0$$

$$(x-a) = 0, \left(y - \frac{2a}{\sqrt{3}} - \frac{x}{\sqrt{3}}\right) = 0, \left(y + \frac{2a}{\sqrt{3}} + \frac{x}{\sqrt{3}}\right) = 0$$

$$\phi = K(x-a)\left(y - \frac{2a}{\sqrt{3}} - \frac{x}{\sqrt{3}}\right)\left(y + \frac{2a}{\sqrt{3}} + \frac{x}{\sqrt{3}}\right)$$

$$\rightarrow \phi = K\frac{-3ax^2 - 3ay^2 - x^3 + 3xy^2 + 4a^3}{3}$$

$$to\ satify\ Puchers\ equation \rightarrow K = \frac{pa}{2h}$$

$$\phi = -\frac{pa}{6h}(3ax^2 + 3ay^2 + x^3 - 3xy^2 - 4a^3)$$

$$\bar{n}_{xx} = \frac{\partial^2 \phi}{\partial y^2} = -\frac{pa}{h}(a - x)$$

$$\bar{n}_{xy} = -\frac{\partial^2 \phi}{\partial x \partial y} = -\frac{pa}{h}y$$

$$\bar{n}_{yy} = \frac{\partial^2 \phi}{\partial x^2} = -\frac{pa}{h}(a + x)$$

$$semi - rigid\ edge\ conditions: \bar{n}_{xx} = \bar{n}_{nn} = 0$$

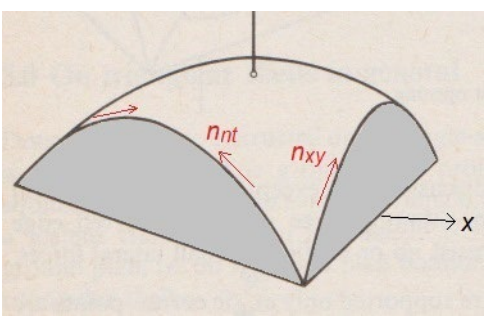

Using the stress function, the correct function for the $\bar{M}$-hill can be constructed. The $\bar{M}$-hill for the semi-rigid boundary conditions will have to include shear forces. The surface of the altered $\bar{M}$-hill will be curved and twisted. This will be reflected in the flow of the vertical forces.

$$v_x = \bar{n}_{xx}\frac{\partial z}{\partial x} + \bar{n}_{xy}\frac{\partial z}{\partial y} = -\frac{pa}{h}(a-x)\cdot\frac{hx}{2a^2} - \frac{pa}{h}y\cdot\frac{hy}{2a^2}$$

$$\rightarrow v_x = -\frac{p}{2a}(ax - x^2 + y^2)$$

$$v_y = \bar{n}_{yy}\frac{\partial z}{\partial y} + \bar{n}_{xy}\frac{\partial z}{\partial x} = -\frac{pa}{h}(a+x)\cdot\frac{hy}{2a^2} - \frac{pa}{h}y\cdot\frac{hx}{2a^2}$$

$$\rightarrow v_y = -\frac{p}{2a}(ay + 2xy)$$

$$v_x = \frac{d\bar{M}}{dx} \rightarrow \bar{M}_x = \int -\frac{p}{2a}(ax - x^2 + y^2)\,dx = -\frac{p}{12a}(6xy^2 - 2x^3 + 3ax^2)$$

$$v_y = \frac{d\bar{M}}{dy} \rightarrow \bar{M}_y = \int -\frac{p}{2a}(ay + 2xy)\,dy = -\frac{p}{12a}(6xy^2 + 3ay^2)$$

$$\rightarrow \bar{M} = \bar{M}_x + \bar{M}_y = -\frac{p}{12a}(3ax^2 + 3ay^2 - 2x^3 + 6xy^2 - C)$$

$$if\ x = -2a\ and\ y = 0\ then\ \bar{M} = 0 \rightarrow C = 28a^3$$

$$\frac{p}{n} = \left(\frac{\partial^2 z}{\partial x^2} + \frac{\partial^2 z}{\partial y^2}\right) \equiv p = -\left(\frac{\partial^2 \bar{M}}{\partial x^2} + \frac{\partial^2 \bar{M}}{\partial y^2}\right)$$

$$z_{"\bar{M}-hill"} = \frac{p}{12an}(3ax^2 + 3ay^2 - 2x^3 + 6xy^2 - 28a^3)$$

$$\rightarrow \left(\frac{(-2x+a)p}{2an} + \frac{(2x+a)p}{2an}\right) = \frac{p}{n}$$

$$with: \bar{M}_{p-load} = -\frac{p(x^2+y^2-a^2)}{4} = -\frac{p}{12a}(3ax^2 + 3ay^2 - 3a^3)$$

$$\bar{M} = -\frac{p}{12a}(\underbrace{3ax^2 + 3ay^2 - 3a^3}_{p-load}\ \underbrace{-2x^3 + 6xy^2 - 25a^3}_{\substack{boundary \\ condition}})$$

This result also adheres to the membrane equation, as would be expected for a $\bar{M}$-hill. From the expression can be seen that the new $\bar{M}$-hill is a tranformed version of the *p*-load $\bar{M}$-hill. This is the result of the boundary conditions. The new surface of the $\bar{M}$-hill is no longer a translation surface, but it now includes twist. Shear membrane forces can be expected in transfering the load.

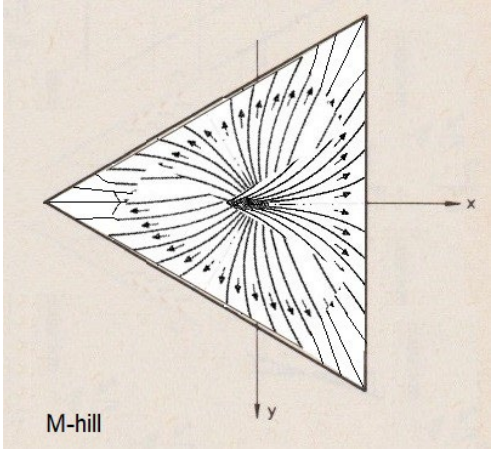

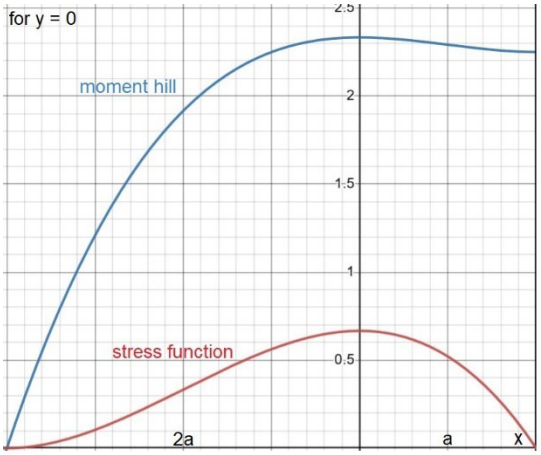

8.5 Boundary conditions

Boundary conditions are important in determining the flow of forces [95]. A straight edge of a shell will not be able to carry a thrust perpendicular to the edge, a funicular arch is better suited [96]. This can be found by an inverted hanging model, either by a physical or numerical model. In the next section will be discussed what this means for an inflated membrane with “free edges”, analogous for a shell with semi-rigid supports.

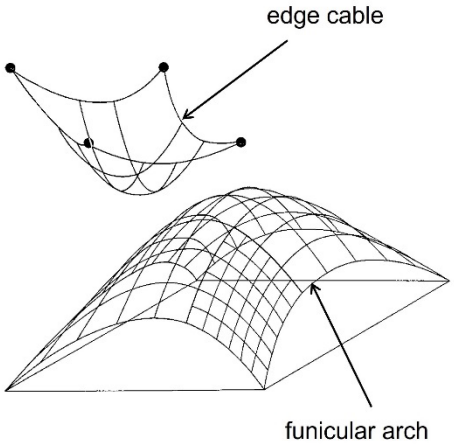

In previous sections it was shown that if the boundary condition is pinned the $\bar{M}$-hill for a uniformly distributed load *p* is an axisymmetric parabola. This fits with a pinned supported circular slab. The equivalent for a square or rectangular slab is a twistless case. The $\bar{M}$-hill strips of the flow of vertical forces are curved but not twisted.

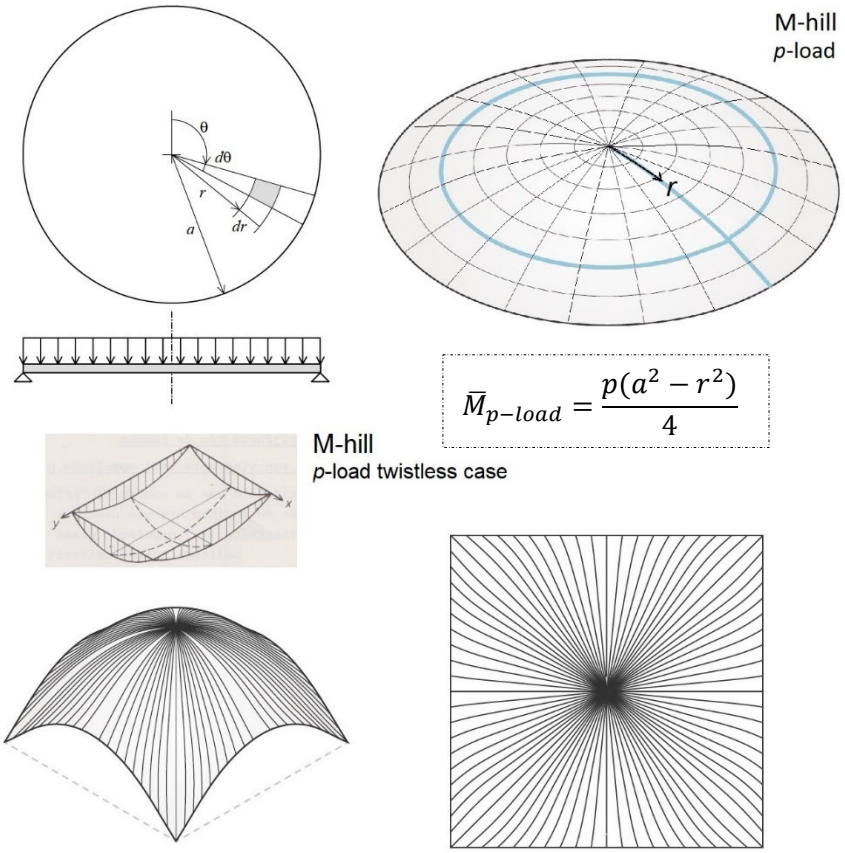

A shell with curved and pinned edges is not a very common solution, it is more theoretical and served its purpose in proving a principle.
Three realistic boundary conditions of shell will be discussed with their slab $\overline{M}$-hill analogy. The first is the square or rectangular based shell with straight edges, like the bubble shell from section 8.3. Its $\overline{M}$-hill analogy is the simply supported plate, the boundary conditions are equivalent and because the shell is square or rectangular the $\overline{M}$-hill strips of the flow vertical forces are curved and twisted.

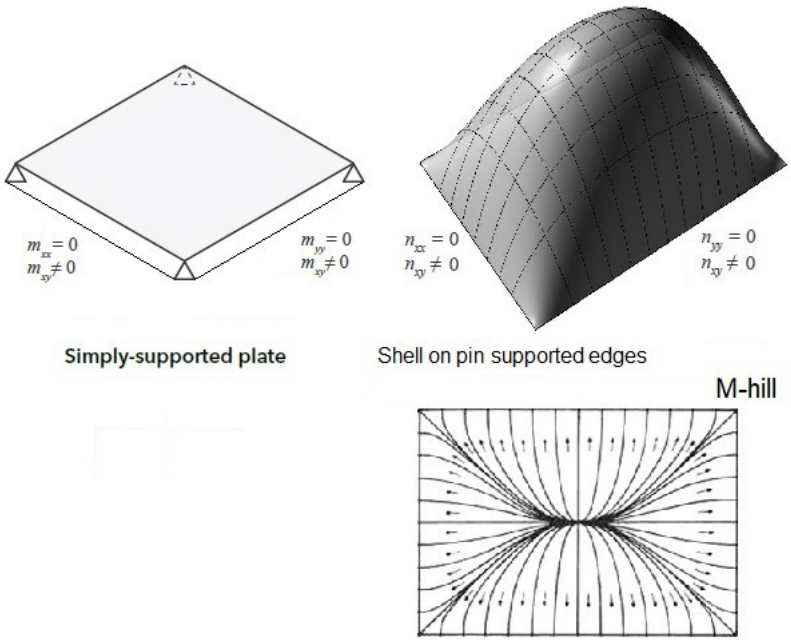

Simply-supported plate

Shell on pin supported edges

For shells with curved edges there two types, those with semi-rigid edges or free edges, like the triangular shell from section 8.4.

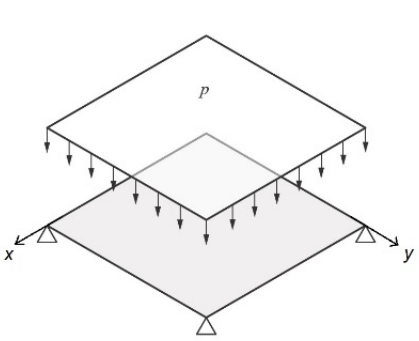

plate subjected to distributed load p

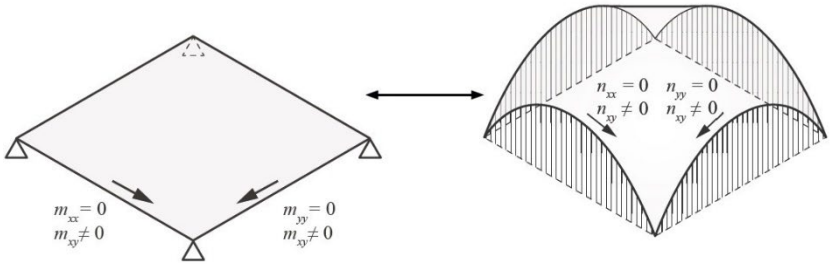

Point supported plate
(with free edges)

Shell on semi-rigid edge supports

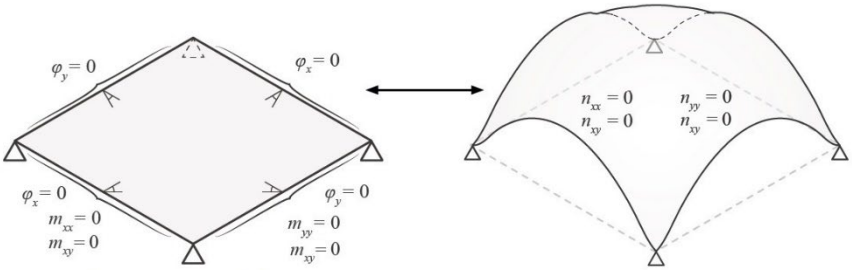

Point supported plate (twistless)
(with free edges, no rotation)

Shell with free edges

Semi-rigid edges take up shear stress, which implies that the surface of the $\bar{M}$-hill has to be twisted as well as bent to be able to accommodate the correct flow of the vertical forces.

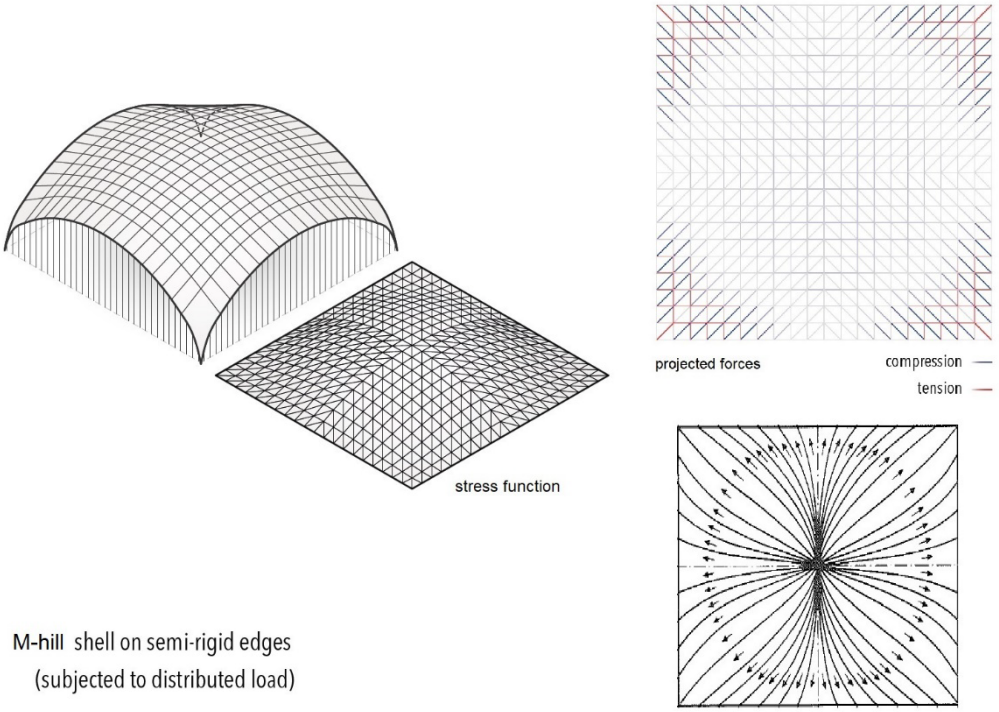

Figure 47 shell surface (shape function) is taken equal to surface of M-hill, its (polyhedral) stress function and the horizontally projected forces and the load distribution [image 101]

For the shell with free edges the accompanying $\bar{M}$-hill needs to have flow trajectories that run parallel along the edges. The continuous slab on columns has such trajectories. Perpendicular to the axis of symmetry the rotations are zero, thus there are no shear forces along the shells edge. This also results in slightly turned up edges for the shell, which is positive for the load transfer.

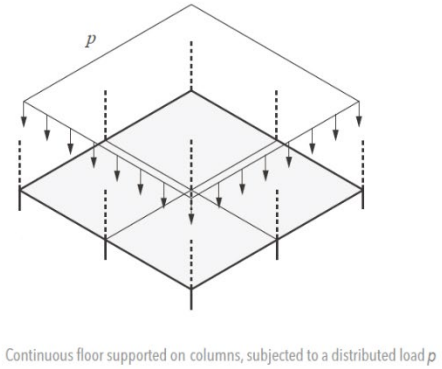

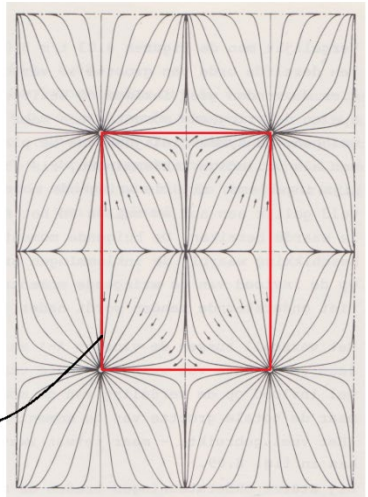

$$\frac{\partial \varphi_x}{\partial y} = \kappa_{xy} = m_{xy} = 0$$

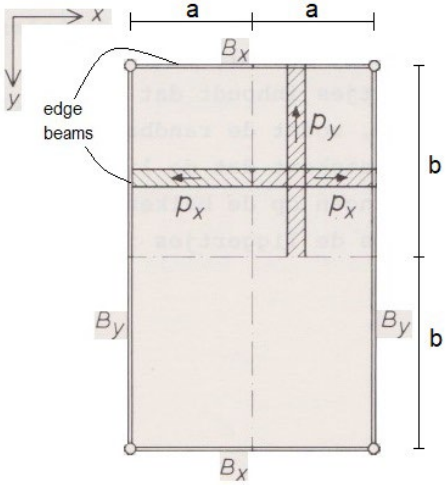

$$B_x \cdot B_y = K_x b \cdot K_y a$$

As long as the rotations perpendicular to the edge are zero there are two types of $\bar{M}$-hill permittable, slabs with a stiffness or the twistless case. For the last situation the shape of the $\bar{M}$-hill depends on the correct ratio of the "edge beam" stiffness *B* and the field stiffness *K*.

$$\frac{p_x}{K_x} = \frac{p_y b}{B_x} \rightarrow B_x = \frac{(1-\beta)}{\beta} K_x b$$
$$\frac{p_y}{K_y} = \frac{p_x a}{B_y} \rightarrow B_y = \frac{\beta}{(1-\beta)} K_y a$$
$$B_x \cdot B_y = K_x b \cdot K_y a$$

The "edge beam" of the $\bar{M}$-hill is equivalent to the edge zone of the shell, usually an upward edge.

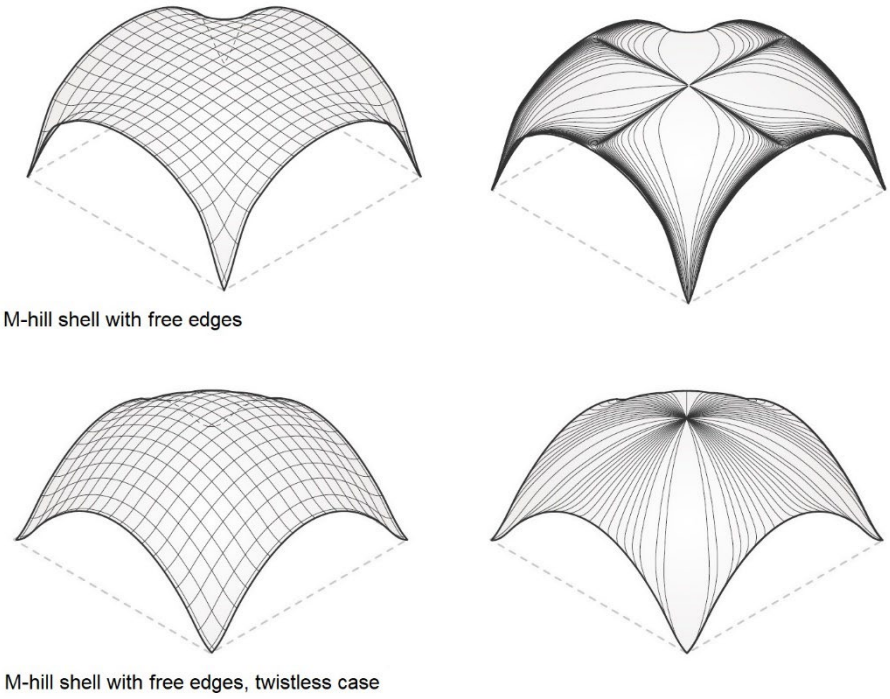

Figure 48 shell surfaces (shape function) is taken equal to surface of M-hill and its load distribution [image 101]

The $\bar{M}$-hill represents the flow of forces *v* of the load for the shell and depends on the boundary condition of the shell. The shape function of the shell, thus its form, and the internal stresses, governed by the stress function, depend on the flow of forces and the $\bar{M}$-hill.

$$\underbrace{\frac{d\bar{M}}{dx}}_{\substack{moment \\ hill}} = v_x = \underbrace{\bar{n}_{xx}\frac{\partial z}{\partial x} + \bar{n}_{xy}\frac{\partial z}{\partial y}}_{\substack{shape\ function\ / \\ stress\ function}}$$
$$\underbrace{\frac{d\bar{M}}{dy}}_{\substack{moment \\ hill}} = v_y = \underbrace{\bar{n}_{yy}\frac{\partial z}{\partial y} + \bar{n}_{xy}\frac{\partial z}{\partial x}}_{\substack{shape\ function\ / \\ stress\ function}}$$
$$p = -\left(\frac{\partial v_x}{\partial x} + \frac{\partial v_y}{\partial y}\right)$$

8.6 The relationship between the four functions

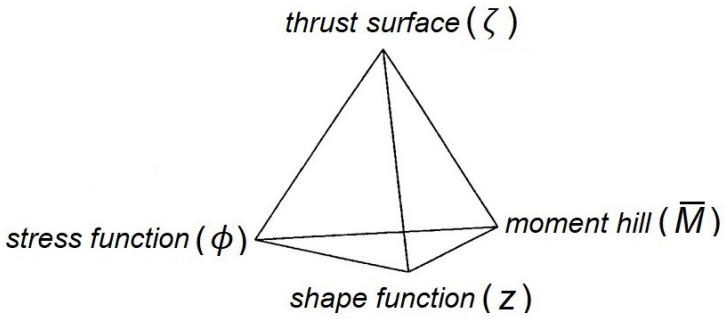

In previous section the close relationship between the four functions was shown that determine the shape of a shell in relation to its flow of forces.

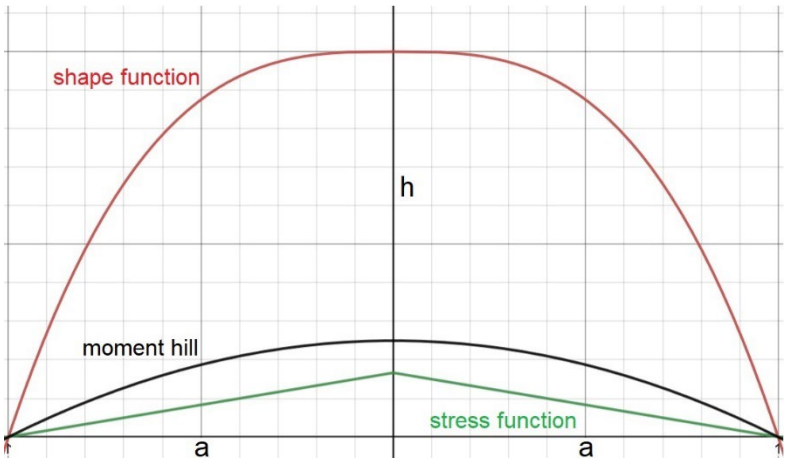

The example of the funicular will be further discussed. The $\bar{M}$-hill for a uniformly distributed *p* load is the parabola. For the equivalent loaded circular slab [97] the M-hill is the summation of the radial m_{rr} and tangential $m_{\theta\theta}$ moments.

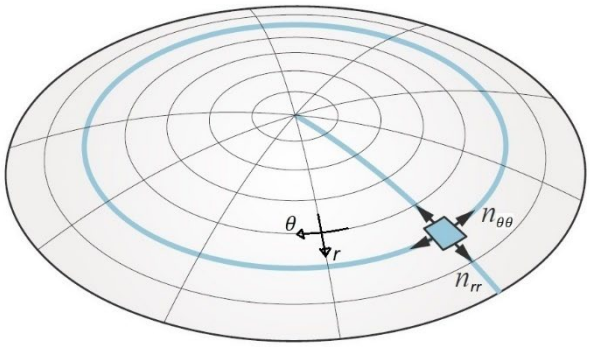

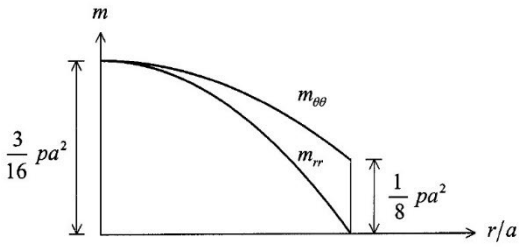

moments of circular slab with load p

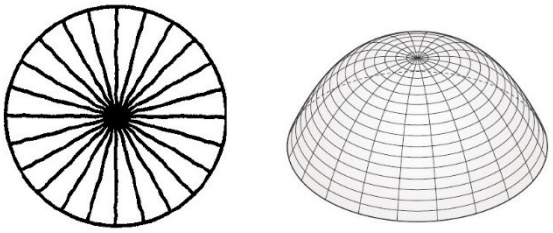

$m_{\theta\theta} = n_{\theta\theta} = 0$

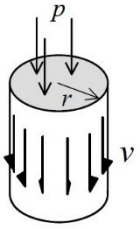

$P = \pi a^2 p$

The part of the radial moment not concerned with equilibrium but which is the result of compatibility issues will be discarded. Because the $\bar{M}$-hill is the summation of the two moments there are equivalent radial and tangential membrane forces in the shell. Both moments contribute to the flow of forces. With the funicular shell there are no radial forces. The funicular shell can be considered as an axisymmetric collection of orange peel shaped beams.
The "natural" flow of a uniformly distributed *p* load is the parabola, the funicular shell is an exception.

$$\frac{p}{n} = \left(\frac{\partial^2 z}{\partial r^2} + \frac{1}{r}\frac{\partial z}{\partial r}\right)$$

$$\rightarrow z_{"\bar{M}-hill"} = \frac{p}{4n}(r^2 - a^2)$$

$$use\ the\ analogy: -p = \left(\frac{\partial^2 \bar{M}}{\partial r^2} + \frac{1}{r}\frac{\partial \bar{M}}{\partial r}\right)$$

$$\rightarrow \bar{M}_{p-load} = \frac{p(a^2 - r^2)}{4} = m_{rr} + m_{\theta\theta,red} = \left(\underbrace{\frac{3p(a^2 - r^2)}{16}}_{m_{rr}} + \underbrace{\frac{p(3a^2 - r^2)}{16} - \frac{pa^2}{8}}_{m_{\theta\theta,red}}\right)$$

$$p\pi r^2 + v_r 2\pi r = 0 \rightarrow v_r = -\frac{pr}{2}\ or:$$

$$v_r = \frac{d\bar{M}}{dr} = \frac{dm_{rr}}{dr} + \frac{dm_{\theta\theta,red}}{dr} = -\frac{3pr}{8} - \frac{pr}{8} = -\frac{pr}{2}$$

$$M_{thrust} = \frac{p_0(a^3 - r^3)}{3a}, with\ p_0 = \frac{P}{2a\pi} = \frac{pa}{2}$$

$$\rightarrow M_{thrust} = \frac{p(a^3 - r^3)}{6}, \qquad and\ m_{\theta\theta} = 0$$

$$if\ r = 0\ then: M_{thrust} = \frac{p_0 a^2}{3} = \frac{pa^3}{6} : "H" = \frac{M}{h} = \frac{pa^3}{6h}$$

$$V_r = \frac{dM_{thrust}}{dr} = -\frac{p_0 r^2}{a} = -\frac{pr^2}{2}$$

$$V_r = v_r \cdot r \rightarrow v_r = -\frac{pr}{2}$$

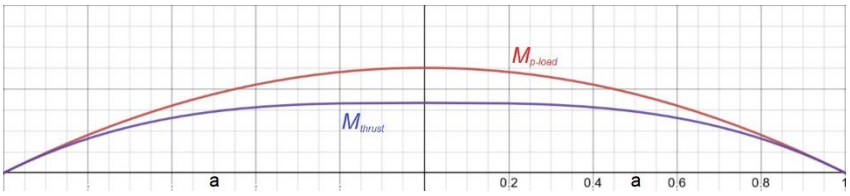

The relations between the functions will be exemplified by the equilateral triangular shell with semi-rigid edges. Start with constructing the $\bar{M}$-hill by virtue of the membrane analogy for slabs with the correct boundary conditions; a slab on three corner supports and with free edges. From the $\bar{M}$-hill follows the flow of forces. Then the shape function of the shell will be introduced. With the help of the projected forces and Pucher's equation the stress function can be derived and finally the internal membrane forces. In the next section the thrust surface will be extracted from the stress function.

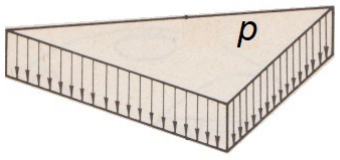

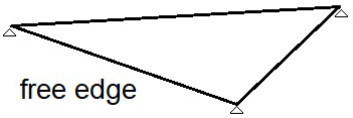

$$solve: \frac{p}{n} = \left(\frac{\partial^2 z}{\partial x^2} + \frac{\partial^2 z}{\partial y^2}\right), including\ the\ appropriate\ boundary\ conditions:$$

$$\rightarrow z_{"\bar{M}-hill"} = \frac{p}{12an}(3ax^2 + 3ay^2 - 2x^3 + 6xy^2 - 28a^3)$$

$$use\ the\ analogy: p = -\left(\frac{\partial^2 \bar{M}}{\partial x^2} + \frac{\partial^2 \bar{M}}{\partial y^2}\right)$$

$$\rightarrow \bar{M} = -\frac{p}{12a}(3ax^2 + 3ay^2 - 2x^3 + 6xy^2 - 28a^3)$$

$$v_x = \frac{d\bar{M}}{dx} = -\frac{p}{2a}(ax - x^2 + y^2) = \bar{n}_{xx}\frac{\partial z}{\partial x} + \bar{n}_{xy}\frac{\partial z}{\partial y}$$

$$v_y = \frac{d\bar{M}}{dy} = -\frac{p}{2a}(ay + 2xy) = \bar{n}_{yy}\frac{\partial z}{\partial y} + \bar{n}_{xy}\frac{\partial z}{\partial x}$$

$$-p = \frac{\partial v_x}{\partial x} + \frac{\partial v_y}{\partial y} \rightarrow -p = \left(\bar{n}_{xx}\frac{\partial^2 z}{\partial x^2} + 2\bar{n}_{xy}\frac{\partial^2 z}{\partial x \partial y} + \bar{n}_{yy}\frac{\partial^2 z}{\partial y^2}\right)$$

$$introduce\ shape\ function: z_{shell} = \frac{h}{4a^2}(x^2 + y^2 - 4a^2)$$

$$\rightarrow \frac{h}{2a^2}(\bar{n}_{xx} + \bar{n}_{yy}) + p = 0$$

$$with: \bar{n}_{xx} = \left(v_x - \bar{n}_{xy}\frac{\partial z}{\partial y}\right)\cdot\frac{\partial x}{\partial z}\ and\ \bar{n}_{yy} = \left(v_y - \bar{n}_{xy}\frac{\partial z}{\partial x}\right)\cdot\frac{\partial y}{\partial z}$$

$$\rightarrow \bar{n}_{xy} = -\frac{pay}{h}, substitute\ \bar{n}_{xy}\ in\ v_x\ and\ v_y\ and\ derive\ \bar{n}_{xx}\ and\ \bar{n}_{yy}$$

$$with: \bar{n}_{xx} = \frac{\partial^2 \phi}{\partial y^2}, \bar{n}_{yy} = \frac{\partial^2 \phi}{\partial x^2}, \bar{n}_{xy} = -\frac{\partial^2 \phi}{\partial x \partial y}\ to\ derive\ \phi$$

$$\rightarrow \phi = -\frac{pa}{6h}(3ax^2 + 3ay^2 + x^3 - 3xy^2 - 4a^3)$$

$$with\ transformation\ equations:$$

$$\lambda = \frac{\cos\varphi}{\cos\theta} = \sqrt{\frac{1 + (\partial z/\partial y)^2}{1 + (\partial z/\partial x)^2}}$$

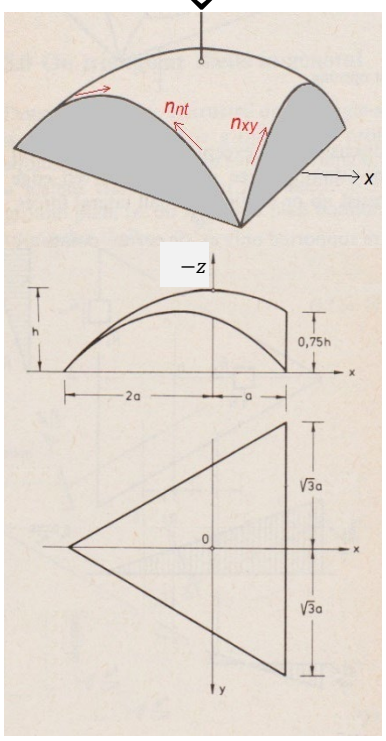

$$the\ solution\ above\ satisfies\ Pucher's\ equation$$

$$and\ corresponds\ with\ classic\ shell\ theory\ [94]: \begin{cases} n_{xx} = \bar{n}_{xx}\cdot\frac{1}{\lambda} = -\frac{pa}{h}(a - x)\cdot\frac{1}{\lambda} \\ n_{yy} = \bar{n}_{yy}\cdot\lambda = -\frac{pa}{h}(a + x)\cdot\lambda \\ n_{xy} = \bar{n}_{xy} = -\frac{pa}{h}y \end{cases}$$

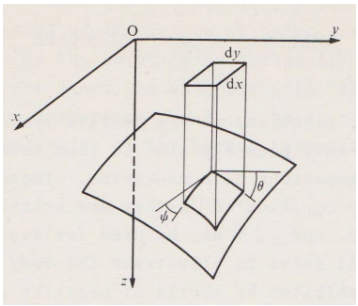

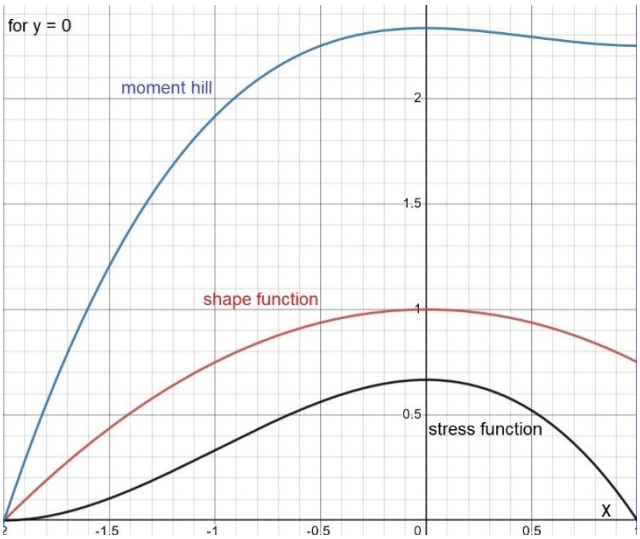

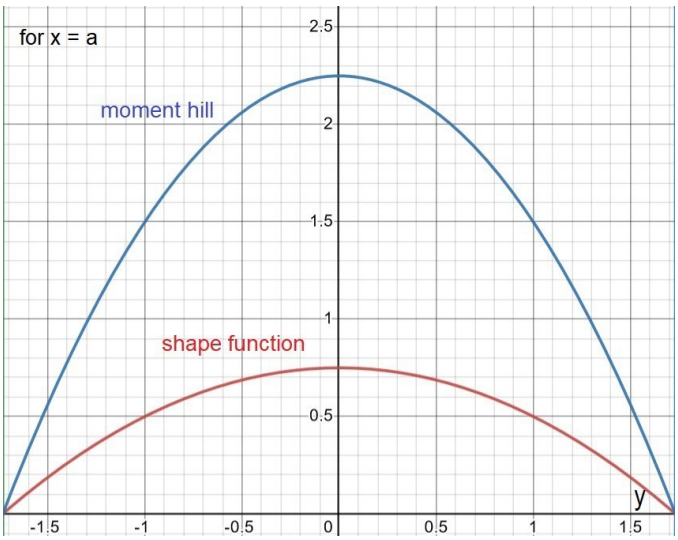

The solution of the membrane analogy is an approximate stylized $\bar{M}$-hill surface. By inspecting the function for the edge of the membrane / $\bar{M}$-hill it can be observed the edge zone of the surface is anti-clastic, this is due to the boundary conditions of the free edges.

$membrane\ equation$:

$$n\left(\frac{\partial^2 z}{\partial x^2}+\frac{\partial^2 z}{\partial y^2}\right)=p$$

$$with: z_{"\bar{M}-hill"}=\frac{p}{12an}(3ax^2+3ay^2-2x^3+6xy^2-28a^3)$$

$$\frac{\partial^2 z}{\partial x^2}=\frac{p}{2an}(a-2x)$$

$$\frac{\partial^2 z}{\partial y^2}=\frac{p}{2an}(a+2x)$$

$$for\ x=a\ \rightarrow z_{edge}=\frac{3p}{4n}(y^2-3a^2)$$

$$\frac{\partial^2 z}{\partial x^2}_{edge}=-\frac{p}{2n},\qquad \frac{\partial^2 z}{\partial y^2}_{edge}=\frac{3p}{2n}$$

$$\rightarrow n\left(-\frac{p}{2n}+\frac{3p}{2n}\right)=p$$

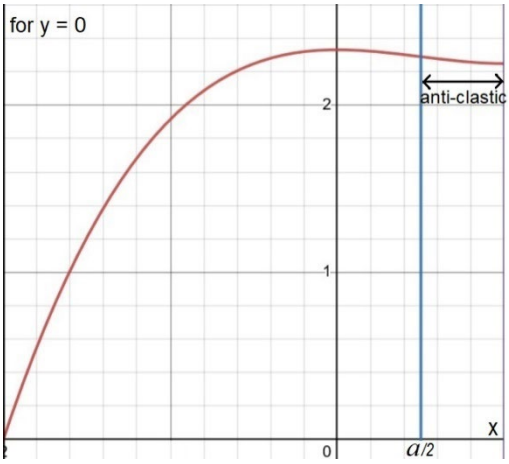

The boundary conditions involves a diaphragm due to the displacement perpendicular u_x to the edge being equal to zero. This results in the surface of the inflated membrane having an anti-clastic zone along the edge. The analogy with its equivalent slab is the concentrated shear force in the “hidden beam” along the edge.

$anti-clastic\ edge\ membrane$:

$$\frac{\partial^2 z}{\partial x^2}_{edge}=-\frac{p}{2n}$$

$$\frac{\partial^2 z}{\partial y^2}_{edge}=\frac{3p}{2n}$$

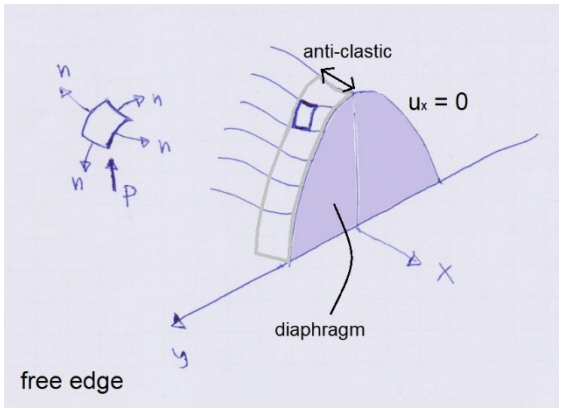

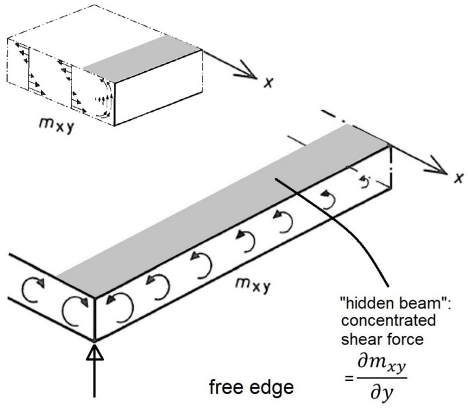

For constructing the surface of the $\bar{M}$-hill the force density method can be used [98, 99]. With this method inflated membrane surfaces can be relatively easily created. For more details see the thesis of Daoxuan Liang, “A Parametric Structural Design Tool (Grashopper Interface) for Plate Structures” [100].

Usually the total set of force density equations have too many unknowns to be solved, but for an inflated membrane the internal stress *n* is constant as is the load *p*. This means that in each link of the discretized mesh the force density is

equal. Together with the correct boundary conditions the equations can be solved resulting in the $\overline{M}$-hill. For a $\overline{M}$-hill with pinned supports the boundary conditions are simple, along all edges $z = 0$.

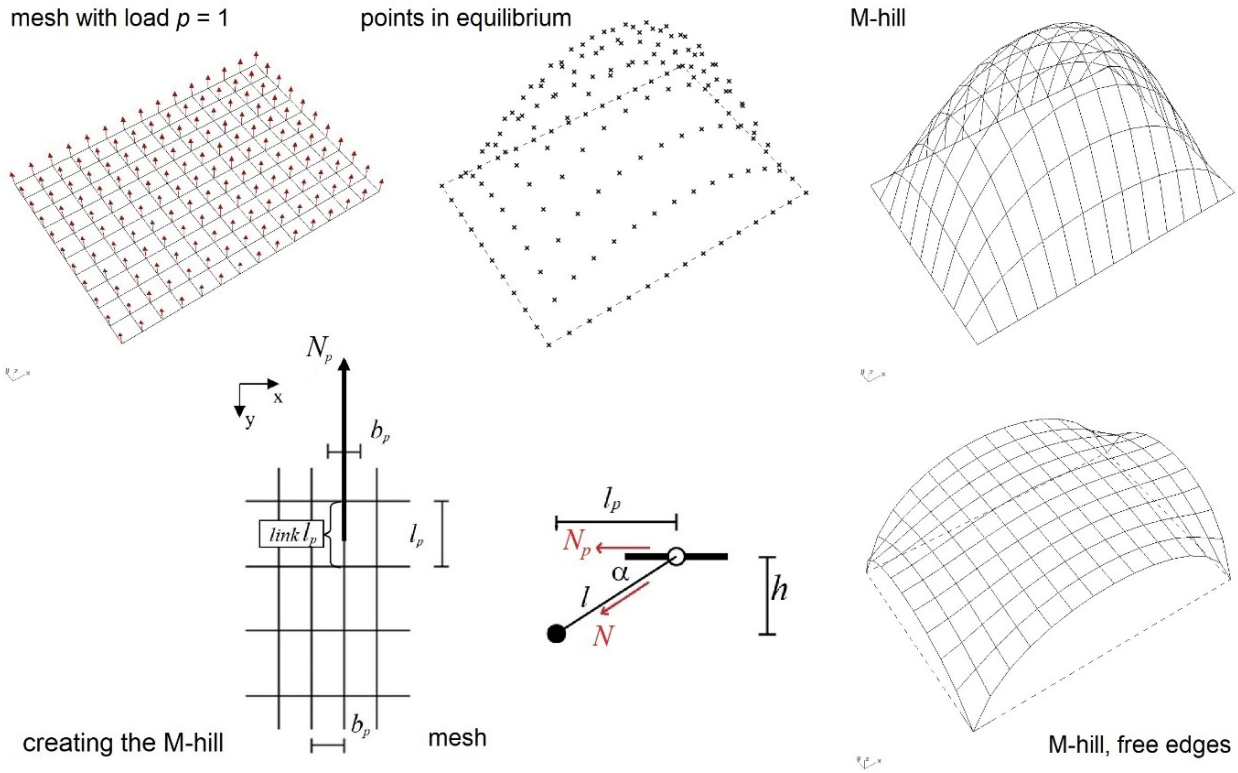

$$\frac{p}{n} = \left(\frac{\partial^2 z}{\partial x^2} + \frac{\partial^2 z}{\partial y^2}\right) \equiv p = -\left(\frac{\partial^2 \bar{M}}{\partial x^2} + \frac{\partial^2 \bar{M}}{\partial y^2}\right)$$

$$force\ density: q = \frac{N}{l} = \frac{N_p}{l_p}, N_p\ and\ l_p\ relate\ to\ the\ horizontal\ projection$$

$$with: N_p = n \cdot b_p \rightarrow q = \frac{nb_p}{l_p}\ and\ n = 1, p = 1$$

$$F_z = p \cdot l_p\ b_p$$

$$solve: \left(\sum \Delta z \cdot \frac{N_p}{l_p}\right) - F_{z,tot} = 0$$

$$include\ boundary\ conditions: \rightarrow \bar{M} - hill$$

Figure 49 constructing the M-hill using force density method [image 98]

But the $\overline{M}$-hill for the case with free edges, like the example of the equilateral triangle, requires that the correct upward curved edges needs to be determined first and then the rest of the surface can be constructed using the force density method. The edges can be determined with the help of the finite difference method.

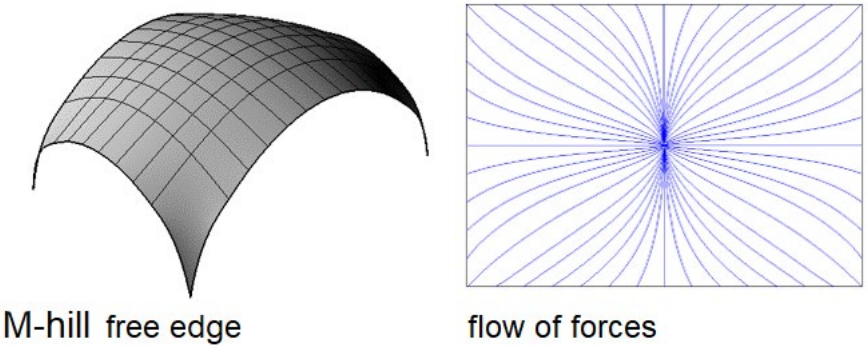

Figure 50 M-hill and its load distribution [images 100]

8.7 The reciprocity of the shape- and stress function

As can be observed from Pucher's equation the shape function and the stress function can be switched given an initial $\bar{M}$-hill as long as the result of their multiplication remains equal as they are reciprocal.
Once again the $\bar{M}$-hill analogy is used to derive the stress function in conjunction with a shape function, but with different boundary conditions. In this case fully pinned and able to take up thrust as well as shear forces.

$$solve: \frac{p}{n} = \left(\frac{\partial^2 z}{\partial x^2} + \frac{\partial^2 z}{\partial y^2}\right)$$

$$including\ the\ appropriate\ boundary\ conditions:$$

$$(x-a) = 0, \left(y - \frac{2a}{\sqrt{3}} - \frac{x}{\sqrt{3}}\right) = 0, \left(y + \frac{2a}{\sqrt{3}} + \frac{x}{\sqrt{3}}\right) = 0$$

$$z_{"\bar{M}-hill"} = K(x-a)\left(y - \frac{2a}{\sqrt{3}} - \frac{x}{\sqrt{3}}\right)\left(y + \frac{2a}{\sqrt{3}} + \frac{x}{\sqrt{3}}\right)$$

$$\rightarrow z_{"\bar{M}-hill"} = K\frac{-3ax^2 - 3ay^2 - x^3 + 3xy^2 + 4a^3}{3}$$

$$to\ satisfy\ the\ membrane\ equation \rightarrow K = -\frac{p}{4an}$$

$$z_{"\bar{M}-hill"} = \frac{p}{12an}(3ax^2 + 3ay^2 + x^3 - 3xy^2 - 4a^3)$$

$$use\ the\ analogy: p = -\left(\frac{\partial^2 \bar{M}}{\partial x^2} + \frac{\partial^2 \bar{M}}{\partial y^2}\right)$$

$$\rightarrow \bar{M} = -\frac{p}{12a}(3ax^2 + 3ay^2 + x^3 - 3xy^2 - 4a^3)$$

$$\bar{M} = -\frac{p}{12a}(\underbrace{3ax^2 + 3ay^2 - 3a^3}_{p-load} \underbrace{+x^3 - 3xy^2 - a^3}_{boundary\ condition})$$

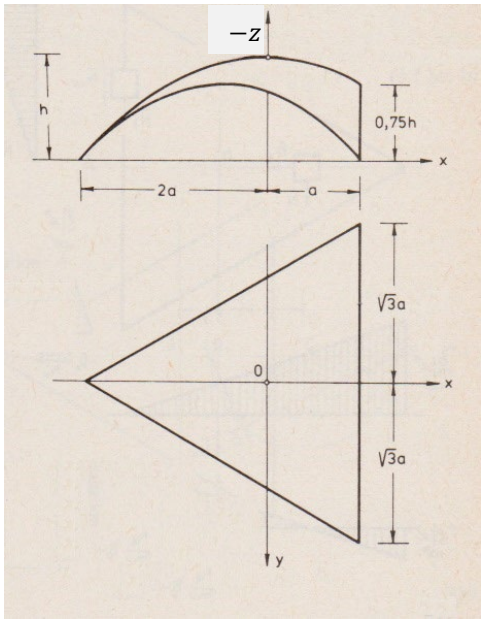

$$pinned\ edge\ conditions:$$
$$\bar{n}_{xx} \neq 0$$
$$\bar{n}_{xy} \neq 0$$

$$v_x = \frac{d\bar{M}}{dx} = -\frac{p}{4a}(x^2 + 2ax - y^2) = \bar{n}_{xx}\frac{\partial z}{\partial x} + \bar{n}_{xy}\frac{\partial z}{\partial y}$$

$$v_y = \frac{d\bar{M}}{dy} = -\frac{p}{4a}(2ay - 2xy) = \bar{n}_{yy}\frac{\partial z}{\partial y} + \bar{n}_{xy}\frac{\partial z}{\partial x}$$

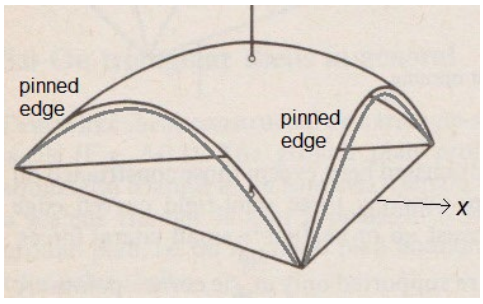

$$-p = \frac{\partial v_x}{\partial x} + \frac{\partial v_y}{\partial y} \rightarrow -p = \left(\bar{n}_{xx}\frac{\partial^2 z}{\partial x^2} + 2\bar{n}_{xy}\frac{\partial^2 z}{\partial x \partial y} + \bar{n}_{yy}\frac{\partial^2 z}{\partial y^2}\right)$$

$$introduce\ shape\ function: z_{shell,1} = \frac{h}{4a^2}(x^2 + y^2 - 4a^2)$$

$$\rightarrow \frac{h}{2a^2}\left(\bar{n}_{xx} + \bar{n}_{yy}\right) + p = 0$$

$$with: \bar{n}_{xx} = \left(v_x - \bar{n}_{xy}\frac{\partial z}{\partial y}\right)\cdot\frac{\partial x}{\partial z}\ and\ \bar{n}_{yy} = \left(v_y - \bar{n}_{xy}\frac{\partial z}{\partial x}\right)\cdot\frac{\partial y}{\partial z}$$

$$\rightarrow \bar{n}_{xy} = \frac{pay}{2h}, substitute\ \bar{n}_{xy}\ in\ v_x\ and\ v_y\ and\ derive\ \bar{n}_{xx}\ and\ \bar{n}_{yy}$$

$$with: \bar{n}_{xx} = -\frac{pa}{2h}(x + 2a), \bar{n}_{yy} = \frac{pa}{2h}(x - 2a), and\ derive\ \phi$$

$$\rightarrow \phi_1 = -\frac{pa}{12h}(6ax^2 + 6ay^2 - x^3 + 3xy^2 - C)$$

$$if\ x = -2a\ and\ y = 0\ then\ \phi = 0 \rightarrow C = 32a^3$$

The $\bar{M}$-hill belongs to the case of a simply supported slab, and thus the shell has pinned edges. After switching the shape function for the stress function the boundary conditions change accordingly, and thus the $\bar{M}$-hill.

$$\textit{the derived solutions satisfy Pucher's equation:}$$
$$\frac{\partial^2 z}{\partial x^2}\frac{\partial^2 \phi}{\partial y^2} - 2\frac{\partial^2 z}{\partial x \partial y}\frac{\partial^2 \phi}{\partial x \partial y} + \frac{\partial^2 z}{\partial y^2}\frac{\partial^2 \phi}{\partial x^2} + p = 0$$

$$\textit{the shape function and the stress function are reciprocal and can be switched:}$$
$$\phi_2 = -\frac{pa}{4h}(x^2 + y^2 - 4a^2)$$
$$z_{shell,2} = \frac{h}{12a^2}(6ax^2 + 6ay^2 - x^3 + 3xy^2 - 32a^3)$$
$$with: \bar{n}_{xx} = -\frac{pa}{2h}, \bar{n}_{yy} = -\frac{pa}{2h}, \bar{n}_{xy} = 0$$

The result is a vault like pinned shell, with no allowable shear forces along the edges.

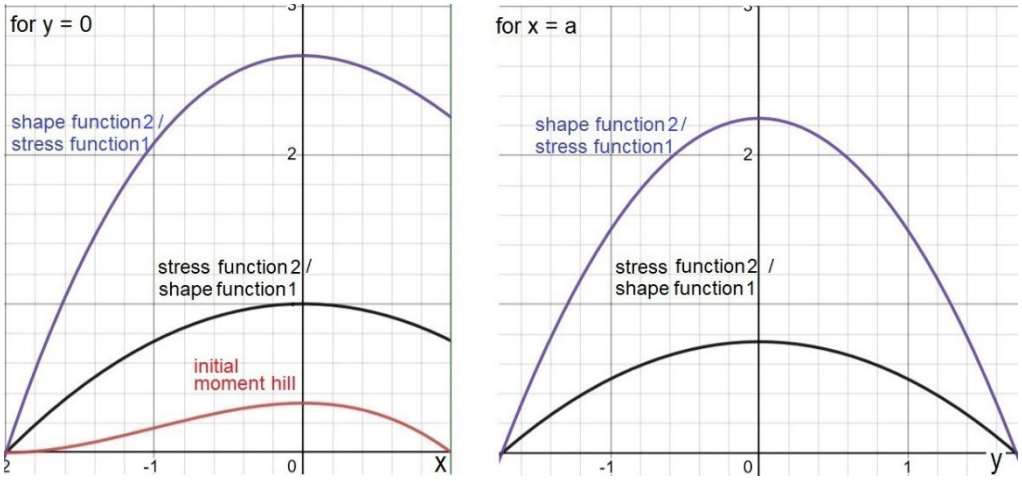

Both solutions satisfy Pucher's equation and carry the same load. But by switching the functions the load distribution changes due to the different boundary conditions.

$$v_x = \bar{n}_{xx}\frac{\partial z}{\partial x} = -\frac{p}{8a}(-x^2 + 4ax + y^2)$$
$$v_y = \bar{n}_{yy}\frac{\partial z}{\partial y} = -\frac{p}{8a}(4ay + 2xy)$$
$$v_x = \frac{d\bar{M}}{dx} \rightarrow \bar{M}_x = \frac{p}{24a}(-6ax^2 - 3xy^2 + x^3)$$
$$v_y = \frac{d\bar{M}}{dy} \rightarrow \bar{M}_y = \frac{p}{24a}(-3xy^2 - 6ay^2)$$
$$\rightarrow \bar{M} = \bar{M}_x + \bar{M}_y = -\frac{p}{24a}(6ax^2 + 6ay^2 - x^3 + 3xy^2 - C)$$
$$if\ x = -2a\ and\ y = 0\ then\ M = 0 \rightarrow C = 32a^3$$

$$\textit{the } \bar{M} - \textit{hill complies with the membrane equation}$$

8.8 From stress function to thrust surface

In the thesis of Pim Buskermolen, “Shell Structures, On the relationship between moment hills, stress functions and thrust surfaces in the design of shell structures” [101] the parametric relation between the stress function and the thrust surface can be found. This was done using a parametric tool based on the reciprocal figure (Maxwell, 1864) [102] of the polyhedron Airy stress function.

But first the other method will be discussed via the force density method and the primal grid.

	Discretized surface	Surface
Horizontal equilibrium	Polyhedral Airy stress function	Airy Stress function
Vertical equilibrium	Force Density Method	Pucher’s Equation

When Pucher’s equation is discretized it results in the force density equations, apart from representing its middle term regarding the membrane shear force. This omission is solved by adding shear panels or diagonals to the network.
A thrust network, in this case with shear panels, or its equivalent diagonals so that the network is form stable, is used. The network can be solved by minimizing its overall total complementary energy (section 4.5) or by solving its stress function using the method from section 8.10. A horizontal projection of the thrust network can be made, the primal grid.

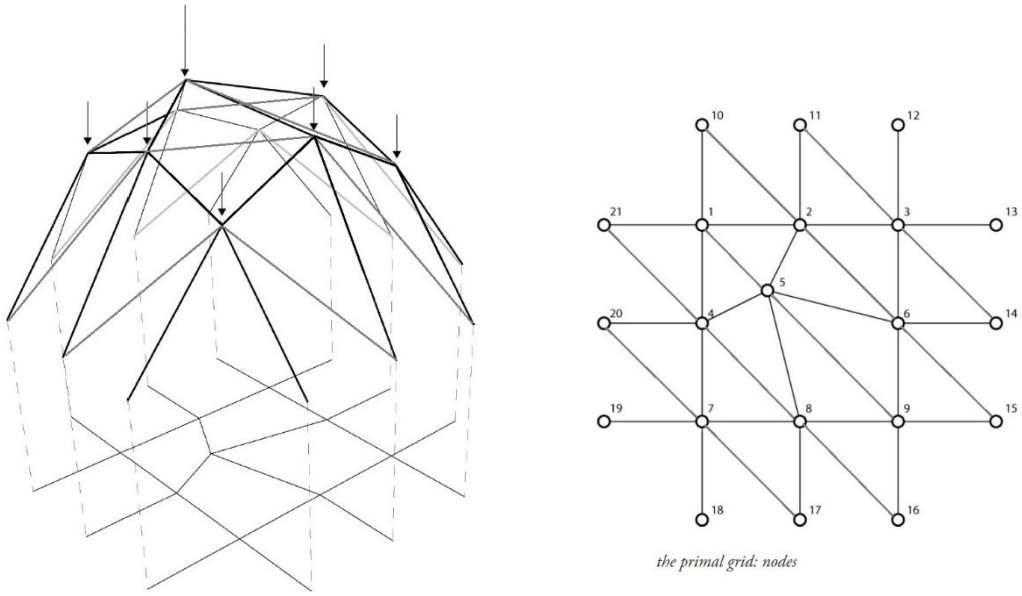

Figure 51 form stable thrust network and its primal grid: the horizontal projection

When the problem has been solved by the complementary energy method the entire geometry of the thrust network is fixed, including the he heights of the nodes of the thrust network.
Alternatively when the stress function has been solved (via the method of section 8.10), the projected forces are known, which lie in the same plane as the primal grid.

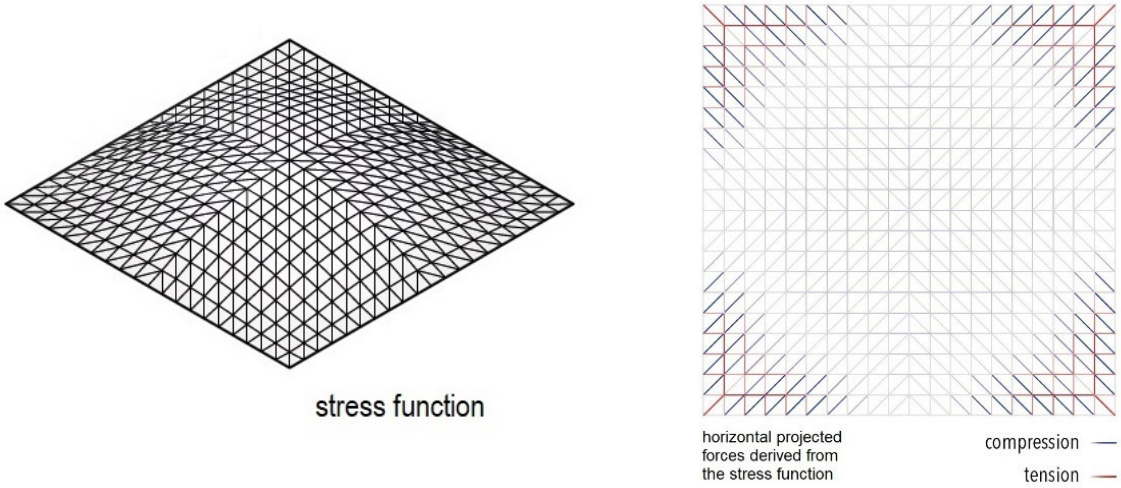

Figure 52 (polyhedral) stress function and its horizontal projected forces [images 101]

From the primal grid the connectivity, projected length and the position of the nodes and bars can be extracted. These can be used together with the force density formulas (section 2.9) to determine the heights of the nodes of the thrust network.

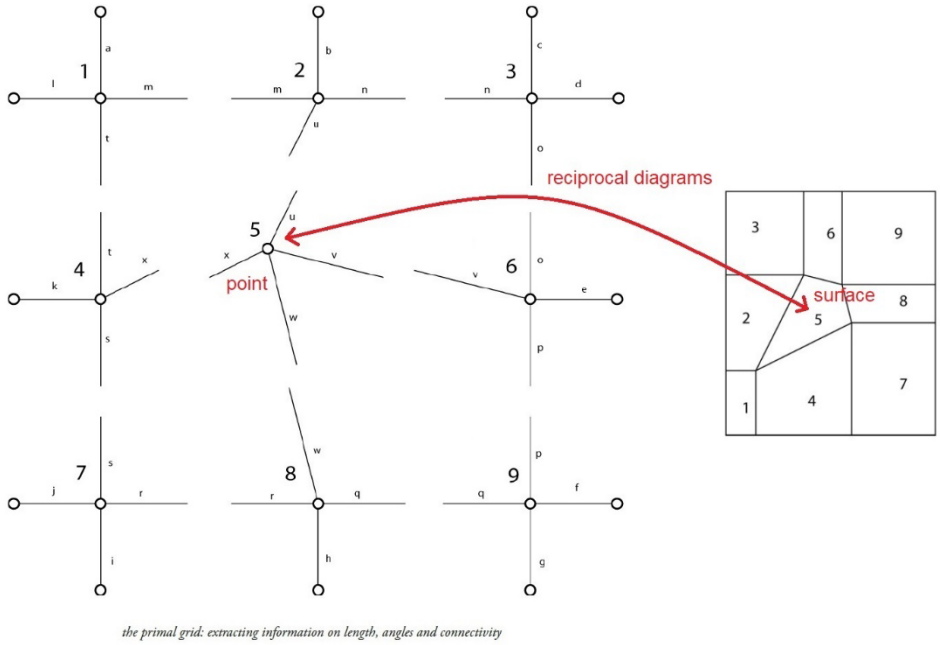

Figure 53 reciprocal diagrams: primal grid and force polygon of horizontal projected forces [images 103]

Normally the force density formulas cannot be solved as there are too many unknowns. But because the projected forces can be taken from the discretized stress function. The force density of a bar in the network is equal to the force density of the projected bar. There is now enough information to be able to solve the equations. Including the boundary conditions, as there are now as many unknowns as equations. All the z-coordinates of the network can be solved [103].

-value's for Force Density from Stress Function $\frac{N_p}{l_p}$ ⟵ projected force taken from stress function

⟵ projected bar length taken from primal gird

$$\sum Z;5: (z_5 - z_2)\frac{N_b}{l_b} + (z_5 - z_6)\frac{N_e}{l_e} + (z_5 - z_8)\frac{N_g}{l_g} + (z_5 - z_4)\frac{N_d}{l_d} - F_{z;5} = 0$$

-remove variables

$$\sum Z;5: (z_5 - z_2)\frac{N_b}{l_b} + (z_5 - z_6)\frac{N_e}{l_e} + (z_5 - z_8)\frac{N_g}{l_g} + (z_5 - z_4)\frac{N_d}{l_d} - F_{z;5} = 0$$

-solve the system $\left(\sum \Delta z * \frac{N_p}{l_p}\right) - F_{z,tot} = 0$

The second method, as described in Buskermolen, uses a reciprocal figure of the stress function for the thrust surface. See image 54: (≡) For this purpose the $\bar{M}$-hill and the shape function of the shell are taken to be equal. (1) The $\bar{M}$-hills have been produced by the method as described in section 8.6. (2) From the $\bar{M}$-hill via the method described in section 8.10 the stress function has been determined.

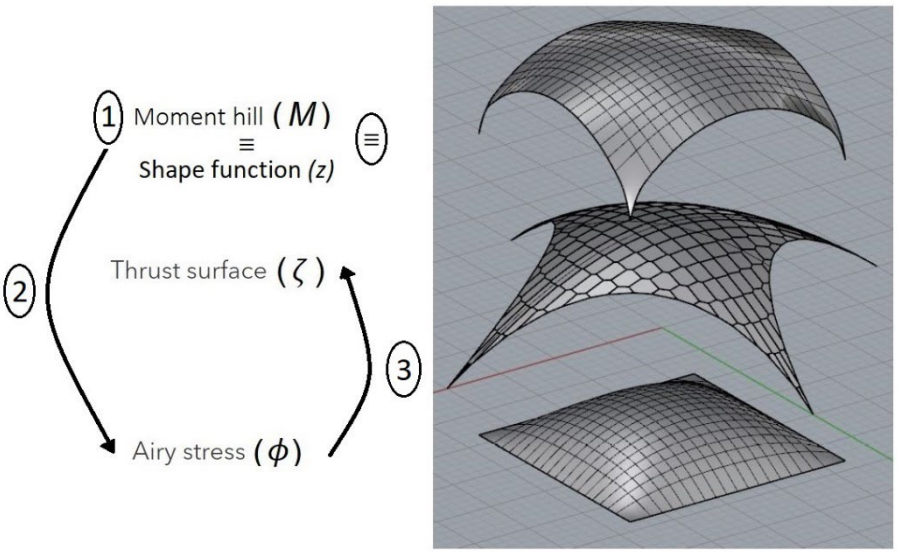

Figure 54 relation of the three surfaces [image 101], whereby for this example the M-hill and the shape function are equal

(3) The discretized stress function is the polyhedral stress function for which there is a reciprocal figure [104], the thrust surface.

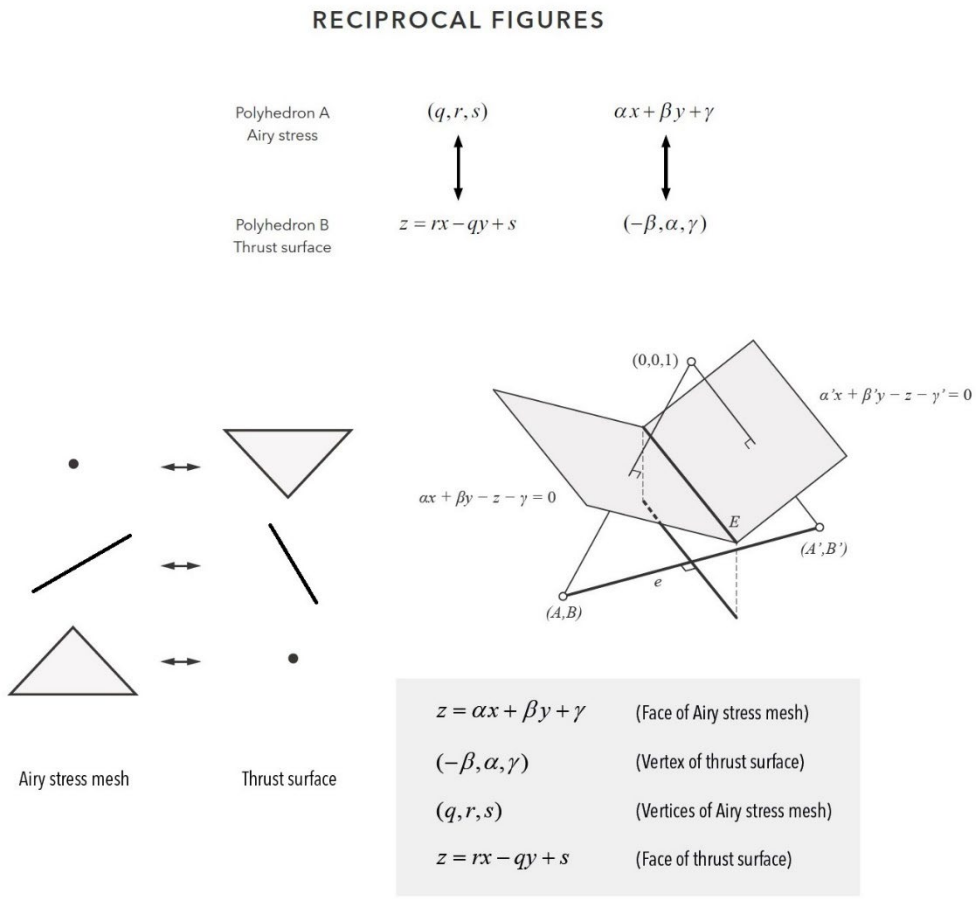

Figure 55 creating reciprocal figures [images 101]

The flow chart and the complete procedure is discussed in the thesis of Pim Buskermolen. Here is a result of an example.

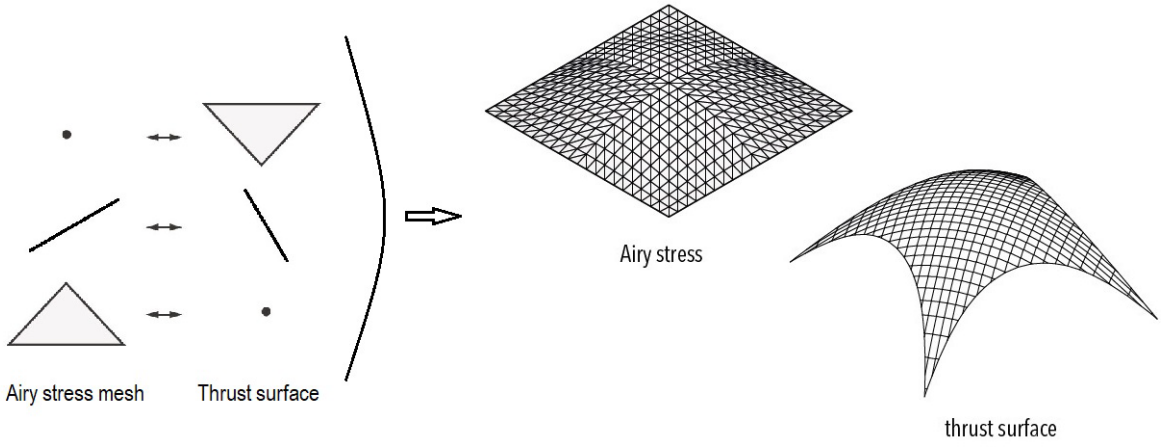

Figure 56 reciprocal figures: (polyhedral) stress function and the thrust surface [images 101]

The $\bar{M}$-hill, the stress function and the thrust surface of the semi-rigid case.

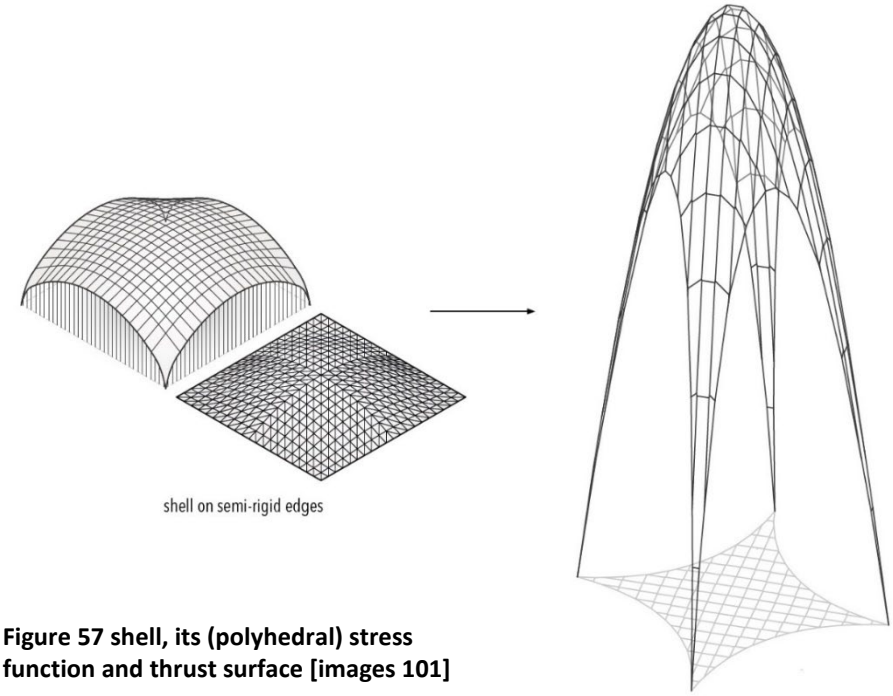

Figure 57 shell, its (polyhedral) stress function and thrust surface [images 101]

It is observed that the thrust surface has a different foot print than that of the $\bar{M}$-hill. The shown thrust surface only contains the compression membrane forces, but for the semi-rigid case with straight edges there are also membrane forces in tension in the edge zone. This result is to be expected, as was explained at the beginning of section 8.5.

The shape function (in this case the $\bar{M}$-hill) on a rectangular base with semi-rigid edges has infinity high (shear) stresses in the corners due to the *p*-load. The membrane state of stress for this case has a stress function which reciprocal diagram results in a non-continuous surface along the edges. It has a turned-up "truss-like" edge, with alternating trajectories of tension and compression.

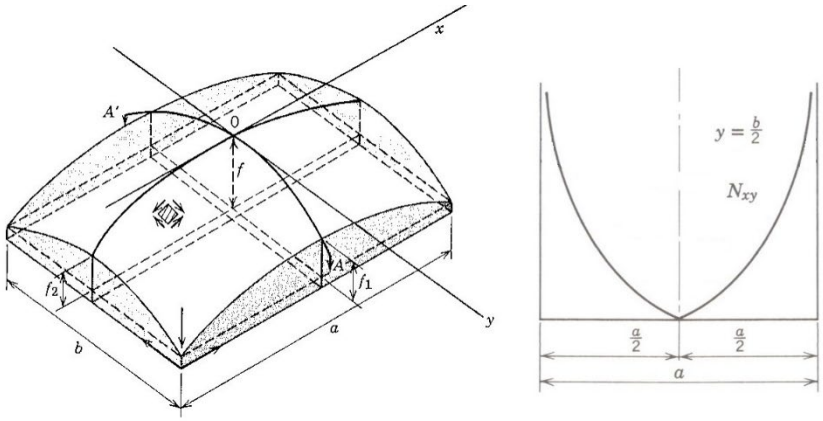

This membrane state of stress is an idealisation and in fact the *p*-load in the corners is predominantly carried by moments and shear forces (p_b-load) and less by membrane forces (p_s-load), see section 8.10.

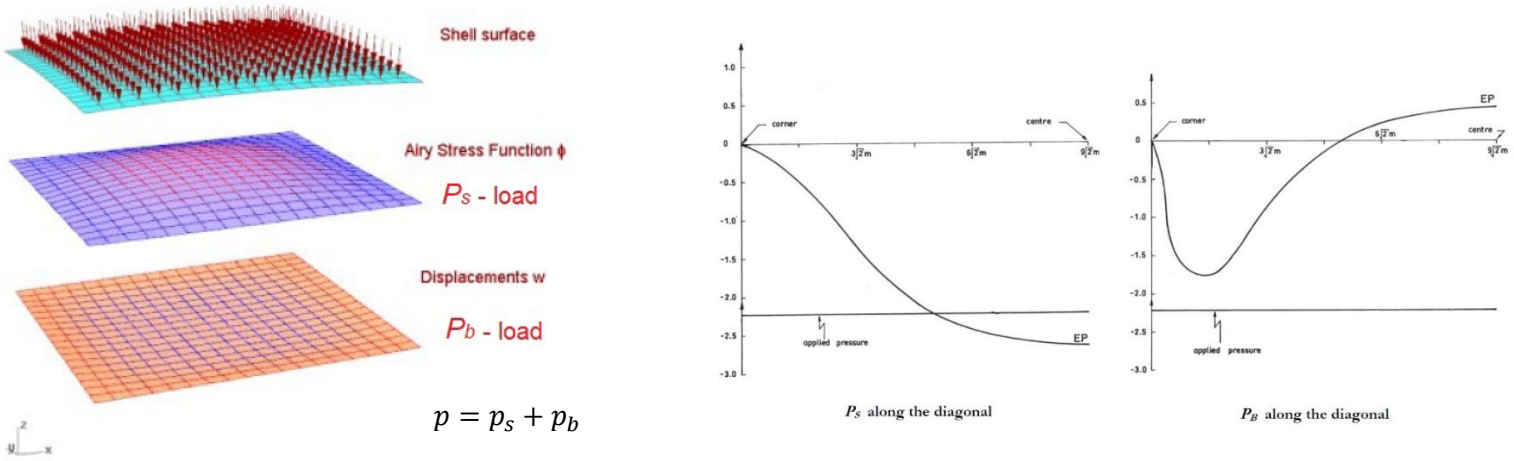

Figure 58 load carried by membrane forces and bending moments [image left 108, right 107]

As with the thrust line of an arch, the height of the thrust surface of a shell can be scaled with the intensity of the load.

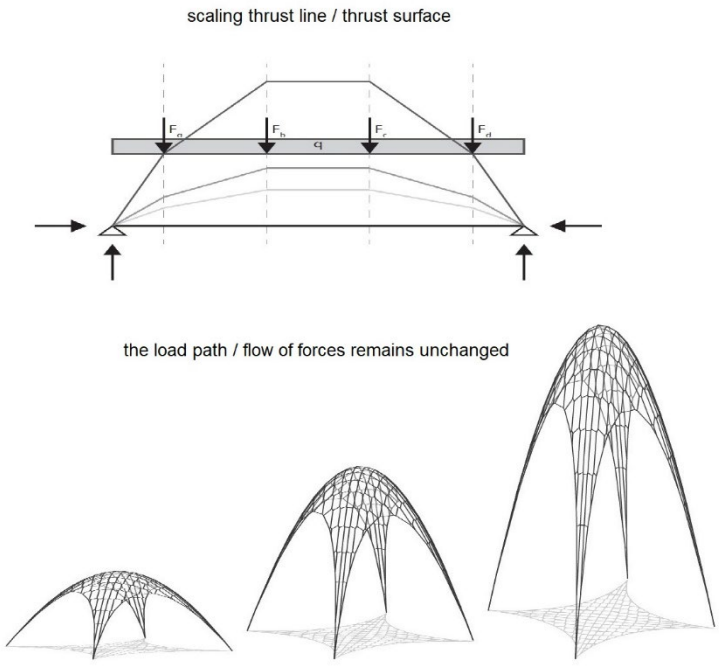

Figure 59 scaling the thrust surface [image 101]

Alternative to the polyhedral stress function, the continuous stress function can be used as described by Maxwell [105] to find the reciprocal diagram, in this case again the thrust surface (ζ).

Maxwell (1868) proposed a mapping between two functions, say $F(x,y)$ and $F^*(\xi,\eta)$:

$$\xi = \frac{\partial F}{\partial x}, \quad \eta = \frac{\partial F}{\partial y}, \quad F^* = x\frac{\partial F}{\partial x} + y\frac{\partial F}{\partial y} - F,$$
$$x = \frac{\partial F^*}{\partial \xi}, \quad y = \frac{\partial F^*}{\partial \eta}, \quad F = \xi\frac{\partial F^*}{\partial \xi} + \eta\frac{\partial F^*}{\partial \eta} - F^*.$$

When $F(x,y)$ and $F^*(\xi,\eta)$ are smoothly differentiable, a point on $F(x,y)$ maps to another point on $F^*(\xi,\eta)$, and vice versa, thus Maxwell classified them as reciprocal diagrams.

Figure 59 mapping of reciprocal diagrams [image 74]

For uniformly distributed *p* load the thrust surface (ζ) will be derived by taking the reciprocal diagram of the stress function of its $\bar{M}$-hill, which is again taken equal to the shape function.

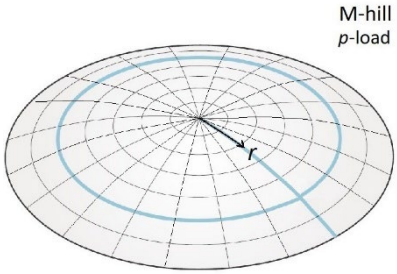

$$\bar{M}_{p-load} = \frac{p(a^2 - r^2)}{4}$$
$$v = \frac{d\bar{M}}{dr} = -\frac{pr}{2}$$

Maxwell's method for mapping reciprocal diagrams will be used for the procedure.

$$take\ for\ the\ shape\ funtion\ the\ moment\ hill: z_{\bar{M}-hill} = \frac{p(a^2 - r^2)}{4}$$
$$\frac{1}{r}\frac{\partial \phi}{\partial r}\cdot\frac{dz}{dr} = \frac{d\bar{M}}{dr} \rightarrow \frac{1}{r}\frac{\partial \phi}{\partial r}\cdot -\frac{pr}{2} = \frac{pr}{2} \rightarrow \phi = \int \frac{\partial \phi}{\partial r}dr = \int -r dr = -\frac{r^2}{2} + C$$
$$with: r = a\ and\ \phi = 0 \rightarrow C = \frac{a^2}{2}$$
$$\phi_{\bar{M}-hill} = \frac{(a^2 - r^2)}{2}$$
$$Maxwell:\ F^* = \frac{\partial F^*}{\partial \xi}\frac{\partial F}{\partial r} - F$$
$$with: F = \phi_{\bar{M}-hill} \rightarrow$$
$$F^* = \left(\frac{\partial F^*}{\partial \xi}\cdot -r\right) - \frac{(a^2 - r^2)}{2}$$
$$and\ take\ \xi = r\ for\ equivalent\ scale$$
$$\rightarrow\ F^* = \zeta = \frac{(\xi^2 - 3a^2)}{6}$$
$$or\ including\ scalefactor\ \varsigma: \frac{(\xi^2 - \varsigma a^2)}{6}$$

The derived formula results in a scalable thrust surface.

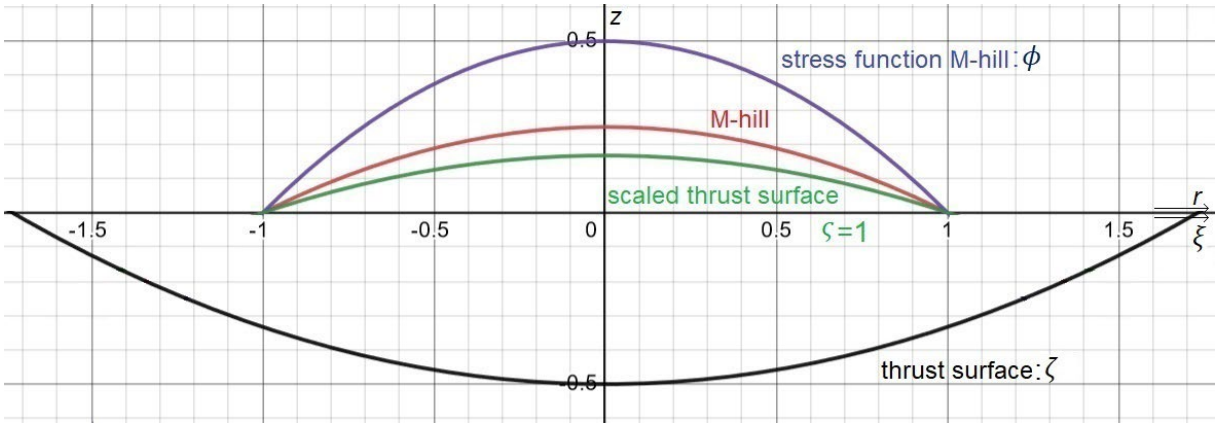

The thrust surface of the *p*-load is parabolic, which means that it has meridian as well as hoop forces in the thrust surface. Just as with the arch, the projected meridian forces $\bar{n}_{rr}$ are constant.

The thrust surface of the *p*-load which has no hoop forces is cubic (section 7.3) and is not the reciprocal diagram of the stress function of the $\bar{M}$-hill. For the cubic thrust surface the horizontal thrust $\bar{N}_r$ is constant and the projected meridian forces $\bar{n}_{rr}$ are not, see also section 7.6.

$$
\begin{aligned}
&parabolic\ thrust\ surface:\\
&\rightarrow thrust\ surface\ is\ the\ reciprocal\ diagram\ of\\
&\bar{M}-hill\ stress\ function\\
&\bar{n}_{rr}=\bar{n}_{\theta\theta}=constant
\end{aligned}
$$

$$
\begin{aligned}
&cubic\ thrust\ surface:\\
&\rightarrow thrust\ surface\ is\ not\ the\ reciprocal\ diagram\ of\\
&\bar{M}-hill\ stress\ function\\
&\bar{N}_r="H"=\bar{n}_{rr}r=constant\\
&\bar{n}_{rr}\neq constant
\end{aligned}
$$

The reason for this is that the cubic thrust surface has no two dimensional state of stress, like the parabolic thrust surface does have.
In fact the cubic thrust surface is a one dimensional corbel-like arch ("*false* arch") turned into a surface of revolution. When the stress function of the cubic funicular arch, of section 7.2, is derived we can compare it with the parabolic funicular arch, see section 6.2.

$$
\begin{aligned}
&\frac{\partial^2\phi}{\partial y^2}\,\frac{\partial^2 z}{\partial x^2}=q=\frac{2q_0x}{a}\\
&z_{arch}(x)=\frac{h(a^3-x^3)}{a^3}\Rightarrow\frac{\partial^2 z}{\partial x^2}=-\frac{6hx}{a^3}\\
&\phi=\iint\frac{\frac{2q_0x}{a}}{-\frac{6hx}{a^3}}dy\Rightarrow\phi=-\frac{q_0a^2}{6h}y^2+\cdots\\
&\frac{\partial^2\phi}{\partial y^2}=-\frac{q_0a^2}{3h}=H
\end{aligned}
$$

Both their stress function is parabolic in one direction, which means that for each case the horizontal thrust *H* is constant. If the comparison is extended to their respective domes (section 7.6), it can be observed that the two stress functions are no longer congruent. The horizontal thrust "*H*" of the cubic dome remains constant

$\underline{parabolic: x^2}$	$\underline{cubic: x^3}$
$arch: \phi = -\frac{qa^2}{4h}y^2, with\ f^* = h$	$arch: \phi = -\frac{q_0 a^2}{6h}y^2$
$dome: \phi = \frac{a^2 p(a^2 - r^2)}{8h}$	$dome: \phi = \frac{a^3 p(a - r)}{6h}$

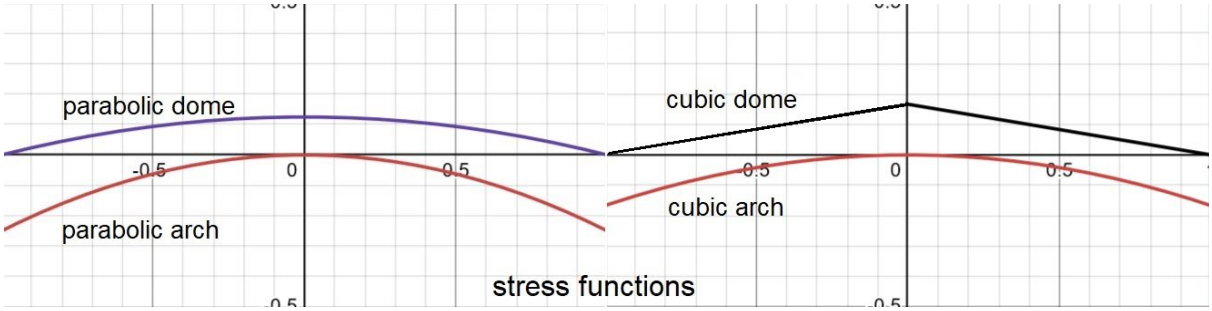

.

8.9 Discussion; bending moments in shells structures

Not for all shapes or boundary conditions for shell design is there a membrane only solution. Some out-of-plan bending is inevitable, this should be minimized as much as possible. In addition to the four basic functions the displacement field, and thus moments and shear forces, play a role when bending is needed to complement the membrane forces in carrying the load, as is explained in section 8.10.

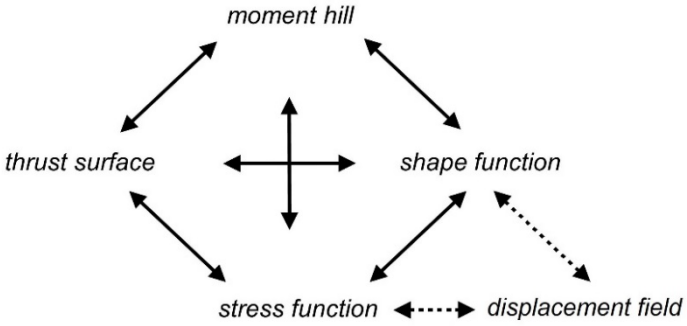

One of the Heinz Isler models scanned and analysed by Peter Eigenraam and Andrew Borgart is the shell design for a series of sports halls built by Isler [106]. For the purpose of analysing its behaviour the author devised a simple method to assess the structural performance of the shell, see section 5.7.

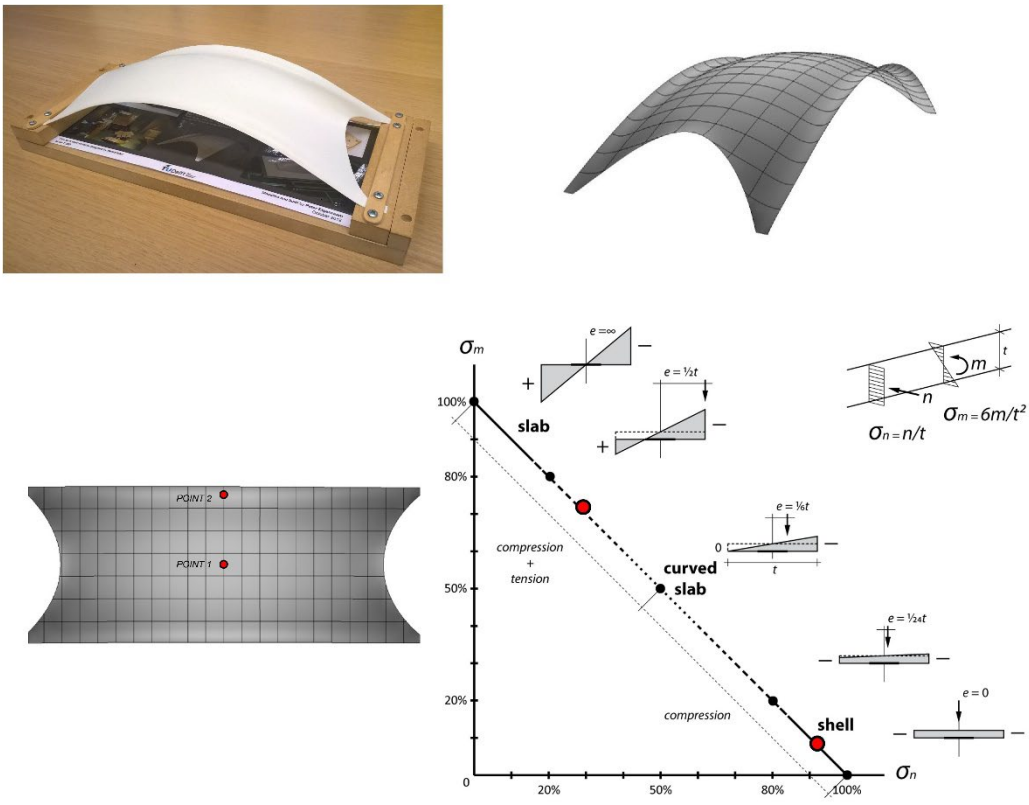

Figure 60 analysing shell Heinz Isler [images 106]

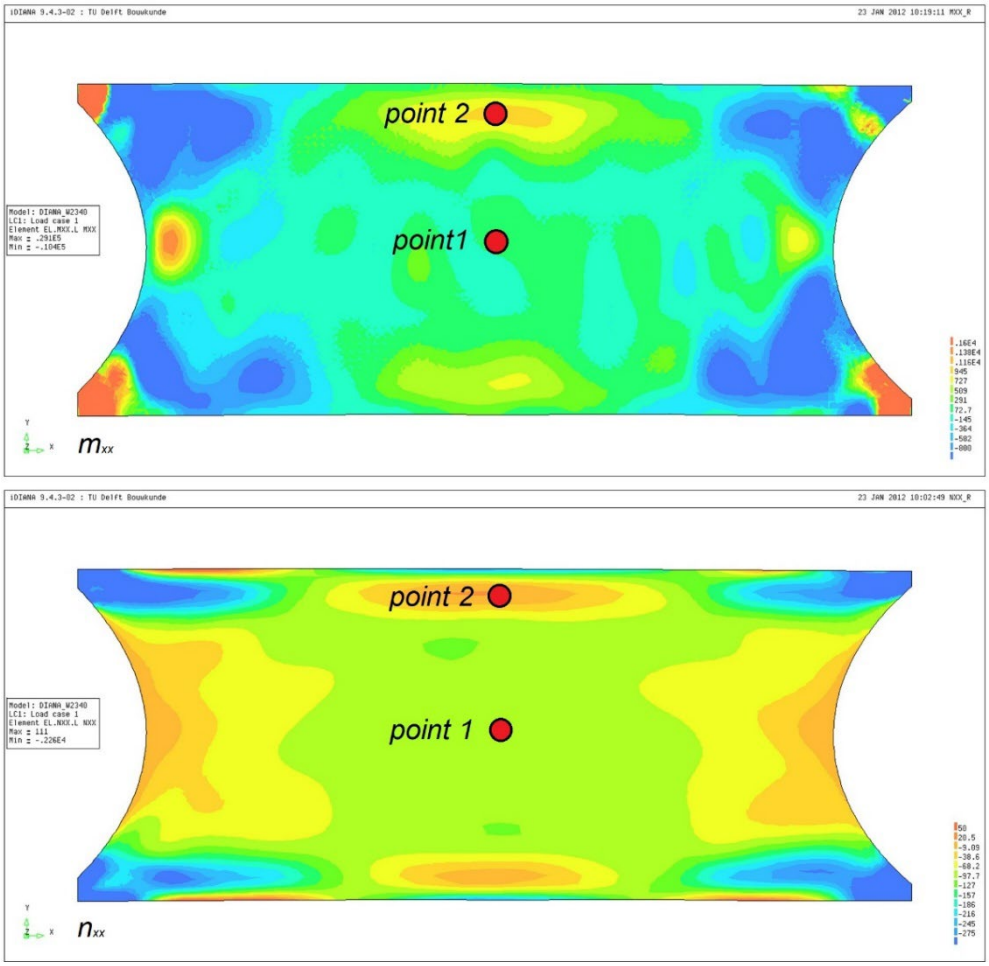

Figure 61 FEM calculations shell Heinz Isler [images 106]

The assessment takes into account the ratio of stresses as a result of internal membrane forces σ_n and of bending moments σ_m, and distinguishes parts of the shell being in compression or a combination of tension and compression. The shell can be assessed as being in a state of a pure membrane, a slab loaded out-of-plane or as something in between, more a curved slab. The assessment is also correlated to the eccentricity of the thrust line with regard to the shells axis.

As can be observed for the Isler shell the curved upward edge zones, needed to limit the deflection as a result of asymmetric loads, have considerable amount of out-of-plane bending. The synclastic curved part of the shell is nearly a perfect membrane shell in compression. This is a nice example of the necessity to have some degree of bending in a shell.

The demonstrated methods in this thesis can be further developed and integrated and used for designing and analysing shell structures. The advantage of a software tool or tools would be its ability to explore the shell's structural

behaviour in a visual manner in a design process. FEM calculation would then only be needed at the very end of the design stage to verify the results.

By optimizing the flow of forces and thus the load distribution a complex geometry shape was found with a minimum of bending moments and most of the loads are carried by membrane forces. The flow of forces is shown a particle “rain shower” which represents the load path, in fact the shape function of this shell was very close to the $\bar{M}$-hill for this case.

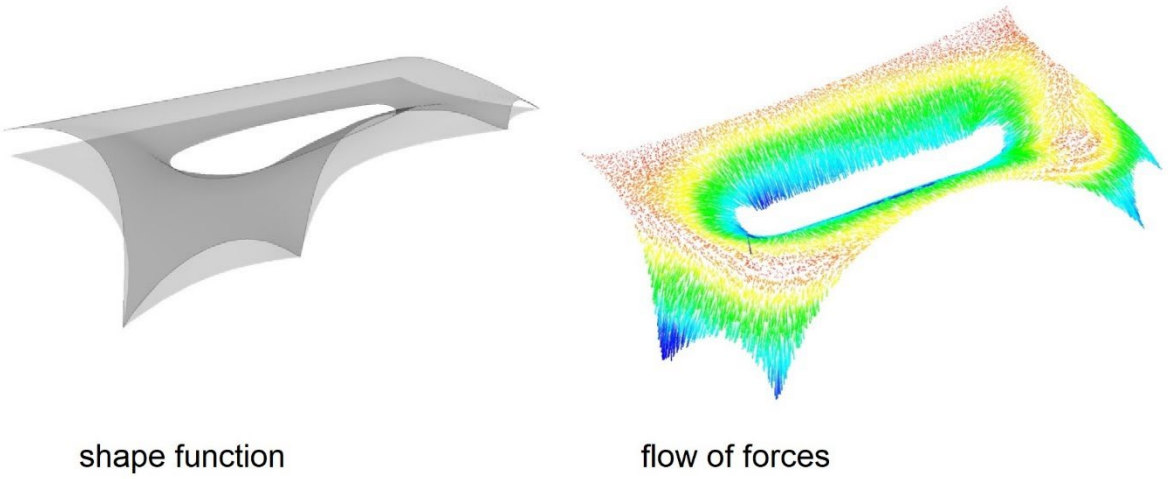

Figure 62 “rain shower” , load distribution of shell [images 52]

During the form finding process the flow of forces was the driving principle and in each iteration of the process it could be observed after each slight modification of the form that the amount of bending moment in the shell decreased.

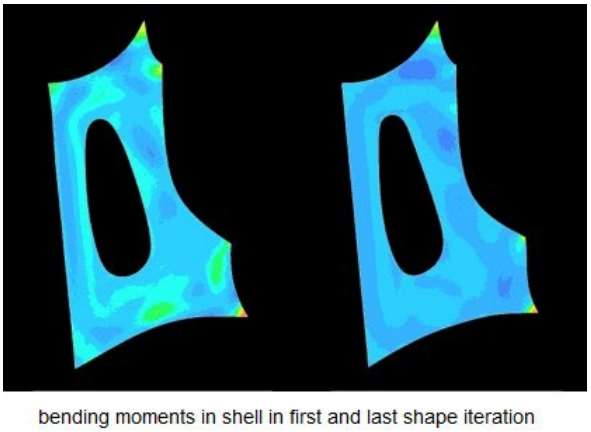

Figure 63 FEM calculation shell, top view [images 52]

In most cases shell structures have a certain degree of bending moments, in the next section it will be explained how these can be determined by solving the static-geometric relations for thin shells, see the next section.

8.10 Numerical procedure for solving the static-geometric relations for thin shells

As concluded in section 8.3 square shells will always have some bending moments and shear forces to help carry the loads, this holds in general for most shells. In other words the thrust surface is no longer material independent, and the flow of forces resulting from the $\bar{M}$-hill can no longer be exclusively resolved into membrane forces.

$$p = p_b + p_s$$

$$v_x = \underbrace{\bar{n}_{xx}\frac{\partial z}{\partial x} + \bar{n}_{xy}\frac{\partial z}{\partial y}}_{p_s} + \underbrace{\frac{\partial m_{xx}}{\partial x} + \frac{\partial m_{xy}}{\partial y}}_{p_b}$$

$$v_y = \underbrace{\bar{n}_{yy}\frac{\partial z}{\partial y} + \bar{n}_{xy}\frac{\partial z}{\partial x}}_{p_s} + \underbrace{\frac{\partial m_{yy}}{\partial y} + \frac{\partial m_{xy}}{\partial x}}_{p_b}$$

$$p = -\frac{\partial v_x}{\partial x} - \frac{\partial v_y}{\partial y} \rightarrow$$

$$p = \underbrace{-\left(\frac{\partial^2 z}{\partial x^2}\frac{\partial^2 \phi}{\partial y^2} - 2\frac{\partial^2 z}{\partial x \partial y}\frac{\partial^2 \phi}{\partial x \partial y} + \frac{\partial^2 z}{\partial y^2}\frac{\partial^2 \phi}{\partial x^2}\right)}_{p_s} - \underbrace{\left(\frac{\partial^2 m_{xx}}{\partial x^2} + 2\frac{\partial^2 m_{xy}}{\partial x \partial y} + \frac{\partial^2 m_{yy}}{\partial y^2}\right)}_{p_b}$$

In this case the full set of shell equations, the static-geometric relations, can be used [107]. The first equation relates to equilibrium, part slab action p_b and part membrane action p_s. The second equation concerns the compatibility expressed in the change of Gaussian curvature g, again one part relating to slab action g_b one to membrane action g_s.

$$equilibrium:$$

$$D\left(\frac{\partial^4 w}{\partial x^4} + 2\frac{\partial^4 w}{\partial x^2 \partial y^2} + \frac{\partial^4 w}{\partial y^4}\right) + \left(\frac{\partial^2 z}{\partial x^2}\frac{\partial^2 \phi}{\partial y^2} - 2\frac{\partial^2 z}{\partial x \partial y}\frac{\partial^2 \phi}{\partial x \partial y} + \frac{\partial^2 z}{\partial y^2}\frac{\partial^2 \phi}{\partial x^2}\right) = p$$

$$p_b + p_s = p$$

$$compatibility:$$

$$\frac{1}{Et}\left(\frac{\partial^4 \phi}{\partial x^4} + 2\frac{\partial^4 \phi}{\partial x^2 \partial y^2} + \frac{\partial^4 \phi}{\partial y^4}\right) = \left(\frac{\partial^2 z}{\partial x^2}\frac{\partial^2 w}{\partial y^2} - 2\frac{\partial^2 z}{\partial x \partial y}\frac{\partial^2 w}{\partial x \partial y} + \frac{\partial^2 z}{\partial y^2}\frac{\partial^2 w}{\partial x^2}\right) = g$$

$$g_s = g_b = g$$

These equations can be solved numerically, for further detailed information see the master thesis of Kris Riemens, "*A Parametric Structural Design Tool for Shell Structures*" [108].

The numerical example shown here is the analysis of an actual shell designed by Heinz Isler, the Hallenbad in Brugg from 1981.

Figure 64 Hallenbad by Heinz Isler [image Peter Eigenraam]

The geometry used for the numeric analysis comes from 3D scans of the real scale models of Heinz Isler, done by Peter Eigenraam together with Andrew Borgart in 2011 [109].

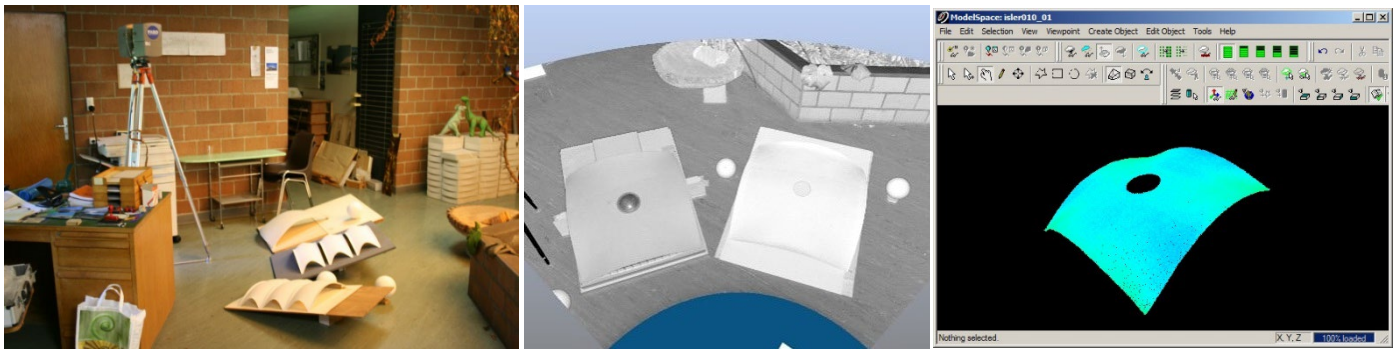

Figure 65 scanning of models by Heinz Isler [images 106]

For simplicity the shell has been analysed with a uniformly distributed load and with semi-rigid edges.

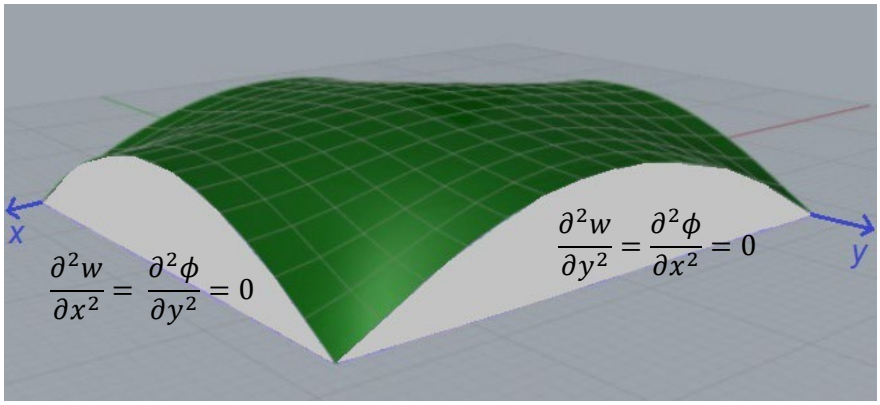

semi rigid edges

The procedure revolves around determining the change of Gaussian curvature for each mesh point of the discretized shell surface. Once this is done the stress function and the displacement field can be determined. The total load *p* can be split into the part that will be carried by membrane forces p_s and the other part by bending moments and shear forces p_b [110].

The global procedure with its different steps is represented below. For the total procedure see the aforementioned thesis of Kris Riemens. A global overview is provided here below, as well as the main results for this example.

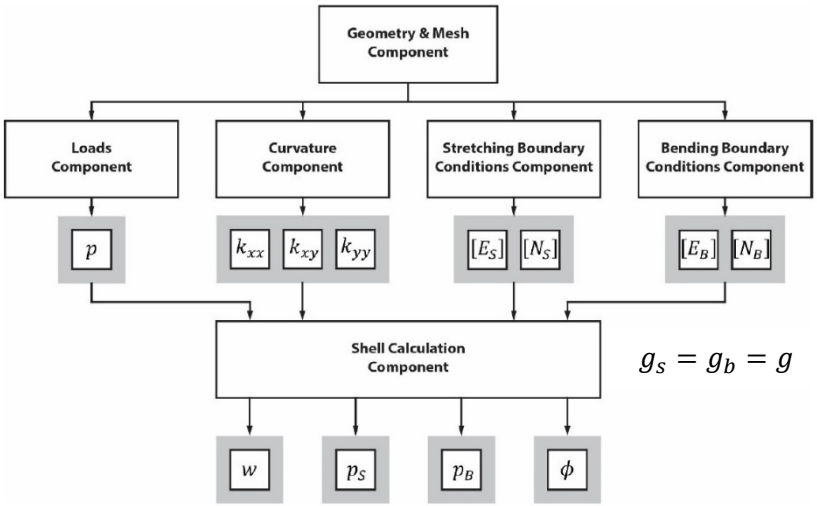

→ *divide the surface of the shell into a mesh*
→ *specify the loads on the mesh*
→ *determine the initial curvatures of the shell surface*
→ *set the boundary conditions*
→ *express the stress function* (ϕ) *and the displacement* (w) *in* (g)
→ *express change of Gaussian curvature* (g) *in the load* (p) *and add the boundary conditions*
→ *solve equations to calculate the change of Gaussian curvate in each mesh point*
→ *determine* (ϕ) *and* (w)
→ *determine* (p_s) *and* (p_b)
→ *determine the support reactions and the internal forces*

$$p_s = \left(\frac{\partial^2 z}{\partial x^2}\frac{\partial^2 \phi}{\partial y^2} - 2\frac{\partial^2 z}{\partial x \partial y}\frac{\partial^2 \phi}{\partial x \partial y} + \frac{\partial^2 z}{\partial y^2}\frac{\partial^2 \phi}{\partial x^2}\right)$$

$$p_b = D\left(\frac{\partial^4 w}{\partial x^4} + 2\frac{\partial^4 w}{\partial x^2 \partial y^2} + \frac{\partial^4 w}{\partial y^4}\right)$$

Figure 66 flow chart procedure [image 108]

After the problem has been solved the internal forces of the shell can be calculated. The result of the stress function and the displacement field is shown in the next image.

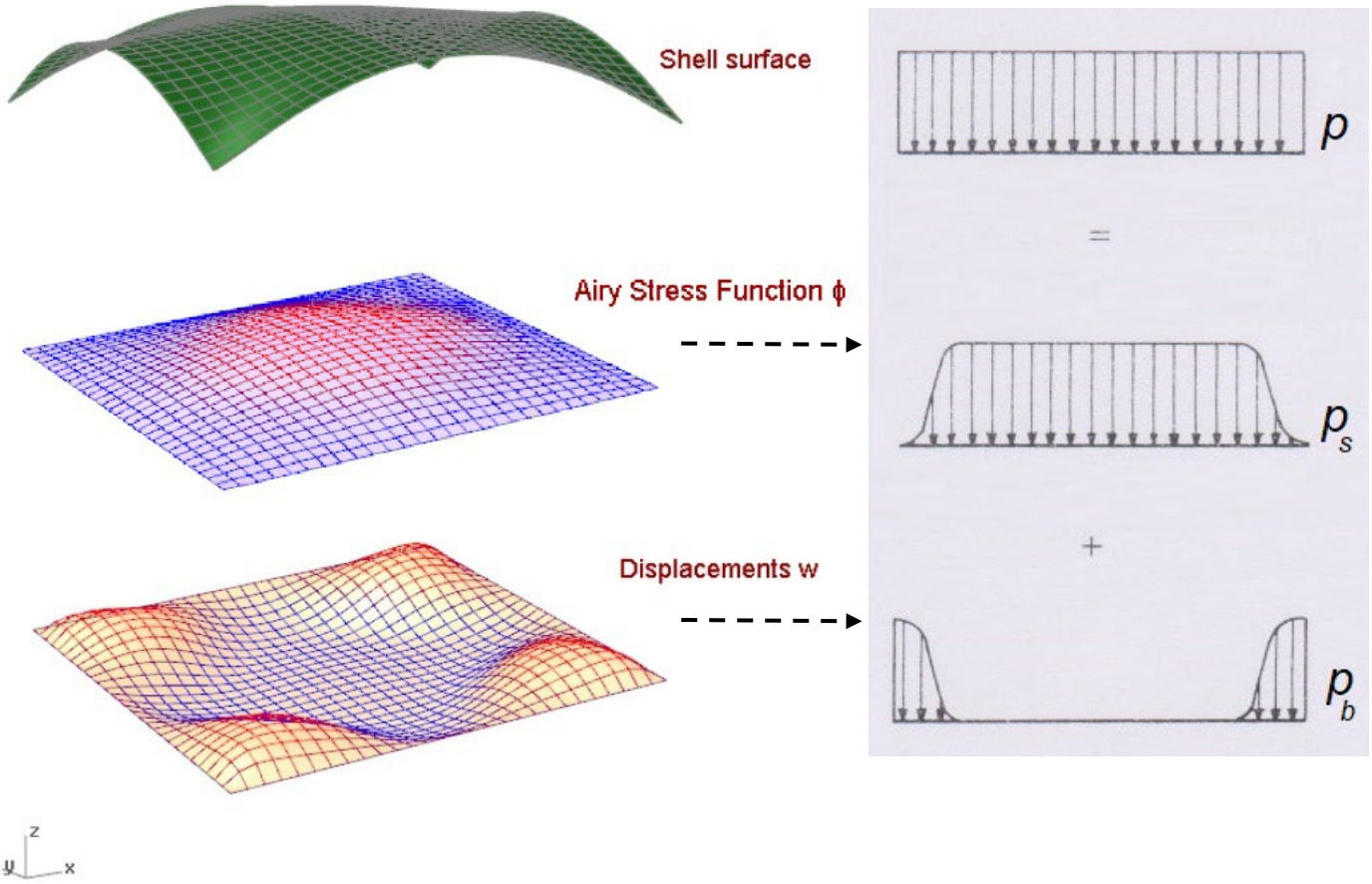

Figure 67 load carried by axial forces or bending moments [images left 108 and right 110]

Using a fine enough mesh the results are very accurate compared to a FEM analysis of the shell. This analysis has been performed by Pim Buskermolen. The calculcated displacement of the axis of symmetry of the shell is shown in the graph below.

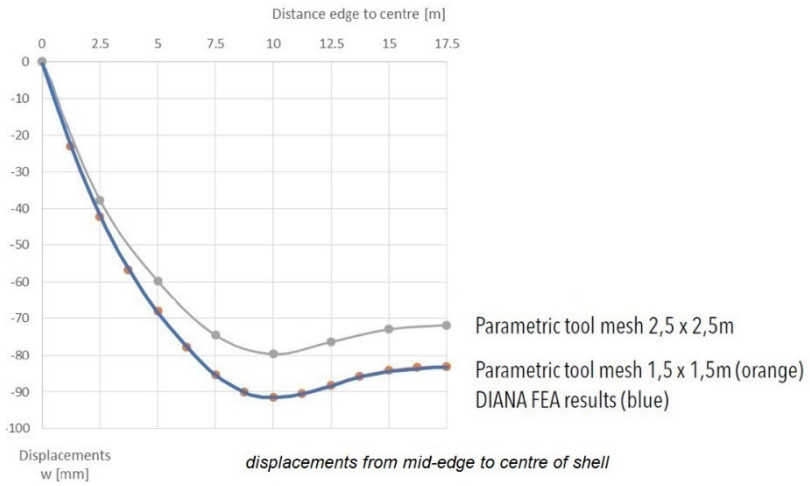

Figure 68 accuracy method [image 108]

9 Conclusions and recommendations

9.1 Conclusions

Different analytical procedures and methods to analyse arches and shells have been described in this thesis. The method set out in chapter 4 is an approximation. The method set out in chapter 8 provides a more insightful set of relations, the slab – shell analogy.

The thesis comprises of three parts, the first part (sections 2 to 4) focusses on 2D and 3D graphic statics, the reciprocal relationship between cables/arches and trusses and (in)determinate graphic statics.

- The relationship between form and force and the equations of equilibrium, force density method, thrust network analysis and the cable equation are essentially the same in which the force density is the scaling factor between the form diagram and the force polygon, this can be explained and visualized by graphic statics (sections 2.6 – 2.9)
- The mutual relationship of trusses and cables/arches can be described by reciprocal structures, this holds for their force polygons, form diagrams and state of rigidity (chapter 3)
- Trusses and cables/arches have a dual relation. For statically indeterminant trusses the sum of the squared bar axial forces weighted by their length has to be minimal, and for cable structures to find their equilibrium geometry the sum of the squared tie lengths weighted by their force densities also has to be minimal (section 3.7)
- Three dimensional graphic statics, such as thrust networks, which are mostly statically indeterminate, can be solved by minimizing the complementary energy. This makes it possible to find the geometry which is in equilibrium which would be the result of a FEM calculation out of the infinite number of possible solutions (sections 3.8, 4.5 & 4.6)

The second part (sections 5 and 6) deals with statically indeterminate arches and their stress functions.

- Maxwell's load path theorem is also applicable to indeterminate arches (section 5.4)
- As with the thrust network the correct thrust line for a statically inderteminate arch can be determined by minimizing the complementary energy of the system

- For arches Pucher's equation, which is normally used to determine axial forces in arches and shells, can be extended to incorporate the eccentricity of the thrust line if it deviates from the arches shape function to determine the amount of bending in the arch (section 6.3)
- It is possible to apply the principles of Mohr's first and second moment-area theorem's to the static-geometric analogy, thus for deflections and the stress function (section 6.4)
- The stress function can be visually represented by graphic statics, just like for cables and arches using a form diagram and stress polygon (section 6.7)

The third part (sections 7 and 8) deals with the relationship between the four fundamental properties of arches and shell structures, namely the shape function, stress function, thrust surface and moment-hill.

- The $\overline{M}$-hill and its load distribution can be used to derive the stress function and thus the internal membrane forces of (axisymmetric) shells, the last in range off results of classic shell theory (chapter 7)
- The $\overline{M}$-hill is an equilibrium surface with the lowest energy considering its load and boundary conditions
- The established beam – arch analogy also holds for shells and their equivalent slabs and is in fact the one dimensional version of the slab – shell analogy (chapter 8)
- The moment-hill of its equivalent slab is responsible for the load distribution in shell structures (chapter 7 and 8)
- For each set of boundary conditions for a shell there is an equivalent slab with dual boundary conditions (section 8.5)
- The shape function, stress function, moment-hill and thrust surface of arch and shell structures are directly related by means of interconnected functions (sections 8.6 and 8.8)
- The shape function and the stress function are reciprocal, with the $\overline{M}$-hill acting as an intermediate and determined by the boundary conditions (section 8.7)
- The out-of-plane moments in shell structures can be determined with the static-geometric relations for thin shells by solving the change of Gaussian curvature *g* (section 8.10)

9.2 Recommendations and outlook

For this thesis some simplifications needed to be made in order to establish the relations without unnecessary complication. A Poisson's ratio of zero has been assumed throughout the thesis and only a uniformly distributed load has been considered. In future research this could be extended.

This could be the basis of a potential parametric design tool, which integrates the theory developed in this thesis used in the thesis and would making it accessible and user friendly.
The procedure would contain the following steps:

- use the force density method including the correct loads and boundary conditions (see section 8.5) to create the $\bar{M}$-hill (see section 8.6), this components can also later be used to show the principle shear forces ("rain flow") in the shell if it contains bending
- use the flow of forces / load distribution of the $\bar{M}$-hill as the basis for deriving the shape and stress function (section 1.3, 8.6 and 8.7)
- once a shape function has been chosen, analytically or with the help of 3D modelling software, generate the stress function numerically using the slab - shell analogy (section 8.3 and 8.6)
- check if it is a membrane only solution (section 8.10)
- derive the membrane forces by using the transformation equations (section 8.6)
- if the solution requires additional bending moments, derive them (section 8.10)
- if required to find another result, alter the shape- or stress function and repeat the process

Recommendations for further research and work that would considerably add to the applicability of the tool to be developed:

- incorporate the self-weight of the shell into the methods, minimizing the eco impact
- extend the different types of boundary conditions available for the method of section 8.10
- further research on generating the thrust surface and its relation with the $\bar{M}$-hill and the stress function

Poisson's ratio can be easily incorporated whilst creating a $\bar{M}$-hill. Although it does change the gradients in the *x*- and *y*-directions and thus the load distribution, for the present research goal it was acceptable to neglect it.

$$\bar{M} = \frac{m_{xx} + m_{yy}}{1 + \nu}$$

The proposed method to add self-weight to the procedure is to generate the M-hill of a flat slab with the correct boundary conditions with horizontally projected load p_w of a hanging model. The load p_w is the projection of the load along the arc surface of the hanging model, similar to that of the catenary. In this way the self-weight of the shell can be approximated and be incorporated into the method in a relatively simple way.

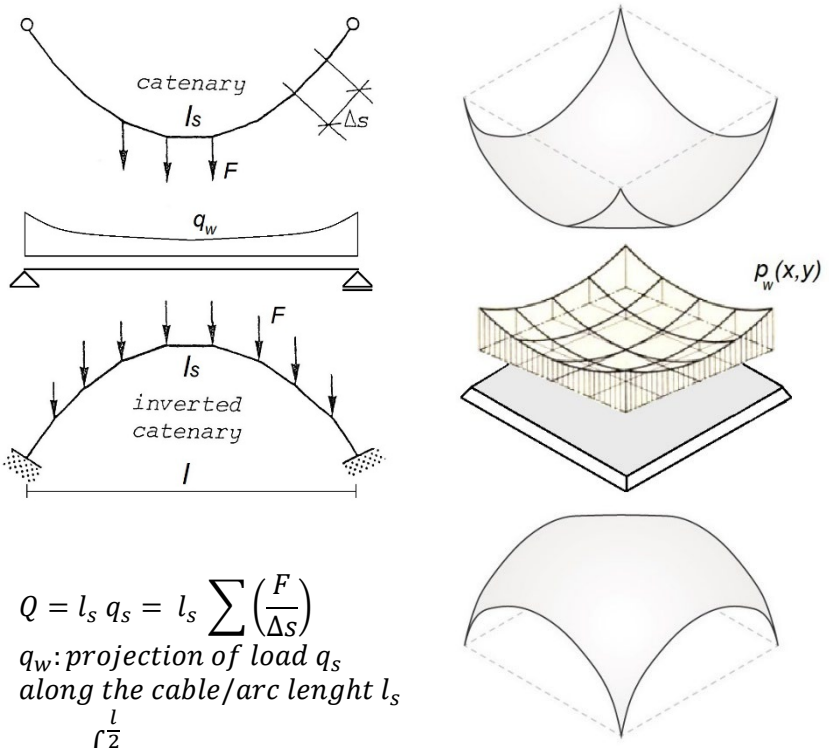

$$Q = l_s\, q_s = \; l_s \sum \left(\frac{F}{\Delta s}\right)$$

q_w: *projection of load* q_s
along the cable/arc lenght l_s

$$Q = \int_{-\frac{l}{2}}^{\frac{l}{2}} q_w \, dx$$

The new possibilities offered by CAM or the advent of 3D printing could be both utilized in the making process for double curved shell. It is worthwhile to investigate if the making process can be part of the parametric design tool.

When taken into account the relationship between the four fundamental functions which govern the structural behaviour of shell structures, their design process can be steered. A shell can be achieved with elegance and efficiency, as has been demonstrated by Candela, Torroja, Nervi and Isler.

Manufacture and loading test of reinforced gypsum shells generated from hanging models – a workshop at Delft University of Technology [111].

References

1. Hilbert, D. and S. Cohn-Vossen, *Geometry and the Imagination*. 1999: AMS Chelsea Pub.
2. Ramm, E. and W.A. Wall, *Shell structures - a sensitive interrelation between physics and numerics.* International Journal for Numerical Methods in Engineering, 2004. **60**(1): p. 381-427.
3. Chilton, J. and H. Isler, *Heinz Isler: the engineer's contribution to contemporary architecture*. 2000: Thomas Telford.
4. Zalewski, W. and E. Allen, *Shaping Structures: Statics*. 1998: Wiley.
5. *Computational design of blobs*. in *Symposium computational design of blobs*. 2004. Delft, The Netherlands: TU-Delft, faculteit bouwkunde.
6. Hanselaar, H., *SnowPalace, Betonnen schaalconstructie voor een Indoor Sneeuwskibaan*, in *Architecture*. 2003, Delft University of Technology.
7. Borgart, A. and T. Kocatürk, *Free form design as the digital "Zeitgeist".* Journal of the International Association for Shell and Spatial Structures, 2007. **48**(4): p. 3-9.
8. Januszkiewicz, K. and M. Banachowicz, *Nonlinear Shaping Architecture Designed with Using Evolutionary Structural Optimization Tools.* IOP Conference Series: Materials Science and Engineering, 2017. **245**: p. 082042.
9. Bletzinger, K.U. and E. Ramm, *Form Finding of Shells by Structural Optimization.* Engineering with Computers, 1993. **9**(1): p. 27-35.
10. Borgart, A., M. Leuw de, and P.C.J. Hoogenboom, *The relationship of form and force in (irregular) curved surfaces*, in *5th International Conference on Computation of Shell and Spatial Structures*, Ramm E., et al., Editors. 2005: Salzburg, Austria.
11. Leuw de, M.W., *'De steilste helling methode' De invloed van de geometrie op het spanningsverloop in willekeurig gekromde schalen*, in *Civil Engineering and Geosciences*. 2005, Delft University of Technology: Delft, Netherlands.
12. Timoshenko, S. and S. Woinowsky-Krieger, *Theory of Plates and Shells*. 1959: McGraw-Hill.
13. Flügge, W., *Stresses in shells*. 2nd edition. ed. 1973, New York: Springer. xi, 525 p.
14. Novozhilov, V.V., *The Theory of Thin Shells*. 1959: P. Noordhoff.
15. Love, A.E.H., *A Treatise on the Mathematical Theory of Elasticity*. 1944: Dover Publications.
16. Haas, A.M., *Design of Thin Concrete Shells: Vol. 2 : Negative Curvature Index*. 1967: John Wiley & Sons.

17. Girkmann, K., *Flächentragwerke: Einführung in die Elastostatik der Scheiben, Platten, Schalen und Faltwerke*. 1948: Springer-Verlag.
18. Billington, D.P., *Thin Shell Concrete Structures*. 1965: McGraw-Hill.
19. Calladine, C.R., *Theory of Shell Structures*. 1983: Cambridge University Press.
20. von Emperger, F., et al., *Dachbauten Schalen und Rippenkuppeln: Hochbau. Bd. 12. Tl. 2*. 1928: Verlag von Wilhelm Ernst & Sohn.
21. Faber, C., *Felix Candela: The Shell Builder*. 1963: Architectural Press.
22. Miret, E.T., *The Structures of Eduardo Torroja: An Autobiography of Engineering Accomplishment*. 1958: F.W. Dodge Corporation.
23. Nervi, P.L., *The Works of Pier Luigi Nervi*. 1957: F.A. Praeger.
24. Isler, H., E. Ramm, and E. Schunck, *Heinz Isler, Schalen: Katalog zur Ausstellung*. 2002: vdf, Hochsch.-Verlag an der ETH.
25. Billington, D.P., *The Tower and the Bridge: The New Art of Structural Engineering*. 1985: Princeton University Press.
26. Tang, G., *An Overview of Historical and Contemporary Concrete Shells, Their Construction and Factors in Their General Disappearance.* International Journal of Space Structures, 2015. **30**(1): p. 1-12.
27. Samuelsson, A. and O.C. Zienkiewicz, *History of the stiffness method.* International Journal for Numerical Methods in Engineering, 2006. **67**.
28. O'Dwyer, D., *Funicular analysis of masonry vaults.* Computers & Structures, 1999. **73**: p. 187-197.
29. Block, P. and J. Ochsendorf, *Thrust network analysis: a new methodology for three-dimensional equilibrium.* Journal- International Association for Shell and Spatial Structures, 2007. **48**: p. 167-173.
30. Beranek, W.J., *Berekening van Platen, deel 1 Theoretische Grondslagen*, T.H. Delft, Editor. 1976.
31. Borgart, A. and L. Tiggeler, *Computational Structural Form Finding and Optimization of Shell Structures*, in *International Association for Shell and Spatial Structures Symposium, Evolution and Trends in Design, Analysis and Construction of Shell and Spatial Structures*, A. Domingo and C. Lazaro, Editors. 2009: Valencia, Spain.
32. Isler, H., *Heinz Isler as Structural Artist*, Art Museum and the School of Engineering and Applied Science Princeton University, Editor. 1980.
33. Kurrer, K.E. and E. Ramm, *The History of the Theory of Structures: From Arch Analysis to Computational Mechanics*. 2012: Wiley.
34. Maxwell, J.C., *I.—On Reciprocal Figures, Frames, and Diagrams of Forces.* Transactions of the Royal Society of Edinburgh, 1870. **26**: p. 1 - 40.
35. Timoshenko, S. and D.H. Young, *Engineering Mechanics: Statics*. 1937: McGraw-Hill book Company, Incorporated.

36. Przemieniecki, J.S., *Theory of Matrix Structural Analysis*. 1967: McGraw-Hill.
37. Linkwitz, K. and H.J. Schek, *Einige Bemerkungen zur Berechnung von vorgespannten Seilnetzkonstruktionen.* Ingenieur-Archiv, 1971. **40**(3): p. 145-158.
38. Beranek, W.J., *Krachtwerking in liggers*, T.H. Delft, Editor. 1980.
39. Irvine, H.M., *Cable Structures*. 1992: Dover Publications.
40. Block, P., *Thrust Network Analysis : exploring three-dimensional equilibrium*. 2009.
41. Miura, K. and S. Pellegrino, *Forms and Concepts for Lightweight Structures*. 2020: Cambridge University Press.
42. Pellegrino, S., *Mechanics of Kinematically Indeterminate Structures*, in *Corpus Christi College*. 1986, University of Cambridge: Cambridge, UK.
43. Mele, T., et al., *Geometry-based Understanding of Structures.* Journal of the International Association for Shell and Spatial Structures, 2012. **53**.
44. Blaauwendraad, J., *Theory of Elasticity, Energy Principles and Variational Methods*, D.U.o. Techology, Editor. 2002: Delft, The Netherlands.
45. Baker, W., et al., *Maxwell's reciprocal diagrams and discrete Michell frames.* Structural and Multidisciplinary Optimization, 2013. **48**.
46. Baker, W.F., et al., *Structural Innovation: Combining Classic Theories with New Technologies.* Engineering Journal-American Institute of Steel Construction, 2015. **52**(3): p. 203-217.
47. Liew, A., et al., *Load-path optimisation of funicular networks.* Meccanica, 2018. **53**(1-2): p. 279-294.
48. Schek, H.-J., *The force density method for form finding and computation of general networks.* Computer Methods in Applied Mechanics and Engineering, 1974. **3**: p. 115-134.
49. Miki, M. and K.i. Kawaguchi, *Extended force density method for form finding of tension structures.* Journal of the International Association for Shell and Spatial Structures, 2010. **51**: p. 291-303.
50. Tabarrok, B. and Y. Xiong, *Some variational formulations for minimum surfaces.* Acta Mechanica, 1991. **89**(1): p. 33-43.
51. Hildebrandt, S. and A. Tromba, *Mathematics and Optimal Form*. 1985: Scientific American Library.
52. Haasnoot, M., *Non-Linear Grid Optimization and "Rain Analysis" on Free Formed Glass Roof*, in *Architecture*. 2007, Delft University of Technology.
53. Loof, H.W., *Vlakke platen op extensie of/en buiging belast*, T.H. Delft, Editor. 1975.
54. Adriaenssens, S., et al., *Shell Structures for Architecture: Form Finding and Optimization*. 2014: Taylor & Francis.

55. Popov, E.V., *On some variational formulations for minimum surface.* Transactions of the Canadian Society for Mechanical Engineering, 1996. **20**: p. 391-400.
56. Popov, E.V. and T. Popova, *Minimal Surface Form Finding and Visualization using Stretched Grid Method.* Scientific Visualization, 2021. **13**: p. 54-68.
57. Kouwenhoven, A., *Form-finding of branching structures supporting freeform architectural surfaces*, in *Architecture*. 2018, Delft University of Technology.
58. Beranek, W.J., *Understanding of structures*, in *Stable-Unstable, Structural consolidation of ancient buildings*, R.M. Lemaire and v.K. Balen, Editors. 1988, Leuven University Press: Leuven, Belgium.
59. Baecke, W., *Het ontwerpen van vouwschalen bestaand uit prefab elementen*, in *Architecture*. 2005, Delft University of Technology.
60. Beranek, W.J., *K3 dictaat ruimtelijke constructies, deel 2*, T.H. Delft, Editor. 1979.
61. Ros, J., *Graphically calculating arcs and shells by using the lowest complementary energy*, in *Architecture*. 2017, Delft University of Technology.
62. Dijk van, N., *Graphic statics in arches and curved beams, finding force equilibrium through total minimum complementary energy*, in *Architecture*. 2014, Delft University of Technology.
63. Rozendaal, R., *Shells and arches, Developing an new method to calculate shells and arches through graphic statics*, in *Architecture*. 2014, Delft University of Technology.
64. Rozendaal, R. and A. Borgart, *Calcularting arches through graphic statics: developing a new method*, in *International Association for Shell and Spatial Structures Symposium, Future Visions*. 2015: Amsterdam, The Netherlands.
65. Matheson, J.A.L., et al., *Hyperstatic Structures: An Introduction to the Theory of Statically Indeterminate Structures*. 1959: Butterworths.
66. Borgart, A., Q. Li, and P. Eigenraam, *Structural behavior assessment and load-transfer analysis of arches and curved beams*. 2018, Delft University of Technology.
67. Li, Q., *Form Follows Force, a theoretical framework for Structural Morphology, and Form-Finding research on shell structures*, in *Department of Architectural Engineering and Technolgy*. 2018, Delft University of Technology: Delft, The Netherlands. p. 276.
68. Heyman, J., *Equilibrium of Shell Structures*. 1977: Clarendon Press.

69. Calladine, C.R., *The static–geometric analogy in the equations of thin shell structures.* Mathematical Proceedings of the Cambridge Philosophical Society, 1977. **82**: p. 335 - 351.
70. Williams, C.J.K. and A. McRobie, *Graphic statics using discontinuous Airy stress functions.* International Journal of Space Structures, 2016. **31**: p. 121 - 134.
71. Hartsuijker, C., *Toegepaste mechanica: deel 2: spanningen, vervormingen en verplaatsingen*. 2001: Academic Service.
72. Vreedenburgh, C.G.J. and J.H. Ploeg van der, *Mathematische Veerkrachtsleer Beginselen van de Schijf- en Plaattheorie Liggers op verende bedding*, T.H. Delft, Editor.
73. Beranek, W.J., *Toegepast Mechanica K-3 vlakke constructiedelen elasticiteitstheorie*, T.H. Delft, Editor. 1974.
74. Chiang, Y.C., *Design and Fabrication of Shell Structures*. 2022, Delft University of Technology: Delft, Netherlands.
75. Beranek, W.J., *Krachtswerking deel 3, Vakwerken Standzekerheid*, D.U.o. Technology, Editor. 2001.
76. Cremona, L., *Graphical Statics: Two Treatises on the Graphical Calculus and Reciprocal Figures in Graphical Statics*. 1890: Merchant Books.
77. Beranek, W.J., *Krachtswerking deel 5, Vervormingen*, D.U.o. Technology, Editor. 2000.
78. Verruijt, A., *Toegepaste Mechanica-I*. 1979: Delftse Uitgevers Maatschappij.
79. Verruijt, A., *Toegepaste Mechanica-II*. 1979: Delftse Uitgevers Maatschappij.
80. Strubecker, K., *Airysche Spannungsfunktion und isotrope Differentialgeometrie.* Mathematische Zeitschrift, 1962. **78**(1): p. 189-198.
81. Heyman, J., *Elements of the Theory of Structures*. 1996: Cambridge University Press.
82. Heyman, J., *Hooke's cubico–parabolical conoid.* Notes and Records of the Royal Society of London, 1998. **52**: p. 39 - 50.
83. Born, J., *Praktische Schalenstatik*. 1968: W. Ernst.
84. Haas, A.M., *Design of Thin Concrete Shells: Vol. 1 : Positive Curvature Index*. 1962: John Wiley & Sons.
85. Isenberg, C., *The Science of Soap Films and Soap Bubbles*. 1992: Dover Publications.
86. Blaauwendraad, J., *Plates and FEM: Surprises and Pitfalls*. 2010: Springer Netherlands.

87. Beranek, W.J. and G.J. Hobbelman, *Space Frames designed as 'Twistless Case'*, in *Third international conference on space structures*, H. Nooshin, Editor. 1984, Elsevier: University of Surrey, UK.
88. Bouma, A.L., *Mechanica van constructies B*, T.H. Delft, Editor. 1981: Delft, The Netherlands.
89. Ramaswamy, G.S., *Design and Construction of Concrete Shell Roofs*. 1968: McGraw-Hill.
90. Dool van den, M., *Optimizing shell structures, by calculating the minimum complementary engergy*, in *Architecture*. 2012, Delft University of Technology.
91. Borgart, A. and Y. Liem, *Force Network Analysis using Complementary Energy*, in *International Association for Shell and Spatial Structures Symposium - IABSE, Taller, Longer, Lighter*. 2011: London, UK.
92. Witteveen, J., *Het berekenen van platen met sprongsgewijs veranderende dikte met behulp van de differentiemethode.* Heron, 1965. **13**(no. 3/4): p. 95-122.
93. Timoshenko, S. and J.N. Goodier, *Theory of Elasticity. (2nd Edition)*. 1951: McGraw Hill Book Company.
94. Csonka, P., *Theory and Practice of Membrane Shells*. 1987: VDI Verlag.
95. Loof, H.W., *Schalen I*, T.H. Delft, Editor. 1974.
96. Engel, H., *Tragsysteme*. 1997: Hatje.
97. Hoogenboom, P.C.J., *Ronde schijven en platen*, D.U.o. Technology, Editor. 2007.
98. Oosterhuis, M., *A parametric design tool for plate and shell structures*, in *Architecture*. 2010, Delft University of Technology.
99. Oosterhuis, M. and A. Borgart, *Parametric model of 3D shear force and bending moment diagrams for out-off-plane loaded plates.*, in *International Association for Shell and Spatial Structures Symposium, Spatial Structures - Permanent and Temporary*, Q. Zhang, L. Yang, and Y. Hu, Editors. 2012: Shanghai, China.
100. Liang, D., *A Parametrci Structural Design Tool (Grasshopper Interace) for Plate Structures*, in *Civil Engineering and Geosciences*. 2012, Delft University of Technology: Delft, Netherlands.
101. Buskermolen, P., *Shell Structures, On the relationship between moment hills, stress functions and thrust surface in the design of shell structures*, in *Architecture*. 2019, Delft University of Technology: Delft, Netherlands.
102. Maxwell, J.C., *XLV. On reciprocal figures and diagrams of forces.* The London, Edinburgh, and Dublin Philosophical Magazine and Journal of Science, 1864. **27**(182): p. 250-261.

103. Liem, Y., *Graphic statics in funicular design, calculating force equilibrium through complementary engergy*, in *Architecture*. 2011, Delft University of Technology
104. Whiteley, W., et al. *Convex Polyhedra, Dirichlet Tessellations, and Spider Webs*. 2013.
105. Maxwell, J.C., *On Reciprocal Diagrams in Space and their relation to Airy's Function of Stress.* Proceedings of the London Mathematical Society 1868. **1**(1): p. 58–63.
106. Borgart, A. and P. Eigenraam, *Scanning in 3D and analysing the models of Heinz Isler, the preliminary results*, in *International Association for Shell and Spatial Structures Symposium - APCS, From Spatial Structures to Space Structures*, S.D. Kim, Editor. 2012: Seoul, South Korea.
107. Mbakogu, F.C. and M.N. Pavlović, *Interaction of bending and stretching actions in shallow translational shells with various Gaussian curvature types.* Engineering Structures, 1999. **21**: p. 538-553.
108. Riemens, K., *A Parametric Structural Design Tool for Shell Structures*, in *Civil Engineering and Geosciences*. 2015, Delft University of Technology.
109. Eigenraam, P., et al., *Structural analysis of Heinz Isler's bubble shell.* Engineering Structures, 2020. **210**.
110. Ernst, L.J., *"De draagwerking van dubbelgekromde schalen, belast met een puntlast"*, in *Afdeling der Weg- en Waterbouwkunde*. 1973, Technische Hogeschool Delft: Delft, The Netherlands.
111. Borgart, A., Q. Li, and P. Eigenraam, *Manufacture and loading test of reinforced gypsum shells generated from hanging models – a workshop developed at Delft University of Technology*, in *Proceedings of the IASS Symposium Creativity in Structural Design*, C. Mueller and S. Adriaenssens, Editors. 2018: Boston, USA.

Curriculum vitae

ANDREW BORGART (1966) studied architectural design at the Rietveld Academy in Amsterdam form 1985 through 1988. From 1988 onwards, he studied architecture and civil engineering at Delft University of Technology, completing his studies in 1997. Since then he has been working as an assistant professor of Structural Mechanics at the Faculty of Architecture and the Built Environment of Delft University of Technology, also teaching at the Faculty of Civil Engineering and Geosciences. He teaches several courses in structural mechanics in the Bachelor programme Architecture and spatial structures as part of the Master track Structural Engineering. Borgart conducts research in the field of structural mechanics and morphology of complex geometry structures. He is a member of the Advisory Board of the International Association for Shell and Spatial Structures (IASS).

Picture back page:
Morpharchitecture workshop in Lyon 2010: snap-through (as result of in-extensional deformation) of shell

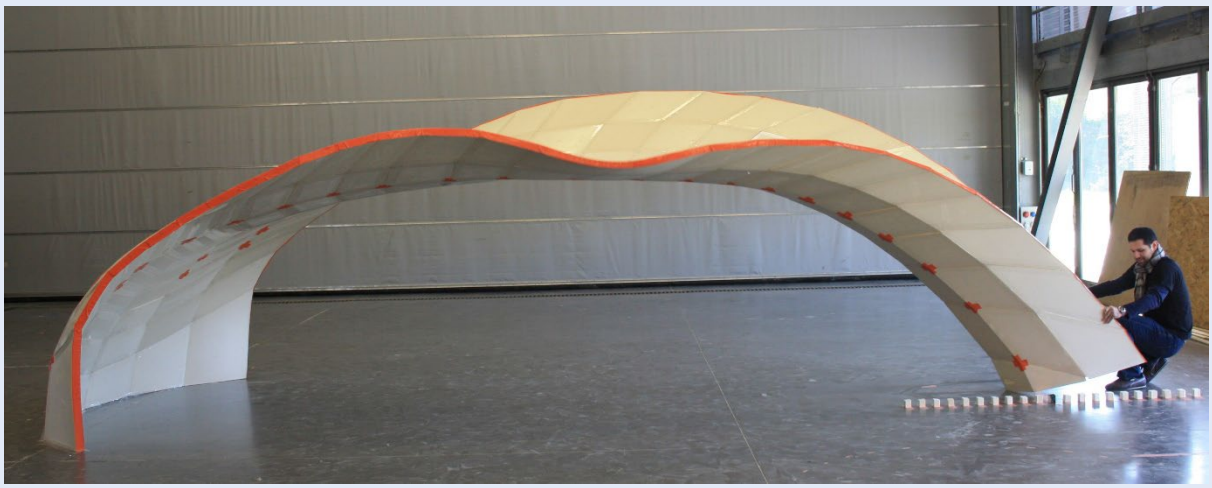

Delft University of Technology
Faculty of Architecture and the Built Environment
Department of Architectural Engineering and Technology